STUDIA UNIVERSITATIS
BABEŞ-BOLYAI

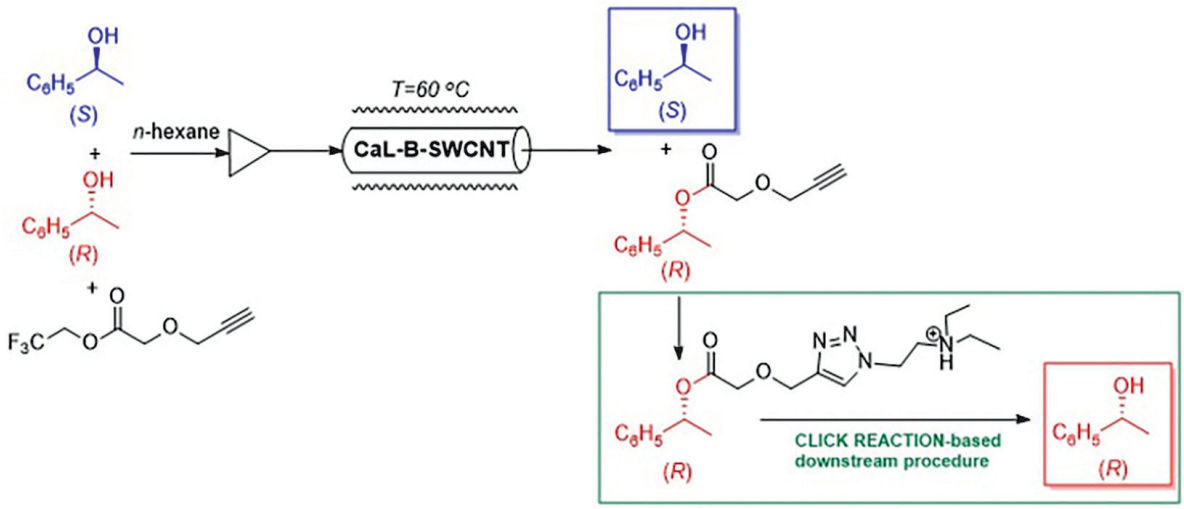

CHEMIA

2/2019
Tom I

STUDIA
UNIVERSITATIS BABEŞ-BOLYAI

CHEMIA

2/2019
Tom I

http://chem.ubbcluj.ro/~studiachemia/; studiachemia@chem.ubbcluj.ro
http://www.studia.ubbcluj.ro/serii/chemia/index_en.html

YEAR **Volume 64 (LXIV) 2017**
MONTH **JUNE**
ISSUE **2**
TOM **I**

S T U D I A
UNIVERSITATIS BABEŞ-BOLYAI
CHEMIA

2

Tom I

ISSUE DOI:10.24193/subbchem.2019.2.I

STUDIA UBB EDITORIAL OFFICE: B.P. Hasdeu no. 51, 400371 Cluj-Napoca, Romania, Phone + 40 264 405352

Dedicated to Professor Florin Dan Irimie on the Occasion of His 65th Anniversary

CUPRINS – CONTENT – SOMMAIRE – INHALT

Studia Universitatis Babes-Bolyai Chemia has been selected for coverage in Thomson Reuters products and custom information services. Beginning with V. 53 (1) 2008, this publication is indexed and abstracted in the following:

- Science Citation Index Expanded (also known as SciSearch®)
- Chemistry Citation Index®
- Journal Citation Reports/Science Edition

STUDIA UBB CHEMIA, LXIV, 2,Tom I, 2019 (p. 7-9)
(RECOMMENDED CITATION)

This issue of our journal is dedicated to Professor Florin Dan Irimie on His 65th Anniversary

Professor Florin Dan Irimie was born on March 30th, 1953 in Brașov, where he completed the primary, gymnasium and high school studies. In 1972, he became a student of the Faculty of Chemistry and Chemical Engineering of the Polytechnic University of Iași, specializing in Technology of Organic Compounds.

He elaborated his diploma project under the guidance of the famous Professor Corneliu Oniscu and he graduated in 1977. During 1997-1982, he was employed as a chemical engineer at Farmec Factory of Cosmetic Products in Cluj-Napoca, first as a coordinator of production activity, afterwards as a researcher of the Research and Development Department. In the period of 1982-1987 he performed research as a chemical engineer at the Biochemistry Department of the University of Agricultural Sciences from Cluj-Napoca. In 1987 he was invited as a teaching assistant to Babeș-Bolyai University (UBB), Faculty of Chemistry and Chemical Engineering to hold Chemical Technology seminars and laboratory works.

Under the supervision of Prof. Dr. Sorin Mager, he obtained the PhD title in chemistry (1993) with a thesis on “Aryl-oxy-carboxylic compounds with potential biologic activity”.

From 1990 he joined as lecturer the staff of the Chemical Technology Department at UBB, where he advanced to associate professor (1993) and to full professor (1999).

He was a research fellow at Mans France University, under the guidance of Prof. Eric Brown (1991) and at Michigan State University, invited by Prof. Rawle Hollingsworth (1995).

During the period 1992-2000, he acted as chancellor of the Faculty of Chemistry and Chemical Engineering of UBB.

In the early 90’s he realized the rapid development of biocatalysis in organic synthesis due to the enhanced chemo-, regio-, stereoselectivities of enzymes. He also recognized the importance of biocatalysis in reduction of environmental impact and also the potential of its contribution to more sustainable chemical industries ranging from pharmaceuticals to biofuels.

For this reason, during his tenure besides teaching General Chemical Technology, he introduced Biochemistry and Biotechnology lectures for existing BSc programs. He was also co-founder of the Catalysis and Biocatalysis MSc programme at the Faculty of Chemistry and Chemical Engineering. In 1995 he founded and continuously directed the most appreciated Biochemical Engineering BSc specialization. Also in this period he developed, together with the Faculty of Biology and Geology, a multidisciplinary MSc programme titled Cellular Biotransformations and then the Organic and Biochemical Processes Engineering MSc programme at the Faculty of Chemistry and Chemical Engineering. He founded and directed the Department of Biochemistry and Biochemical Engineering during the period 1999-2012. During this time, he developed several new disciplines at the Faculty of Chemistry and Chemical Engineering like Biochemistry, Biotechnology, Biocatalysis, Enzymatic and Fermentative Technologies, Bioprocess Engineering, Genetic Engineering, etc. He founded the Bioprocessing of Organic Substrates research group, which in time was transformed into the Biocatalysis and Biotransformation Research Centre, one of the most relevant integrated research units for biocatalyst development and enzyme assisted organic reactions in Central and Eastern Europe. He coordinated more than ten research projects.

From 2001-2002, the group coordinated by Professor Irimie joined to the CEEPUS Network “*Teaching and Learning Bioanalysis*”, leaded by the University of Pécs, Hungary**,** a network of universities aimed to establish cooperation in research and teaching activities.

He was invited lecturer at several prestigious universities such as: Karl-Franzens University of Graz, Austria, University Rouen, France, Budapest University of Technology and Economics Hungary, Eötvös Loránd University

of Budapest, Hungary, Ivanovo State University of Chemistry and Technology, Russia, University of Pecs, Hungary, “Constantine the Philosopher” University of Nitra, Slovakia, Charles University of Prague, Czech Republic, “Neofit Rilski” University of Blagoevgrad, Bulgaria, University of Zagreb, Croatia and University of Warsaw, Poland, Escuela Superior Politecnica de Chimborazo-Ecuador, Hanoi University of Science and Technology-Vietnam, National University of Laos.

Among his many scientific contacts, the most fruitful collaboration with the Bioorganic Chemistry Group from Budapest University of Technology and Economics should be mentioned, underlined by many common publications.

He is a member of the Doctoral School of Chemistry and he was the scientific supervisor of 13 PhD theses, all in the field of biocatalysis.

Prof. Florin-Dan Irimie, as a devoted researcher, was the corresponding author of several valuable publications dealing with cellular and enzymatic biocatalysis, immobilized enzymes in stereoselective organic synthesis, multienzymatic cascade reactions, enzymatic biofuel synthesis etc. His numerous publications in prestigious journals like *Tetrahedron: Asymmetry, Journal of Molecular Catalysis B: Enzymatic, Process Biochemistry, ChemCatChem, Bioresource Technology, European Journal of Organic Chemistry, ACS Sustainable Chemistry and Engineering, Proceedings of the National Academy of Sciences of the United States of America, Angewandte Chemie*, etc. played an important role in increasing the international visibility of Romanian science.

He is also author and co-author of five books written in Romanian and three book chapters in English (CRC press, Elsevier, Springer).

In 2018 the Babeș-Bolyai University awarded Professor Florin-Dan Irimie with the title of Professor Emeritus to honor his sustained and distinguished educational and research service brought to the University.

Currently, Professor Florin Dan Irimie is continuing untiringly and with commitment his educational and scientific activity. The guest editors and his collaborators from the Biocatalysis and Biotransformation Research Centre would like to express their best wishes to him. May he continue to enjoy many more years of successful Biocatalysis in good health.

GUEST EDITORS

Prof. Dr. Monica Ioana TOȘA
Prof. Dr. László POPPÉ
Prof. Dr. Csaba PAIZS

STUDIA UBB CHEMIA, LXIV, 2,Tom I, 2019 (p. 11-21)
(RECOMMENDED CITATION)
DOI:10.24193/subbchem.2019.2.01

Dedicated to Professor Florin Dan Irimie on the Occasion of His 65th Anniversary

MODELING THE L(+) LACTIC ACID PRODUCTION VIA R. ORYZAE NRRL 395 FERMENTATION ON BIODIESEL CRUDE GLYCEROL

EVA-H. DULF[a], DAN C. VODNAR[b], FRANCISC V. DULF[b]*

ABSTRACT. Similar to the petroleum industry, biodiesel industry generates unwanted by-products. Biodiesel production generate huge amount of crude glycerol- one part of glycerol is produced at every ten parts of biodiesel, and has a negative influence on the biodiesel price. A solution to reduce the negative environmental problems and the cost of biodiesel is to use crude glycerol as carbon source for microbial growth media in order to produce valuable organic chemicals. Recently, the research group from University of Agricultural Sciences and Veterinary Medicine Cluj-Napoca developed sustainable opportunities for L (+) lactic acid production via R. oryzae NRRL 395 fermentation on biodiesel crude glycerol. The current research aims at improving the production of L-lactic acid using crude glycerol as substrate, immobilized spores and inhibited alcohol dehydrogenase of R. oryzae in discontinuous and semi continuous fermentation processes in order to make the process more efficient. According to several experimental dataset under different process parameters, multiple regression methods were employed to establish mathematical models for prediction of the L lactic acid production. Determination coefficient values states that predicted values were in good agreement with the experimental values. Introducing the fractional order in models lead to a good phenomenological description. The resulted models can be used both in optimization process and prediction instead of time and resource consuming experiments.

Keywords: *biodiesel; crude glycerol; process optimization, mathematical model, fractional order model*

[a] *Technical University of Cluj-Napoca, Faculty of Automation and Computer Science, 28 Memorandumului str., RO-400014, Cluj-Napoca, Romania*
[b] *University of Agricultural Sciences and Veterinary Medicine Cluj-Napoca, Faculty of Food Science and Technology, 3-5 Manastur str., RO- 400372, Cluj-Napoca, Romania*
** Corresponding author: francisc_dulf@usamvcluj.ro*

INTRODUCTION

Nowadays, having the authority's pessimistic prospects for the future regarding the absolute dependency on fossil fuels, the political and economic policies are to stimulate the development of sustainable alternatives to fossil fuels. Biodiesel represent an alternative for the substitution of fossil fuels, which is the most common biofuel in Europe [1]. Similar to the petroleum industry, biodiesel industry generate unwanted by-products [2]. Biodiesel production generate huge amount of crude glycerol- one part of glycerol is produced at every ten parts of biodiesel [3], and has a negative influence on the biodiesel price.

The glycerine phase from biodiesel industry causes environmental problems regarding to the management of this waste. A solution to reduce the negative environmental problems and the cost of biodiesel is to use crude glycerol as carbon source for microbial growth media in order to produce valuable organic chemicals [4-6].

L(+)-lactic acid is an important chemical which has applications in many industries: food, cosmetics, pharmaceuticals; etc. It can be used as a feedstock for the production of poly-lactic acid (PLA), a polymer present in medical applications and environmentally friendly biodegradable plastics with high socio-economic impact, which can be substituted for synthetic plastics derived from petroleum resources [7, 8].

It is obvious that the optimization of lactic acid fermentation is a highly discussed problem. Still, the problem is not solved from many points of view, and the substrate plays a vital role in the improvement of the process. Raw materials can reduce the cost of substrates. However, pre-treatment cost and low productivity in fermentation using raw materials are the remaining drawbacks to be solved.

More recently, the research team from University of Agricultural Sciences and Veterinary Medicine Cluj-Napoca developed and analysed sustainable opportunities for L(+) lactic acid production via R. oryzae NRRL 395 fermentation on biodiesel crude glycerol [9, 10]. Apart from the large group of bacteria, filamentous fungi, especially R. oryzae proved that is a good lactic acid producer. Importantly, the filamentous fungus R. oryzae can produce an optically pure L(+)-lactic acid from media without expenses pre-treatment costs. R. oryzae NRRL 395 can utilize crude glycerol as carbon source, and unlike its competitors of lactic acid producing bacteria tolerate high impurities, has lower nutrition requirements which reduce the fermentation cost and simplifies downstream product separation.

The current research of the authors aim at improving the production of L-lactic acid using crude glycerol as substrate, immobilized spores and inhibited alcohol dehydrogenase of R. oryzae in discontinuous and semi-continuous

fermentation processes in order to make the process more efficient. Rigorous mathematical models would be useful both in prediction and in the optimization stage. To the best of our knowledge, there are no such models available for the studied processes. The paper presents the developed mathematical models, highlighting the advantages and disadvantages of each model.

MATERIALS AND METHODS

The aim of the current paper is to mathematically describe the potentialities of valorisation of crude glycerol by pelletized R. oryzae NRRL 395, in order to analyse and optimize the production of L(+)-lactic acid in media supplemented with laboratory nutrients or with lucerne green juice (LGJ). The model of the L lactic acid production process was developed in Matlab®, based on the data published by the authors in [9]. In this investigation, the input or decision variables consist of the amount of inorganic nutrients and time. As mathematical tool is used the multiple regression, both in linear or nonlinear form [11, 12]. Are also developed fractional order models, being recognized for the advantages introduced in modeling the complexity of the dynamics of some real-world systems [13, 14].

RESULTS AND DISCUSSION

The first developed model describes the dependency of the crude glycerol concentration for cultivating R. oryzae NRRL 395 in trials without LGJ addition and in trial with LGJ.

Noting with x_1 and x_2 the crude glycerol (CG) contents supplemented with different amount of inorganic nutrients (IN) and time, respectively, the mathematical model of productivity, y, resulted by the multiple linear regression is:

$$y = -1.1914 + 0.1571x_1 - 0.4286x_2 + 0.0806x_1x_2 \quad (1)$$

The corresponding simulation results, for values of x_1 in the range 10-80 g/L and x_2 in the range 20 – 90g/L are presented in Figure 1, in comparison with the experimental data (blue dots). The resulted statistical data are: R_2= 0.8416 and p-value=3.41e-08.

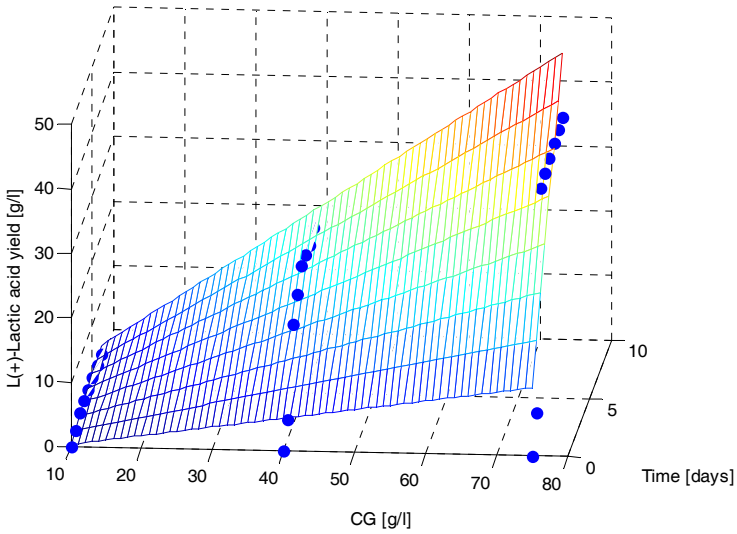

Figure 1. Simulation result with the linear model of x_1, x_2

For a better process description is developed also a nonlinear model, including the quadratic terms:

$$y = -8.3012 + 0.2280x_1 + 5.7439x_2 + 0.0806x_1x_2 - \\ - 0.0008x_1^2 - 0.8818x_2^2 \quad (2)$$

The corresponding simulation result is in Figure.2 for the same range of parameters x_1 and x_2, highlighting o good match, with R_2= 0.9092 and p-value= 9.081e-09.

It has been shown that fractional calculus in general and fractional order differ-integrals models in particular can characterize very well the phenomenology of biochemical processes [15]. Another advantage of these equations is that is simple to derive further a transfer function model from in its Laplace equivalent. The great deal of success is due to the fact that explains complex phenomena with a startling simplicity [16].

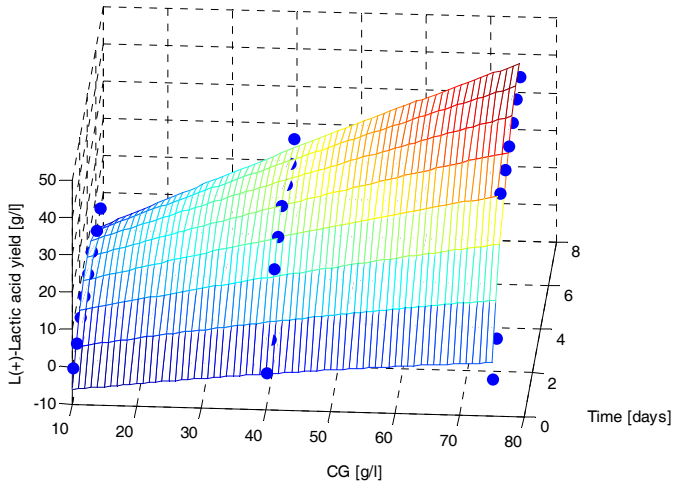

Figure 2. Simulation result with the classical nonlinear model of x_1, x_2

Having this in mind it were developed a series of fractional order models. The best results were obtained for the fractional order model:

$$y = -7.9601 + 0.14646x_1^{1.2} + 7.8152x_2^{1.2} + 0.0806x_1^{1.7} - \\ - 3.0646x_2^{1.7} \tag{3}$$

with R_2= 0.9101 and p= 8.35e-09.

The graphical plot from Figure 3 reveals a great phenomenological fit.

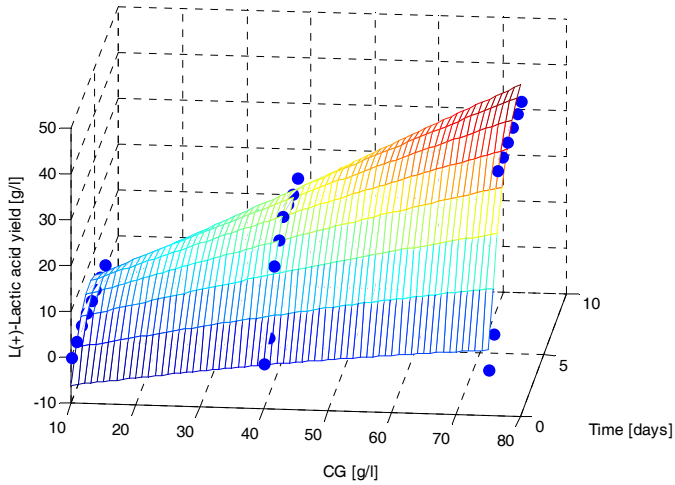

Figure 3. Simulation result with the fractional order model of x_1, x_2

In the same manner were developed models including the L(+)-lactic acid yield during R.oryzae NRRL 395 fermentaion in media containing different ratio of crude glycerol (CG) (10, 40, 75 g/l) supplemented with lucerne green juice (LGJ) (90, 60, 25 g/l), noted with variable x1 and x3. The linear model is:

$$y = 18.5414 - 0.1936x_1 + 9.0227x_3 - 0.0931x_1x_3 \quad (4)$$

The nonlinear model becomes:

$$y = 4.3191 + 0.0679x_1 + 17.4021x_3 - 0.0931x_1x_3 - \\ - 0.0023x_1^2 - 1.1971x_3^2 \quad (5)$$

while the fractional order model is:

$$y = 2.5961 + 0.1699x_1^{0.85} + 19.6730x_3^{0.85} - 0.0925x_1x_3 - \\ - 0.0038x_1^{1.9} - 0.9404x_3^{1.9} \quad (6)$$

The corresponding simulation results are presented in Figure 4, Figure 5 and Figure 6. The corresponding statistical measures are: R_2=[0.8077, 0.8950, 0.8936] and p=[2.32e-07 3.28e-08 3.72e-08], highlighting once again the advantage of fractional order.

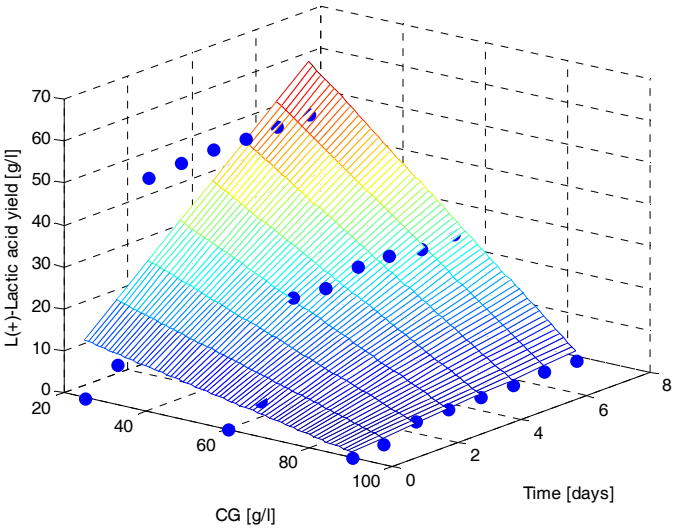

Figure 4. Simulation result with the linear model of x_1, x_3

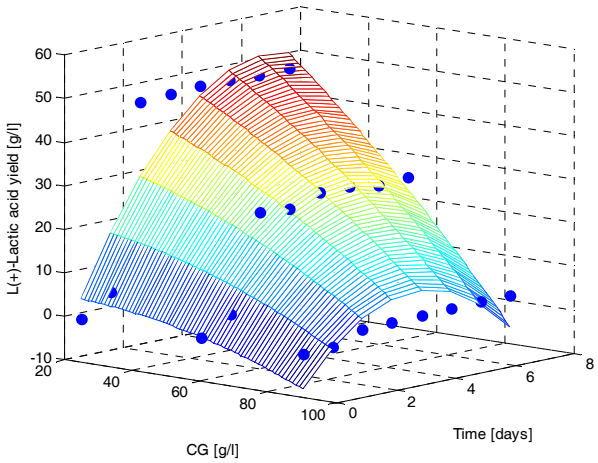

Figure 5. Simulation result with the classical nonlinear model of x_1, x_3

The mathematical model containing all three parameters is:

$$y = -116.3715x_2 + 1.3855x_1x_2 + 0.8672x_1x_3 + 0.7246x_2x_3 - \\ - 0.1050\,x_1x_2x_3 + 0.0113x_1^2 + 1.1389x_2^2 + 6.7875x_3^2 \quad (7)$$

with a mean square error of $3.6274 \cdot 10^{-13}$.

In this case is also obtained the minimum error for the fractional order model: $6.8359 \cdot 10^{-14}$, having the form:

$$y = -4.5443x_2 + 0.0306x_1x_2 - 0.0153x_1x_3 + \\ + 0.0115x_2x_3 - 0.0032\,x_1x_2x_3 + 0.0258x_1^{1.8} + 0.4457x_2^{1.8} + \quad (8) \\ + 1.7604x_3^{1.8}$$

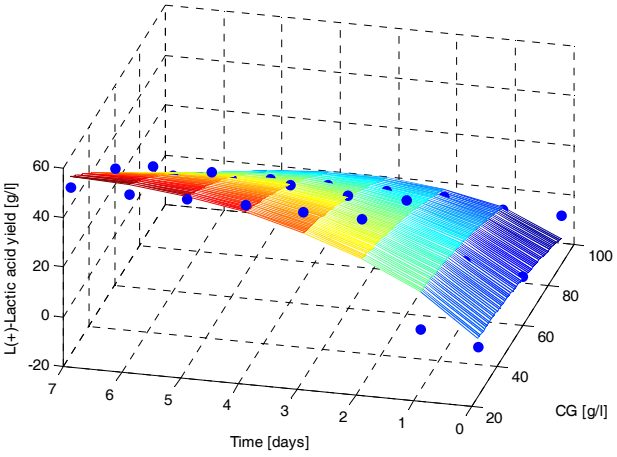

Figure 6. Simulation result with the fractional order model of x_1, x_3

The kinetics study of lactic acid production in bioreactor consisted in the analysis of the capacity of R. oryzae NRRL 395 for sugar utilization as model media. Processing the experimental results of R. oryzae NRRL 395 in producing L (+)-lactic with classical identification method, namely the Instrument Variable approach, lead to the integer order model in Laplace form:

$$H(s) = \frac{60}{(0.3s+1)(0.65s+1)} \tag{9}$$

where the system input is the ratio of crude glycerol (CG) and the output is the L (+)-lactic yield. The resulted mean square error is of 1.54. The corresponding fractional order model, identified as in [13, 14] is:

$$H(s) = \frac{60}{(0.3s^{1.2}+1)(0.65s^{0.8}+1)} \tag{10}$$

with a mean square error of 0.89. The comparative plot resulted with these two models is presented in Figure 7.

The linear mathematical model describing the R. oryzae NRRL 395 for sugar utilization for different ratio of crude glycerol (CG) resulted as:

$$H(s) = \frac{100}{(0.4s+1)(0.8s+1)} \tag{11}$$

with a mean square error of 3.27. The fractional order model has the form:

$$H(s) = \frac{100}{(0.4s^{1.3}+1)(0.8s^{0.8}+1)} \tag{12}$$

and the corresponding error is less than 0.45. The comparative simulation results of integer order and fractional order models are presented in Figure 8.

The next analysis consists on the lactic acid production by R. oryzae NRRL 395 on crude glycerol supplemented with inorganic nutrients. The results highlight once again the superiority of the fractional order models, Figure 9. The obtained values are in agreement with the data reported in the specific literature.

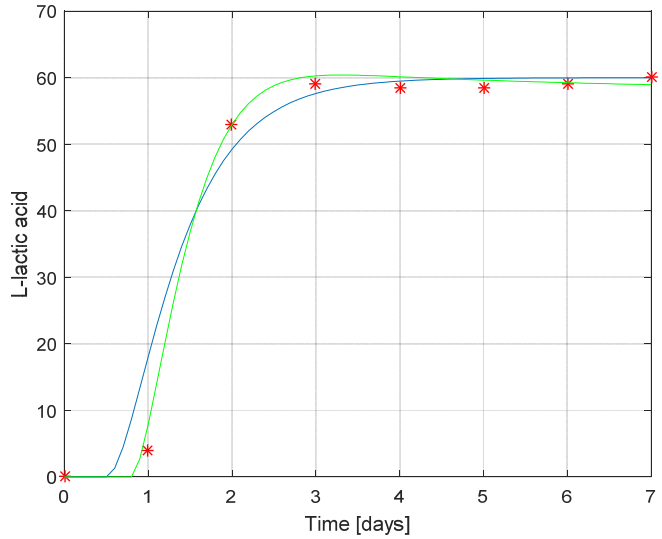

Figure 7. Simulation results for an integer order and fractional order model in producing L (+)-lactic (red stars-experimental data, blue line – linear model, green line – fractional order model)

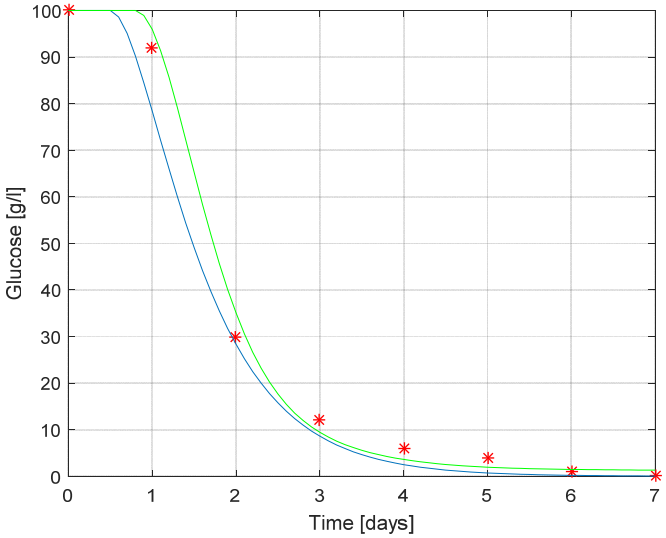

Figure 8. Simulation results for an integer order and fractional order model in sugar utilization (red stars-experimental data, blue line – linear model, green line – fractional order model)

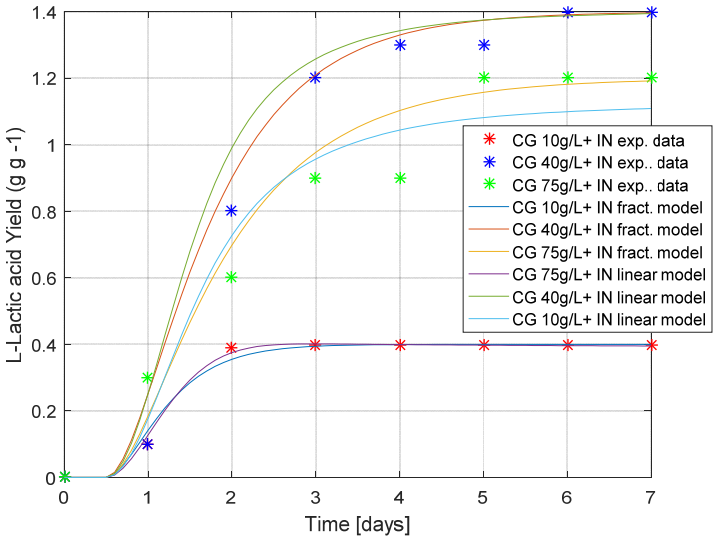

Figure 9. Simulation results for L (+)-lactic acid production obtained in trials with crude glycerol (CG) (10, 40, and75 g l-1)

CONCLUSIONS

The aim of the current paper was to mathematically describe the phenomena in the L(+) lactic acid production via R. oryzae NRRL 395 fermentation on biodiesel crude glycerol, in order to analyze and optimize the production in media supplemented with laboratory nutrients or with Lucerne green juice (LGJ). From the obtained mathematical models the best results are provided with the fractional order models, describing very well the nonlinear phenomena and being easy to use for optimization. The obtained mean square error is $6.8359 \cdot 10^{-14}$. The kinetic study of lactic acid production leads to a mean square error of 0.45 with the fractional order model, while with the integer order model is 3.27.

Future works include the application of different optimization methods for these processes.

ACKNOWLEDGMENTS

This work was supported by a grant of the Romanian National Authority for Scientific Research, CNDI– UEFISCDI, project number PN-III-P2-2.1-PED-2016-1237, contract 17PED/2017 and project PN-III-P1-1.2-PCCDI2017-0056 contract 2PCCDI/2018.

REFERENCES

1. A. Drozdzynska, K. Leja, K. Czaczyk, *J Biotechnol Comp Bio Bionanotechnol.,* **2011**, *92*, 92.
2. R. Dobson, V. Gray, K. Rumbold, *J Ind Microbiol Biotechnol.,* **2012**, *39*, 217.
3. D.M. Rossi, J.B. da Costa, E.A. de Souza, M.C.R. Perelba., M.A.Z. Ayub, *Renew Energ*, **2012**, *39*, 223.
4. A. Kosmider, A. Drozdzynska, K. Blaszka, K. Leja, K. Czaczyk, *Pol J Environ Stud*., **2010**, *19*, 1249.
5. F. Yang, M.A. Hanna, R. Sun,*Biotechnol Biofuel*., **2012**, *5*(13), 1.
6. K. Xu, P. Xu, *Bioresour Technol*., **2014**, *153*, 23.
7. M.A. Abdel-Rahman, Y.Tashiro, K. Sonomoto, *Biotechnol Adv.*, **2013**, *31*, 877.
8. Y. Wang, Y. Tashiro, K. Sonomoto, *J Biosci Bioeng*, **2014**, available online.
9. D.C. Vodnar, F.V. Dulf, O.L. Pop, C. Socaciu, *Microb Cell Fact.*, **2013**, *12*, 92.
10. D.C. Vodnar, L.F. Calinoiu, F.V. Dulf, B.E. Stefanescu, G. Crisan, C. Socaciu, *Food Chemistry*, **2017**, *231*, 131.
11. D. Olive, “Linear Regression”, Springer Verlag, **2017**.
12. B.R. Darlington, A.F. Hayes, “Regression Analysis and Linear Models Concepts, Applications, and Implementation”, The Guilford Press, **2016**.
13. J.A.T Machado;V. Kiryakova, F. Mainardi, *Communications in Nonlinear Science and Numerical Simulation*, **2011**, *16(3)*, 1140.
14. C.A. Monje, Y.Q.Chen, B.M. Vinagre, D. Xue, V. Feliu, “Fractional-order Systems and Controls”, Springer Verlag, **2010**, chapter 4.
15. E.H Dulf, F.V. Dulf, C.I. Pop, *Chemical Engineering Communication*, **2015**, *202(12)*,1600.
16. E.H. Dulf, C.I. Muresan, M.L. Unguresan, *Journal of Mathematical Chemistry*, **2014**, *52(1)*, 115.

STUDIA UBB CHEMIA, LXIV, 2,Tom I, 2019 (p. 23-34)
(RECOMMENDED CITATION)
DOI:10.24193/subbchem.2019.2.02

Dedicated to Professor Florin Dan Irimie on the Occasion of His 65th Anniversary

USE OF FACTORIAL DESIGN TO OPTIMIZE THE EFFICIENCY OF BACTERIAL TRANSFORMATION

GHEORGHITA MENGHIU[a,b], LAURIANA-EUNICE ZBÎRCEA[a,b] AND VASILE OSTAFE[a,b] *

ABSTRACT. A Plackett-Burman factorial design of experiments was created to optimize the protocols of preparation of *E. coli* DH5α competent cells and transformation of these cells by heat shock method using a *chi*A_pUC57 plasmid. The numerical parameters to be optimized were: the pH, the concentration of $CaCl_2$, the cell concentration of the culture used for the preparation of the competent cells, the temperature of defrosting of the competent cells, the concentration of plasmid DNA. It was also considered a qualitative factor that might influence the transformation efficiency, namely the use of ultrasound in the heat shock step of transformation protocol. A design of experiments based on 26 experimental values was created. Analyzing this experimental setup by both, Plackett-Burman factorial design and surface response design, it was highlighted that the pH, the concentration of calcium chloride and the concentration of plasmid DNA have a significant influence on the transformation efficiency. The optimal conditions for the preparation and transformation of *E. coli* DH5α competent cells with *chi*A_pUC57 plasmid where when the pH of a 40 mM $CaCl_2$ solution was 6, the competent stock cells were thawed slowly on ice and in the heat shock step the cells were subjected to ultrasounds treatment.

Keywords: *design of experiments; Minitab; Plackett-Burman factorial design; surface response design; competent cell; heat shock transformation.*

[a] *West University of Timisoara, Faculty of Chemistry, Biology, Geography, Department of Biology - Chemistry, 16 Pestalozzi, 300115 Timisoara, Romania.*

[b] *West University of Timisoara, Advanced Environmental Research Laboratory,4 Oituz, 300086, Timisoara, Romania.*

** Corresponding author: vasile.ostafe@e-uvt.ro*

INTRODUCTION

A common issue encountered in experimental research is when there are several protocols or methods published in scientific journals and all claim to provide the best results. Although the published protocols are reproducible, the results are not as good as it was expected. Another common situation is when in a long list of chemicals and materials used currently in a laboratory protocol one item has to be changed and after that, the expected results are not anymore as they were before. In all these cases, an optimization procedure is recommended to be performed in that lab, using the instruments, chemicals, materials, and so on, that are available at that time. This optimization procedure may be time and other resources consuming unless a design of experiments technique is applied.

The most used method for bacterial transformation is based on the induction of bacterial cell competency by calcium chloride treatment and exposure of bacteria to a heat shock in the stage of plasmid inclusion [1]. This "classical" method of bacterial transformation can provide various degree of transformation efficiency if some of the parameters of the methods are slightly changed. Efficiency of bacterial transformation is influenced by several factors such as concentration of $CaCl_2$ solution [2, 3], plasmids size and plasmid concentration [4, 5], heat shock [5-8], optical density of cell cultures (cells concentration) [9], bacterial strain [3], time of cells incubation in $CaCl_2$ solution [10], rotation speed of cells [11] and so on.

The "classical" practice for optimizing an experimental protocol is the one-factor-at-a-time method, i.e. to change in an experimental series only one experimental parameter. There are several options offered by the design of experiments approach, like factorial design, which imply the simultaneous optimization of all the factors at once. In this work, there is presented an example of the use of a Plackett-Burman factorial design and surface response design approaches to optimize the method of bacterial transformation by heat shock in the presence of calcium chloride.

RESULTS AND DISCUSSION

There are many reasons when an optimization of the experimental procedure has to be performed in a laboratory: introducing a new method or a new version, changing a few of the instruments, reagents or other sources of materials. Instead of using the one-factor-at-a-time strategy, one may save time, money and other resources by selecting a strategy to design the experiment, like the factorial design. In this strategy, there are selected some parameters that are considered to have an influence on the outcomes of the

experimental procedure and the values of these factors are changed in the same series of experiments. For example, for the transformation of *E. coli DH5α* strain with the plasmid pUC57 (that have a gene inserted, in this case, the gene of chitinase (*chiA*), following the general procedure based on calcium chloride and heat shock, one may consider the following factors: the concentration of calcium chloride solution used to make the competent cells, the pH of this solutions, the concentration of plasmid DNA (in fact the volume of plasmid DNA used in the transformation procedure, i.e. 0.5, 1 and 2 μL, respectively), the temperature used to thaw the competent cells preserved at -80°C and the use in the heat shock step of a ultrasonic bath.

In the bacterial transformation process, the calcium chloride plays an important role by the binding of plasmid DNA to lipopolysaccharides from the cell membrane. Positively charged calcium ions attract the negatively charged backbone phosphate groups from DNA molecule. The plasmid DNA can then enter into the cell under heat shock (+42°C for a short time). [12] It was shown that when the concentration of calcium chloride is over 200 mM and under 50 mM, the bacterial transformation efficiency is minimal [2, 13]. In many protocols for bacterial transformation, calcium chloride concentrations used is 75 mM [11, 14], 100 mM [1, 3, 15-17], 200 mM [10]. Most often, the pH value of the solution of calcium chloride is not specified. Normally, the pH of calcium chloride solutions varies between 8.0 and 9.0 as other components, like TRIS, are present. Only in a few transformation protocols, the pH of $CaCl_2$ solution is specified to be around 7.0 [14].

We also considered two factors whose influence has not been studied so far. The duration of the cell defrost step can be reduced if the cell kept at –80°C are thawed rapidly at 37°C instead to slowly thaw them on ice. This is why we have considered the thawing temperature as a factor in the design of the experiments. The other factor considered was the use of an ultrasonic bath (operating frequency 44KHz, ultrasonic power 14 W/L) in the step of the heat shock.

Considering all these numerical and qualitative factors a complex design of experiment (DOE) was realized. For the numerical factors, at least two values (considered as minim and maxim) were selected, and in some cases, intermediate values were added, to see if the variation of the experimental response (i.e. conversion efficiency) depends linearly on the considered factors. Based on these factors, a Placket-Burman type factorial design was created in Minitab software (Table I).

The most intuitive graphical representation of the influence of the considered factors on the transformation efficiency is the Pareto chart of standardized effects (Figure 1).

In the Pareto chart of standardized effects, the higher is the influence of a factor (independent variable) on the response (dependent) variable, the greater is its value. The chart displays the absolute value of the effects and draws a reference line on the chart. Any effect that extends past this reference line is statistically significant.

Table I. The Plackett-Burman DOE matrix, for four numerical factors and one qualitative factor, with some central values for the numerical factors

Run Order	$CaCl_2$ conc. (mM)	pH units	Plasmid Volume (µL)	Thaw Temperature (°C)	Ultrasonic Bath	Transformation Efficiency (Colony forming units/µg DNA)
1	80	6	2	0	No	76872
2	80	8	0.5	37	No	3276
3	40	8	2	0	Yes	4187
4	80	6	2	37	No	4875
5	80	8	0.5	37	Yes	3528
6	80	8	2	0	Yes	897
7	40	8	2	37	No	3975
8	40	6	2	37	Yes	93452
9	40	6	0.5	37	Yes	397865
10	80	6	0.5	0	Yes	34532
11	40	8	0.5	0	No	16785
12	40	6	0.5	0	No	421675
13	40	7	1	0	No	96167
14	60	7	1	0	No	69101
15	80	7	1	0	No	8383
16	40	6	1	0	No	186047
17	60	6	1	0	No	102814
18	80	6	1	0	No	15568
19	40	8	1	0	No	7964
20	60	8	1	0	No	2574
21	80	8	1	0	No	1616
22	50	7	0.5	0	No	29419
23	50	7	1	0	No	16155
24	50	7	2	0	No	8604
25	50	7	1	25	No	15767
26	50	7	1	37	No	15199

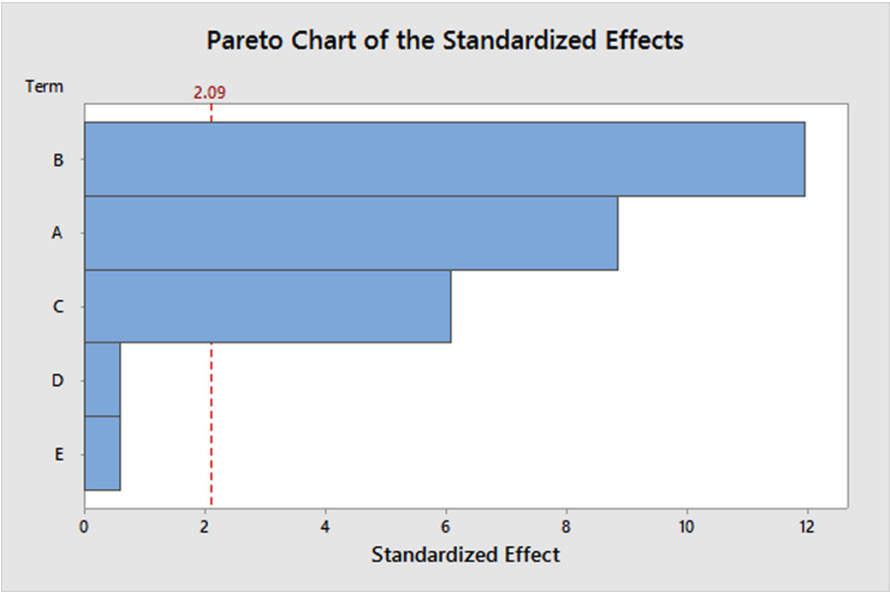

Figure 1. Pareto diagram highlighting the factors that significantly influence the transformation efficiency. Factors: A = $CaCl_2$ concentration (mM) used to make competent cells, B = pH value of $CaCl_2$ solutions, C = volume (µL) of plasmid DNA solution used in the transformation protocol, D = the temperature in the thawed step of the competent cells kept at –80°C, E = a qualitative factor, indicating the use (Yes or No) of a ultrasonic bath in the heat shock step. Response is efficiency of transformation at α = 0.05.

The analysis of the Pareto chart reveals that the most pronounced effect on the efficiency of transformation of *E. coli* cells is due to the pH value of the calcium chloride solution (factor B), followed by effect of the concentration of the $CaCl_2$ solution (factor A) and plasmid concentration in the mixture of the reaction (factor C). The other factors considered - use of ultrasounds in the membrane labilization stage and temperature of the defrosting step of competent cells have little influence on the transformation efficiency.

The same data were also analyzed using as model a response surface approach. The investigation of the interactions among the factors (Figure 2) shows that between the concentration of calcium chloride and the pH of this solution is a strong interaction as the variation curves intersect at different angles and the curves have different slopes. This means that their effect is cumulative, modifying the value of a parameter will influence the response function for an initial value of the other parameter. The x-axis represents the levels for each factor and the y-axis represents the response.

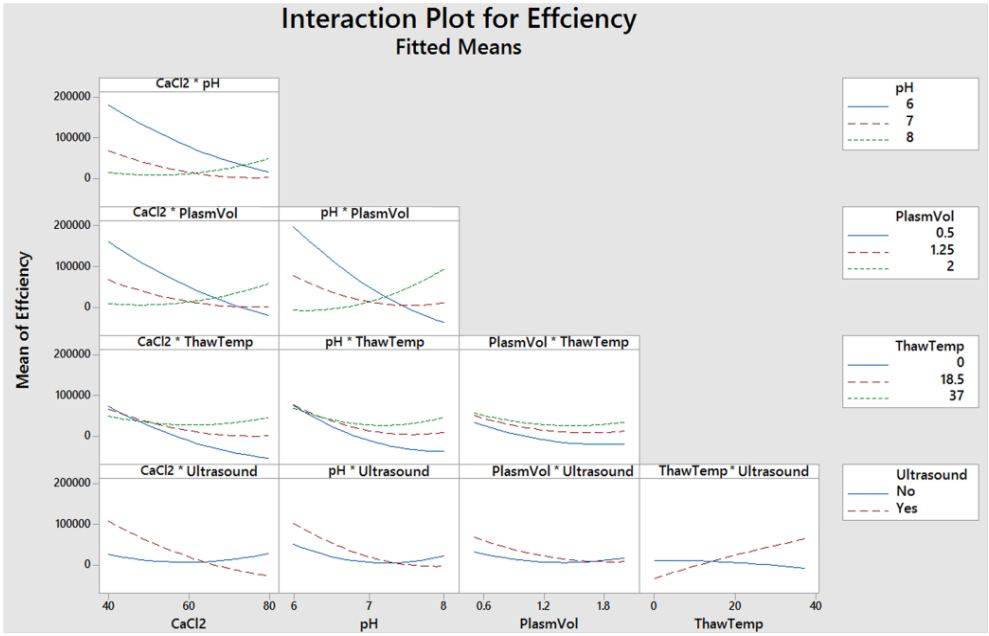

Figure 2. The interaction curves between the factors considered in the study to have an influence on transformation efficiency of E. coli DH5α cells.

Similarly, one may see that there is an interaction between the pH values of the calcium chloride solution and the plasmid DNA concentration (volume of solution used). On the other side, curves of the thawed temperature of the competent cells do not interact with the other factors, unless, maybe, with the use of ultrasounds in the heat shock stage, but even here the influence is relatively insignificant. In all the cases of the interaction of the thawing temperature with the other parameters, the curves are almost parallel. An analogous situation is in the case of interaction of ultrasound factor with the other parameters, no interaction is revealed as the curves have similar slopes. It is worth to mention that when the competent cells are defrosted slowly, on ice, the use of ultrasounds in the heat shock stage may be justified as it conducts to an increase of the transformation efficiency.

Considering the interaction plots and also other types of graphs that Minitab can provide, and that were not presented here, one may conclude that the optimal conditions for the transformation of *E. coli* DH5α cells with pUC57 plasmid (considering all the experimental details presented in Experimental chapter) are: 40 mM calcium chloride concentration (to prepare the competent cells) having a pH value of 6, the cells should be defrosted slowly on ice and the use of ultrasounds in the heat shock step is beneficial.

From that plate that was inoculated with the cell suspension from the vial that fulfills these optimal conditions seven colonies were randomly chosen and grown on liquid selective LB media. The plasmid of these cells was purified by miniprep protocol and subjected to EcoRI digestion. These seven samples were subjected to agarose gel electrophoresis.

Confirmation of the transformation procedure

In order to prove that the transformed cells obtained in those optimal conditions revealed by the analysis of the interaction curves are indeed transformed, *i.e.* contain the plasmid *chi*A_pUC57, seven colonies randomly chosen were verified by subjecting to agarose gel electrophoresis (Figure 3) the samples obtained after the purification of the plasmids and their digestion with the EcoRI restriction enzyme.

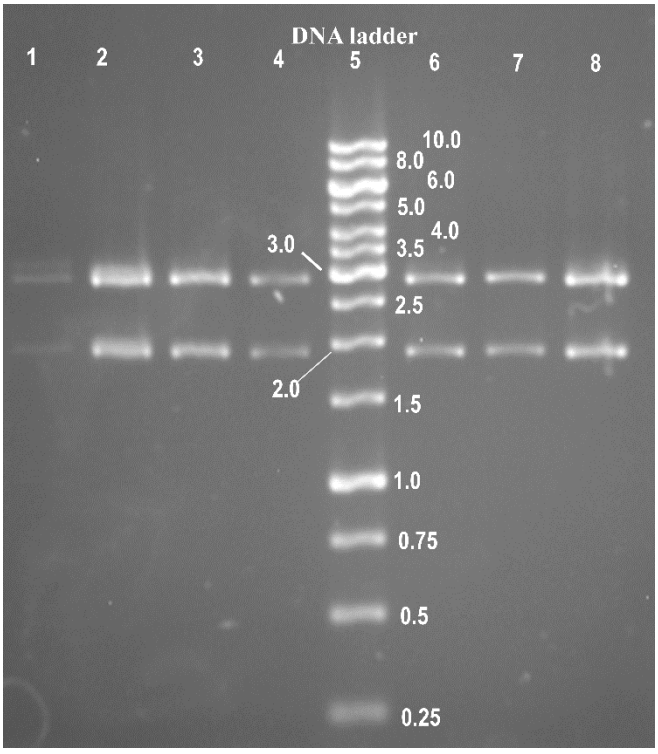

Figure 3. Agarose gel electrophoresis of *chi*A_pUC57 digestion with EcoRI. The lines 1 to 8 (except line 5 that is DNA ladder, in kbp) represent fragments of 2855 bp and respectively 1874 bp obtained after the digestions of the purified plasmids from 7 clones collected from that Petri dish where were cultured the cells transformed in the optimal conditions.

CONCLUSIONS

Using 26 experimental values, based on Plackett-Burman and response surface models of design of experiments, there were highlighted the factors that most influence the transformation efficiency of *E. coli* cells, i.e. the pH and concentration of calcium chloride solution used in the process of preparation of *E. coli* DH5α competent cells and the concentration of plasmid DNA used to transform the competent cells. Both models, factorial and response surface, have indicated that the temperature at which the competent cells are defrosted and the use of ultrasound in the heat shock step do not significantly influence the transformation efficiency.

EXPERIMENTAL SECTION

Reagents, solutions, and instruments

Reagents and Enzymes

The reagents were analytical or molecular biology grade: *Eco*RI (Thermo Fisher Scientific Inc #ER0271), yeast extract (Carl Roth, #2363.3), agar (Carl Roth, #X928.1), casein hydrolysate (Carl Roth, #A157.1), NaCl (Carl Roth, #9265.1), ampicillin sodium salt (Carl Roth, #K029.2), peptone (Carl Roth, # 2366.1),$MgCl_2$ (Carl Roth, # KK36.2), $MgSO_4$ (Carl Roth, # P027.2); glucose (Carl Roth, #HN06.4), EDTA (Ethylenediamine tetra acetic acid)(Carl Roth, #CN06.3), Tris-HCl (Carl Roth, #4855.5), sodium hydroxide (Carl Roth, #6771.3), sodium dodecyl sulfate (SDS) (Carl Roth, #2326.2), ethanol (Carl Roth, #P075.3), 2-propanol (Carl Roth, # AE73.2), DNA loading dye and gene ruler 1 kb DNA ladder 250 to 10.000 bp kit (Thermo Fisher Scientific Inc, #R0611), ethidium bromide (Sigma Aldrich, # 46065).

Culture media, solutions and buffers

LB liquid media: 0.5% (w/v) yeast extract, 0.5% (w/v) NaCl, 1% (w/v) casein hydrolysate; *LB solid media* additionally contain 2% (w/v) agar; *SOC media*: 0.5% (w/v) yeast extract, 0.05% (w/v) NaCl, 2% (w/v) peptone, 1 M $MgCl_2$, 1 M $MgSO_4$, 20% glucose; *$CaCl_2$ solution*: 40, 60, 80 mM $CaCl_2$, 15% glycerol, 10 mM Tris, pH 6.0, 7.0, 8.0 (adjusted with HCl solution); *Alkaline lysis solution I* (GTE): 50 mM glucose, 25 mM Tris-HCl, 10 mM EDTA, pH 8.0; 100μg/mL RNase; *Alkaline lysis solution II* (P2): 200 mM sodium hydroxide, 1% SDS; *Alkaline lysis solution III* (K-acetate solution): 4 M CH_3COOK; 6X DNA loading dye kit (10 mM Tris-HCl (pH 7.6), 0.03% bromophenol blue, 0.03% xylene cyanol FF, 60% glycerol, 60 mM EDTA) [18].

Strains and plasmids

The experiments were performed with *Escherichia coli* DH5α strain for transformation, kindly donated by Fraunhofer IME, Germany [19]. The exogenous recombinant DNA taken in experimental working was a *chi*A_pUC57 plasmid, which was purchased from Gene Script (#SD1176).

Instruments

Water bath (Julabo MA-4 Heating Circulator, # 9153504), Ultrasonic water bath operating at 44KHz, ultrasonic power 14 W/L (Barnstead/Lab-Line, Aqua Wave 9375, #034737037) Nanophotometer (IMPLEN P300, # DI-2110), UV Transilluminator (Vilber Lourmat, # Z363782), DNA Electrophoresis (SCIE-PLAS HU 6 Mini, # N562.1), Microcentrifuge (Hettich Mikro 22 R, # D-78532), Centrifuge (Hettich Universal 320R, # 1401).

E. coli DH5α competent cells preparation

E. coli DH5 growth conditions

An aliquot from the glycerol stock of *E. coli* DH5α cells was taken with a loop and zigzag scattered on an LB agar plate. The plate was incubated overnight at 37°C. One colony from the plate was inoculated in 3 mL LB and incubated overnight at 37°C and 250 rpm. From the overnight culture, 1 mL was inoculated in 100 mL LB media and incubated at 37°C and 250 rpm until OD 620 nm reached at 0.3-0.4 a.u. [20]

Preparation of competent cells with different concentration of $CaCl_2$ and pH

The 100 mL culture was divided into nine Falcon tubes and kept on ice for 10 minutes. The cells were centrifuged for 10 min at 3000 rpm. The collected cells were washed two times in 10 mL ice-cold $CaCl_2$ solution at different concentrations (40, 60, 80 mM) and pH (6.0, 7.0, 8.0) and centrifuged at 3000 rpm for 5 minutes. After the last centrifugation, the cells were kept on ice for 30 minutes and in each vial was added 1 mL of $CaCl_2$ solution having different concentrations and pH values. From each of these cell suspensions, portions of 100 µL were pipetted in sterile Eppendorf tubes and frozen at -80°C [21].

Calcium chloride transformation of E. coli DH5

From a stock solution containing *chi*A_pUC57 plasmid at 2.228 µg/µL, portions of 0.5, 1 or 2 µL were added at aliquots of 100 µL of competent cells prepared, as described above, at different pH values (6; 7 and 8) and different calcium chloride concentrations (40, 60 and 80 mM). The cell suspensions were kept on ice for 30 minutes. In the next step, the competent cells were exposed to heat shock at 42°C for 45 seconds and after that, the cells were incubated on ice for 2 minutes. To the transformation mixtures, portions of 1 mL of SOC media were added. After 1 h of incubation at 37°C, 100 µL of transformed cells were plated on LB selective media. The plates where incubated around 22 hours at 37°C. The colonies were counted after 10 hours of incubation until 22 hours of incubation [12].

Transformation efficiency calculation

The transformation efficiency represents the number of transformed cells (number of colonies) per amount (µg) of plasmid DNA spread on a plate [22].

Confirmation of the transformation procedure

Growth conditions

Several colonies of *E. coli* DH5α cells transformed with *chi*A_pUC57 plasmid were transferred in different Falcon tubes containing 3 mL selective LB liquid media with ampicillin (100 µg/mL final concentration). The tubes were incubated overnight at 37°C, 250 rpm. DNA plasmid isolation was performed from overnight culture [23].

Isolation of chiA-pUC57 plasmid (Miniprep)

The overnight liquid culture was transferred to a centrifuge tube and centrifuged for 1 min at 13,000 rpm. The *chi*A_pUC57 plasmids were isolated using the alkaline lysis method [25] by a series washes with GTE (150 µL), P2 (300 µL), K-acetate (450 µL), isopropanol and 75% ethanol solutions and centrifugation at 13,000 rpm. Plasmids harvested by centrifugation were dried by incubation at 45°C for 30 minutes. The dried plasmids were dissolved in sterile distilled water and their concentration was calculated based on their optical density at 260 nm. Different concentrations of plasmid were considered for plasmid restriction digestion [24].

Plasmid restriction digests

The plasmid DNA was cut with EcoRI restriction enzyme. All of the ingredients in a restriction digest mixture were kept on ice until the reaction was started. Restriction digest started by mixing of the plasmid solution (4 µL of DNA plasmid at a concentration between 1 and 3 µg/µL) with EcoRI restriction enzyme (0.5 µL, 10 U/µL) and with 10X EcoRI buffer (1 µL). The ingredients were mixed in the reaction tube and the tube was incubated at 37°C for 2 hours. To stop the digestion reaction, the mixture was incubated at 65°C for 20 minutes. Once the restriction digest was completed, the digested fragments were separated by size performing an agarose gel electrophoresis [22].

DNA agarose gel electrophoresis.

For agarose gel electrophoresis, 5 µL of restriction mixture mixed with 1 µL 6X DNA loading dye were used. To estimate the size of the separated DNA fragments, a gene ladder was used on a distinct line. The agarose gel concentration of 1% was prepared in 1xTAE buffer. The following parameters were established for the agarose gel electrophoresis: The electrophoretic separation was run at 80V, 200 mA, 300 W for 45 min. When the process was completed, the agarose gel was transferred in ethidium bromide solution (0.5 µg/mL) for 10 min and visualized under UV light.

The design of experiments

The designs of these experiments were realized using Minitab software (Minitab Inc., State College, PA, USA). The experimental designs try to explore the dependence of some measured value on a number of independent parameters (factors), each taking value, in such a way as to minimize the variance of the estimates of these dependencies using a limited number of experiments [26]. Plackett-Burman designs (Screening design) allow fractionation of the full factorial design, giving numbers of parameter combinations that are a multiple of four. Response Surface designs are useful for building a model for the response variable without needing to use a complete three-level factorial experiment. The response dependent variable was transformation efficiency. Four numerical parameters and one qualitative were considered. The numerical parameters were the pH and the concentration of the calcium chloride solution used in the preparation of competent cells, the temperature of defrosting the stock of the competent cells kept at -80°C, and the volume of plasmid DNA solution (in fact the concentration of plasmid DNA). The qualitative factor was the use of an ultrasonic bath in the stage of heats shock in the transformation procedure. The matrix of the design of experiments consisted of 26 experimental values and the results were analyzed by both Plackett-Burman factorial design and response surface design.

ACKNOWLEDGMENTS

G. Menghiu acknowledges that this work was supported by the strategic grant POSDRU/159/1.5/S/137750, Project “Doctoral and Postdoctoral programs support for increased competitiveness in Exact Sciences research”. The authors also acknowledge the GRANT PNIII-P3-284, ChitoWound - Biotechnological tools implementation for new wound healing applications of byproducts from the crustacean seafood processing industry.

REFERENCES

1. Chan, W.T., C.S. Verma, D.P. Lane, and S.K. Gan, *Bioscience Rep*, **2013**, *33*, e00086.
2. Lim, G., D. Lum, B. Ng, and C. Sam, *J Exp Microbiol Immunol*, **2015**, *19*, 1-6.
3. Liu, X., L. Liu, Y. Wang, X. Wang, Y. Ma, and Y. Li, *Pak J Pharm Sci*, **2014**, *27*, 679-684.
4. Chan, V., L.F. Dreolini, K.A. Flintoff, S.J. Lloyd, and A.A. Mattenley, *J Exp Microbiol Immunol*, **2002**, *2*, 207-223.
5. Campos-Guillen, J., F. Fernandez, X. Pastrana, and A.M. Loske, *Ultrasound Med Biol*, **2012**, *38*, 1078-1084.
6. Morimoto, R.I., *Cancer Cell*, **1991**, *3*, 295-301.
7. Divya Prakash, G., R.V. Anish, G. Jagadeesh, and D. Chakravortty, *Anal Biochem*, **2011**, *419*, 292-301.
8. Van der Rest, M.E., C. Lange, and D. Molenaar, *Appl Microbiol Biotechnol*, **1999**, *52*, 541-545.
9. Tang, X., Y. Nakata, H.-O. Li, M. Zhang, H. Gao, A. Fujita, O. Sakatsume, T. Ohta, and K. Yokoyama, *Nucleic Acids Res*, **1994**, *22*, 2857-2858.
10. Rudchenko, O.N., N.A. Likhacheva, N.V. Timakova, and B.N. Il'iashenko, *Genetika*, **1975**, *11*, 101-1019.
11. Li, X., X. Sui, Y. Zhang, Y. Sun, Y. Zhao, Y. Zhai, and Q.Y. Wang, *Afr J Biotechnol*, **2010**, *9*, 8549-8554.
12. Dagert, M. and S.D. Ehrlich, *Gene*, **1979**, *6*, 23-28.
13. Loske, A.M., J. Campos-Guillen, F. Fernandez, and E. Castano-Tostado, *Ultrasound Med Biol*, **2011**, *37*, 502-510.
14. Zhiming, T., H. Guangyuan, X.L. Kexiu, J.C. Mingjie, C. Junli, C. Ling, Y. Qing, P.L. Dongping, Y. Huan, S. Jiantao, and W. Xuqian, *Electron J Biotechnol*, **2005**, *8*, 114-120.
15. Maeda, S., A. Sawamura, and A. Matsuda, *FEMS Microbiol Lett*, **2004**, *236*, 61-64.
16. Xiaofeng, L., L. Lin, W. Yonggang, W. Xiaoli, M. Yanling, and L. Yunchun, *J Chem Pharm Res*, **2013**, *12*, 450-453.
17. Chan, J., C. Davis, and I. Jokic, *J Exp Microbiol Immunol*, **2006**, *9*, 92-96.

18. Liou, J.T., B.H. Shieh, S.W. Chen, and C. Li, *Prep Biochem Biotechnol*, **1999**, *29*, 49-54.
19. Blazic, M., G. Kovacevic, O. Prodanovic, R. Ostafe, M. Gavrovic-Jankulovic, R. Fischer, and R. Prodanovic, *Protein Expres Purif*, **2013**, *89*, 175-180.
20. Zhou, A., X. Jiang, and X. Xu, *BioTechniques*, **1997**, *23*, 592-594.
21. Aich, P., M. Patra, A.K. Chatterjee, S.S. Roy, and T. Basu, *Protein J*, **2012**, *31*, 366-373.
22. Green, R. and E.J. Rogers, Transformation of chemically competent *E. coli*, in *Methods in Enzymology*, J. Lorsch, Academic Press: New York, United States, **2013,** Volume 529, 28, p. 329-336.
23. Carstens, M., M.A. Vivier, and I.S. Pretorius, *Transgenic Res*, **2003**, *12*, 497-508.
24. Stephen, D., C. Jones, and J.P. Schofield, *Nucleic Acids Res*, **1990**, *18*, 7463-7464.
25. O'Sullivan D, J. and T.R. Klaenhammer, *Appl Environ Microbiol*, **1993**, *59*, 2730-2733.
26. Carro, N., I. Garcia, M. Ignacio, and A. Mouteira, *Anal Lett*, **2012**, *45*, 2161-2175.

STUDIA UBB CHEMIA, LXIV, 2,Tom I, 2019 (p. 35-47)
(RECOMMENDED CITATION)
DOI:10.24193/subbchem.2019.2.03

Dedicated to Professor Florin Dan Irimie on the Occasion of His 65th Anniversary

CHANGES OF OXIDATIVE STRESS CAUSED BY PHYSICAL ACTIVITY

ELVINA MIHALAŞ[a,c], LĂCRĂMIOARA IONELA ŞERBAN[b], DANIELA MATEI[c*], DAN CAŞCAVAL[a], ANCA IRINA GALACTION[c]

ABSTRACT. Free radicals and reactive oxygen species are produced in the human body as a part of metabolic processes. Reactive species in low levels are important for cellular activities. Excessive amounts of reactive species can be harmful because they can produce lipid peroxidation, proteins and ADN oxidation. For reduce these harmful effects the organism requires an antioxidant defence. Oxidative stress is involve in atherosclerosis, coronary heart disease, metabolic syndrome, type 2 diabetes mellitus. The aerobic and anaerobic exercises have different effects on the muscles, but both influence positively the biomarkers of oxidative stress. Studies prove that aerobics increase endogenous antioxidant status. Regular moderate exercises produce an increase in antioxidant activity, due to the changes in redox homeostasis. The aim of this review is to discuss the importance of a constant physical activity for increase the body's antioxidant system and to protect against oxidative stress.

Keywords: *Free radicals, reactive oxygen species, oxidative stress, metabolic syndrome, aerobic exercises, anaerobic exercises, antioxidant system*

[a] *"Gheorghe Asachi" Technical University of Iasi, Faculty of Chemical Engineering and Environmental Protection, 73 D. Mangeron str., RO-700050 Iasi, Romania*

[b] *"Grigore T. Popa" University of Medicine and Pharmacy Iasi, Romania, Faculty of Medicine, 16 Universitatii str., RO-700115, Iaşi, Romania*

[c] *"Grigore T. Popa" University of Medicine and Pharmacy Iasi, Romania, Faculty of Medical Bioengineering, 9-13 M. Kogălniceanu str., RO-700454 Iasi, Romania*

[*] *Corresponding author: daniela.matei@umfiasi.ro*

INTRODUCTION

Oxidative stress (OS) is characterized by an imbalance between the production or inactivation of reactive oxygen species, and imbalance between oxidants and antioxidants in favour of oxidants with a destructive and pathogenic effect [1]. Free radicals are substances that are derived from incomplete oxidized compounds having in their structure oxygen groups capable of initiating aggressive oxidation reactions on the cells.

Reactive species such as reactive oxygen and nitrogen species (ROS and RNS) in low levels are important for gene expression, cellular growth, infection defense, regulating cell signalling pathways, regulating blood flow, and controlling superior nerve activity. Excessive amounts of ROS and RNS can be harmful because they can produce lipid peroxidation, proteins and ADN oxidation [2]. The most active free radicals are ions: superoxide, peroxide, hydroxide, nitric acid [2].

Most endogenous free radicals occur at the level of: mitochondria (during generation the ATP-adenosine triphosphoric acid), peroxisomes, cytochrome P450, and phagocytes. At the mitochondria level, following the molecular oxygen reduction reaction by cell respiratory cytochromes, about 2% of the total amount of ROS occurs. Superoxide is produce by NADH dehydrogenase, cytochrome C oxidoreductase or succinate dehydrogenase [3].

Peroxisomes are primarily responsible for oxygen consumption in the cell and maintain low ROS production by the balance of enzyme concentration or activity, such as catalase. Thus, destruction of peroxisomes allows the release of hydrogen peroxide in the cell and oxidative stress. Phagocytes play an important role in the inflammatory response of the body. Increased oxygen consumption and activation of NADPH-oxidase accompany the main bactericidal, oxygen-dependent mechanism [2]. Cytochrome P450 is a group of enzymes present in almost every cell of the body that plays a role in the metabolism of steroids, fat soluble vitamins, fatty acids, prostaglandins and alkaloids. Some enzymes of this group detoxify drugs and some environmental pollutants [2].

Under abnormal environmental conditions such as excessive heat, ultraviolet radiation, pollutants, the levels of ROS increase dramatically, resulting in serious cellular damage. Nitrogen reactive species are a family of antimicrobial molecules derived from nitric oxide and superoxide, produced by the activity of NOS2 enzymes and NADPH-oxidase, resulting peroxynitrite [2]. NOS are present under three isoforms: NOS-1 (in the nervous tissue), NOS-2 inducible enzyme (expressed primarily in macrophages) and NOS-3 (in endothelial cells).

For fight against the ROS are antioxidant enzymes such as superoxide dismutase (SOD), glutathione peroxidase (GPx), catalase (CAT), and other antioxidant molecules: ascorbic acid (vitamin C), tocopherol (vitamin E),

vitamin A, flavonoid, and ubiquinone [4]. Glutathione protects cells against free oxygen radicals by formation of glutathione disulphide (GSSG) which is reduced to free glutathione (GSH) under the action of glutathione reductase. The GSH / GSSG ratio can be used as a marker of increased intracellular oxidative stress.

The measurement of free radicals is very difficult because they are in low concentrations and have a short life span. For determination are used different methods such as: the total oxidative status, total antioxidant capacity, oxidative stress index (ISO- ratio of oxidants to antioxidants), evaluating lipid peroxides by determining Malonyldialdehyde (MDA), measure carboxylates proteins by determining carbonyl groups, measure of serum thiols by determination of total sulfhydryl groups (SH), determination of serum glutathione [5].

Determination of loss of unsaturated fatty acids is useful for evaluating lipid peroxidation stimulated by certain pro oxidants. The system studied has to be decomposed (lipids extracted from cells or lipoproteins) and the lipids have to be hydrolysed to release fatty acids that can be measured by high performance liquid chromatography (HPLC) or converted to volatile products and separated by gas-liquid chromatography (GLC) [5].

Direct methods such as determination of iodine concentration, oxidation of ferric ions detected with xylene-orange (FOX), determination of glutathione peroxidase, cyclooxygenase (COX) determination, degradation of peroxides by hem, gas chromatography (GC) and mass spectrometry (MS) are used for the determination of lipid peroxides (aldehydes, isoprostanes, cholesterol peroxides / cholesterol esters) [6].

Other methods used are methods which determine antioxidant activity such as total peroxyl radical trapping antioxidant parameter (TRAP method), determines the ability of plasma antioxidants (vitamin E, urate, ascorbate but not albumin) to reduce Fe (III) to Fe^{2+} at low pH, incubating ABTS® [2, 2-azabis (3-ethylbenzothiazoline-6-sulfonate)] with a peroxidase-meth globin and H_2O_2 to produce $ABTS^{+}$ cation [6]. In all these methods a radical is generated and purified by antioxidants. When all the antioxidant systems have been depleted, the radical reacts with a target molecule to produce colour, fluorescence, chemiluminescence, loss or gain of electron spin resonance signal [5, 6]. Methods for determining the total antioxidant capacity in biological fluids are useful in measuring relative antioxidant activity and changes occurring under clinical conditions.

Nowadays the involvement of oxidative stress in pathogenic processes with socio-economic impact such as atherosclerosis, coronary heart disease, metabolic syndrome, type 2 diabetes mellitus, hypertension, is accepted and partially demonstrated [7].

The metabolic syndrome is present when three or more of the following signs are occurring: increased blood pressure, abdominal circumference, serum triglycerides, and low levels of HDL cholesterol and insulin resistance. This syndrome is often characterized by increased generation of reactive oxygen species and decreased activity of antioxidant systems such as low serum vitamin C levels, α-tocopherol and decreased superoxide dismutase activity. In addition, these patients have an increase in malondialdehyde and carbonyl groups levels [8].

Oxidized LDL-cholesterol, a biomarker of oxidative stress, activates circulating monocytes and increases their ability to infiltrate the vascular wall, in the initial stage of plaque formation. Lipid peroxidation can produce changes in permeability of membranes and also enzymatic membrane equipment can be damage. Cytotoxic products resulting from lipid peroxidation contributes to endothelium damage, platelet aggregation, release growth factors stimulating proliferation of smooth muscle cells, and inflammatory response. ROS production stimulates the release of proinflammatory cytokine such as, interleukin-1 (IL-1), IL-6, leptin, and adiponectin, by monocytes and macrophages through activation of the transcription factor nuclear kB (NFkB) [9]. Cytotoxic products may also increase the release of chemotactic factor for polymorphonuclear cells and alter phospholipase A2 activity with the subsequent formation of prostaglandin and endoperoxides [9]. Through these mechanisms oxidative stress may trigger an inflammatory response directly involved in the pathogenesis of atherosclerosis. High plasma levels of oxidized LDL-cholesterol were associated with an increased risk of myocardial infarction, independent of LDL-cholesterol and other cardiovascular risk factors, indicating that LDL-oxidized would be a predictive value biomarker [9].

Oxidative stress can damage proteins and may produce changes in their aggregation, in enzymes activity, ions transport, and also can induce proteolysis. ROS contribute to the activation of protein, tyrosine kinases, protein kinase C, and the MAP kinase cascade which play an important role in cellular responses such as activation, proliferation, and differentiation. Also high levels of ROS can inactivate mitochondrial enzymes, causes DNA damage and hence higher frequency of mutation [10]. ROS can activate NFkB which regulates the expression of genes which are associated with atherosclerosis and diabetes (Figure 1).

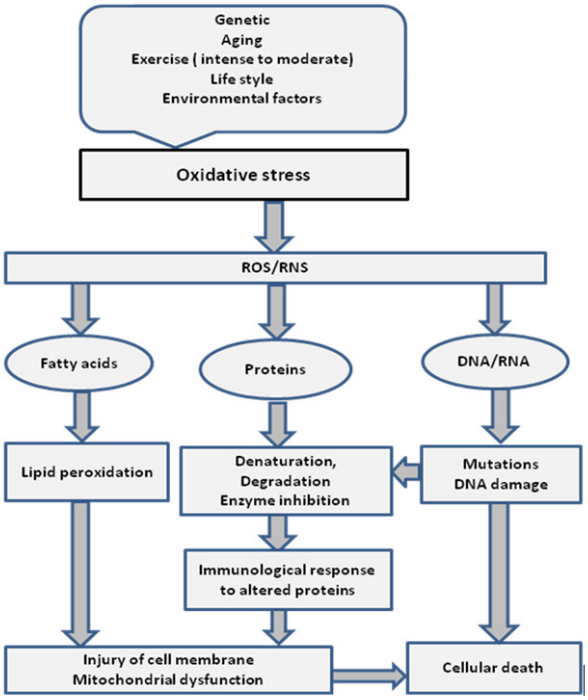

Figure 1. The pathophysiological mechanism by which oxidative stress contributes to the occurrence of various diseases

High levels of plasma glucose can increase oxidative stress through activation of protein kinase C (PKC), increased hexosamine pathway flux, increased advanced glycation end products (AGEs), and increased polyol pathway flux [11]. Increased AGEs will determine to bind to AGEs receptors (RAGEs) on endothelial cells and increase the production of growth factors and cytokines which will contribute to endothelial dysfunction [11]. High glucose level and free fatty acid stimulate reactive oxygen species production which can directly alter the production of NO or reduce the bioavailability of nitric oxide already produced reducing vasodilatation that contributes to hypertension. Nitric oxide is synthesized from L-arginine under the influence of the enzyme NO synthase. NO inhibits oxidation of LDL-cholesterol, proliferation and migration of smooth muscle cells, adhesion and platelet aggregation and produce vasodilatation. NO can reacting with superoxide anion forming peroxynitrite, which can oxidize NOS making it unstable. NOS inhibitors, such as the asymmetric dimethyl-arginine (ADMA), can contribute to hypertension through vasoconstriction [12]. Hyperglycaemia increases the production of endothelin-1, a powerful vasoconstrictor involved in endothelial dysfunction.

Muscles consume high quantities of oxygen and can generate ROS and RNS during muscle contraction. ROS and RNS have multiple effects on muscle excitability, contractility, and calcium homeostasis. On the other hand, they are involved in the muscular fatigue during strenuous physical activity.

Nowadays it is discussed that ROS and RNS plays a role in the development of sarcopenia leading to a reduction in muscle mass quantity and strength [13]. OS act on mitochondria leading to alteration of oxidative phosphorylation which contribute to decreased intracellular ATP. OS can reduce acetylcholine release at the synaptic cleft and impair neuromuscular transmission, also can lower the release of calcium from sarcoplasmic reticulum and impair excitation–contraction coupling and contractile properties of myofilaments [13, 14].

A good understanding of the link between oxidative stress and disease can be a real support in discovery of targeted treatment strategies for a better health.

Oxidative Stress and Physical Activity

There are several types of physical effort and each type has a different effect on oxidative stress. According to the type of contraction are isotonic (dynamic), isometric (static), and isokinetic effort. According to effort intensity are high, moderate, low intensity efforts. Based on the oxygen supply of the body there are aerobic, anaerobic, mixed effort.

Inactivity and high-intensity physical exercise increases OS, but moderate intensity exercise is linked to a reduction in OS levels [15]. Physical activities with intensities between 50% and 80% of VO_2max (the maximum rate of oxygen consumption) and with a frequency of three sessions per week are indicate for prevention OS [15].

Regular physical activity is recommended for prevention cardiovascular diseases. It is known that approximately 30 minutes per day of exercise training at moderate-intensity decrease the cardiovascular events [3]. For sedentary subjects the physical activity should be increased progressively in intensity and duration, to avoid excessive fatigue, muscle pain, or injuries.

The regular physical activity decreased blood pressure, cholesterol and body mass index which are important especially in prevention of the clinical sequel of atherosclerosis [16]. The 20 elderly women who were over 65 years of age had 30% body fat, underwent a 12-week healthy life exercise program. To evaluate the effects of the healthy life exercise program, measurements were performed before and after the healthy life exercise program in all the subjects. After the healthy life exercise program, MCP-1 and the arteriosclerosis adhesion molecules sE-selectin and sVCAM-1 were statistically significantly decreased. The 12-week healthy life exercise program

reduced the levels of arteriosclerosis adhesion molecules. Therefore, the results of the study suggest that a healthy life exercise program may be useful in preventing arteriosclerosis and improving quality of life in elderly obese women [16].

Further studies demonstrate the beneficial effects of the regular physical training on myocardial vasodilation improving O2 consumption and produces cardio protection. Two-hundred coronary artery disease (CAD) patients (LVEF > 40%, 90% men, mean age 58.4 ± 9.1 years) were randomized to a supervised 12-week cardiac rehabilitation program of three weekly sessions of either AIT – aerobic interval training (90–95% of peak heart rate (HR) or ACT – aerobic continuous training (70–75% of peak HR) on a bicycle. Primary outcome was peak VO2; secondary outcomes were peripheral endothelial function, cardiovascular risk factors, quality of life and safety [17]. Peak VO_2 (ml/kg/min) increased significantly in both groups (AIT 22.7 ± 17.6% versus ACT 20.3 ± 15.3%; $p < 0.001$). In addition, flow-mediated dilation (AIT +34.1% (range –69.8 to 646%) versus ACT +7.14% (range –66.7 to 503%); $p < 0.001$) quality of life and some other cardiovascular risk factors including resting diastolic blood pressure and HDL-C improved significantly after training. Improvements were equal for both training interventions. Contrary to earlier smaller trials, it was observed similar improvements in exercise capacity and peripheral endothelial function following AIT and ACT in a large population of CAD patients [17].

On the other hand, it is well known that aerobic exercise can increase endothelial function and can mediate the alternation between vasoconstriction and vasodilatation. In literature there is a lack of information as far as that goes the effects of exercise on vascular endothelial function particularly throughout the post exercise period and relation to oxidative stress, production of endothelin-1 (ET-1) and exercise intensity. Twenty one healthy, young men (24 ± 5 years) underwent assessment of brachial artery FMD (flow-mediated dilatation) using high-resolution ultrasound before and after 30-min of moderate-intensity cycle exercise (80% maximal heart rate). Subsequently, subjects performed five 30-min cycle exercise bouts at 80% maximal heart rate across a 2-week period, followed by repeat assessment of resting brachial FMD post-training [18]. Correcting for changes in diameter and shear, FMD did not change after the initial exercise bout ($P = 0.26$). However, a significant correlation was found between post-exercise changes in FMD and adaptation in resting FMD after training ($r = 0.634$, $P = 0.002$), where an acute decrease in post-exercise FMD resulted in a decrease in baseline FMD after 2 weeks and vice versa. We also found a positive correlation between shear rate during exercise and change in FMD% after acute exercise and after exercise training ($r = 0.529$ and 0.475, both $P < 0.05$) [18].

It has been observed a reduction of potent vasoconstrictor ET-1 after aerobic exercise training and an increase of endothelin-1 at the end of acute intense exercise [19]. Moreover, hard aerobic exercise is associated with transient reductions of flow-mediated dilation and moderate-intensity exercise confers good effects which improve production of reactive oxygen species at higher effort [20].

During exercise the production of ROS is increased by 50-100 times more than during rest [1]. It was found that MDA and lipid peroxidation were elevated after high-intensity physical activity [21]. But in other study the ROS have been shown to decrease among participants with regular exercise training or low-intensity physical activity [22]. Also higher physical activity was associated with a decreased SOD activity and an inverse relationship between physical activity and SOD levels was found [23].

Other activities such as intermittent team sport activities, short durations rock-climbing, cycling exercise were linked with high levels of markers of the oxidative stress [24, 25].

The type, intensity and duration of exercise being utilized are dependent in ROS production. The ROS were found elevated at greater exercise intensities 25 vs. 50 vs. 75 % of percentage of maximal exercise capacity VO2max after 30 min stationary cycling [26]. Also longer durations (120 vs. 60 vs. 30 min) of stationary cycling at 75 % VO_2 produced more oxidative stress marker [27].

During strenuous exercise IL-6 is produced in muscles proportionally with duration of the exercise and acts as a myokine [28]. Beside IL-6 other pro-inflammatory molecules such as tumour necrosis factor (TNF)-α, interleukin (IL)-1β and macrophage inflammatory protein (MIP)-1 are found [29].

The aerobic and anaerobic exercises have different effects and responses on the muscles, but both influence positively the biomarkers of oxidative stress. It has not been elucidated the method that would explain benefits from daily aerobic and anaerobic exercises. Some studies prove that aerobics increase endogenous antioxidant status and protect against oxidative stress [30]. In a study with 113 untrained subjects undergoing treadmill exercise the authors evaluated total antioxidant capacity, peroxide, oxidative stress index and DNA damage. They found that during exercise ROS increased, antioxidant capacity and vitamin C decreased [31]. In another study were investigated if half-marathon or marathon run in healthy hobby runners can alter DNA, antioxidant capacity in lymphocytes and plasma. Increases in the levels of oxidative DNA damage in lymphocytes were found. Also the number of granulocytes and monocytes able to generate oxidative burst were significantly increased after both races, but the lytic activity of NK cells was significantly increased at the end of the half-marathon [32].

The anaerobic intense physical activity can induce OS and results in damage of proteins, glucose, lipids and nucleic acids in muscle cells. In aerobic exercise the ROS and RNS are produce during mitochondrial respiration, but in anaerobic exercise oxidative stress may result from the ischemia/reperfusion cycle of muscle contraction and/or immune system responses following muscle damage [33].

Recent studies have proved that free radicals produced during exercise are keys to adaptive processes [34]. Regular moderate exercises produce an increase in antioxidant activity and resistance to oxidative stress, due to the changes in redox homeostasis [35]. On the other hand, it has been show that subjects expose to large amount of physical activity have impaired cardiovascular health.

Exercise causes oxidative stress only in overload training (in large volume or long-term period) and can lead to an impaired antioxidant defense. But if exercise is practiced in moderation, it can increase the antioxidant enzymes. During exercise MAP kinases are activate and in turn activated the NF-kappa B pathway and the expression of superoxide dismutase, an antioxidant enzymes [36]. For that exercise it can be considered an antioxidant [36].

Overload training may lead to inflammation which is also associated with increased oxidative stress. In overload training in untrained subjects exercise leads to increases of ROS, which cannot be eliminated by endogenous antioxidants. During regular exercise, in trained persons, ROS increased production contribute to body adaptation by improving antioxidant capacity, mitochondrial biogenesis, insulin sensitivity and aerobic capacity of skeletal muscle [37].

Oxidative stress can be detected immediately after exercise but the long-term effects are better observed when we measure antioxidant activity. For example, decreased levels of enzymatic antioxidants have been reported 19 days after an ironman triathlon competition [38].

During physical overtraining increased levels of urinary isoprostanes, serum levels of TBARS, protein carbonyls, CAT, GPX, and GSSG and decreased levels of GSH, the GSH/GSSG ratio, and total antioxidant capacity in blood serum were found [39].

Chronic exercises, during a long period of time, were found to increase the antioxidant capacity (Figure 2).

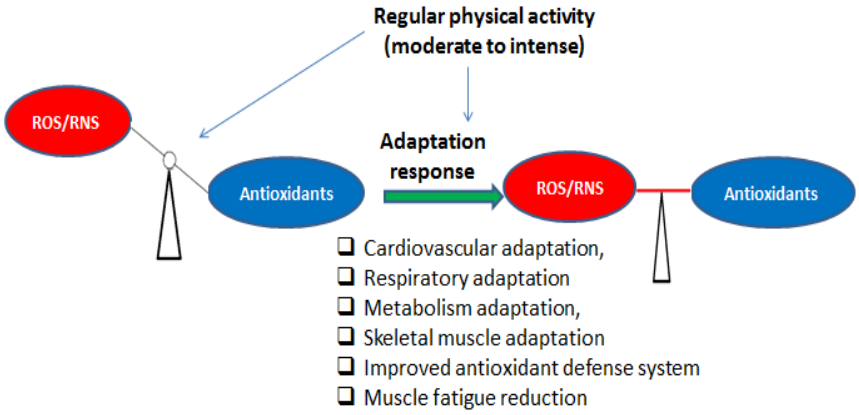

Figure 2. The physiologic process of body adaptation to regular physical activities

Beside physical training the increase of exogenous antioxidant defence, can be obtained by administrations a natural antioxidant nutrition or supplementation with non-nutritional antioxidants.

The exogenous antioxidants such as vitamin C, E, and carotenoids, have the positive effect and can protect against oxidative stress. Was demonstrating that a diet poor in antioxidants, during intensive short-term exercise can increases oxidative stress, and supplementation with multivitamins, before and during the marathon, was found to prevent the increase of lipid peroxidation [40].

To find out if a diet supplemented with vitamin C and E can be considered beneficial during exercise, Ristow et al. [41] investigated the effects on exercise induces insulin sensitivity as established by glucose infusion rates during a hyperinsulinemic euglycemic clamp before untrained and pre-trained healthy young men. Has been demonstrated that exercise increase parameters of insulin sensitivity only in default of antioxidants, both for trained and untrained individuals. At the same time, it was observed the increase expression of ROS-sensitive transcriptional regulators of insulin sensitivity and ROS defense capacity. The exercise induced molecular mediators of endogenous ROS defense (Mn-SOD, Cu, Zn-SOD, GPX) and this effect was again blocked by antioxidant supplementation. The authors concluded that exercise induced oxidative stress ameliorates insulin resistance and causes an adaptive response promoting endogenous antioxidant defense capacity and that supplementation with antioxidants may preclude these health-promoting effects of exercise in humans. The exercise causes an activation of mitogen-activated protein kinases which activates nuclear factor

in the muscles and consequently the expression of important enzymes associated with defense against ROS (SOD) and adaptation to exercise – endothelial nitric oxide synthase (eNOS) and inducible nitric oxide synthase (iNOS) [36, 42].

The advantages of exercise are widely known, but there is a lack of information about correct mode, type, length, frequency of exercise necessary to gain such benefits. The quality of low volume exercise performed with high intensity has become more and more noteworthy with facts showing comparable efficiency of high intensity interval workout and traditional training based on resistance in metabolic control of skeletal muscle and cardiovascular system activity [43, 44]. Besides promotions of physical exercise, having an antioxidant-rich diet with healthy eating habits can prevent oxidative stress. A dietary with caloric restriction and surplus of vitamins are known in relieve of oxidative stress.

CONCLUSIONS

Cardiovascular pathology is linked to oxidative stress, inflammation and endothelial dysfunction. Physical activity is recognized as an important component of healthy lifestyle but when are practiced strenuously it causes OS and cell damage. Moderate exercise is recommended to improve the physiological and functional capabilities because it increases the expression of antioxidant enzymes. Mechanistic analysis of free radicals may be useful for physiotherapists and health professionals, in particular when comparing different exercise doses, trying to outline appropriate recommendation for physical exercise in guidelines for health.

REFERENCES

1. S.K. Powers, M.J. Jackson, *Physiol Rev*, **2008**, *88*, 1243.
2. A.C. Montezano, R.M. Touyz, *Basic Clin Pharmacol Toxicol*., **2012**, *110*, 87.
3. R.L. Goncalves, C.L. Quinlan, I.V. Perevoshchikova, M. Hey-Mogensen, M.D. Brand, *J. Biol. Chem*., **2015**, *290*, 209.
4. A. Kunwar, K. Priyadarsini, *J Med Allied Sci*., **2011**, *1*, 53.

5. C.A. Rice-Evans, "Techniques in Free Radical Research", Elsevier, Amsterdam **1991**, chapter **1**.
6. B. Halliwell, J.M.C. Gutteridge, "Free radicals in biology and medicine", Oxford University Press Inc, New York**, 1999**, 351.
7. E. Braunwald, *N Engl J Med*, **2015**, *337*, 1360.
8. L. Moreto, E. P de Oliveira, R. M. Manda, R. C Burini, *Oxid Med Cell Longev*. **2014**, *505368*.
9. A. Isogawa, M. Yamakado, M. Yano, T. Shiba, *Diabets Res Clin Pract*. **2009**, *86*, 213.
10. A. Rahal, A. Kumar, V. Singh, B. Yadav, R. Tiwari, S. Chakraborty, K. Dhama, *Biomed Res Int,*. **2014**, *76*, 1264.
11. S. Golbidi, S. A. Ebadi, I. Laher, *Curr Diabetes Rev*, **2011**, *7*, 106.
12. J. Rysz, A. Gluba-Brzózka, B. Franczyk, Z. Jabłonowski, A. Ciałkowska-Rysz, *Int J Mol Sci*., **2017**, *18*, 1702.
13. M.J. Gomes, P.F. Martinez, L.U. Pagan, R.L. Damatto, M.D. Cezar, A.R.R. Lima, K. Okoshi, M. P. Okoshi*, Oncotarget*. **2017**, *8*, 20428.
14. C.W. Baumann, D. Kwak, H. M.Liu, L.V. Thompson, *J Appl Physiol Bethesda,* **2016**, *121*, 1047.
15. M.A. Bouzid, E. Filaire, A. McCall, C. Fabre, *Sports Med*., **2015**, *45*, 1245.
16. S. Lim, S. Min, H. Park, J. Park, *J Phys Ther Sci,* **2015**, *27*, 1529.
17. T. Luk, Y. Dai, C. Siu, K. Yiu, H. Chan, S. W.Lee et al., *Eur J Prev Cardiol*, **2012**, *19*, 830.
18. E.A. Dawson, D.J. Green, N.T. Cable, and D.H.J. Thijssen, *Journal of Applied Physiology*, **2013**, *115*, 1589.
19. S. Maeda, T. Miyauchi, T. Kakiyama et al., *Life Sciences*, **2001**, *69*, 1005.
20. B.D. Johnson, J. Padilla, and J.P. Wallace, *European Journal of Applied Physiology*, **2012**, *112*, 33.
21. J. Liu, H.C. Yeo, E. Övervik-Douki, T. Hagen, S.J. Doniger, D.W. Chu, et al., *J Appl Physiol*, **2000**, *89*, 21.
22. M.G. Nikolaidis, V. Paschalis, G. Giakas, I.G. Fatouros, Y. Koutedakis, et al., *Med Sci Sports Exerc*, **2007**, *39*, 1080.
23. S. Yang, M.K. Jensen, P. Mallick, E.B. Rimm, W.C. Willett, et al. *J Community Med Health Educ*, **2015**, *5*, 377.
24. A. Ascensão, A. Rebelo, E. Oliveira, F. Marques, L. Pereira, J. Magalhães, *Clinical Biochemistry*, **2008**, *41*, 841.
25. J. Magalhaes, R. Ferreira, F. Marques, E. Olivera, J. Soares, A. Ascensao, *Med Sci Sports Exerc*, **2007**, *39*, 955.
26. R.J. Bloomer, A.H. Goldfarb, L. Wideman, M.J. McKenzie, L.A. Consitt, *J Strength Cond Res*, **2005**, *19*, 276.
27. R.J. Bloomer, A.H. Goldfarb AH, *Can J Appl Physiol*., **2004**, *29*, 245.
28. P. Steinbacher, P. Eckl, *Biomolecules*., **2015**, *5*, 356.
29. H.G. Nielsen, O. Øktedalen, P.K. Opstad, T. Lyberg, *J Sports Med*., **2016**, 7186137.
30. Y.A. Shin, J.H. Lee, W. Song, T.W. Jun, *Mech Ageing Dev*., **2008**, *129*, 254.

31. R. Demirbag, R. Yilmaz, S. Guzel, H. Celik, A. Kocyigit, E. Ozcan, *Anadolu Kardiol Derg,* **2006**, *2*, 135.
32. K. Briviba, B. Watzl, K. Nickel, S. Kulling, K. Bos, S. Haertel, et al., *Redox Rep*, **2005**, *10*, 325.
33. S.R. McAnulty, L.S. McAnulty, D.C. Nieman, J.D. Morrow, A.C. Utter, C.L. Dumke, *Free Radic Res*., **2005**, *39*, 1219.
34. L.L. Ji, *Free Radic Biol Med*, **2008**, *44*, 142.
35. Z. Radak, H.Y. Chung, S. Goto, *Free Radic Biol Med*, **2008**, *44*, 153.
36. M.C. Gomez-Cabrera, E. Domenech, J., *Free Radic Biol Med.,* **2008**, *44*, 126.
37. M.A. Smith, M.B. Reid, *Respir. Physiol. Neurobiol,* **2006**, *151*, 229.
38. O. Neubauer, D. Konig, N. Kern, L. Nics, K. H. Wagner, *Med Sci Sports Exerc*, **2008**, *40*, 2119.
39. K. Margonis, I.G. Fatouros, A.Z. Jamurtas, M.G. Nikolaidis, I. Douroudos, A. Chatzinikolaou, A. Mitrakou, G. Mastorakos, I. Papassotiriou, K. Taxildaris et al., *Free Radic. Biol. Med.*, **2007**, *43*, 901.
40. G. Machefer, C. Groussard, S. Vincent, H. Zouhal, H. Faure, J. Cillard, Z. Radák, A. Gratas-Delamarche, *J Am Coll Nutr*., **2007**, *26*, 111.
41. M. Ristow, K. Zarse, A. Oberbach, N. Klöting, M. Birringer, M. Kiehntopf, M. Stumvoll, C.R. Kahn, M. Blüher, *Proc. Natl. Acad. Sci. USA*, **2009**, *106*, 8665.
42. M.C. Gomez-Cabrera, C. Borrás, F.V. Pallardó, J. Sastre, L.L. Ji, J. Viña, *J. Physiol.*, **2005**, *567*, 113.
43. M.J. Gibala, J.P. Little, M.J. Macdonald, and J. A. Hawley, *The Journal of Physiology*, **2012**, 590, 1077.
44. N. Steckhan, C.D. Hohmann, C. Kessler, G. Dobos, A. Michalsen, H. Cramer, *Nutrition,* **2016**, *32*, 338.

STUDIA UBB CHEMIA, LXIV, 2,Tom I, 2019 (p. 49-60)
(RECOMMENDED CITATION)
DOI:10.24193/subbchem.2019.2.04

Dedicated to Professor Florin Dan Irimie on the Occasion of His 65th Anniversary

ISOLATION, PURIFICATION AND CHARACTERIZATION OF ASCORBATE OXIDASE AND PEROXIDASE FROM *CUCURBITA PEPO MEDULLOSA*

ALINA-MARIANA CRAINIC[a], AUGUSTIN C. MOȚ[a], RADU SILAGHI-DUMITRESCU[a*]

ABSTRACT. Ascorbate oxidase is a well-known copper-containing enzyme however, its biological role and mechanism are still unclear. Reported here is a new protocol for purification of ascorbate oxidase from *Cucurbita pepo medullosa* (field pumpkin), with improved yields. The enzyme is biochemically characterized, including Michaelis-Menten parameters. Also, purification and characterization of the peroxidase from the same source is described, featuring an unusually high affinity for hydrogen peroxide(low-micromolar).

Keywords: *ascorbate oxidase, peroxidase, field pumpkin, purification*

INTRODUCTION

Ascorbate oxidase (AO) is a homodimeric enzyme (2×70 kDa) that catalyzes the oxidation of ascorbate to dehydroascorbate, using O_2 as electron acceptor. The active site features a mononuclear type I (T1) blue copper center—where the color is due to a cysteine-to-sulfur charge transfer, and the rest of the coordination sphere consists of two histidines and a methionine—where ascorbate is oxidized by one-electron donation to Cu(II); the resulting ascorbyl radical is thought to immediately dismutate to ascorbate and dehydroascorbate. In order to provide the oxidizing equivalents, AO also features a three-copper active site (type III, T3, colorless and magnetically coupled, ligated only by histidines and with an oxo or hydroxo bridge in the oxidized form), where the ascorbate-derived electrons are stored as Cu(I) and

[a] *Department of Chemistry, Babes-Bolyai University, 1 Mihail Kogalniceanu street, Cluj-Napoca 400084, Romania*
** Corresponding author: rsilaghi@chem.ubbcluj.ro*

then used for reducing molecular oxygen to water [3, 8] [9] [10]. These features, as well as the multimeric nature of the protein (with three equivalent units, each containing a trinuclear and a mononuclear site, are shared by several other multicopper oxidases (also known as blue copper oxidases), such as laccase and ceruloplasmin [1-3]. AO is selective towards ascorbate, due to interactions at the surface of the protein, where histidine and tryptophan residues bind to the lactone ring of the substrate [11]. Nevertheless, other compounds can also serve as reducing substrates, such as catechol or dichlorohydroquinone [2]. Beyond this, the mechanistic details of AO remain unclear, especially at the T3 center.

AO was the first of the blue copper oxidases whose structure was solved by x-ray diffraction, with several examples now available [11, 14]. Biochemical features of the enzyme, including thermostability, pH dependence and Michaelis-Menten parameters for the ascorbate oxiase cycle were also reported [3].

AO is found predominantly in higher plants, especially in *Cucurbitacee*, although it has also been observed in microorganisms such as *Acremmonium sp* (fungi) [8]. By comparison, laccase is found in microbes and in some plants, while ceruloplasmin is exclusively found in blood [3]. The biological role of AO is still unclear. In plants, ascorbate is part of the defense mechanism against oxidative stress and is located predominantly in leaves, extracellularly. AO is also found extracellularly, in the apoplast, where its expression is upregulated by light [12]. A role for AO in regulating the redox potential of the cells has been proposed, via tuning the ratio of ascorbate vs. dehydroascorbate. Also noted was an involvement of AO in cellular elongation [15].

AO also has practical applications, such as in biochemical sensors [15], or as a useful reagent for generating anaerobic conditions in biochemical laboratory experiments. It also provides an opportunity for exploring the mechanistic features of multicopper oxidases, with implications for enzymes with even larger numbers of practical applications – laccases and ceruloplasmin.

AO purification was first reported in 1940, from the yellow pumpkin *Cucurbita pepo condensa* [1]; a number of other purification protocols have since been reported [1, 2, 8].

Peroxidases (PX) are found in a wide range of organisms and have physiological/biological functions involving defense against oxidative stress, biochemical synthesis, and possibly others. By far the most common peroxidases are the ones featuring a heme at the active site (as seen, e.g., in horseradich peroxidase HRP or in chloroperoxidase CPO) – to the extent that the term “peroxidase” is generally assumed to refer to heme-containg peroxidases; other types of peroxidases feature active sites based on cysteine, or selenocysteine, or vanadium, or a binuclear di-iron center. The practical applications of peroxidases are vast and have been described elsewhere [16-19].

Reported here is an improved protocol of purification for AO from green pumpkin *Cucurbita pepo medullosa*, as well as a biochemical characterization of this enzyme. Purification of a peroxidase is also reported from these preparations, as a side-product.

RESULTS AND DISCUSSION

AO isolation and purification

Figure 1 shows the hydrophobic interaction chromatogram of the resuspended total protein pellet obtained by ammonium sulfate and acetone treatment. The brown color of the latter, alongside the general knowledge of peroxidases (PX) as relatively abundant enzymes in plant extracts, is the reason why the fractions were monitored not only at 610 nm (T1 AO – specific) but also at 405 nm (heme – specific). It may be seen that the presumed peroxidase impurity is present in most AO-containing fractions. Considering that the extinction coefficient of the heme is one order of magnitude larger than that of the charge-transfer band in the T1 copper of AO, the ratio of the 610 nm to 405 nm absorbances in the fractions suggests that AO is the dominant component over PX in most fractions, except at ~50 min where the two are sensibly equal.

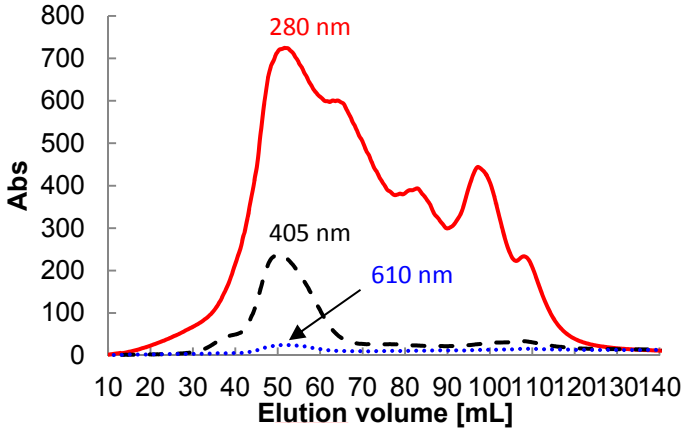

Figure 1. Hydrophobic interaction chromatogram of the resuspended total protein pellet by ammonium sulfate and acetone

Figure 2 shows that anion exchange chromatography does allow for separation of the peroxidase component to a good degree. However, the major AO fraction does still feature absorbance at 405 nm. The PX was mainly present in the flow-through fraction, which was collected for further analysis and purification in parallel with the AO-containing fraction. At this stage the two fractions contained predominantly the proteins of interest as shown by SDS-PAGE analysis.

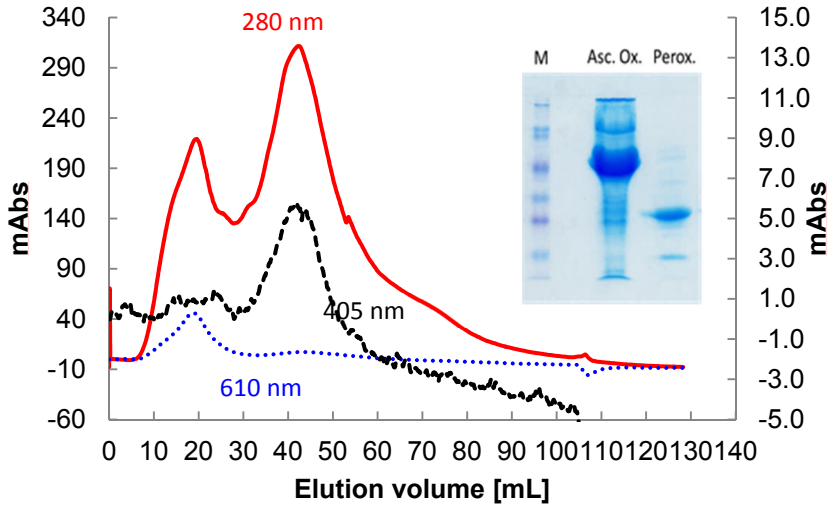

Figure 2. Anion-exchange chromatogram of the AO-containing fraction collected from hydrophobic interaction separation. Inset: SDS-PAGE analysis of the same fractions.

The AO and PX fractions were further subjected to preparative native gel electrophoresis, followed by a final purification step (hydrophobic interaction for AO, cation exchange for PX). As seen in Figure 3, this yields proteins of excellent purity.

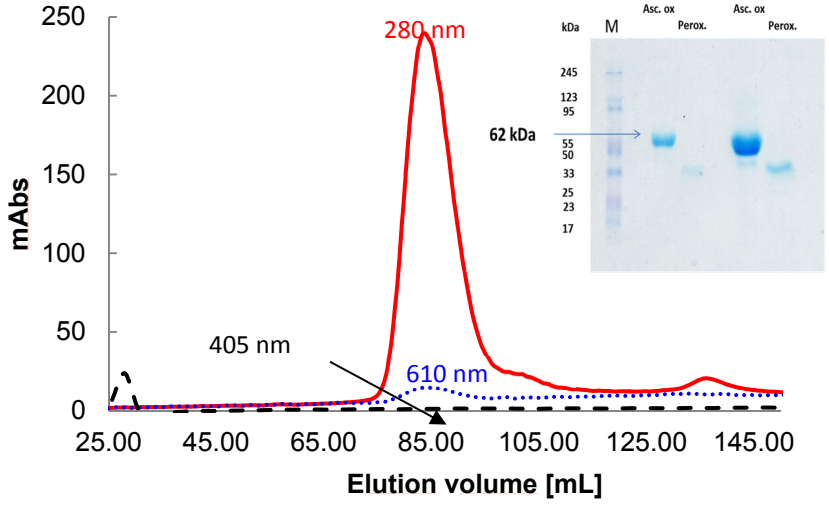

Figure 3. Hydrophobic exchange chromatogram for the final purification step of AO. Inset: SDS-PAGE of the purified AO and PX at two levels of concentration.

The UV-vis spectra of the purified AO and PX are shown in Figure 4. The ratio of absorbances due to the protein component (280 nm) vs. specific to the copper center (610 nm) can be used as purity indicator; a value of 25.3 was noted, in excellent agreement with an average of 25±0.5 seen in the literature.

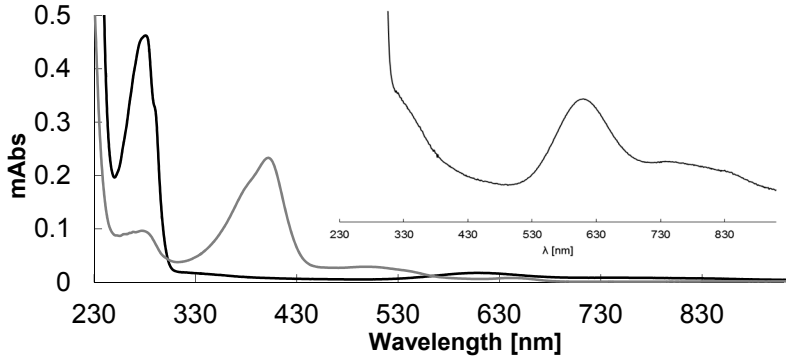

Figure 4. Molecular absorbtion UV-vis spectra of AO (black) and PX (grey). Inset – enlarged visible domain for AO spectrum.

Figure 5 summarizes the progress of the puritication steps; the maximum specific activity was 1056 μmoli/(min × mg), and the purification factor was 91.3. The latter value is ~ double to that of 43 reported for previous protocols [21], while the quantitative yields were 12.5% vs. 18%.

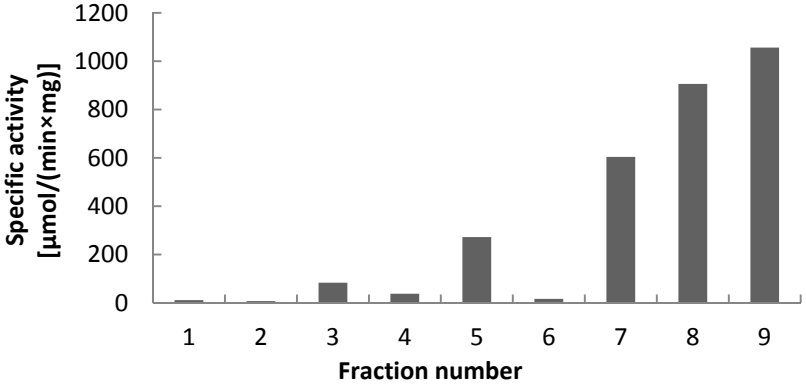

Figure 5. Specific activity of AO across the purification procedure. Fraction description:1-extract from blended peels (7200 mL), 2-After first ammonium sulfate procedure (1850 mL), 3-After precipitation with acetone (750 mL), 4-After first ammonium sulfate procedure (1240 mL), 5-AO fraction from first hydrophobic interaction purification, after dialysis (335 mL), 6-PX fraction after anion exchange (350 mL), 7-AO fraction after anion exchange (63 mL), 8-AO after native electrophoresis (42 mL), 9-AO at the end of purification protocol (26 mL). Fraction volumes are derived from a 50 kg starting point of raw material.

Figure 6 shows similarly obtained data as in Figure 5 – in this case for the purification of the PX. The purification factors at the final two fractions are 5.5 – 6.7, two orders of magnitude lower than for AO. This may be explained by the fact that in the initial extract several peroxidases are expected to be present – and several fractions were also present at various chromatographic steps, out of which only the dominant one, from the anion-exchange flow-through, was selected for purification. The highest specific activities were 162.5 and 118.9 μmol/(min×mg), respectively.

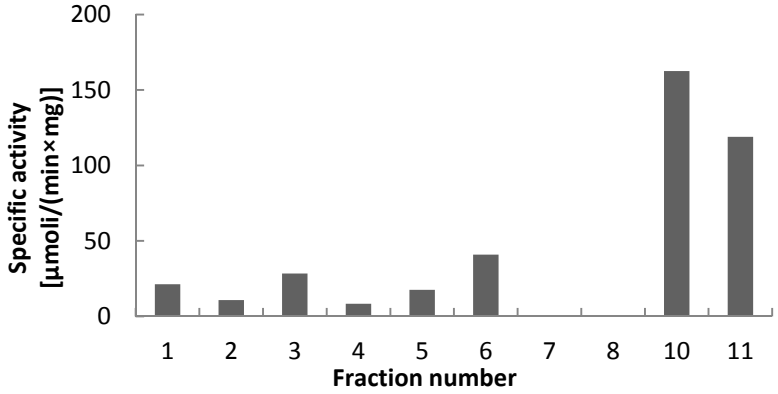

Figure 6. Specific activity of PX across the purification procedure.
Fraction description: as in Figure 6, with two additions –
10 PX after cation exchange, fraction 1 (11 mL),
11 PX after cation exchange, fraction 1 (6.5 mL).

Michaelis-Menten analysis

For ascorbate, a K_m value of 124 μM at V_{max} = 2.356 UA/min was measured vs. AO, using an Eadie Hofstee plot as shown in Figure 7.

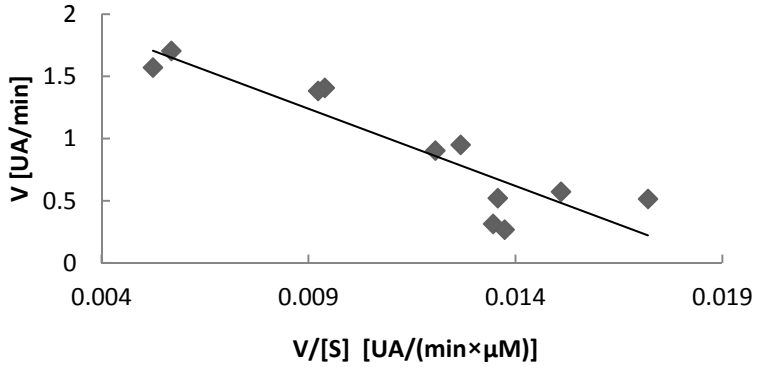

Figure 7. Eadie Hofstee plot for AO activity vs. ascorbate concentration.

In the case of PX, the Km values for the two substrates were 9 μM for H_2O_2 (at V_{max} = 0.017 UA/min) and 664 μM for ABTS (which was employed as model reducing substrate; V_{max} = 0.012 UA/min), according to Figure 8. Typical affinities of heme enzymes for peroxide are closer to the range of 1 mM. From this point of view, the PX purified here constitutes a particular exception, rivalling the non-heme peroxidases in this respect [16].

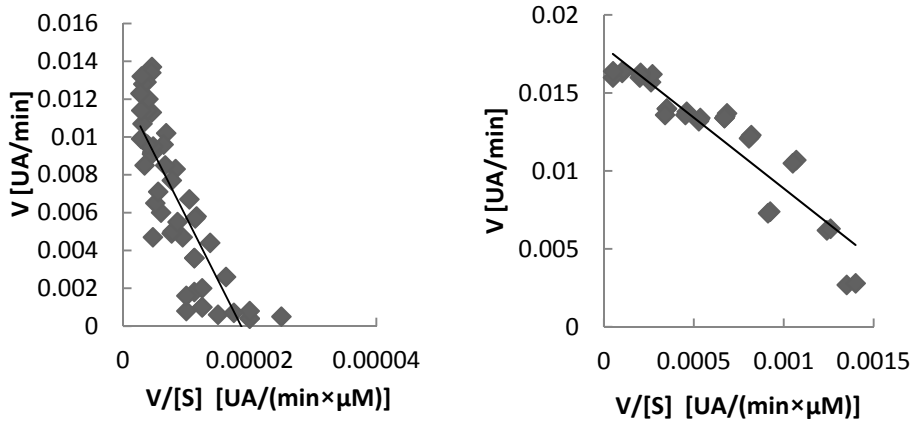

Figure 8. Eadie Hofstee plot for PX activity vs. ABTS (left) and peroxide (right) concentration.

Stability and dependence on reaction conditions

Figure 9 shows the pH dependence of the activity, for the two enzymes purified – AO and PX. The peroxidase shows a distinctly higher pH dependence, losing almost all of the activity above pH 5 – unlike AO for which the activity varies to a much smaller degree between pH 4 and 8.

Working at a pH close to optimum pH for both enzymes but not very close to the denaturation limit (pH 4, cf. Figure 9), the temperature dependence was examined cf. Figure 10. First, when measuring the activity immediately after exposing to the respective temperature, an optimal temperature of 50°C is noted for AO. Moreover, at 60°C essentially all AO activity is lost within 20 minutes – while at 50°C 80% of the activity is retained after 1 hr (data not shown), while for PX the maximum is at 70°C yet with only very small differences to 80°C.

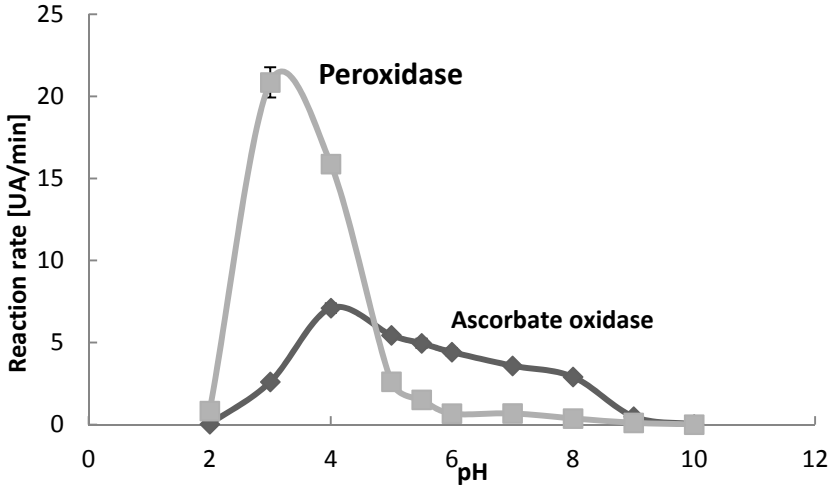

Figure 9. pH dependence of AO and PX activities.

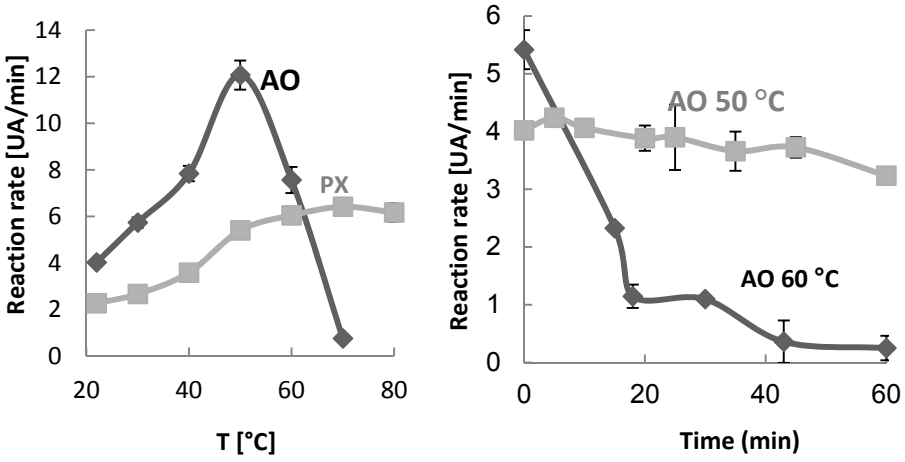

Figure 10. Influence of temperature on AO and PX.
Left: exposure immediately after mixing. Right: thermostability.

A number of potential inhibitors were also tested on AO and PX, cf. Figure 11, from a range typical of biotechnological applications. Expectedly, SDS is efficient, presumably via denaturation; notably, AO is completely inhibited even at 1 mM SDS, where PX retains most of its reactivity; this, alongside the temperature-dependent reactivity discussed above, reinforces PX as a more stable enzyme than AO. On the other hand, AO is much more

stable than PX towards ethanol, remarkably withstanding 20% without major loss of activity. Azide and fluoride (as typical exogenous metal ligands) inhibit peroxidase less than they do than AO.

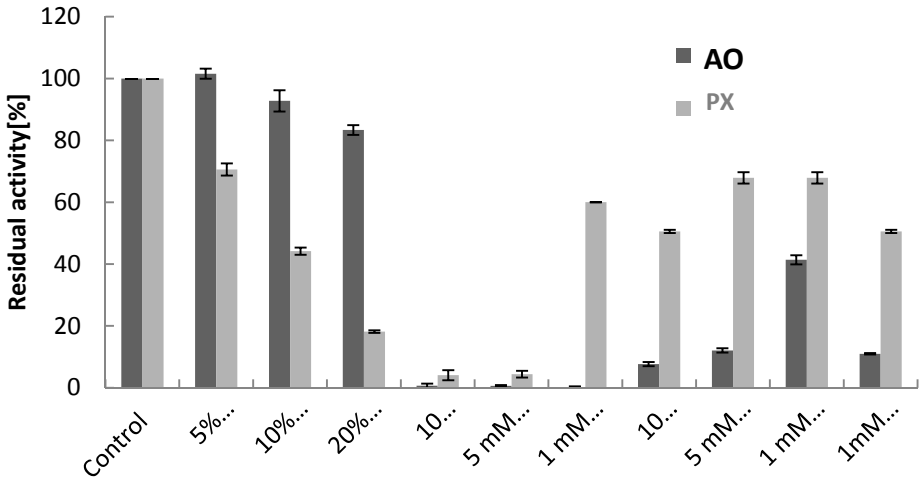

Figure 11. Influence of tested inhibitors on the activities of AO and PX.

MATERIALS AND METHODS

TrisHCl and ascorbic acid were purchased from Sigma-Aldrich (Germany), sodium tetraborate and sodium chloride from Reactivul Bucharest (Romania), ammonium sulfate from Lachner (Czech Republic), ABTS from TCI (Japan), sodium hydrogen phosphate from Chempur (Germany).

The AO purification protocol was based on previous reports [2], and involved 50 kg of green pumpkins per run. The majority of ascorbate oxidase is located in the peel of the fruit [6], which accounts for 20% of the total weight of the fruit. The pumpkins were washed, after which the peels were removed, with a thickness of 3 mm. The peels were subsequently homogenized in a blender (Kempo Juice Extractor, Green power) and squeezed thoroughly through a layer of cloth to maximize juice extraction. The pH of the ruslting suspension was adjusted to 6.7-6.9 by adding solid $Na_2B_4O_7$ (approximately one spatula per 500 mL). Solid ammonium sulfate (65%, (408 g/L) was subsequently added, and the mixture was stirred overnight in a cold room. The precipitate was collected decanted and centrifuged (5000 rpm, 10 min). At this stage the supernatant had negligible AO activity. The precipitate was then resuspended in ultrapure water (4℃, 1 L per 500 g solid), and then

centrifuged (10000 rpm, 10 min). At this stage, AO activity was by far confind to the supernatant. Solid sodium chloride was then dissploved in the supernatant to 13 g/L, after which acetone (pre-cooled to -30°C) was gradually added under stirring to a final volume ratio of 0.9 (acetone) : 1 (supernatant). The precipitate was decanted and centrifuged (5000 rpm, 10 min; AO activity was confined to the precipitate) and was then resuspended in ultrapure water (300 mL water to 150 mL precipitate). The resulting suspension was centrifuged (13000 rpm, 10 min), then the supernatant was subjected to chromatographic purification. The precipitate, when resuspended in water overnight with stirring, also contained residual AO activity but was not further employed.

The supernatant was adjusted to contain 1.6 M ammonium sulfate and was subjected to hydrophobic interaction chromatography on a *HiTrap Phenyl HP* 5 mL column (A: TRIS 10 mM, $(NH_4)_2SO_4$ 1.6 M; B: TRIS 10 mM) using a GE Healthcare FPLC chromatograph. Among others, this procedure allows for removal of nucleic acids, as they do not bind to the column. The fractions were monitored at 610 nm (absorbance specific to the AO T1 center), 280 nm (protein-specific) and 405 nm (heme-specific, chosen due to the brown color of the extract and on the assumption that this color was due to a heme protein). The major AO-containing fraction (40-70 mL elution volume cf. Figure 1) was collected and dialyzed against Tris 5 mM, pH=7.6, then centrifuged (15000 rpm, 15 min) loaded onto a *HiTrap QFF* 5 mL anion exchange column (A: TRIS 5 mM; B: TRIS 5 mM, NaCl 1 M), again monitored at 280, 405 and 610 nm. At this stage two separate fractions were collected: one with high 405 absorbtion (flow-though) and one with high 610 nm absorption (35-50 mL elution volume).

The resulting AO and PX fractions were then each concentrated using Amicon concentrators and were subjected to native electrophoresis using a preparative native PAGE gel. The migration time was kept to a minimum in order to avoid heating of the gel and autoreduction of AO as witnessed in loss of the blue color (nevertheless, this color is readily recovered upon elution from the gel).

The resulting AO fraction was adjusted to 1.6 M ammonium sulfate and subjected to one more round of hydrophobic interaction chromatography. The PX fraction obtained from native electrophoresis was dyalized and then loaded onto a cation-exchange column *HiTrap SP FF* 1 mL (A: Na_2HPO_4 5 mM; B: Na_2HPO_4 200 mM). A 12.5% yield was noted at the end of the procedure, for AO purification starting from the initial blended peels.

Protein contents were estimated using the Bradford method, with bovine serum albumin as standard and using a range of protein concentrations from 0 to 12 µg/mL. For ech measurement, 950 µL of Bradford reagent were mixed with up to 50 µL of sample as needed, after which ultrapure water was added to a total volume of 1 mL. Measurements were performed in duplicates.

AO activity was monitored at 240 nm in pH 5.5 acetate,10 mM, at room temperature. ABTS peroxidase reactivity was monitored at 420 nm [20].

Enzyme purity was verified by SDS-PAGE by standard protocols [16].

CONCLUSIONS

Reported here is a new protocol for purification of ascorbate oxidase from *Cucurbita pepo medullosa* (field pumpkin), with improved yields. The enzyme is biochemically characterized, including Michaelis-Menten parameters. Also, purification and characterization of the peroxidase from the same source is described, featuring an unusually high affinity for hydrogen peroxide (low-micromolar).

ACKNOWLEDGEMENTS

AMC thanks the World Federation of Scientists for a scholarship. Funding from the Romanian National Authority for Scientific Research and Innovation, CNCS – UEFISCDI, grants PCE 488/2012 (RSD) and PN-II RU-TE-2014-4-2555 (ACM), is gratefully acknowledged.

REFERENCES

1. W.H. Powers, S. Lewis, C.R. Dawson, *The Journal of General Physiology*, **1943**, *27*, 167.
2. A. Marchesini, P.M.H. Kroneck, European *Journal of Biochemistry*, **1979**, *101*, 65.
3. A. Messerschmidt, Multi-copper oxidases, World Scientific Publishing, Singapore, **1997**, C151-281.
4. T. Shirasawa, M. Izumizaki,Y. Suzuki, A. Ishihara, T. Shimizu, M. Tamaki, F. Huang, K. Koizumi, M. Iwase, H. Sakai, E. Tsuchida, K. Ueshima, H. Inoue, H. Koseki, T. Senda, T. Kuriyama, I. Homma*, Journal of Biological Chemistry*, **2003**, *278*, 5035.
5. M.H. Lee, C.R. Dawson, *Journal of Biological Chemistry*, **1973**, *248*, 6603.
6. K. Murata, N. Nakamura, H. Ohno, *Biochemical and Biophysical Research Communications*, **2008**, *367*, 457.
7. L. Santagostini, M. Gullotti, L. De Gioia, P. Fantucci, E. Franzini, A. Marchesini, E. Monzani, L. Casella, *Biochemical and Biophysical Research Communications*, **2004**, *36,* 881.
8. H. Dhillon, K. Sharma, R. Gehlot, S. Kumbhat, *Electrochemical Communications*, **2009**, *11*, 878.

9. A. Messerschmidt, R. Ladenstein, R. Huber, M. Bolognesi, L. Avigliano, R. Petruzzelli, A. Finazzio-Agro, *Journal of Molecular Biology*, **1992**, *224*, 179.
10. C. Pignocchi, J.M. Fletcher, J.E. Wilkinson, J.D. Barnes, C.H. Foyer, *Plant Physiology and Biochemistry*, **2003**, *132*, 1631.
11. Y. Kisu, Y. Harda, M. Goto, M. Esaka, *Plant and Cell Physiology*, **1997**, *38*, 631.
12. A. Messerschmidt, A. Rossi, R. Ladenstein, R. Huber, M. Bolognesi, G. Gatti, A. Marchesini, R. Petruzzelli, A. Finazzio-Agro, *Journal of Molecular Biology*, **1989**, *206*, 513.
13. K. Rekha, M.D. Gouda, M.S. Thakur, N.G. Karanth, *Biosensors and Bioelectronics*, **2000**, *15*, 499.
14. D. Hathazi, A.C. Mot, A. Vaida, F. Scurtu, I. Lupan, E. Fischer-Fodor, G. Damian, D.M. Kurtz Jr., R. Silaghi-Dumitrescu, *Biomacromolecules*, **2014**, *15*, 1920.
15. R. Silaghi-Dumitrescu, *Studia UBB Chemia*, **2010**, *55*, 207.
16. R. Silaghi-Dumitrescu, *European Journal of Inorganic Chemistry*, **2008**, 5404.
17. A.C. Mot, C. Bischin, B. Muresan, M. Parvu, G. Damian, L. Vlase, R. Silaghi-Dumitrescu, *Natural Product Research*, **2016**, 1315.
18. A. Mot, G. Damian, C. Coman, C. Miron, C. Sarbu, R. Silaghi-Dumitrescu, *Food Chemistry*, **2014**, *143*, 214.
19. S. Pundir, A. Gera, C.S. Pundir, *Artificial Cells, Blood Substitutes, and Biotechnology*, **2011**, *39*, 324.

STUDIA UBB CHEMIA, LXIV, 2,Tom I, 2019 (p. 61-68)
(RECOMMENDED CITATION)
DOI:10.24193/subbchem.2019.2.05

Dedicated to Professor Florin Dan Irimie on the Occasion of His 65th Anniversary

CLOSANTEL AS A POTENTIAL LIPOPOLYSACCHARIDE BIOSYNTHESIS INHIBITOR IN *SHIGELLA SONNEI* 4303

LAURA DEUTSCH-NAGY[a,b,*], PÉTER URBÁN[b], HUNOR SZEBENI[c], BEÁTA ALBERT[c], BÉLA KOCSIS[d], FERENC KILÁR[a,c,*]

ABSTRACT. *Shigella spp.* are Gram-negative intracellular pathogenic bacteria belonging to the family *Enterobacteriaceae*. The pathophysiological impact of the bacteria is highly related to the composition and structural variability of lipopolysaccharides. Serum sensitivity and biofilm forming ability are correlated with the length of these molecules, while bacteria with truncated lipopolysaccharides are more sensitive to hydrophobic antibiotics. Inhibitors of lipopolysaccharide biosynthesis have the potential to develop new antimicrobial agents or antibiotic adjuvants. Bacterial two-component systems enable bacteria to sense and to respond to the changes in different environmental conditions. This study focuses on the inhibition of the *rfaD* gene encoding the ADP-L-glycero-D-mannoheptose-6-epimerase, which is involved in the lipopolysaccharide biosynthesis. Although, there are some inhibitors presumed for bacterial two-component systems like Closantel, their impact on lipopolysaccharide biosynthesis has not been examined previously. The *Shigella sonnei* 4303 strain was involved in the experiments with known lipopolysaccharide structure. The effect of Closantel on lipopolysaccharide biosynthesis and the limitations of its use are presented.

Keywords: *lipopolysaccharide, lipooligosaccharide, lipopolysaccharide biosynthesis, Closantel, Shigella sonnei*

[a] *Institute of Bioanalysis, Medical School, University of Pécs, Szigeti út 12., 7624 Pécs, Hungary*
[b] *Szentágothai Research Center, University of Pécs, Ifjúság útja 20., 7624 Pécs, Hungary*
[c] *Department of Bioengineering, Sapientia Hungarian University of Transylvania and Emergency County Hospital, Piața Libertății nr. 1., 530104 Miercurea Ciuc, Romania*
[d] *Department of Medical Microbiology and Immunology, Medical School, University of Pécs, Szigeti út 12, 7624 Pécs, Hungary*
**Corresponding authors: nagylottii@gmail.com, ferenc.kilar@aok.pte.hu*

INTRODUCTION

Shigella sonnei is a Gram-negative, enteric pathogen, causing bacillary dysentery. Among all *Shigella* species, *S. sonnei* is the most prevalent one in developed countries [1]. With low infectious dose (as low as 10^2 colony-forming units) *Shigella* species are highly contagious. Well-described structure and genetic background of the surface lipopolysaccharide (LPS) of *S. sonnei* 4303 (*phase II* bacteria) made this strain of *S. sonnei* to be perfect for biosynthesis investigations. *S. sonnei* 4303 was first isolated and described in Pécs, Hungary [2], when the phenomenon of phase variations was examined. This *phase II* rough (*R*) strain was formed by spontaneous plasmid loss from the *S. sonnei phase I* smooth (*S*) strain due to the instable nature of the virulence plasmid [3]. Several *R*-type isogenic derivatives were further generated from this *S. sonnei* 4303 strain to perform structural and biosynthetic analysis on their truncated lipopolysaccharides [4-8]. A detailed description of the genes responsible for lipopolysaccharide biosynthesis in *S. sonnei* 4303 has also been carried out [9].

Lipopolysaccharides, as important cell wall constituents of *Gram-negative* bacteria, play significant role in the intraspecies and host-bacteria interactions. LPS molecules comprise three chemical regions: a hydrophobic lipid A moiety anchored to the outer membrane, a hydrophilic core oligosaccharide, and a hydrophilic O-oligosaccharide extending outwards from the cell surface. While the lipid A part is associated with endotoxicity, the polysaccharide chain is responsible for O-specific immunogenicity. The number and size-variation of the repeating units in the polysaccharide parts on the surface are associated with pathogenic characteristics and antibiotic sensitivity of the strains.

The core oligosaccharide domain (attached directly to lipid A) contains sugars like L-glycero-D-manno-heptose and 3-deoxy-D-manno-oct-2-ulosonic acid (Kdo) and minor non-carbohydrate components. However, defects in the biosynthesis of lipid A and Kdo are lethal for the bacteria, and the blockade in the heptose biosynthesis results in shorter lipopolysaccharides and an increasing antibiotic susceptibility [10, 11]. Heptoses are not present in mammalian cells, thus the inhibition of their biosynthetic pathway provides a selective target to design novel antimicrobial agents.

The biosynthesis of heptoses is quite universal across the different bacterial species. In *S. sonnei*, the pathway of heptose biosynthesis (Figure 1) starts with sedoheptulose-7-phosphate obtained from the reaction of fructose-6-phosphate with ribose-5-phosphate catalyzed by transketolase (TktA). Sedoheptulose-7-phosphate is then converted into D-glycero-D-manno-heptose-7-phosphate by ketose-aldose-isomerase (GmhA). This is followed by the anomeric phosphorylation with the bifunctional D-β-D-heptose 7-phosphate kinase (HldE). The next step is the dephosphorylation at the C-7 position by

the phosphatase GmhB. Then, the HldE enzyme catalyzes an adenylyl transfer to the phosphate group at the C-1 position, which leads to ADP-D-glycero-β-D-manno-heptose. Lastly, an epimerase (RfaD) performs the inversion of the D-stereochemistry of the C-6 hydroxyl group creating the ADP-L-glycero-β-D-manno-heptose, which will be incorporated into the lipopolysaccharides. While the ADP-D-glycero-β-D-manno-heptose might also be incorporated into lipopolysaccharides, disturbances in this biosynthesis pathway may lead to truncated lipopolysaccharides, and an increased sensitivity against heat and hydrophobic antibiotics [12,13].

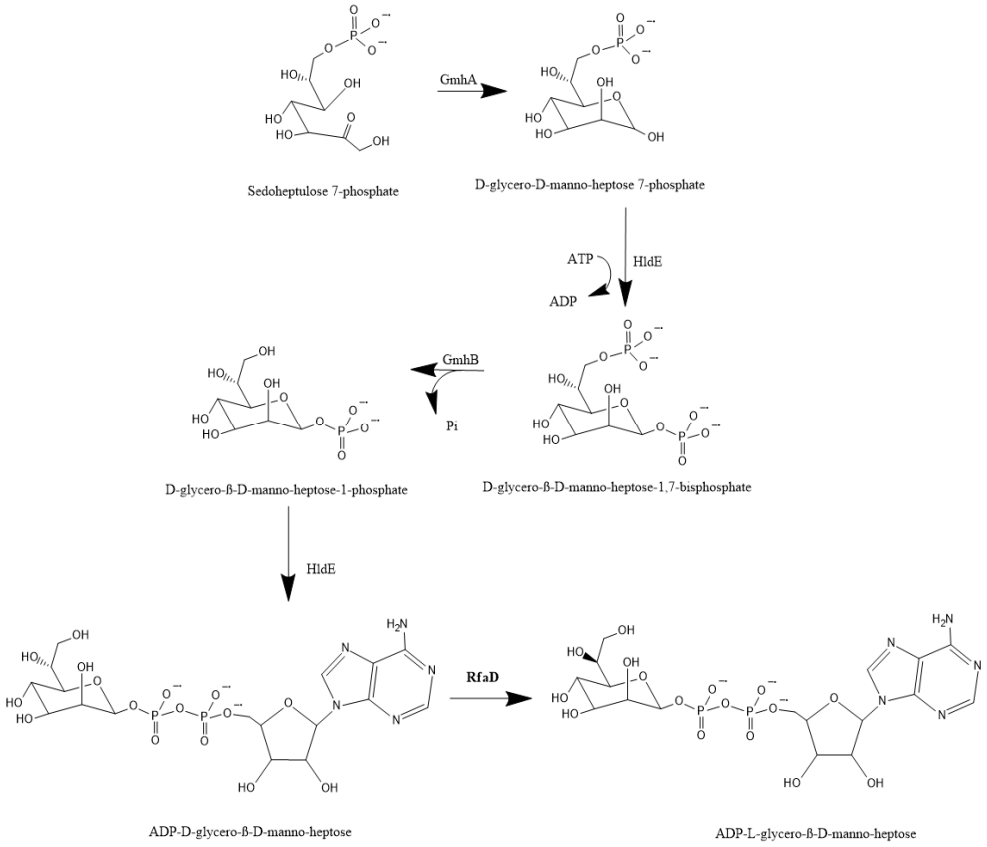

Figure 1. The biosynthesis pathway of ADP-L-glycero-β-D-manno-heptose

Since LPSs are secondary gene products, the inhibition of the LPS biosynthesis may occur in two ways, either within the gene expression or by alteration in the enzyme activity. The connection between the LPS biosynthesis and the bacterial two-component system opens possibilities to influence the structure and integrity of LPSs.

Closantel, a veterinary anthelmintic agent, is a potential histidine kinase (HK) inhibitor with described effect on the bacterial two-component regulatory system [14, 15]. However, the connection between Closantel and lipopolysaccharide biosynthesis has not yet been examined. Despite the low solubility of the molecule in aqueous solutions (16 mg/L), an active inhibitory effect was shown in *in vitro* experiments with different buffers. The potential influence of Closantel on *rfaD* expression was studied in this study.

RESULTS AND DISCUSSION

S. sonnei 4303 bacteria, having three L-glycero-β-D-manno-heptose molecular constituents in the core structure of their lipopolysaccharides, were grown in liquid medium in the absence and presence of Closantel. After culturing the cells, RNA was extracted, and cDNA was transcribed to perform qPCR analysis. In the experiments comparative analysis of the relative quantities can be performed by measuring the fluorescent signal. Figure 2 shows the fluorescent signal (ΔRn) of the amplification plotted against the cycles.

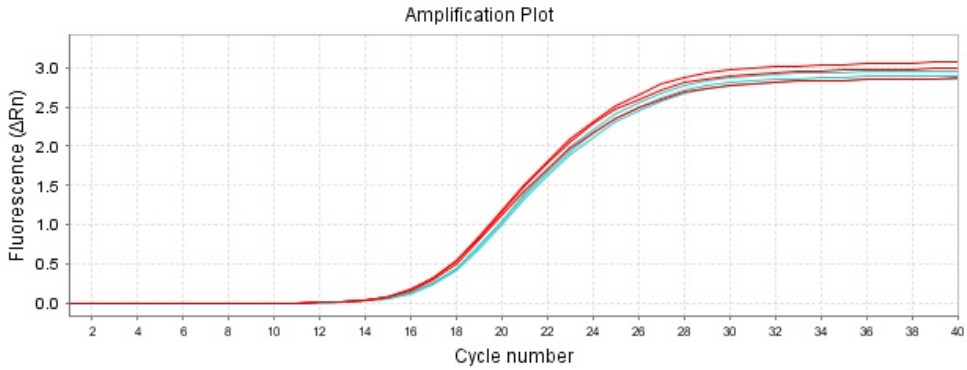

Figure 2. Amplification plot of the qPCR experiment showing the accumulation of the *rfaD* gene in Closantel treated (shown in blue) and in control (shown in red) *Shigella sonnei* 4303 samples. The ΔRn value is the difference between the normalized reporter value of the reaction and the baseline signal generated by the instrument.

A fluorescence level was selected at the exponential section of the amplification curves to mark a threshold. The cycle value where the curve reaches this fluorescence value is called threshold cycle (C_T). The relative amount was compared with the Livak or the $\Delta\Delta C_T$ method, which take into account the changes in the control sample. First, the normalization of the

$C_{T(rfaD)}$ level was made with the $C_{T(uidA)}$ level, and the ΔC_T was calculated for the treated and control samples, respectively. In the second step, the ΔC_T value of the control (untreated) sample was subtracted from the ΔC_T value of the treated sample. As last step, the expression ratio, or fold change difference was calculated. The amount of normalized *rfaD* in the sample is described with a relative quantity (RQ value) where $RQ=2^{-\Delta\Delta C_T}$. The results are presented in Table 1.

Although, the absolute difference in the relative quantity values between the treated and untreated samples attained less than RQ=1, there is a mild difference (corresponding to 9.1%) in the gene expression of *rfaD* in *S. sonnei* 4303 cells treated with Closantel (Figure 3). Although, the difference in the relative fold change is low, it confirms that there is a detectable downregulation effect of this substance.

Table 1. Relative gene expression data and statistical values of qPCR measurements of the *rfaD* and *uidA* genes in *Shigella sonnei* 4303 cultures treated with 16 mg/L Closantel and in untreated *S. sonnei* 4303 cells (control). Means were calculated from three replicates

Sample	Target	C_T Mean	ΔC_T Mean	ΔC_T SE	$\Delta\Delta C_T$	RQ
Control	*rfaD*	17.48	-0.24	0.04	0.00	1.00
Treated	*rfaD*	17.87	-0.11	0.03	0.14	0.91

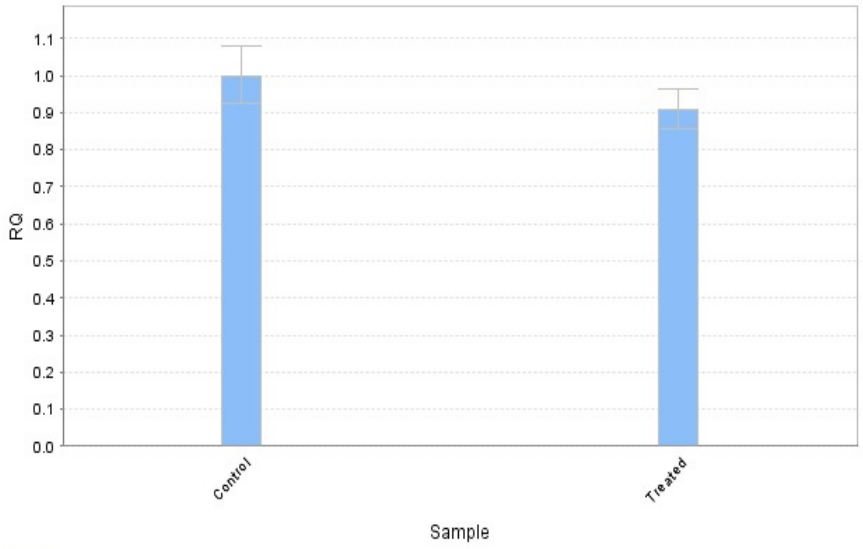

Figure 3. Box plot diagram of RQ values: relative gene expression of *rfaD* in treated and untreated *Shigella sonnei* 4303 cells

The connection between the LPS biosynthesis and the bacterial two-component system have been examined earlier. LpxC inhibitors, known as potential active substances on the posttranscriptional level [16], or inhibitory components of heptose biosynthesis with proven effect studied by *in vitro* experiments have been described [17]. In parallel with enzyme inhibition, the silencing of different LPS biosynthesis genes has also been investigated. The downregulation of the *rfaD* gene and its effect on LPS structure was described, *e.g.*, in *ntrC* null mutant *Vibrio vulnificus* bacterium [18] (the *ntrC* is a regulatory protein of the bacterial two-component regulatory system), where the absence of the transcriptional activator *ntrC* leads to the deficit of ADP-L-glycero-D-mannoheptose-6-epimerase as shown by comparative proteome analysis.

CONCLUSIONS

Relationship has been shown between the *rfaD* gene and the bacterial two-component regulatory system, which leads to possibilities of influencing the biosynthesis of lipopolysaccharides. The search for *rfaD* inhibitors is an important goal in successful medical treatment. Based on our results, it could be concluded that the presence of Closantel during cell growth has an effect on the expression of the *rfaD* gene in *S. sonnei* bacterium. The mild connection between the presence of Closantel and the inhibition of LPS biosynthesis is, nevertheless, probably due to the low solubility of Closantel in aqueous media (*i.e.*, in the broth medium for cell cultures). Therefore, further studies are needed applying different agents as possible two-component system inhibitors to investigate the endotoxin biosynthesis in *Gram-negative* bacteria.

EXPERIMENTAL SECTION

The experiments were performed with *Shigella sonnei* 4303 strain (*S. sonnei* 4303) with known lipopolysaccharide structure [7, 8] and genetic background [9]. Closantel in analytical standard grade (chemically N-(5-chloro-4-((4-chlorophenyl)(cyano)methyl)-2-methylphenyl)-2-hydroxy-3,5-diiodobenzamide) was purchased from Sigma-Aldrich (Saint Louis, Missouri, USA).

Bacteria were cultured for 36 hours in Luria-Bertani (LB) liquid medium in the presence of 16 mg/L of Closantel. This concentration value corresponds to the limit of solubility in LB liquid medium and this concentration is identical to the highest concentration used in pharmacokinetic examinations in animals [19].

Table 2 shows the TaqMan qPCR primers and probes (IDT, Coralville, Iowa, USA) developed by using the gene sequences obtained from the National Center for Biotechnology Information database (https://www.ncbi.nlm.nih.gov). To normalize the differences in relative expression, *uidA* (beta-glucuronidase) gene was used as endogenous control.

Cells were disrupted with liquid nitrogen, and a NucleoSpin RNA kit (Macherey-Nagel, Düren, Germany) was used to extract total RNA from 2mL of lysed cell culture. DNase, included in the kit, was used to degrade any remaining DNA. Complementary DNA (cDNA) library was created by the High-Capacity cDNA Reverse Transcription Kit (Thermo Fischer Scientific, Waltham, Massachusetts, USA).

Table 2. Primer and probe sequences used to amplify *uidA* and *rfaD* sequences

uidA	
Forward primer	GAATACGGCGTGGATACGTTAG (sense)
Reverse primer	GATCAAAGACGCGGTGATACA (antisense)
Probe	TGAAGAGTATCAGTGTGCATGGCTGG (sense)
rfaD	
Forward primer	CGTTGAACGTCTACGGTTACTC (sense)
Reverse primer	CCTTCACGCGGTCCATAAA (antisense)
Probe	TCGCAGATTGTTGGCTTCCGCTAT (sense)

After aqueous dilutions for equal concentrations, qPCR analyses were performed with the StepOne Plus (Thermo Fischer Scientific, Waltham, Massachusetts, USA), with the TaqMan Real-Time PCR Master Mix (Thermo Fischer Scientific, Waltham, Massachusetts, USA), and with TaqMan Mini Kit (IDT, Coralville, Iowa, USA) to analyze the expression level of *rfaD* in control (*S. sonnei* 4303 strains grown in the absence of Closantel) and treated cells. Measurements were performed in three biological replicates.

ACKNOWLEDGEMENTS

This work was supported by the grants NKFIH K-125275 and PTE-AOK-KA-2017-19.

REFERENCES

1. C.N. Thompson; P.T. Duy; S. Baker; *PLoS Negl Trop Dis*, **2015**, *9*, e0003708.
2. K. Rauss; I. Kétyi; A. Verténvi; S. Vörös; *Acta Microbiol Acad Sci Hung*, **1961**, *8*, 53-63.
3. R. Schuch; A.T. Maurelli; *Infect Immun*, **1997**, *65*, 3686-3692.
4. B. Kocsis; T. Kontrohr; V. László; H. Milch; *Acta Microbiol Acad Sci Hung*, **1980**, *27*, 217.
5. T. Kontrohr; B. Kocsis; *J Biol Chem* **1981**, *256*, 7715-7718.
6. B. Kocsis; T. Kontrohr; *J Biol Chem*, **1984**, *259*, 11858-11860.
7. A. Bui; A. Kilár; A. Dörnyei; V. Poór, K. Kovács; B. Kocsis; F. Kilár; *Croat Chem Acta*, **2011**, *84*, 393–398
8. A. Kilár; A. Dörnyei; A. Bui, Z. Szabó, B. Kocsis, F. Kilár; *J Mass Spectrom,* **2011**, *46*, 61-70.
9. L. Deutsch-Nagy; P. Urbán; Z. Tóth; Z. Bihari; B. Kocsis; C. Fekete; F. Kilár; *Gut Pathog*, **2018**, *10*, 47.
10. M.A. Valvano; P. Messner; P. Kosma; *Microbiology*, **2002**, *148*, 1979-1989.
11. P.L. Taylor; K.M. Blakely; G.P. de Leon; J.R. Walker; F. McArthur; E. Evdokimova; K. Zhang; M.A. Valvano; G.D. Wright; M.S. Junop; *J Biol Chem*, **2008**, *283*, 2835-2845.
12. Karow; S. Raina; C. Georgopoulos; O. Fayet; *Res. Microbiol*, **1991**, *142*, 289-294
13. H. Osada; T. Beppu; *Agric Biol Chem*, **2014**, *49:6*, 1813-1819
14. D.J. Hlasta; J.P. Demers; B.D. Foleno; S.A. Fraga-Spano; J. Guan; J.J. Hilliard; M.J. Macielag; K.A. Ohemeng; C.M. Sheppard; Z. Sui; G.C. Webb; M.A. Weidner-Wells; H. Werblood, J.F. Barrett; *Bioorg Med Chem Lett*., **1998**, *8*, 1923-1928.
15. K. Stephenson, Y. Yamaguchi, J.A. Hoch; *J Biol Chem*, **2000**, *275*, 38900-38904.
16. M.C. Pirrung; L.N. Tumey; C.R. Raetz; J.E. Jackman; K. Snehalatha; A.L. McClerren; C.A. Fierke; S.L. Gant;, K.M. Rusche; *J Med Chem* **2002**, *45*, 4359-4370.
17. G.P. De Leon; N.H. Elowe; K.P. Koteva; M.A. Valvano; G.D. Wright; *Chem Biol*, **2006**, 13, 437-441.
18. H.S. Kim; M.A. Lee; S.J. Chun; S.J. Park; K.H. Lee; *Mol Microbiol*, **2007**, *63*, 559-574.
19. M. Michiels, W. Meuldermans, J. Heykants; *Drug Metab Rev*, **1987**, *18*, 235-251.

STUDIA UBB CHEMIA, LXIV, 2,Tom I, 2019 (p. 69-78)
(RECOMMENDED CITATION)
DOI:10.24193/subbchem.2019.2.06

Dedicated to Professor Florin Dan Irimie on the Occasion of His 65th Anniversary

COVALENT IMMOBILIZATION OF LIPASES ON ACTIVATED HOLLOW SILICA MICROSPHERES

BIANKA SZOKOL[a], GÁBOR HORNYÁNSZKY,[a,b] JÓZSEF NAGY[a*]

ABSTRACT. This study explores the covalent immobilization of three lipases (Lipase AK, from *Pseudomonas fluorescens*; Lipase PS, from *Burkholderia cepacia*; and CrL, from *Candida rugosa*) on four supports prepared by functionalization of mesoporous hollow silica microspheres (M540) with various bisepoxides as activating agents for production of novel lipase biocatalysts for enantiomer selective biotransformations of secondary alcohols. The influence of length, rigidity and hydrophobicity of the bisepoxide activating agents was investigated on the efficiency of immobilization and catalytic properties of the resulted twelve lipase biocatalysts. The hollow silica particles modified with the most beneficial bisepoxide activating agents resulted in novel biocatalysts capable for kinetic resolution of racemic 1-phenylethanol *rac*-**1a** and racemic octan-2-ol *rac*-**1b** with high activity and enantioselectivity.

Keywords: *hollow silica microspheres, bisepoxide surface activation, kinetic resolution, lipase, immobilization*

INTRODUCTION

Due to the effective catalytic properties and green nature of the enzymes and to the progress of modern biotechnology, enzyme industry witnessed a rapid development over the past decades [1,2]. Nowadays, several different enzymes are available for the practicing organic chemists and biotechnologists for a variety of different transformations [1–5].

[a] *Department of Organic Chemistry and Technology, Budapest University of Technology and Economics, H-1111 Budapest, Műegyetem rkp 3., Hungary*
[b] *SynBiocat, Ltd, H-1172 Budapest, Szilasliget u 3, Hungary*
**Corresponding author: jnagy@mail.bme.hu*

Hydrolytic enzymes such as lipases (triacylglycerol ester hydrolases, EC 3.1.1.3) play a prominent role among biocatalysts [6,7]. Lipases are one of the most used enzymes, applied as biocatalysts in synthetic organic chemistry using their hydrolytic capacity in aqueous medium as well as their catalytic ability of the reverse reaction in organic solvents for various synthetic biotransformations related to carboxylic acid esters [8–11].

However, similarly to other enzymes, native lipases can easily become deactivated and their recovery for reuse may be challenging [12–14]. Therefore, especially in large-scale processes, lipases are often applied in immobilized form in order to facilitate their recovery and enhance their activity, thermal and operational stability [15–17]. Enzyme immobilization can be carried out by different methods and the selection of the mode of immobilization is crucial for preventing the loss of enzyme activity by stabilizing of its active conformation [18–20].

Surface-modified silica gel-based particles proved to be efficient supports in our practice for the immobilization of several lipases [21–26]. Therefore, in this study our aim was to extend the immobilization of further lipases [Lipase AK from *Pseudomonas fluorescens* (Lipase AK), Lipase PS from *Burkholderia cepacia* (Lipase PS) and Lipase from *Candida rugosa* (CrL)] using bisepoxide-activated mesoporous hollow silica microspheres to produce efficient biocatalysts for kinetic resolution of secondary alcohols.

RESULTS AND DISCUSSION

Previous results of our research group indicated that surface grafted mesoporous silica gel supports can be advantageously applied for easy-to-perform adsorptive immobilization of lipases leading to biocatalysts with useful activity and selectivity in kinetic resolution of racemic secondary alcohols [27]. Lipases could be immobilized by sol-gel-entrapment or entrapment within nanostructured polymeric systems including electrospun fibers [17,19]. Such entrapment-based immobilization methods proved to be advantageous in enzyme stabilization, as the enzyme molecules could be rigidified by the embedding matrix. Covalent immobilization carried out on bisepoxide-activated aminoalkyl polymer resins resulted in hydrophobic stabilization of the immobilized enzyme by a relatively rigid and hydrophobic spacer arm and contributed significantly to preservation of enzyme activity and selectivity at higher temperatures [28]. To expand the usefulness of enzyme immobilization methods for industrial applications [29], the application of mechanically resistant, bisepoxide-activated mesoporous hollow silica microspheres for enzyme immobilization were extended to immobilization of three further lipases [Lipase AK from *Pseudomonas fluorescens* (Lipase AK), Lipase PS from *Burkholderia cepacia* (Lipase PS) and Lipase from *Candida rugosa* (CrL)].

Immobilization of the lipases on bisepoxide-activated M540 supports

After activation of the MatSpheres 540 hollow silica microspheres (M540) with four different bisepoxides, the three selected lipases (Lipase AK, Lipase PS and CrL) were immobilized covalently resulting in twelve different lipase biocatalysts (Figure 1).

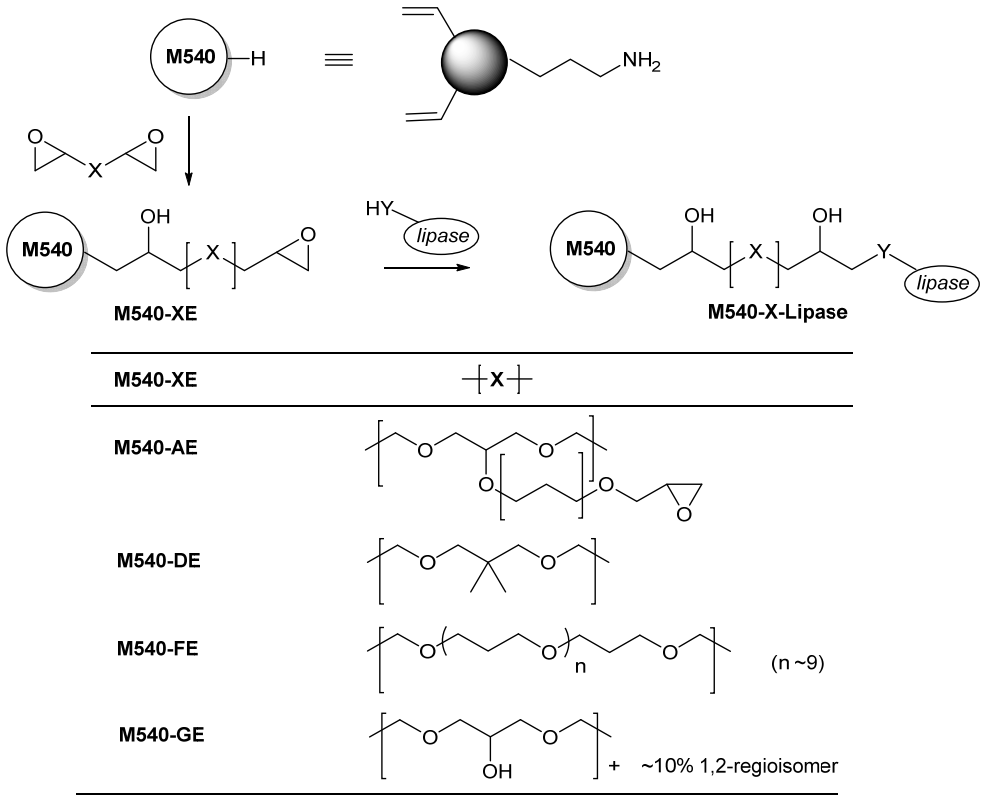

Figure 1. Lipase immobilization on bisepoxide-activated M540 supports.

The morphology of the immobilized lipase biocatalysts was investigated by scanning electron microscopy (SEM). As an example, the results with Lipase AK immobilized on M540-GE supports are shown in Figure 2. SEM investigations revealed than in all cases the biocatalyst particles were uniform in appearance with good monodispersity.

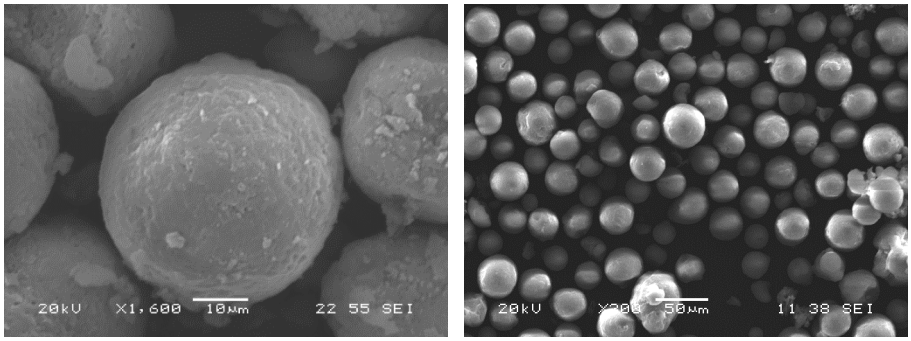

Figure 2. SEM images of Amano Lipase AK immobilized on activated M540-GE.

Kinetic resolution with lipases on bisepoxide-activated M540 supports

The catalytic performance of the immobilized biocatalysts was evaluated by investigation of their activity and selectivity in enantiomer selective acylation of racemic secondary alcohols 1-phenylethanol *rac*-**1a** and octan-2-ol *rac*-**1b** with vinyl acetate (Figure 3).

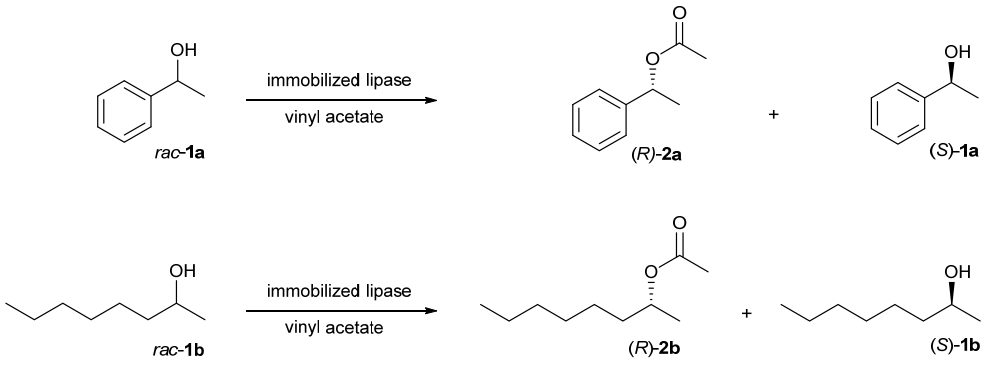

Figure 3. Kinetic resolution of alcohols *rac*-1a,b catalyzed by the novel biocatalysts.

Conversion (*c*) and enantiomeric excess (*ee*) in the kinetic resolution of *rac*-**1a,b** were determined by gas chromatography (GC) on enantioselective stationary phase. To characterize the degree of enantiomer selectivity, the enantiomeric ratio (*E*) for the reactions was calculated from the values of *c* and $ee_{(R)\text{-}\mathbf{2a,b}}$. The activity of the biocatalysts in the acylation of *rac*-**1** could be described by their specific biocatalyst activity (U_B) which was calculated using the equation $U_B = n_P/(t \times m_B)$ (where n_P [mol] is the amount of the product (*R*)-**2a,b**, *t* [min] is the reaction time and m_B [g] is the mass of the applied biocatalyst).

Studies with the lipases immobilized on the activated M540 supports

We have found that lipase AK, lipase PS and CrL can be efficiently immobilized by covalent linkages onto the surface of bisepoxide-activated M540 supports. The nature of the M540 activation significantly influenced not just the productivity but also the selectivity of each immobilized lipase biocatalyst in kinetic resolution of racemic 1-phenylethanol *rac*-**1a** (Table 1) and octan-2-ol *rac*-**1b** (Table 2).

Table 1. Kinetic resolution of *rac*-1a with vinyl acetate catalyzed by native and immobilized forms of lipases (30 °C, after 1 h)

Enzyme	Cross linker	*c* %	$ee_{(R)\text{-}2a}$ %	*E* -	U_B U/g
PS[a]	free	17.0	98.7	58	8.7
	AE	21.9	98.9	>200	30.2
	DE	19.5	99.1	>200	26.9
	FE	33.3	99.9	»200	45.6
	GE	23.5	99.5	»200	32.4
AK	free	20.4	46.6	3.1	28.1
	AE	33.3	99.0	>200	45.9
	DE	42.5	98.7	>200	58.6
	FE	39.2	99.2	>200	54.1
	GE	32.6	99.2	>200	44.9
CrL[b]	free	7.4	83.1	11.7	10.2
	AE	9.7	93.8	34.8	13.3
	DE	38.1	89.7	32.9	52.4
	FE	38.2	98.7	>200	52.6
	GE	4.3	63.5	4.7	5.9

[a] Results agreed with our previous study on immobilization of lipase PS [30]; [b] Results after 24 h

Table 2. Kinetic resolution of *rac*-1b with vinyl acetate catalyzed by native and immobilized forms of several Lipases at 30 °C after 2 h

Enzyme	Cross linker	*c* %	$ee_{(R)\text{-}2a}$ %	*E* -	U_B U/g
PS	free	14.1	96.4	>100	19.4
	AE	41.6	72.1	10.3	43.7
	DE	40.3	69.4	14.4	42.5
	FE	45.7	96.5	>100	57.8
	GE	22.6	78.5	10.4	23.7
AK	free	6.7	57.8	3.9	6.4
	AE	9.0	62.2	4.6	9.4
	DE	14.0	62.6	4.8	14.7
	FE	17.7	69.2	6.3	18.6
	GE	49.8	99.4	»200	52.3
CrL[a]	free	9.2	99.1	»200	12.6
	AE	12.4	85.6	14.7	17.1
	DE	32.8	89.4	28.2	45.2
	FE	40.6	99.7	»200	55.9
	GE	47.9	98.8	»200	66.1

[a] Results after 24 h

In case of Lipase PS, all the bisepoxide-activated M540-based biocatalysts had better selectivity and specific activity in kinetic resolution of *rac*-1a and *rac*-1b than the native Lipase PS powder form. The best biocatalytic properties could be achieved by the Lipase PS immobilized on the M540-FE support, resulting in 33.3% conversion from *rac*-1a with excellent enantiomer selectivity (*E* »200, $ee_{(R)\text{-}2a}$= 99.9%) in 1 h reaction time and 45.7% conversion from *rac*-1b with good enantiomer selectivity (*E* >100, $ee_{(R)\text{-}2b}$= 96.5%) in 2 h reaction time.

In case of Lipase AK, all the bisepoxide-activated M540-based biocatalysts surpassed the biocatalytic ability of the native Lipase AK powder form in kinetic resolution of *rac*-1a,b as well. The most active form was the M540-DE-AK biocatalyst resulting in 42.5% conversion from *rac*-1a in 1 h reaction time, whereas the highest enantiomer selectivity (*E* >200, $ee_{(R)\text{-}2a}$= 99.2%) was observed with the M540-FE-AK biocatalyst with this substrate. The effect of the linker properties was quite remarkable in case of kinetic resolutions from *rac*-1b with the immobilized AK biocatalysts. Although the AK biocatalysts on AE-, DE-, or FE-activated M540 supports were all more active and selective than the native AK form, the M540-GE-AK biocatalyst was far the most active and selective biocatalyst resulting in almost complete KR (*c*= 49.8%) with remarkable enantiomer selectivity (*E* »200, $ee_{(R)\text{-}2b}$= 99.2%). This example indicated that the quite moderate enantiomer selectivity of a lipase in KR of *rac*-1b (*E*= 4-6) can be significantly enhanced (up to *E* »200) just by fine-tuning the properties of activation agent of the support for immobilization.

The immobilized biocatalysts containing lipase from *Candida rugosa* (CrL) followed the general trend, as all bisepoxide-activated M540-based biocatalysts turned out to be more active in KRs from *rac*-**1a,b** than the native lipase powder. Although the immobilized CrL biocatalysts were less active than the PS or AK preparations (the suitable conversions required 24 h), there were suitable bisepoxide activating agents for KRs of both substrates *rac*-**1a,b**. The most active and most selective form was the M540-FE-CrL biocatalyst resulting in 38.2% conversion from *rac*-**1a** with remarkable high enantiomer selectivity (*E* >200, $ee_{(R)\text{-}\mathbf{2a}}$= 98.7%) in 24 h reaction time. The importance of fine-tuning the properties of the immobilization support is also indicated by the fact that in case of the KRs from the aliphatic alcohol *rac*-**1b** the M540-GE-CrL form proved to be the most suitable biocatalyst resulting in almost perfect KR with 47.9% conversion and high enantiomer selectivity (*E* »200, $ee_{(R)\text{-}\mathbf{2a}}$= 98.8%) in 24 h reaction time.

Besides the improvement in activity and enantiomer selectivity, the immobilization of lipases enabled also convenient handling, easier product separation, and offered reusability in batch reactions, thus making the lipase-catalyzed synthetic processes more cost-effective. In order to evaluate the

reusability and operational stability of the three types of lipase biocatalysts, the M540-FE forms of each lipase were investigated in five repeated cycles of kinetic resolution of *rac*-**1a** (Figure 4). All samples proved to be very durable when recycled up to 5 times, indicating that the M540-based lipase biocatalysts were mechanically and functionally stable.

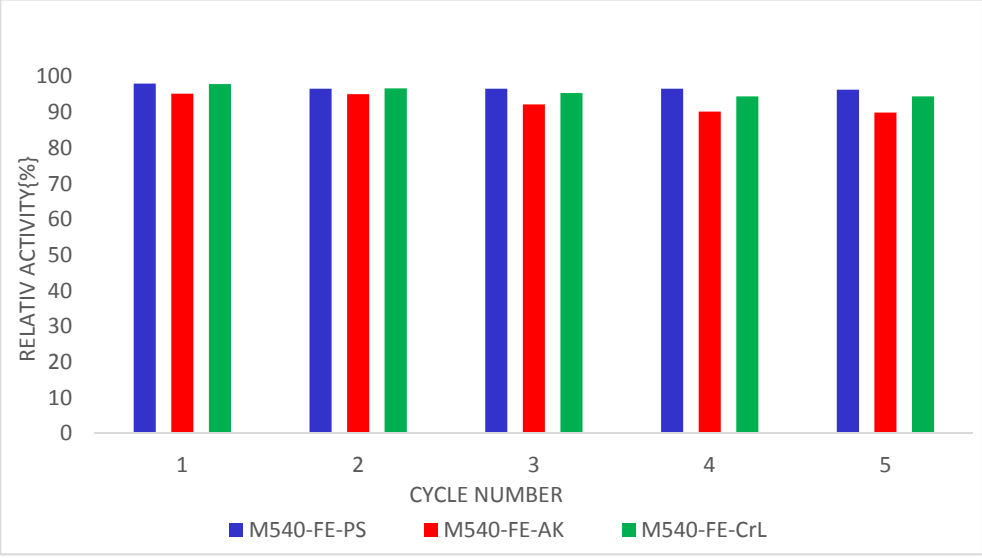

Figure 4. Reusability of the three M540-FE-lipase biocatalysts in 5-cycles of kinetic resolution from racemic 1-phenylethanol *rac*-1a

After the recycling experiments the morphology of the biocatalysts was checked by scanning electron microscope again, proving that the particles were not shattered or mechanically deteriorated.

CONCLUSIONS

Covalent immobilization of three lipases (Lipase AK, from *Pseudomonas fluorescens*; Lipase PS, from *Burkholderia cepacia*; and CrL, from *Candida rugosa*) was successfully carried out on bisepoxide-activated silica microspheres (M540). Our study with four bisepoxides of different properties as activating agents for M540 hollow silica microspheres bearing amine functions at the surface as support proved that immobilization of lipases on bisepoxide-activated M540 could enhance the biocatalytic properties of the lipases as compared to their native powder form. Recycling studies of the resulted preparations

indicated that bisepoxide-activated M540 lipases were suitable and fine-tunable biocatalysts for synthetic biotransformations such as kinetic resolution of racemic secondary alcohols.

EXPERIMENTAL SECTION

Chemicals and enzymes

Racemic 1-phenylethanol, octan-2-ol, propan-2-ol (IPA), 2-amino-2-(hydroxymethyl)propane-1,3-diol (Tris), vinyl acetate, hexane, acetone, and ethanol were commercial products of Alfa-Aesar Europe (Karlsruhe, Germany), Sigma–Aldrich (Saint Louis, MO, USA) or Merck (Darmstadt, Germany). M540 (Matspheres 540) was the product of Materium Innovations. M540-AE, M540-DE, M540-FE and M540-GE supports were the products of SynBiocat LLC. (Budapest, Hungary; the bisepoxide-activated derivatives of the M540 hollow silica microspheres were prepared according to a previously published method [31].

Lipase from *Pseudomonas fluorescens* (Lipase AK), from *Burkholderia cepacia* (Lipase PS), and from *Candida rugosa* (CrL) for immobilization experiments were obtained from Sigma–Aldrich (Saint Louis, MO, USA).

Analytical methods

GC analyses were carried out on Agilent 4890 instrument equipped with FID detector and Hydrodex-6TBDM column [25 m × 0.25 mm, 0.25 μm film of heptakis-(2,3-di-*O*-methyl-6-*O*-*t*-butyldimethylsilyl)-ß-cyclodextrin]; Macherey & Nagel) using H_2 as carrier gas (injector: 250 °C; FID detector: 250 °C; head pressure, 12 psi; split ratio, 50:1, oven: 120 °C; 8 min). GC: t_r (min) for **1** and **2**: 4.0 [(*S*)-**2**], 4.4 [(*R*)-**2**], 5.8 [(*S*)-**1**], 6.0 [(*R*)-**1**].

The structure and morphology of different M540-based lipase preparations were investigated with a JEOL JSM-5500LV scanning electron microscope (SEM). Samples were prepared by placing some silica support on a copper grid coated with carbon and coated with gold layer by a nebuliser prior to analysis. Electron beam energy of 20-22 kV was used.

Enzyme immobilization onto bisepoxide-activated M540 supports

Bisepoxide-activated support (150 mg; either of M540-AE, M540-DE, M540-FE, M540-GE) was suspended in Tris buffer (15 mL, 100 mM, p*H* 7.5) containing the selected lipase (3 mg/mL). The suspension was shaken at room temperature for overnight. The resulted suspension was washed three times with 100 mM Tris buffer (100 mM, p*H* 7.5, 3 × 10 mL) and stored at 4 °C for further experiments.

Enantiomer selective acetylation of racemic 1-phenylethanol *rac*-1a and octan-2-ol *rac*-1b

To a solution of the racemic alcohol *rac*-**1a** or *rac*-**1a** (50 mg) in hexane/*t*-butyl methyl ether/vinyl acetate 6/3/1 (1100 µL) immobilized lipase (25 mg) was added in a sealed amber glass vial and the resulting mixture was shaken (1000 rpm) at 30 °C for 24 h. The reactions were analyzed by GC after the time indicated in Tables 1 and 2 (1 h, 2 h or 24 h).

ACKNOWLEDGEMENTS

The authors thank to Materium Innovations (Granby, Canada) for M540 silica supports. This work was supported by the Higher Education Excellence Program of the Ministry of Human Capacities in the frame of Biotechnology research area of Budapest University of Technology and Economics (BME FIKP-BIO).

REFERENCES

1. W.Aehle, *Enzymes in Industry*, 3rd ed., Wiley-VCH, Weinheim, Germany, **2007**, 99.
2. K. Drauz, H. Gro, *Enzyme Catalysis in Organic Synthesis,* 3rd ed., Wiley-VCH, Weinheim, Germany, **2012**, 14.
3. P. Falus, Z. Boros; P. Kovács, L. Poppe, J .Nagy, *Journal of Flow Chemistry,* **2014**, *4*, 125.
4. M. Oláh, Z. Boros, G.Hornyánszky, L. Poppe, *Tetrahedron,* **2016**, *72*, 7249.
5. D. Weiser, A. Varga, K. Kovács, F. Nagy, A. Szilágyi, B.G. Vértessy, C. Paizs, L. Poppe, *ChemCatChem* **2014**, *6*, 1463.
6. S. Hama, H. Noda, A. Kondo, *Current Opinion in Biotechnology,* **2018**, *50*, 57.
7. S.V. Pawar, G.D. Yadav, *Journal of Industrial and Engineering Chemistry,* **2015**, *31*, 335.
8. E.P. Cipolatti, E.A. Manoel, R. Fernandez-Lafuente, D.M.G. Freire, *Biotechnology Research and Innovation,* **2017**, *1*, 26.
9. Q. Cai, C.Hu, N. Yang, Q. Wang, J. Wang, H. Pan, Y. Hu, C. Ruan, *International Journal of Biological Macromolecules,* **2018**, *109*, 1174.
10. M. Babaki, M. Yousefi, Z. Habibi, J. Brask, M. Mohammadi, *Biochemical Engineering Journal,* **2015**, *101*, 23.
11. I.M. Ferreira, R.H.V. Nishimura, A.B.D. A Souza, G.C. Clososki, S.A. Yoshioka, A. L. M. Porto, *Tetrahedron Letters,* **2014**, *55,* 5062.
12. A. Fabry-Wood, M.E. Fetrow, C.W. Brown, N.A. Baker, N. Fernandez Oropeza, A.P. Shreve, G.A. Montaño, D. Stefanovic, M.R. Lakin, S.W. Graves, *ACS Applied Materials and Interfaces,* **2017**, *9*, 30185.

13. S. Gihaz, D. Weiser, A. Dror, P. Sátorhelyi, M. Jerabek-Willemsen, L. Poppe, A. Fishman, *ChemSusChem,* **2016**, *9*, 3161.
14. M.V.M. Silva, J.F. Bassut, I.I. Junior, S.P. de Souza, M.L.G. Estrada, L.S.M. Miranda, R.O.M.A. de Souza, *RSC Advances,* **2015**, *5*, 102409.
15. X.N. Yang, X.B. Huang, R.Q. Hang, X.Y. Zhang, L. Qin, B. Tang, *Journal of Materials Science,* **2016**, *51*, 6428.
16. R.A. Meryam Sardar, *Biochemistry & Analytical Biochemistry,* **2015**, *4,* 1.
17. D. Weiser, P. L.Sóti, G. Bánóczi, V. Bódai, B. Kiss, Á. Gellért, Z. K. Nagy, B. Koczka, A. Szilágyi, G. Marosi, L. Poppe, *Tetrahedron,* **2016**, *72*, 7335.
18. N. Rueda, J.C.S. dos Santos, R. Torres, O. Barbosa, C. Ortiz, R. Fernandez-Lafuente, *RSC Advances,* **2015**, *5*, 55588.
19. D. Weiser, F. Nagy, G. Bánóczi, M. Oláh, A. Farkas, A. Szilágyi, K. László, Á. Gellért, G. Marosi, S. Kemény, L. Poppe, *Green Chemistry,* **2017**, *19*, 3927.
20. Z. Gao, J. Chu, T. Jiang, T. Xu, B. Wu, B. He, *Process Biochemistry,* **2018**, *64*, 152.
21 .J. Agustian, A.H. Kamaruddin, H.Y. Aboul-Enein, *Chirality* **2017**, *29*, 376.
22. Z. Zhou, F. Piepenbreier, V.R.R.Marthala, K. Karbacher, M. Hartmann, *Catalysis Today,* **2015**, *243*, 173.
23. Y.T. Zhu, X.Y. Ren, Y.M. Liu, Y. Wei, L. Qing, Liao, X. Sen, *Materials Science and Engineering C,* **2014**, *38* , 278.
24. C. Hou, H. Zhu, Y. Li, X. Wang, W. Zhu, R. Zhou, *Applied Microbiology and Biotechnology* **2014**, *99*, 1249.
25. B. Nagy, Z. Galla, L.C. Bencze, M.I. Toşa, C. Paizs, E. Forró, F. Fülöp, *European Journal of Organic Chemistry,* **2017**, *2017*, 2878.
26. A. Suescun, N. Rueda, J.C.S. Dos Santos, J.J. Castillo, C. Ortiz, R. Torres, O. Barbosa, R. Fernandez-Lafuente, *Process Biochemistry,* **2015**, *50*, 1211.
27. L. Nagy-Győr, Z. Boros, L. Poppe, *Periodica Polytechnica Chemical Engineering,* **2013**, *57*, 37.
28. E. Abaházi, D. Lestál, Z. Boros, L. Poppe, *Molecules,* **2016**, *21*, 767.
29. D. Weiser, Z. Boros, J. Nagy, G. Hornyánszky, E. Bell, P. Sátorhelyi, L. Poppe, *Biocatalysis: An Industrial Perspective*; Catalysis series no 29. Royal Society of Chemistry, Cambridge, United Kingdom, **2018**, 397.
30. F. Nagy, K. Szabó, P. Bugovics, G. Hornyánszky, *Periodica Polytechnica Chemical Engineering***, 2019**, 1.
31. M. Oláh, S. Suba, Z.Boros, P. Kovács, M. Gosselin, C. Gaudreault, G. Hornyánszky, *Periodica Polytechnica Chemical Engineering*, **2018**, *62*, 519.

STUDIA UBB CHEMIA, LXIV, 2,Tom I, 2019 (p. 79-86)
(RECOMMENDED CITATION)
DOI:10.24193/subbchem.2019.2.07

Dedicated to Professor Florin Dan Irimie on the Occasion of His 65th Anniversary

CONTINUOUS-FLOW ENZYMATIC KINETIC RESOLUTION MEDIATED BY A LIPASE NANOBIOCONJUGATE

MĂDĂLINA ELENA MOISĂ, LÁSZLÓ CSABA BENCZE, CSABA PAIZS, MONICA IOANA TOŞA*

ABSTRACT. This study describes the development of a continuous-flow procedure for the enzymatic kinetic resolution of *rac*-1-phenylethan-1-ol with the clickable acylating agent 2,2,2-trifluoroethyl 2-(prop-2-yn-1-yl-oxy)acetate, which allows facile click reaction-based downstream, enabling the large-scale chemo-enzymatic synthesis of both secondary alcohol stereoisomers with high enantiopurity. The influence of flow rate, acylating agent and substrate concentration upon the productivity of the packed-bed reactor was investigated. In addition to this, the performances of continuous-flow and batch reactors were compared.

Keywords: *enzymatic kinetic resolution, secondary alcohol, lipase, continuous-flow process, batch process, productivity*

INTRODUCTION

An important aspect when developing a new process is its applicability on industrial scale, consequently scaling-up becomes pivotal. Currently the use of continuous-flow technology is gaining more and more attention as it generally affords processes with increased efficiency and productivity [1,2,3]. Moreover, facile automatic control, reproducibility, lower costs and increased mass and heat transfer make continuous-flow processes an advantageous alternative to traditional batch processes [4].

Babeş-Bolyai University, Faculty of Chemistry and Chemical Engineering, Biocatalysis and Biotransformations Research Center, 11 Arany Janos str., RO-400028, Cluj-Napoca, Romania
**Corresponding author: mtosa@chem.ubbcluj.ro*

Flow technology represents an attractive tool for developing efficient biocatalytic processes and numerous comparative studies prove its superior performance over batch processes [5-8].

Generally, for enzyme-catalysed reactions the preferred type of reactor is the packed-bed reactor, which consists in a column filled with the enzyme (usually immobilized). With the aid of a pump, allowing control of residence time, the reaction media (substrate and reagent dissolved in a solvent) is passed through the enzyme-packed column. The reactor is frequently connected to a thermostat permitting temperature control. Beside the simple construction, the packed-bed reactor has the advantages of extended biocatalyst lifetime through the lack of stirring, which might damage the biocatalyst particles and also through simplified reaction workup since catalyst removal at the end of the process is not required [9-11].

Enzymatic kinetic resolution (EKR) is one of the most employed biocatalytic methods to access enantiomerically pure compounds, mainly due to its simplicity and versatility. The major disadvantage of this method is represented by the maximal theoretical yield of 50%, requiring separation of the two enantiomers at the end of the process which raises practical and economical issues at industrial scale.

Encouraged by our previous results [12], in order to apply the newly developed click reaction-aided EKR products separation strategy for large-scale production of both enantiomerically enriched stereoisomers of secondary alcohols (see **Figure 1**), the EKR step was investigated in continuous-flow mode using a packed-bed reactor.

Accordingly, the efficient clickable acylating agent 2,2,2-trifluoroethyl 2-(prop-2-yn-1-yl-oxy)acetate was applied in the continuous-flow enzymatic transesterification of racemic 1-phenylethan-1-ol (frequently employed as model aromatic chiral alcohol) mediated by the highly stable and thermotolerant lipase B from *Candida antarctica* immobilized on single-walled carbon nanotubes (CaL-B-SWCNT), with reported increased operational stability [13].

RESULTS AND DISCUSSION

Preliminary experiments with CaL-B-SWCNT in continuous-flow acylations of various (hetero)aromatic ethanols revealed 60 °C as the optimal temperature, therefore this biocatalyst was employed in the continuous-flow acylation of *rac*-1-phenylethan-1-ol *rac*-**1** with 2,2,2-trifluoroethyl 2-(prop-2-yn-1-yl-oxy)acetate **2** in *n*-hexane at 60 °C in a packed-bed reactor (30 × 4.6 mm, **Figure 1**).

The productivity (the specific reaction rate, r) was employed as a measure of system performance and was calculated with **Equations 1** and **2** for continuous-flow (r_{flow}) and batch reactions (r_{batch}) [14].

$$r_{batch} = \frac{n_P}{t \times m_e}\left[\frac{\mu mol}{min \times g}\right]$$ **Equation (1)**

$$r_{cont} = \frac{[P] \times f}{m_e}\left[\frac{\mu mol}{min \times g}\right]$$ **Equation (2)**

where n_p: the amount of formed product [µmol]
t: the reaction time [min]
m_e: the mass of the applied biocatalyst [g]
[P]: the product concentration [µmol mL^{-1}]
f: the flow rate [mL min^{-1}]

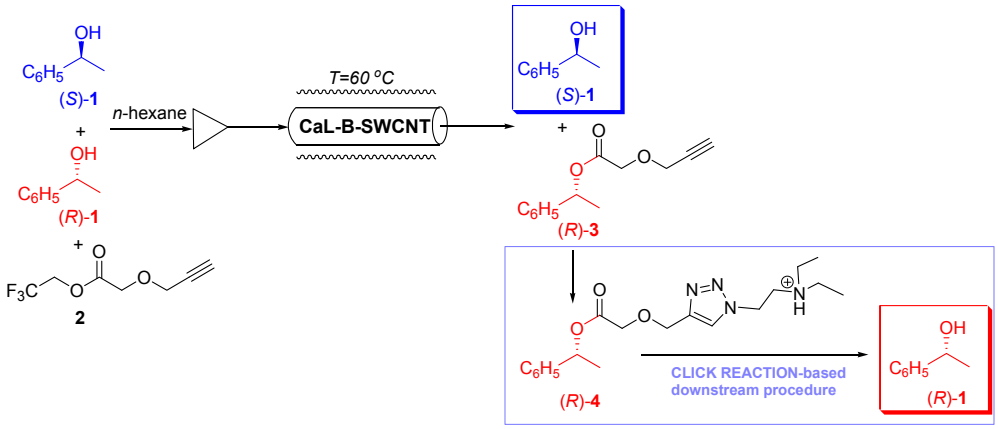

Figure 1. Transesterification of *rac*-1-phenylethan-1-ol *rac*-**1** with 2,2,2-trifluoroethyl 2-(prop-2-yn-1-yl-oxy)acetate **2** in *n*-hexane at 60 °C in a continuous-flow packed-bed reactor, followed by click reaction-based downstream procedure

In order to effectively apply the click chemistry-type downstream, the presence of the reactive enantiomer of the substrate in the effluent is not desired, therefore the flow rate and the acyl donor and substrate concentrations must be well adjusted to ensure complete transformation.

The continuous-flow EKR was initially studied using a 10 mM substrate concentration and 0.75 equiv. of acyl donor **2** at 60 °C, varying the flow rate in the range of 0.1 – 0.5 mL min^{-1}. The maximum conversion attained within this experiment was 42% at 0.1 mL min^{-1} (**Figure 2A**). Consequently, with the aim to reach the maximum conversion of 50%, higher amounts of the acylating agent **2** were tested (2, 3 and 4 equiv.).

The obtained results (**Figure 2A**) confirm the beneficial impact of the increased molar *ratio* of acyl donor on the conversion in the continuous-flow EKR. Accordingly maximum conversion was reached at 0.1 mL min^{-1} flow rate with 3 and 4 equiv. of ester **2**, allowing a productivity of 4.2 μmol min^{-1} g^{-1}. Moreover, when using 4 equiv. of the ester the 50% conversion was also reached at 0.2 mL min^{-1}, affording a two times higher productivity (**Figure 2B**). Since no considerable variations in conversion were seen from 0.1 to 0.5 mL min^{-1} using 4 equiv. of **2** (48-50% *c*), this amount of acylating agent was selected as optimal for the next experiments. Noteworthy, the continuous-flow transesterification proceeded with high enantioselectivity (*E*»200), affording product (*R*)-**3** with maximum enantiomeric excess (ee_P>99%) in all experiments.

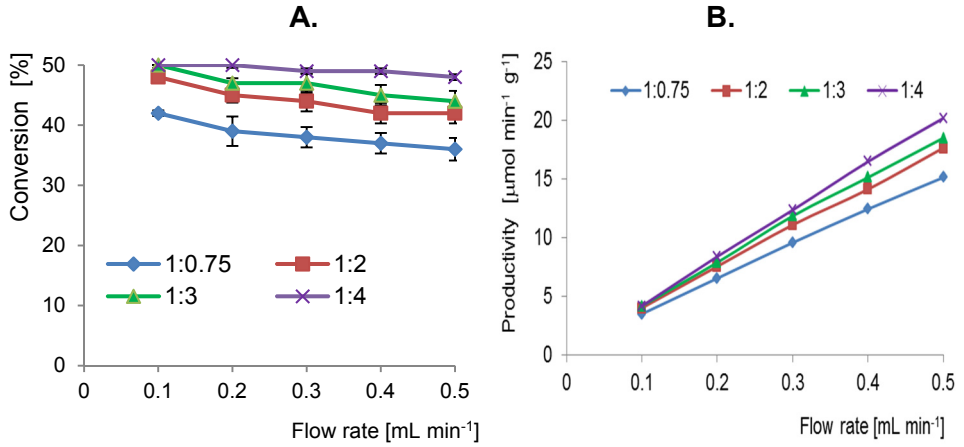

Figure 2. Influence of substrate: acylating agent *ratio* on the conversion (**A**) and productivity (**B**) of CaL-B-SWCNT-mediated continuous-flow transesterification of *rac*-**1** (10 mM) with trifluoroethyl 2-(prop-2-yn-1-yl-oxy)acetate **2** in *n*-hexane at 60 °C. Error bars represent standard deviations from average. The productivity was calculated using the average value of conversion.

Further, in order to increase the productivity, different substrate concentrations (10 – 100 mM) were tested at 0.1 and 0.5 mL min^{-1} flow rate using 4 equiv. of acyl donor (**Figure 3**). As expected, the productivity increased with the substrate concentration, the maximum value being obtained at 100 mM *rac*-**1** and 0.5 mL min^{-1} flow rate (88.2 μmol min^{-1} g^{-1}, **Figure 3B**). Although higher productivities were obtained at the higher flow rate, the significant decrease in conversion at 0.5 mL min^{-1} (**Figure 3A**) must be considered when deciding which flow rate is more advantageous. Analyzing the theoretical maximum productivity calculated for the maximum conversion (represented with dotted

lines in **Figure 3**), it can be noticed that at 0.1 mL min^{-1} flow rate the actual productivity values are close to the maximum theoretical ones, while at 0.5 mL min^{-1} flow rate the difference in actual and theoretical values drastically increases with substrate concentration.

It is worth mentioning that even at the highest studied substrate concentration (100 mM) the system afforded a high conversion of *rac*-**1** (45% at 0.1 mL min^{-1}). In addition to this, the enantioselectivity of the process was not altered throughout the investigated substrate concentration domain (*E*»200).

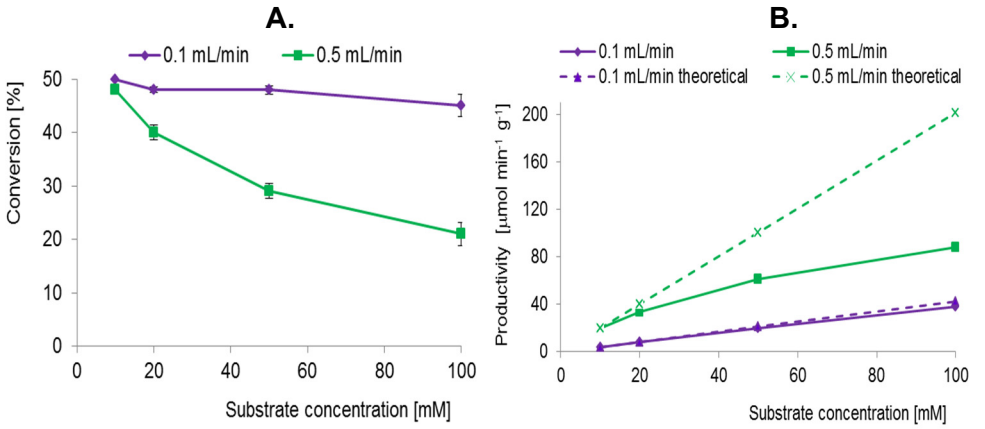

Figure 3. Influence of substrate concentration on the conversion (**A**) and productivity (**B**) of CaL-B-SWCNT-mediated continuous-flow transesterification of *rac*-**1** with trifluoroethyl 2-(prop-2-yn-1-yl-oxy)acetate **2** (4 equiv.) in *n*-hexane at 60 °C. Error bars represent standard deviations from average. The productivity was calculated using the average value of conversion. The theoretical productivity was calculated for the maximum conversion (obtained at 10 mM *rac*-**1**) without considering the decrease in conversion with increased substrate concentration.

Furthermore, the productivities obtained in continuous-flow and batch systems were compared under identical experimental conditions (substrate and acyl donor concentrations, solvent and temperature) at the same degree of conversions [14]. The continuous-flow reactor proved remarkable productivity as compared to the batch system (r_{batch} = 1.0 µmol min^{-1} g^{-1}, r_{flow} = 17.6 µmol min^{-1} g^{-1}, at 42% conversion, 60 °C, 10 mM substrate concentration, 2 equiv. of acyl donor **2** and 0.5 mL min^{-1} flow rate), demonstrating the superior performance of the continuous-flow system over the batch process.

CONCLUSIONS

An efficient continuous-flow procedure for performing lipase-mediated kinetic resolution of *rac*-1-phenylethan-1-ol with 2,2,2-trifluoroethyl 2-(prop-2-yn-1-yl-oxy)acetate was developed using a packed-bed reactor. By combining this continuous-flow EKR with the click reaction-based downstream, the large-scale production of both enantiomers of secondary alcohols can be effectively achieved.

EXPERIMENTAL SECTION

Materials and methods

Chiral HPLC (Agilent 1200 Series instrument) using LUX-3 Phenomenex column (4.6 × 250 mm) and a mixture of *n*-hexane:2-propanol 9:1 v/v at 1 mL min^{-1} flow rate as mobile phase was employed for the quantitative analysis of the enzymatic kinetic resolution [(*S*)-**1**: 6.5 min; (*R*)-**1**: 7.1 min; (*S*)-**3**: 15.4 min; (*R*)-**3**: 18.0 min; 25 °C].

The enantiomeric excesses of the substrate ee_S and product ee_P were determined from peak areas of HPLC chromatograms. The enantiomeric *ratio* *E* was calculated with the equation $E = \ln[(1-c)(1-ee_S)]/\ln[(1-c)(1+ee_S)]$, using the calculated conversion: $c = ee_S/(ee_S+ee_P)$ [15].

CaL-B-SWCNT was obtained by covalently immobilizing lipase B from *Candida antarctica* on carboxy-functionalized single-walled carbon nanotubes ($SWCNT_{COOH}$) as previously described [13].

HPLC grade *n*-hexane and 2-propanol were purchased from VWR.

Batch enzymatic reactions were performed in a Heidolph Vibramax 110 shaker equipped with an incubator module (Heidolph, Germany) while continuous-flow experiments were carried out in a stainless steel column (30 × 4.6 mm) attached to the pump and thermostat modules of an Agilent 1200 Series HPLC instrument.

Enzymatic procedures

All experiments were performed in triplicate.

1. Continuous-flow lipase-mediated transesterification of *rac*-1-phenylethan-1-ol *rac*-1 with 2,2,2-trifluoroethyl 2-(prop-2-yn-1-yl-oxy)acetate 2 in a packed-bed reactor

Continuous-flow reactions were performed in a thermostated stainless steel column (30 × 4.6 mm) filled with the immobilized lipase (119 mg of CaL-B-SWCNT) attached to an Agilent 1200 Series HPLC pump. Prior to performing

the reaction, the lipase-filled column was washed with *n*-hexane at 0.5 mL min^{-1} for 30 min. The solution of the substrate *rac*-**1** (10, 20, 50 or 100 mM) and 2,2,2-trifluoroethyl 2-(prop-2-yn-1-yl-oxy)acetate **2** (0.75, 2, 3 or 4 equiv.) in *n*-hexane was pumped through the reactor thermostated at 60 °C at different flow rates (0.1 – 0.5 mL min^{-1}). Samples of 50 µL were collected periodically, diluted with *n*-hexane (500 µL) and analysed by HPLC. The steady-state condition was reached within 30-90 min, depending on the flow rate. Between experiments the enzyme-filled reactor was washed with *n*-hexane at 0.5 mL min^{-1} for 30 min and stored overnight at 4 °C.

2. Batch mode lipase-mediated transesterification of *rac*-1-phenylethan-1-ol *rac*-1 with 2,2,2-trifluoroethyl 2-(prop-2-yn-1-yl-oxy)acetate 2

Into the solution of *rac*-**1** (10 µmol) in *n*-hexane (1 mL), 2,2,2-trifluoroethyl 2-(prop-2-yn-1-yl-oxy)acetate **2** (2 equiv.) and the immobilized lipase CaL-B-SWCNT (2.4 mg) were added and shaken at 700 rpm at 60 °C until 42% conversion was reached (28 hours). Samples taken as previously described were subjected to HPLC analysis.

ACKNOWLEDGMENTS

This work was supported by a grant of the Romanian National Authority for Scientific Research, CNDI–UEFISCDI, project number PN-II-PT-PCCA-2013-4-0734.

Financial support for project NEMSyB, ID P37_273, Cod MySMIS 103413 [funded by National Authority for Scientific Research and Innovation (ANCSI) and European Regional Development Fund, Competitiveness Operational Program 2014-2020 (POC), Priority axis 1, Action 1.1] is gratefully acknowledged.

REFERENCES

1. F.M. Akwi, P. Watts, *Chemical Communications*, **2018**, *54*, 13894.
2. R. Porta, M. Benaglia, A. Puglisi, *Organic Process Research & Development*, **2016**, *20*, 2.
3. A.S. de Miranda, M.V. de M. Silva, F.C. Dias, S.P. de Souza, R.A.C. Leão, R. O.M.A. de Souza, *Reaction Chemistry & Engineering,* ***2017****, 2,* 375.
4. G. Jas, A. Kirschning, *Chemistry – A European Journal,* **2003**, *9*, 5708.
5. M.P. Kamble, G.D. Yadav, *Industrial & Engineering Chemical Research,* **2017**, *56(7)*, 1750.
6. J.C. Thomas, B.B. Aggio, A.R.M. de Oliveira, L. Piovan, *European Journal of Organic Chemistry,* **2016**, *36*, 5964.

7. M.E. Moisă, C.G. Spelmezan, C. Paul, J.H. Bartha-Vári, L.C. Bencze, F.D. Irimie, C. Paizs, F. Péter, M.I. Toşa, *RSC Advances*, **2017**, *7*, 52977.
8. V.M.M. Silva, J. Bassut, I. Ivaldo Jr., S.P. de Souza, M.L. G. Estrada, L.S.M. Miranda, R.O.M.A. de Souza, *RSC Advances,* **2015**, *5*, 102409.
9. Eş, J.D.G. Vieira, A.C. Amaral, *Applied Microbiology and Biotechnology,* **2015**, *99(5)*, 2065.
10. I. Itabaiana Jr, L.S.M. Miranda, R.O.M.A. de Souza, *Journal of Molecular Catalysis B: Enzymatic,* **2013**, *85–86*, 1.
11. H.M. Salvi, M.P. Kamble, G.D. Yadav, *Applied Biochemistry and Biotechnology,* **2018**, *184(2)*, 630.
12. M.E. Moisă, L. Poppe, C.A. Gal, L.C. Bencze, F.D. Irimie, C. Paizs, F. Péter, M.I. Toşa, *Reaction Chemistry & Engineering,* **2018**, *3*, 790.
13. L.C. Bencze, J. H. Bartha-Vári, G. Katona, M.I. Toşa, C. Paizs, F.D. Irimie, *Bioresource Technology* **2016**, *200*, 853.
14. C. Csajági, G. Szatzker, E.R. Tőke, L. Ürge, F. Darvas, L. Poppe, *Tetrahedron: Asymmetry,* **2008**, *19*, 237.
15. C.S. Chen, Y. Fujimoto, G. Girdaukas, C.J. Sih, *Journal of American Chemical Society*, **1982**, *104*, 7294.

STUDIA UBB CHEMIA, LXIV, 2,Tom I, 2019 (p. 87-99)
(RECOMMENDED CITATION)
DOI:10.24193/subbchem.2019.2.08

Dedicated to Professor Florin Dan Irimie on the Occasion of His 65th Anniversary

7-AMINOCEPHALOSPORANIC ACID – PRODUCTION AND SEPARATION

ALEXANDRA TUCALIUC[a], MĂDĂLINA POȘTARU[b,*], DAN CAȘCAVAL[a], ANCA-IRINA GALACTION[b]

ABSTRACT. Cephalosporins, a large group of β-lactam antibiotics, contain a 7-aminocephalosporanic acid (7-ACA) nucleus which is derived from cephalosporin C, and substitutions of chemical groups or modifications of 7-ACA side-chains resulting in varying pharmacologic properties and antimicrobial activities, development of useful antibiotic agents, also. Cephalosporin C obtained by fungus fermentation can be transformed to 7-ACA by two-step or one step enzymatically conversion process. The most important step in 7-ACA downstream process is represented by its separation from enzymatically produced reaction mixture. Among the used methods new separation techniques have been developed and applied to bioseparations, like reactive extraction and pertraction which have considerable potential.

Keywords: *7-aminocephalosporanic acid, cephalosporin C, enzymatic reaction, pertraction, reactive extraction*

INTRODUCTION

Over the past 50 years, the industrial production of β-lactam antibiotics by fermentation is one of the outstanding examples of biotechnology. Cephalosporins are a large group of β-lactam antibiotics that are closely related to the penicillins. They are used for the treatment of infection diseases caused by gram-positive and

[a] *"Gheorghe Asachi" Technical University of Iasi, "Cristofor Simionescu" Faculty of Chemical Engineering and Environmental Protection, Dept. of Organic, Biochemical and Food Engineering, D. Mangeron 73, 700050 Iasi, Romania*

[b] *"Grigore T. Popa" University of Medicine and Pharmacy of Iasi, Faculty of Medical Bioengineering, Dept. of Biomedical Science, M. Kogălniceanu 9-13, 700454 Iasi, Romania*

**Corresponding author: many.north@gmail.com*

gram-negative bacteria. They now comprise a group of antibiotics having a wide range of activity and low toxicity. Since their discovery in the 1950s, cephalosporins have become one of the largest classes of antibiotics. The class is divided into generations or subclasses, which are grouped by chemical properties and subsequent generalized microbiologic spectra. There are now more than 50 marketed cephalosporins [1].

Cephalosporins are widely used for treating and preventing bacterial diseases through disrupting the synthesis of the peptidoglycan layer of cell walls in both gram-positive and gram-negative bacteria [2].

Fungus *Cephalosporium acremonium* produces cephalosporin C (CPC) that is not potent for clinical use. Its molecule can be transformed to 7-aminocephalosporanic acid (7-ACA) as the intermediate compound for making semisynthetic cephalosporin derivatives that are of current interest with important applications in biopharmaceutical industries with a share of about 29% of the estimated worldwide antibiotic market.

PRODUCTION OF 7-AMINOCEPHALOSPORANIC ACID

The improved fermentation technology, by using producer microorganisms, like *Acremonium chrysogenum (syn. Cephalosporium acremonium)*, has enhanced the productivity and substantial cost reduction of the cephalosporins antibiotics production [3].

Enzymatic process technology for 7-aminocephalosporanic acid is also highly efficient (~80 - 90%), with new enzyme technology leading to major cost reductions over the past decade [4].

Cephalosporins contain a 7-aminocephalosporanic acid nucleus which is derived from cephalosporin C, and substitutions of chemical groups or modifications of 7-ACA side-chains resulting in varying pharmacologic properties and antimicrobial activities, development of useful antibiotic agents, also.

The diversity of structural types, coupled with potent antibacterial or β-lactamase inhibitory activity, provided a new incentive for expansion in the area of β-lactam chemistry directed towards semi- or total-synthesis of these new agents and analogues. The toxicity level of cephalosporin antibiotics is low and, as penicillin, hypersensitivity is the most common adverse effect.

7-aminocephalosporanic acid is the building-block chemical structure (Figure 1) of cephalosporin antibiotics and intermediates. Modifications of side-chains of 7-ACA affect the antibacterial activity and can lead to the alteration of pharmacokinetic properties and receptor binding affinity, thus creating new class of cephalosporin antibiotics with important clinical uses [5].

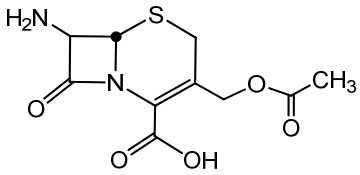

Figure 1. Chemical structure of cephalosporin C [6]

The most commonly used method to produce 7-ACA at industrially scale is chemical deacylation of chephalosporin C, a β-lactam antibiotic obtained by fermentation processes (Figure 2).

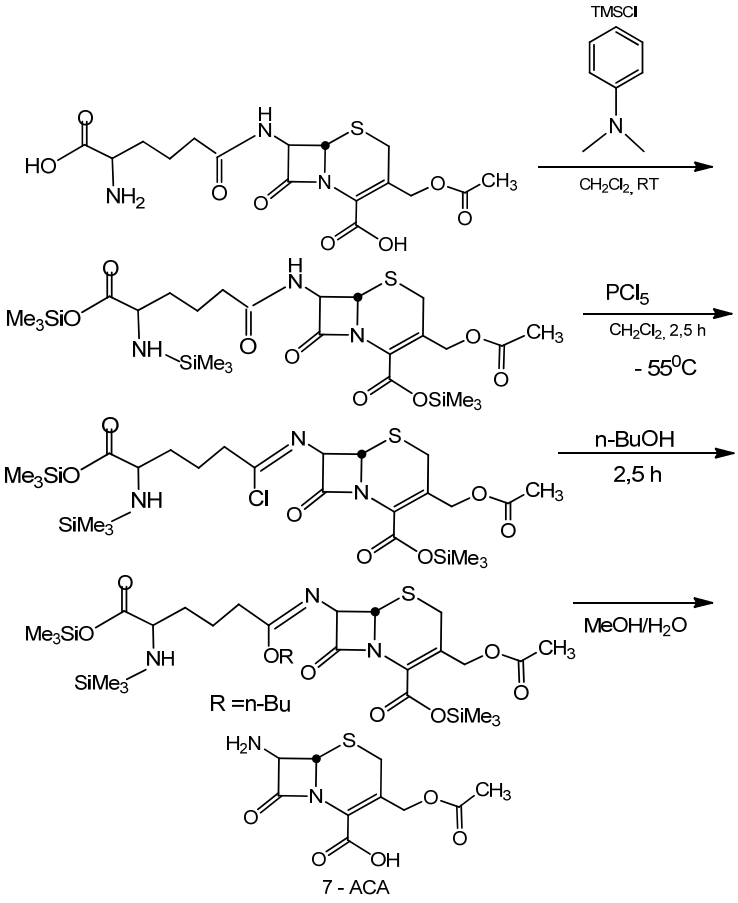

Figure 2. Chemical 7-ACA route starting from cephalosporin C [6]

However, this production method has many environmental and safety disadvantages, due to the large quantities of organic solvents and the production of toxic chemical waste. This process also utilizes many costly techniques in order to overcome environmental and ecological problems [6].

In the past decade, enzymatic methods for deacylation have attracted more attention in the manufacturing of cephalosporin antibiotics, and several enzyme-based methods have been developed. Therefore an enzymatic conversion of CPC to 7-ACA was developed, which reduce the process costs and has a positive environmental impact. Two principle enzymatic routes are proposed:

– Two-step cleavage with D-amino acid oxidase (DAAO) and glutarylacylase (GA) (Figure 3, left);

– One-step hydrolysis of CPC with a CPC acylase (CA) (Figure 3, right).

Industrial standard for 7-ACA production is represented by chemo-enzymatic hydrolysis of cephalosporin C by a two-step enzymatic process (Figure 3).

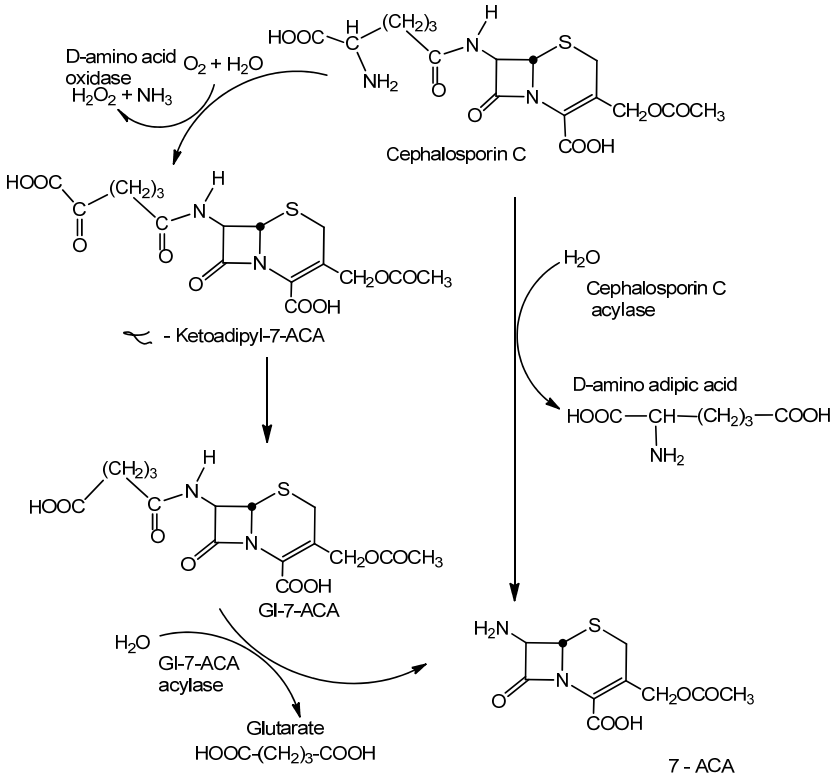

Figure 3. Chemo-enzymatic hydrolysis of cephalosporin C with 7-ACA production [7]

The transformation of cephalosporin C to 7-ACA and glutarate involves two step enzymatic conversions with the participation of three main intermediates: hydrogen peroxide (H_2O_2), α-ketoadipyl- (AKA-7-ACA), 7-β-(4-carboxybutanamido)-cephalosporanic acid (GL-7-ACA) [8].

The main problem of the method that involves one step 7-ACA bioconversion is the presence of H_2O_2 during the reaction process, which results in the inactivation of the employed enzymes, especially DAAO. In order to eliminate this main drawback of the enzymatic process, Lopez-Gallego et al. developed a system in which DAAO was co-immobilized with catalase (CAT), which is able to fully eliminate in situ the hydrogen peroxide formed by the neighboring DAAO molecules. For that, the oxidative deamination of CPC must produce only α-ketoadipyl-7-ACA, the kinetic parameters of GAC (glutaryl acylase) derivate being presented in Table 1. The conversion of cephalosporin C to 7-ACA was achieved with more than 80% yield in 180 minutes and only 2.5% of α-ketoadipyl-7-ACA was not hydrolyzed [9].

Table 1. Kinetics parameters of GAC with GL-7-ACA and α-ketoadipyl-7-ACA [9]

Kinetic parameters	Glutaryl amidase activity	α-ketoadipyl amidase activity
K_m [mM]	1.06 ± 0.05	4.9 ± 0.3
K_{cat} [min^{-1}]	97.8 ± 0.7	2.8 ± 0.5
K_{cat}/K_m [min^{-1} x mM^{-1}]	82.8 ± 0.4	0.56 ± 0.02

Another study reported the conversion of CPC to 7-ACA in a single reactor, by a fed-batch strategy, by simultaneous action of DAAO in the permeabilized *Pichia pastoris* cells and immobilized glutaryl-7-aminocephalosporanic acid acylase on support. The results indicated that CPC could be converted by simultaneous action of the two enzymes in the two different forms, to 90.9% 7-ACA, 5% AKA-7-ACA and 4.1% unidentified by-product within 2.5 h [10].

Direct conversion of cephalosporin C into 7-ACA was optimized by using cephalosporin C acylase from *Pseudomonas* N176 (named VAC). Conti et al. obtained 7-ACA as the main reaction product by converting over 98% cephalosporin C, under optimal conditions, thus obtaining approximatively 81 mg of 7-ACA in 41 hours from 15 mM cephalosporin C. All variants of VAC used were active on both substrates, cephalosporin C and Gl-7-ACA. The kinetic properties are presented in Table 2 [11].

Development of DAAO and GA into an industrial biocatalyst includes the fermentative production, the isolation, purification, and immobilization of the enzymes. Enzyme purification is needed to eliminate any unwanted catalytic activities found in cell extracts. DAAO as well as GA are both inactivated by separation of their subunits; to avoid this immobilization of the

enzymes on a solid support greatly increases their stability. Both enzymes have been immobilized as whole cells or as cell extracts in gels or on prefabricated carriers [12,13].

Table 2. Comparison of kinetic properties of VAC variants on CPC and GI-7-ACA substrates [11]

VAC variants	CPC substrate		GI-7-ACA substrate	
	K_m [mM]	V_{max}/K_m	K_m [mM]	V_{max}/K_m
VAC wild-type	9.5 ± 0.3	0.08	1.5 ± 0.2	24.3
VAC H57βS-H70βS	12.2 ± 0.9	0.24	6.9 ± 0.7	0.70
VAC HS-HS-F72βR	16.4 ± 2.3	0.10	2.0 ± 0.2	26.4
VAC HS-HS-L154βY	4.5 ± 0.7	0.73	2.0 ± 0.6	3.95

Pollegione et al. obtained ~90% conversion of cephalosporin C to 7-amino-cephalosporanic acid in a single deacylation step, starting from a known glutaryl-7-amino cephalosporanic acid acylase as the protein scaffold, an acylase gene optimized for expression in *Escherichia coli* and for molecular biology manipulations. The activity of the synthetic used gene (VAC) variants on CPC and GI-7-ACA substrates was investigated in order to determine the changes in substrate specificity. The most significant increase in activity on CPC was recorded by M4 mutant, while in the case of activity on GI-7-ACA, a significant increase in K_m was recorded for M5 and M6 mutants (Table 3) [14].

Table 3. Kinetic properties of mutant VAC on CPC and GI-7-ACA as substrates [14]

VAC mutants	CPC substrate		GI-7-ACA substrate	
	K_m [mM]	V_{max} (U/mg)	K_m [mM]	V_{max} (U/mg)
VAC wild-type	11	0.7	1.6	24.2
M1 (F270M)	6.5	0.7	2.7	24.6
M2 (A215Y)	6.9	1.8	1.7	16
M3 (D416Y)	7.2	0.7	1.7	4.9
M4 (D416Y-H417Y)	13.0	4.2	9.0	1.2
M5 (I44V-E49stop-D416Y-H417Y)	32.0	0.13	25.0	0.06
M6 (S22P-T394P-D416Y-H417Y)	24.5	0.02	37.2	0.11
M7 (E89A-A215Y)	18.9	0.10	1.1	0.66
M8 (A215Y-F270S)	10.1	1.56	2.0	23.8

Because two-step protocol shows some limitation, one-step protocol for 7-ACA production was developed, which can involve two aspects, i.e. the direct conversion of CPC to 7-ACA by a single enzyme, cephalosporin acylase or mutant of glutarylamidase [13].

A new challenge is represented by the utilization of Cephalosporin C acylase for the one-step enzymatic process to convert CPC into 7-ACA directly (Figure 4).

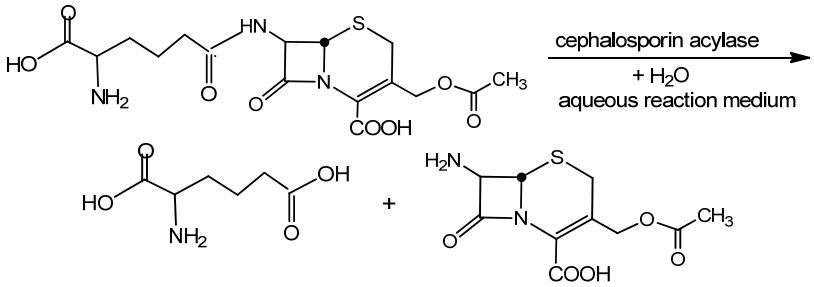

Figure 4. Mechanism conversion of CPC into D-α-aminoadipic acid and 7-ACA catalyst by CPC acylase [6]

But Cephalosporin C acylase produced by microorganisms (*Achromobacterxylosoxidans*, *Aeromonas* sp., *Arthrobacterviscosus*, *Bacillus laterosporus*, *Flavobacterium* sp., *Paecilomyces* sp., and *Pseudomonas* sp.) has low activity, therefore to increase its activity needs genetic engineering [15].

SEPARATION OF 7-AMINOCEPHALOSPORANIC ACID BY EXTRACTION

Following the enzymatic conversion process of cephalosporin C to 7-aminocephalosporanic acid, the product must be isolated from the reaction mixture. This separation process raises difficulties because the concentration of acid in the mixture is reduced and due to the presence of α-aminoadipic acid as by-product impurity. A general process flow diagram of production and separation of 7-ACA is presented below (Figure 5):

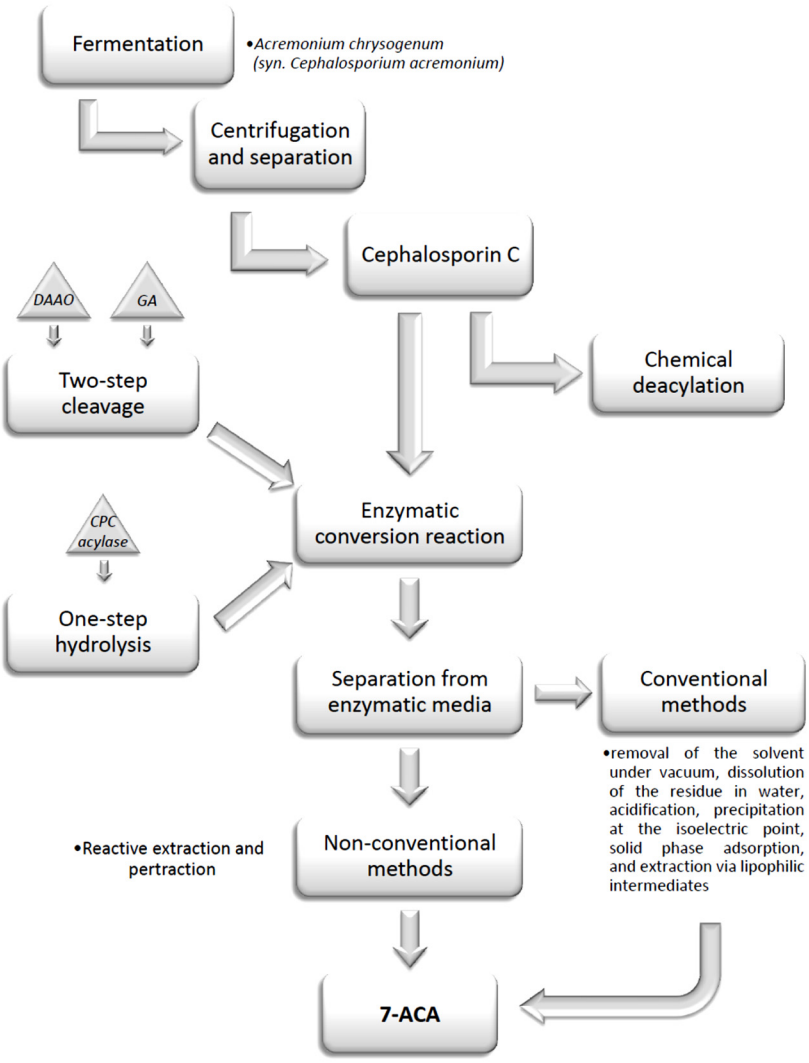

Figure 5. Process flow diagram of production and separation of 7-ACA

Since 7-ACA is an amphoteric molecule, physical solvent extraction is difficult. Various methods of extraction and purification of cephalosporin antibiotics have been studied (removal of the solvent under vacuum, dissolution of the residue in water, acidification, and precipitation at the isoelectric point of 7-ACA (pH = 3.5). These methods, along with solid phase adsorption, and extraction via lipophilic intermediates, have important materials and energy costs [16-18].

A study on the separation of 7-ACA aimed to remove the antibiotic from wastewater by using lipid-accumulating microalgae [19]. The results demonstrated that the microalgae strains that were tested, *Chlorella* sp. Cha-01, *Chlamydomonas* sp. Tai-03, and *Mychonastes* sp. YL-02, exhibited high resistance to 7-ACA in terms of cell growth and lipid production, for high 7-ACA contamination level at 100 mg 7-ACA l^{-1}. 7-ACA was mainly removed from antibiotic wastewater by hydrolysis, photolysis, and adsorption onto microalgae. The studied influential factors in microalgae cultivation were visible-light illumination, stirring and CO_2 aeration. 7-ACA removal efficiency was above 75% at 24 h in Cha-01 group.

In aqueous solutions, 7-ACA exists in ionic forms of different charges depending on the pH of the media. At pH below 2.02 (pK_{a1} = 2.02), the predominant form of 7-ACA is cationic, at pH above 4.42 (pK_{a2} = 4.42) is anionic, and in this range the zwitterion is predominant (Figure 6) [18,20].

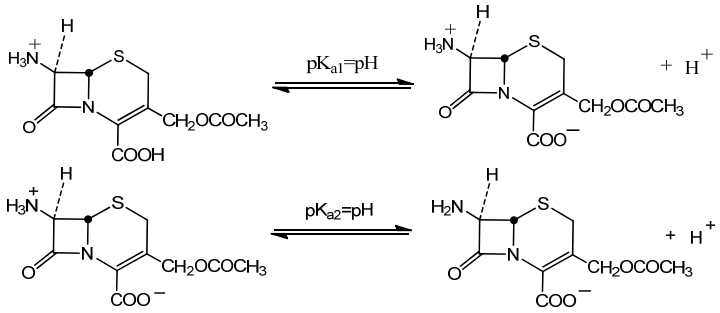

Figure 6. The chemical form of 7-ACA depending on the pH of the aqueous solution [20]

Therefore, a viable method for the separation of 7-ACA is extraction accompanied by chemical reaction with an extractant, namely reactive extraction [21]. There are two mechanisms of reactive extraction of β-lactams [17]: ion-pair extraction (the extractant dissolves in an organic phase and reacts with the β-lactam anions and a proton in the aqueous phase) and liquid-liquid ion exchange (the removal of a β-lactam anion from the aqueous phase by an ion-exchange with the anion of the extractant, typically a quaternary salt, dissolved in the organic phase).

The reactive extraction of 7-ACA using secondary and tertiary amines and a quaternary ammonium salt was studied by Bora et al. [18]. 7-ACA dissociates in the aqueous phase to give an anion and a proton. The dissolved amine in the organic phase reacts with 7-ACA anion and the proton, in the aqueous phase. The experiments were carried out using various carriers in butyl acetate: dioctylamine, Amberlite LA-1, Amberlite LA-2, trioctylamine, and Aliquat-336. According to this study, the most effective amine carrier was

Amberlite LA-2, which, however, exhibits opposite pH dependence on the distribution coefficient (K_d) to that achieved with Aliquat-336 (liquid-liquid ion-exchange extraction). As both extraction and back-extraction were easily performed at pH values of 8 and, respectively 5, Aliquat-336 was the preferred choice for the reactive extraction of 7-ACA.

Following the results of their previous study, the scientists analyzed the equilibrium and kinetics of 7-ACA extraction with Aliquat-336 dissolved in n-butyl-acetate as the solvent [22]. Varying the pH value of the aqueous solutions, the obtained equilibrium constant (K_P) for extraction of 7-ACA with Aliquat-336 was $20x10^2$ at a pH value of 8 and $5x10^2$ at a pH value of 5. The equilibrium constant increases with the pH of the aqueous solution, attributed to the increase in ionization of 7-ACA. The proposed mathematical model for the extraction of 7-ACA confirmed that the interfacial chemical reaction controls the extraction rate, the interfacial reaction between the 7-ACA anion and adsorbed solute-carrier complex playing a significant role in the extraction kinetics over the pH and concentration ranges that were studied.

In another study, 7-ACA and certain β-lactam antibiotics (7-aminodeacetoxy cephalosporanic acid (7ADCA), cephalexin, 6-aminopenicillanic acid (6-APA), and cephalosporin-C) were extracted from aqueous solution with Aliquat-336 dissolved in n-butyl acetate with a complimentary stripping kinetic study [23]. The feed phase pH value was maintained between 8 and 10 by using phosphate and carbonate buffer. The stripping phase pH varied between 3 and 5 in order to assess the pH effect on stripping rate.

Table 4. Maximum percentage stripping of various β-lactams and the corresponding pH values [22]

β-lactam	pH	% of stripping	J_S (mol/(cm^{2}s))
6-APA	4	67.4	3.74×10^{-10}
Cephalosporin-C	4	72.9	4.0×10^{-10}
Cephalexin	4	74.1	3.4×10^{-10}
7-ACA	4	75.5	3.22×10^{-10}
7-ADCA	3	83.3	5.15×10^{-10}

Table 4 offers a comparison of the extent of stripping and pH dependence of the stripping rate (*Js*), and indicates the role of the molecular structure of the β-lactams whose pK_a values are different from each other.

One of the most recent separation techniques, pertraction or permeation through liquid membrane, consists in the transfer of a solute between two aqueous phases through a liquid solvent membrane interposed between them. The extraction dynamic is based on the difference in pH value

and concentration between the feed and the stripping phase, thereby offering the possibility to transport the solute against its concentration gradient. Compared to physical extraction, this method reduces the solvent loss and requires small quantities of solvent and carrier agent, because of their constant regeneration [24].

Ghosh et al. reported some preliminary results on reactive extraction of cephalosporin C in a supported liquid membrane consisting in a mixture of Aliquat-336 as carrier and butyl acetate. The permeation rate of CPC depended on the carrier concentration in the membrane and the chloride ion concentration in the aqueous feed phase. By maintaining a fixed concentration of Cl^- ion, the increase of Aliquat-336 concentration led to an increase of the permeation coefficient (P) values, to a maximum at about 300-400 mol/m^3 of Aliquat-336 [25]. Based on this previous study, Sahoo at al. investigated the facilitated transport of 7-ACA in a bulk liquid membrane also of butyl acetate and Aliquat-336, positioned above the two aqueous phases [20].

The distribution coefficient increased up to 1.3 at a value of pH of 9.2, beyond which it decreased. The decrease of the distribution coefficient was attributed to the hydrolytic decomposition of 7-ACA at high pH values. However, since 7-ACA is stable in the pH range of 5 - 8, the experiments were carried out using aqueous solutions of pH = 8 - 9 and stripping phase pH = 5 - 6.

CONCLUSIONS

7-Aminocephalosporanic acid is an important intermediate in the production of semisynthetic cephalosporin antibiotics. The primary method for industrial production of 7-ACA is chemical deacylation of cephalosporin C, but this method has many environmental and safety disadvantages.

In recent years, enzymatic conversion of CPC to 7-ACA was developed, which reduces the process costs and has a positive environmental impact, by two-step cleavage with D-amino acid oxidase and glutarylacylase or one-step hydrolysis of CPC with a CPC acylase. Under optimized conditions, the conversion of CPC to 7-ACA was higher than 90%, with byproduct formation lower than 4%.

The separation of 7-ACA from an enzymatically produced reaction mixture was performed by numerous methods that have important materials and energy costs. Therefore, new techniques of separation were studied, namely reactive extraction and transport through bulk liquid membranes. The results published so far indicate that using Aliquat-336 as an extractant or carrier agent dissolved in different solvents may present a promising method for efficiently separate 7-ACA from enzymatic media, with over unity permeation and distribution coefficients for pH-values of 7- ACA aqueous solutions of 8.

These biotechnological achievements are industrial benchmarks in modern biocatalysis and separation processes and can lead to the industrial implementation of highly economical and sustainable production of 7-aminocephalosporanic acid.

ACKNOWLEDGMENTS

This work was supported by a grant of Ministry or Research and Innovation, CNCS –UEFISCDI, project number PN-III-P4-ID-PCE-2016-0100, within PNCDI III.

REFERENCES

1. R.P. Elander, *Applied Microbiology and Biotechnology*, **2003**, *61*, 385.
2. A. Magdaleno, M.E. Saenz, A.B. Juarez, J. Moretton, *Ecotoxicology and Environmental Safety*, **2015**, *113*, 72.
3. J.C. Kim, Y.S. Song, D.H. Lee, S.W. Kang, S.W. Kim, *Biotechnology Letters*, **2007**, *29(1)*, 51.
4. M.S. Barber, U. Giesecke, A. Reichert, W. Minas, *Advances in Biochemical Engineering / Biotechnology*, **2004**, *88*, 179.
5. L.L. Brunton, B.A. Chabner, B.C. Knollman, "The pharmacological basis of therapeutics", McGraw-Hill Medical, New York, **2011**.
6. H. Gröger, M. Pieper, B. König, T. Bayer, H. Schleich, *Sustainable Chemistry and Pharmacy*, **2017**, *5*, 72.
7. L. Pollegioni, E. Rosini, G. Molla, *Applied Microbiology and Biotechnology*, **2013**, *97(6)*, 2341.
8. H. Luo, H.M. Yu, Q. Li, Z.Y. Shen, *Enzyme and Microbial Technology*, **2004**, *25*, 514.
9. F. Lopez-Gallego, L. Batencor, A. Hidalgo, C. Mateo, R. Fernandez-Lafuente, J.M. Guisan, *Advanced Synthesis & Catalysis*, **2005**, *347*, 1804.
10. Q. Tan, Q. Song, D. Wei, *Enzyme and Microbial Technology*, **2006**, *39*, 1166.
11. G. Conti, L. Pollegioni, E. Rosini, *Catalysis Science & Technology*, **2015**, *5*, 1854.
12. V.K. Nigam, S. Kundu, P. Ghosh, *Applied Biochemistry and Biotechnology*, **2005**, *126*, 13.
13. V.C. Sonawane, *Critical Reviews in Biotechnology*, **2006**, *26*, 95.
14. L. Pollegioni, S. Lorenzi, E. Rosini, G.L. Marcone, G. Molla, R. Verga, W. Cabri, M.S. Pilone, *Protein Science*, **2005**, *14*, 3064.

15. D. W.Hardianto, B. Isdiyono, F.X. Ivan, *Indonesia Journal of Biotechnology and Biosciences*, **2016**, *3*, 89.
16. F.M. Huber, P.R. Chauvette, B.G. Jackson, "Cephalosporins and penicillins: Chemistry and Biology", Academic Press, New York, **1972**.
17. A.C. Ghosh, R.K. Mathur, N.N. Dutta, *Advances in Biochemical Engineering / Biotechnology*, **1997**, *56*, 111.
18. M.M. Bora, N.N. Dutta, K.G. Bhattacharya, *Journal of Chemical & Engineering Data*, **1998**, *43*, 318.
19. W.Q. Guo, H.S. Zheng, S. Li, J.S. Du, X.C. Feng, R.L. Yin, Q.L. Wu, N.Q. Ren, J.S. Chang, *Bioresource Technology*, **2016**, *221*, 284.
20. G.C. Sahoo, A.C. Ghosh, N.N. Dutta, R.K. Mathur, *Journal of Membrane Science*, **1996**, *112*, 147.
21. D. Cascaval, L. Kloetzer, A.I. Galaction, *Journal of Chemical & Engineering Data*, **2011**, *56(6)*, 2521.
22. M.M. Bora, N.N. Dutta, K.G. Bhattacharya, *Chemical Engineering Communications*, **2000**, *179*, 15.
23. M.M. Bora, S. Borthakur, P.G. Rao, N.N. Dutta, *Chemical Engineering and Processing*, **2008**, *47*, 1.
24. D. Cascaval, M. Postaru, A.I. Galaction, L. Kloetzer, A.C. Blaga, *Industrial & Engineering Chemistry Research*, **2013**, *52*, 2685.
25. A.C. Ghosh, S. Borthakur, M.K. Roy, N.N. Dutta, *Separations Technology*, **1995**, *5*, 121.

STUDIA UBB CHEMIA, LXIV, 2,Tom I, 2019 (p. 101-110)
(RECOMMENDED CITATION)
DOI:10.24193/subbchem.2019.2.09

Dedicated to Professor Florin Dan Irimie on the Occasion of His 65th Anniversary

ENHANCED HETEROLOGOUS EXPRESSION IN *E.COLI*

KATALIN NAGY[a], ZITA KOVÁCS[b], PÁL SALAMON[b], CSONGOR-KÁLMÁN ORBÁN[c,*], SZABOLCS LÁNYI[b,c], BEÁTA ALBERT[a,c]

ABSTRACT. Apoptotic regulation has been implicated in many human diseases, including cancer, autoimmune disease, inflammation and neuro degradation. Mapping up critical apoptosis regulators is a strategy for the development of new therapies [1, 2].

Present work highlights optimization of heterologous expression conditions for the X-linked inhibitor of apoptosis protein (XIAP). Genes of target protein containing pGEX-4T vector was transformed in chemically competent *E. coli* Rosetta™(DE3)pLysS cells. The recombinant construct contained a glutathione S-transferase (GST) fusion partner, which assured the purification of the protein by affinity chromatography. In the next step we examined the growth dynamics of the expression culture in M9 minimal medium, meanwhile we also determined the appropriate time of induction. Following this we carried out the optimization of expression, examining the expression's effectiveness under different conditions. On the basis of these fermentation experiments the target protein expression was the most prominent at 18 °C with 0.2 mM IPTG induction for 12 hours. During large scale fermentation experiments, we followed the optical density (OD), dry cell weight and substrate utilization. Finally, recombinant protein expression inhancement in the presence of 3% ethanol was successfully achieved in bioreactor. In this case the target protein was expressed in inclusion bodies, therefore solubilisation and refolding is necessary.

Keywords: *XIAP, heterologous expression, optimization, bioreactor, ethanol*

[a] *University POLITEHNICA of Bucharest, Faculty of Applied Chemistry and Materials Science, Str. Gh. Polizu, Nr. 1-7, Sector 1, 011061 Bucuresti, Romania*

[b] *University of Pécs, Faculty of Sciences, Ifjúság útja 6., 7624 Pécs, Hungary*

[c] *SAPIENTIA Hungarian University of Transylvania, Faculty of Economics, Socio-Human Sciences and Engineering, Department of Bioengineering, 1 Libertatii Square, RO-530104, Miercurea Ciuc, Romania*

**Corresponding author: orbancsongor@uni.sapientia.ro*

INTRODUCTION

Biologically active human proteins are useful for studying the biological functions of genes in different disease, for the development of therapeutic drugs and biomaterials in biotechnology industry [1].

In multicellular organism, apoptosis –genetically programmed cell death– is an ordinary and important process. Apoptotic regulation has been implicated in cancer. About 7 million people die from cancer-related cases per year, and it is estimated that there will be more than 16 million new cancer cases every year by 2020 [3].

The inhibitor of apoptosis proteins (IAPs) contains approximately 70 amino acid motifs termed baculovirus IAP repeat domains (BIR) [4]. Human X-linked inhibitor of apoptosis protein (XIAP), contains 3 BIR domains in the N-terminal region, a RING domain and UBA domain. The BIR1 domain interacts with TAK1 (TGFβ-activated kinase) and TAB1 (TAK1 binding protein 1) [5]. The BIR2 domain mediates interaction of XIAP's with active caspase-3 and -7 [6]. The BIR3 domain binds to procaspase-9 [7]. Beside BIR domains, XIAP contains an UBA domain, which mediates association with mono- and polyubiquitin chains [8]. The RING domain (zinc finger domain) confers E3 ubiquitin ligase activity [9].The IAP family member's cIAP1 and cIAP2 have an architecture similar to XIAP. As the most potent caspase inhibitors in IAP family, XIAP binds to and thus inhibits caspases in the initiation (caspase-9) and execution (caspase-3 and-7) phases of apoptosis. The inhibitory function of XIAP is antagonized by Smac-DIABLO (second mitochondria-derived activator of caspases–direct IAP binding protein with low pI).

According to literature, high levels of XIAP have been found in several cancer cell lines. The physiological amount of Smac-DIABLO released from the mitochondria may not be sufficient to overcome the inhibitory effect of XIAP on the caspases, thus preventing apoptosis [10]. Inactivation of overexpressed XIAP by Smac mimetic molecules may relieve caspase binding, thereby promoting apoptosis in malignant cells[11][12].

Nowadays, many therapeutic proteins and peptides are produced by biosynthesis. Insertion of the gene in the heterologous host is performed by recombinant techniques. In literature many reviews have covered the heterologous expression systems with great detail [13] [14]. In practice, planning an expression and carrying out it seems difficult. Many factors and circumstances need to be considered during expression planning. First of all, we need to examine ways to isolate gene of interests. Planning an expression system include the following factors: choosing the appropriate and well-functioning expression plasmid (vector), choosing the convenient organism for expression, troubleshooting the recombinant protein production, purification and structural analysis. *E. coli* expression system remain to be the preferred system for laboratory investigations and initial development in

commercial activities because is a well-established host with short culturing time and easy genetic manipulation. Within *E. coli* expression, the T7 system is the most popular approach for producing proteins. In this system, an expression vector containing a gene of interest cloned downstream of the T7 promoter is introduced into a T7 expression host.

The GST fusion system can be characterized as a versatile expression system. Expression is under the control of the *tac* promoter and a repressor protein transcribed by *lacI*^{q} gene, thus maintaining tight control over expression of the insert. Promoter is the key component of an expression system because of its role in controlling the transcription initiation. An ideal promoter is strong enough to allow product accumulation up to 50% of the total cellular proteins, and is tightly regulated to prevent product toxicity. As a very strong hybrid promoter, *tac* promoter consists of the -35 region of the *trp* (tryptophan) promoter and the -10 region of the *lac* promoter. The GST fusion proteins can be purified from bacterial lysates by affinity chromatography using immobilized glutathione.

Enhancing recombinant protein expression level in most cases is limited. We found studies with the goal to develop food-grade expression systems by eliminating antibiotic selection markers [15]. These expression systems proved to be biosafe and also substantially increase final recombinant protein yields. Another possibility for improvement expression is secretion. For example, Shruti and coworkers developed a novel signal peptide sblggt (native signal of Bacillus licheniformis ER15 ggt gene) recognized and cleaved by signal peptidases of *E. coli BL21 (DE3)* cells which allowed high secretion to medium [16].

In our research we have used various molecular strategies to express XIAP in pGEX-4T expression system by optimizing various parameters such as, cultivation temperature, inducer concentrations, cell growth, and use of additives in culture medium. Gaurav and co-workers investigated ethanol, as an additive in culture medium [17]. Based on their results, ethanol proved to be efficient additive to increase protein expression in *E. coli*.

RESULTS AND DISCUSSION

Determination of cell culture growth parameters

The unlimited growth of a bacterial population has an exponential nature, with cells doubling after generation time. In a closed culture vessel, the exponential growth of the bacteria cannot continue indefinitely, as no fresh medium is added to the culture during the cultivation, the nutrient concentration is continuously decreasing and thus the number of cells over time can be divided into characteristic phases. Representing different stages of growth as a function of time gives the growth curve of bacterial populations.

Heterologous expression is characterized by de novo fermentation, which can be divided into two phases. If protein production is intracellular, the amount of target protein is directly proportional to the amount of biomass, consequently first phase is biomass formation. Thereafter, induction of the cells results in the expression of the protein. For sensitive heterologous proteins, it is necessary to optimize expression conditions to achieve higher yields.

At this stage of our research the growth of the cell culture was examined in the interest of determine optimal cell density for induction. The cell growth media is chemically well-defined nutrient solution (M9 minimal medium), in which bacterial metabolism is different compared to a most commonly used (Luria-Bertani broth) medium.

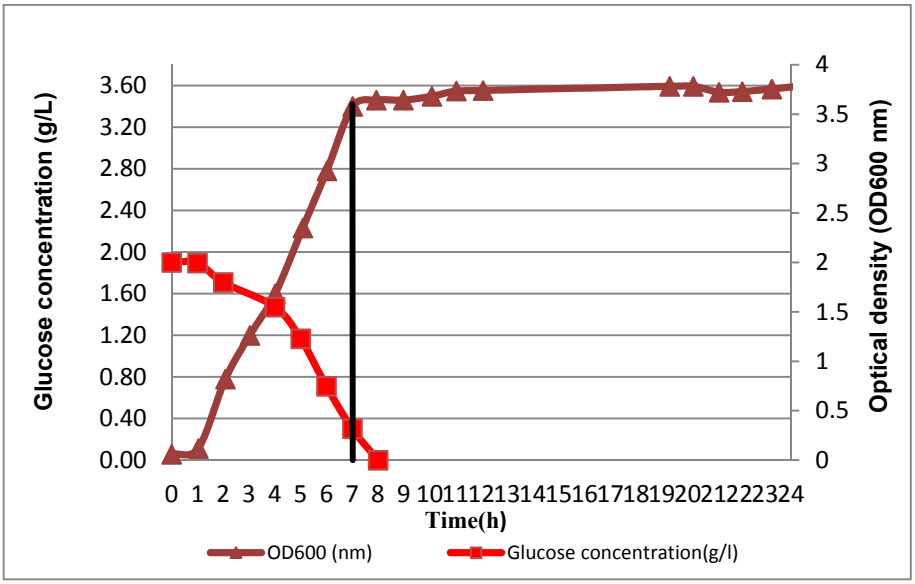

Figure 1. *E. coli Rosetta™(DE3)pLysS* growth curve

According to our experiments, cell culture growth is characterized: 1 hour passed from an adaptive phase (lag phase) to an exponential phase that lasted for 7 hours, then the metabolism of the cells slowed down, their growth stopped and entered a stationary phase. The glucose concentration from the samples was determined by HPLC on CARBOSep COREGEL 87H3 column. If we examine the glucose concentration in the exponential phase we can declare that between the first and the seventh hour, the average glucose depletion rate is 0.278 g/h.

Since glucose concentration reached 0.317 g/mL at the 7th hour, and then cells were transferred to the stationary phase, it can be assumed that this low glucose concentration results in reduced cellular metabolism.

The specific growth rate of cell culture was calculated using the optical density values, and the Monod model was used for the calculation (0.304 h^{-1}). Conditions for selecting the induction time are as follows: primarily, the cell culture should be in an exponential phase, since the metabolism of the cells is set for self-replication and not for survival.

By examining the growth curve and the glucose depletion rate, we decided to induce the cell culture at OD_{600} = 1.5, because the broth contains plenty of glucose and is in the exponential phase of cell culture.

Optimization of XIAP protein expression

Results about shake flask expression in M9 minimal medium induced with different final concentrations of IPTG are summarized in this section. Samples taken every 3-3 hours in the interest of determine target protein concentration were investigated by SDS-PAGE analysis. These samples from whole cells were too small amount to pass through a purification phase. Our results are shown in the figures below.

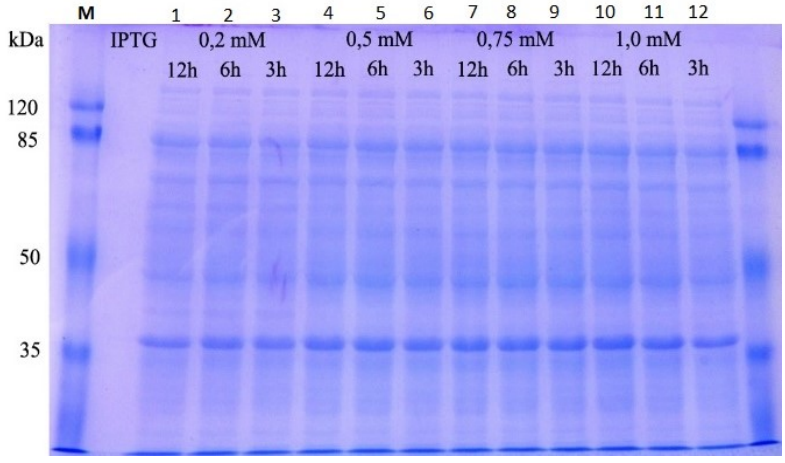

Figure 2. 10% SDS-PAGE gel analysis of expressed XIAP-GST at 37 °C.Protein samples were separated by 10% SDS-PAGE and stained with CBB. (M)-PageRuler^{TM} Prestained NIR Protein Ladder, (molecular weight marker from Thermo Scientific^{TM}); (1)-0.2 mM IPTG induction-12h; (2)-0.2 mM IPTG induction-6h; (3)-0.2 mM IPTG induction-3h; (4)-0.5 mM IPTG induction-12h; (5)-0.5 mM IPTG induction-6h; (6)-0.5 mM IPTG induction-3h; (7)-0.75 mM IPTG induction-12h; (8)-0.75 mM IPTG induction-6h; (9)-0.75 mM IPTG induction-3h; (10)-1.0 mM IPTG induction-12h; (11)-1.0 mM IPTG induction-6h; (12)-1.0 mM IPTG induction-3h.

Figures 2. and 3. shows expression level of XIAP at 18 and 37 °C, varying IPTG concentration and incubation time. XIAP is a 53 kDa (http://media.cellsignal.com/pdf/2042.pdf) sized protein and with GST it has 78 kDa. It is observed that proteins were produced only at 18 °C for 12 hours. We can observe differences at concentration of inducer. Unfortunately, the target proteins were expressed in inclusion bodies. In conclusion we declare no protein expression were observed at 37 °C.

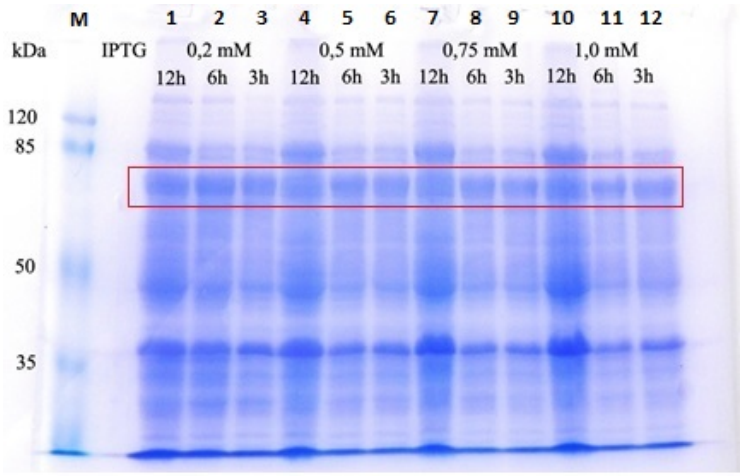

Figure 3. 10% SDS-PAGE gel analysis of expressed XIAP-GST at 18 °C.Protein samples were separated by 10% SDS-PAGE and stained with CBB. (M)-PageRuler^{TM} Prestained NIR Protein Ladder, (molecular weight marker from Thermo Scientific^{TM}); (1)- 0.2 mM IPTG induction-12h (2)-0.2 mM IPTG induction- 6h; (3)-0.2 mM IPTG induction- 3h; (4)- 0.5 mM IPTG induction-12h; (5)- 0.5 mM IPTG induction-6h; (6)-0.5 mM IPTG induction-3h; (7)-0.75 mM IPTG induction-12h; (8)-0.75 mM IPTG induction-6h; (9)-0.75 mM IPTG induction-3h; (10)-1.0 mM IPTG induction-12h; (11)-1.0 mM IPTG induction-6h; (12)-1.0 mM IPTG induction-3h.

Considering the cell growth over expression (Table 1), a slight difference is observed in optical density increase, as the concentration of IPTG increases, the optical density decreases.

Table 1. Changes in optical density of cell culture during XIAP expression at 18 and 37 °C

XIAP/18°C	**0,2 mM**	**0,5 mM**	**0,75 mM**	**1,0 mM**
3 h	0,68	0,768	0,712	0,712
12 h	2,736	2,656	2,544	2,488
XIAP/37°C	**0,2 mM**	**0,5 mM**	**0,75 mM**	**1,0 mM**
3 h	0,712	0,704	0,792	0,76
12 h	1,664	1,264	1,152	1,112

As a result of over-expression, the induction causes the protein production to start and the proteins to poison the cells.

Finally, it can be concluded that the protein expression in bioreactor should be performed at 18 °C for 12 hours with 0.2 mM IPTG inducer concentration.

Enhanced expression of human recombinant XIAP protein in bioreactor

To ensure high-yield production of target protein, a bioreactor system was used for cultivation of transformed expression strains under controlled process parameters offering the possibility to obtain high biomass levels, and consequently, high protein production rates.

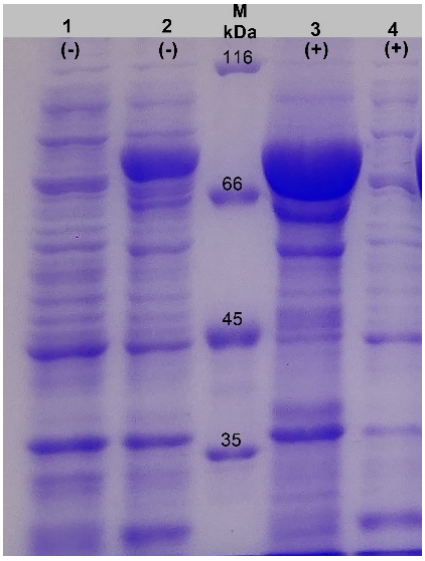

Figure 4. 10% SDS-PAGE gel analysis of increased XIAP production. Protein samples were separated by 10% SDS-PAGE and stained with CBB.(1)-supernatant after cell disruption in absence of ethanol (-); (2)-pellet after cell disruption in absence of ethanol I (-); (M)-peqGold Prestained protein marker I. (molecular weight marker from VWR); (3)-pellet after cell disruption in presence of ethanol (+); (4)-supernatant after cell disruption in presence of ethanol (+)

To enhance the expression, and increase the production of recombinant protein, the feed broth contained 3% ethyl alcohol. The amount of recombinant protein expression was increased 8.55 fold, but also in this case the proteins were expressed in inclusion bodies. Expression of recombinant proteins in *E. coli* under ethanol treatment is a unique technique. Ethanol can affect the cellular environment including membrane fluidity, membrane transport, membrane lipid composition and also the assembly of membrane proteins.

DNA replication is a membrane associated phenomena therefore it is affected by ethanol concentration. Among future plans we'll design appropriate solubilization and refolding of XIAP from inclusion body.

CONCLUSIONS

In the current phase of our research we proved a successful expression procedure for biosynthesis of XIAP. Firstly, expression conditions were optimized successful, and also investigation of expression in bioreactor was effective. The best expression level was achieved at the following parameters: 0.2 mM IPTG, 18 °C, and 12 hours.

The 3% ethyl alcohol used to increase the production of recombinant protein was able to increase protein levels, but unfortunately in inclusion bodies, therefore solubilisation and refolding are necessary steps towards protein purification.

EXPERIMENTAL SECTION

All chemicals, bacterial growth media used for our experiments were purchased from commercial sources (*Sigma Aldrich, Merck, BioLabs and Thermo scientific*). Bacterial strains were also obtained from commerce (*AddGene, BioZyme*).

Investigation of cell culture growth parameters

Our goal was to determine the optimal point for induction on the exponential phase of cell growth, as a function of substrate concentrations. We measured the optical density of cell culture and concentration change of glucose during fermentation. To determine the growth curve, we prepared the inoculum as a first step. 100 µl of the transformed stock of *E. coli* Rosetta™(DE3)pLysS was inoculated into 10 ml of Ampicillin-containing LB medium in 50 ml centrifuge tubes and incubated for 4 hours at 37 °C. In a second step, the pre-culture was inoculated into a 500 ml Erlenmeyer flask containing 200 ml M9 minimal medium and then incubated at 37 °C, 250 rpm. 1 ml of sample was taken per hour and the optical density (OD) was measured at 600 nm. 1 ml of sample was centrifuged at 10,000 rpm for 10 minutes and the supernatant stored in a refrigerator for subsequent glucose measurement. The growth of the bacterium was monitored in triple repetitions for 18 hours. Components of M9 minimal medium are the followings: Na_2HPO_4 (3,548 g/L), KH_2PO_4 (3,401 g/L), NaCl (0.5 g/L), $(NH_4)_2SO_4$ (2 g/L), $C_6H_{12}O_6$ (2 g/L), $MgSO_4$ (2 mM), $CaCl_2$ (0,02 mM), Trace elements(1x), Antibiotic (Ampicillin,100 µg/mL).

Optimization of XIAP heterologous expression

Optimization of heterologous expression of XIAP was investigated in *E. coli* Rosetta™(DE3)pLysS cell line at different temperatures, with 0.2-1 mM IPTG inducer concentrations for 12 hours. The expression of XIAP protein was investigated using the following methods at 37 °C. At first, we prepared the inoculum: *E. coli* Rosetta™(DE3)pLysS with pGEX-4T-XIAP transformed cells were inoculated into 8x10 mL LB-Ampicillin broth and incubated in shaking incubator (250 rpm) at 37 °C for 4 hours. Thereafter, 100 µl of the preculture in LB broth was transferred to 8 sterile centrifuge tubes containing 10-10 ml of M9 minimal medium and incubated in shaking incubator (250 rpm) at 37 °C.

The cell density was measured hourly. When it reached OD_{600}=1.5, the protein expression was induced with isopropyl-thiogalactopyranoside (IPTG) at various concentration (0.2 mM, 0.5 mM, 0.75 mM, 1 mM). After 3, 6 and 12 hours, 1-1 ml of sample was taken, centrifuged at 10,000 rpm, 10 min, the supernatant was discarded and lysis buffer (50 mM Tris-HCl (pH 7,5), 250 mM NaCl, 2 mM DTT, 1 mM PMSF, protease inhibitor cocktail) was added to the pellet-containing tubes, diluted to OD_{600}=1.5, wherewith was resuspended. 2X Laemmli Sample buffer was added to the tubes and placed in incubator with 98 ℃ for 10 minutes. After the incubation time, the cells were sonicated, then centrifuged and assayed by SDS-PAGE gel electrophoresis. Following this process, next experiment was performed at 18 °C using the same procedure.

Expression of human recombinant XIAP protein in bioreactor

Recombinant protein production was carried out in a 1 L capacity Sartorius Biostat®A Plus Bioreactor, using BioPAT ® MFCS/DA Supervisory Control and Data Acquisition (SCADA) Software. The reactor was firstly loaded with 0.7 L basic M9 minimal medium. The system was autoclaved for 20 minutes at 120 °C, in order to ensure sterility. After sterilization, the reactor was connected to aeration, acid and base solutions, temperature control system and control unit. After the reactor has cooled down (40 ºC), thermally unstable compounds were added through a sterile filter (0.25 µm). In order to homogenize the system, mixing, temperature, and pH control were launched: 400 RPM, 37 ºC, pH 6.9. After the stabilization of the reactor, the media was inoculated under sterile conditions with 15 mL inoculum. The culture at this stage was grown at 37 °C, with a dissolved oxygen level above 40%, and pH 6.9. When the cell density reached OD_{600}=8, the temperature was set to 18 ºC and the protein expression was induced with isopropyl-thiogalactopyranoside (IPTG) (0.2 mM final concentration). Protein expression was carried out at 18 ºC, O.N. (12 hours).

In order to harvest the cells, 0.7 L culture was centrifuged (12,000xg for 10 min at 4 ºC), and the cell pellets were stored at -80 °C until further processing (Thermo Scientific FORM 88000 series).

Cell lysis was performed as follows: 1 gram of cells were resuspended in 5 mL of lysis buffer (50 mM Tris-HCl (pH 8), 150 mM NaCl, 2 mM DTT, 1 mM PMSF, 1x protease inhibitor cocktail). Cell disruption was performed with a Microfluidizer LM10, in order to increase the efficiency, the micro-flight compression was performed twice. The resulting cell extract was centrifuged at 4 ºC, 60,000xg, for 60 minutes in order to separate the solubilized proteins from cellular debris.

For quantification of expressed XIAP recombinant protein we used GelQuant, NET software provided by biochemlabsolutions.com.

ACKNOWLEDGMENTS

The research work was supported by the project: Controlul funcţiilor celulelor dendritice cu semnale anti-inflamatoare şi de moarte celulară- DCFANS (Code Project: PN-II-PT-PCCA-2013-4; Financing: Cerere de finanţare Proiecte Colaborative de Cercetare Aplicativă).

REFERENCES

1. S. Nagata, *Annu. Rev. Immunol.*, **2018**, 36, 489-517.
2. A.C. West, B.P. Martin, D.A. Andrews, S.J. Hogg, A. Banerjee, G. Grigoriadis, R. W. Johnstone, and J. Shortt, *Oncogenesis*, **2016**, 5, 1-6.
3. R. Hammami and I. Fliss, *Drug Discov. Today*, **2010**,15, 540–546.
4. K. Welsh, D. Finlay, R.J. Ardecky, S. Reddy, M. González-lo, Y. Su, P. Teriete, P.D. Mace, S.J. Riedl, K. Vuori, J.C. Reed, and N.D.P. Cosford, *Bioorg. & Med. Chem lett.*, **2011**, 21, 4332–4336.
5. R. Hofer-warbinek, J.A. Schmid, C. Stehlik, B.R. Binder, J. Lipp, and R. De Martin, *JBC,* **2000**, 275, 22064–22068.
6. Y. Suzuki, Y. Nakabayashi, K. Nakata, J.C. Reed, and R. Takahashi, *JBC*, **2001**, 276, 27058–27063.
7. E.N. Shiozaki, J. Chai, D.J. Rigotti, S.J. Riedl, P. Li, S.M. Srinivasula, E.S. Alnemri, R. Fairman, and Y. Shi, *Mol. Cell*, **2003**, 11, 519–527.
8. M. Gyrd-Hansen, M. Darding, M. Miasari, M.M. Santoro, L. Zender, W. Xue, T. Tenev, P.C.A. Fonseca, M. Zvelebil, J.M. Bujnicki, S. Lowe, J. Silke, and P. Meier, *Nat Cell Biol.*, **2008**, 10, 1309-1317.
9. D.L. Vaux, J. Silke, T. Walter, and E. Hall, *Nat. Rev. Mol. Cell Biol.*, **2005**, 6, 287-297.
10. E. Mastrangelo, F. Cossu, M. Milani, G. Sorrentino, D. Lecis, D. Delia, L. Manzoni, C. Drago, P. Seneci, C. Scolastico, V. Rizzo, and M. Bolognesi, *J. Mol. Biol.*, **2008**, 384, 673–689.
11. S. Fulda, Clin. *Cancer Res.*, **2015**, 21, 5030–5037.
12. S.W. Haiying Sun, Zaneta Nikolovska-Coleska, Chao-Yie Yang, Dongguang Qian, Jianfeng Lu, Su Qiu, Longchuan Bai, Yuefeng Peng, Qian Cai, *Acc. Chem. Res.*, **2009**, 41, 1264–1277.
13. R. Chen, *Biotechnol. Adv.*, **2012**, 30, 1102–1107.
14. G.L. Rosano and E. A. Ceccarelli, *Front. Microbiol*, **2014**, 5, 1–17.
15. P.H. Oliveira and J. Mairhofer, *Trends Biotechnol.*, **2013**, 31, 539–547.
16. S. Bindal, V.K. Dagar, M. Saini, Y. P. Khasa, and R. Gupta, *Enzyme Microb. Technol.*, **2018,** 116, 23-32.
17. J. Kaur, A. Kumar, and J. Kaur, *Int. J. Biol. Macromol.*, **2018**, 106, 803–822.

STUDIA UBB CHEMIA, LXIV, 2,Tom I, 2019 (p. 111-126)
(RECOMMENDED CITATION)
DOI:10.24193/subbchem.2019.2.10

Dedicated to Professor Florin Dan Irimie on the Occasion of His 65th Anniversary

ANTHOCYANINS, CAROTENOIDS AND ANTIOXIDANT ACTIVITY OF COLOURED COMMERCIALLY AVAILABLE JUICES

ANDREA BUNEA[a], SANDA ANDREI[a,*], CRISTINA EL-MAHDI[b], ALINA CUCERDEAN[c], FLORIN DUMITRU BORA[d], ZORITA DIACONEASA[a], ADELA PINTEA[a]

ABSTRACT. The phytochemical composition of apple, cranberry, pomegranate, carrot, and beetroot juices was determined in terms of carotenoids, anthocyanins, betalains and ascorbic acid concentration. Antioxidant potential of these beverages was also assessed using the colorimetric DPPH radical scavenging assay. The results showed that pasteurized and unpasteurized carrot and apple juices contain significant amount of *β*-carotene and *cis*-*β*-carotene. High total betalain content was observed in beetroot juice. Major anthocyanins detected in cranberry and pomegranate juices were glycosides of cyanidin, malvidin, and delphinidin. Notable ascorbic acid content and antioxidant potential were observed in unprocessed carrot juices, while beetroot juice exhibited the highest percentage of free radical inhibition.

Keywords: *juices, ascorbic acid, carotenoids, anthocyanins, antioxidant activity*

[a] *Department of Biochemistry, University of Agricultural Sciences and Veterinary Medicine, Cluj-Napoca*
[b] *Department of Fundamental Science, University of Agricultural Sciences and Veterinary Medicine, Cluj-Napoca*
[c] *Agrico Research, Bant, Holand*
[d] *Department of Physico-Chemistry and Biochemistry, Research Station for Viticulture and Enology Târgu Bujor*
**Corresponding author: sandrei@usamvcluj.ro*

INTRODUCTION

A growing interest in consumption of fruits and vegetables has been recently observed, due to their nutritional and medicinal value. This effectiveness is thought to be mainly related to bioactive compounds present in the plants, such as carotenoids, betalains, anthocyanins, flavonoids, and ascorbic acid.

In the last few years, many reviews were published focusing on the chemistry, bioavailability, and health and nutrition benefits of carotenoids [1, 2]. So far the most analyzed and studied carotenoids are *β*-carotene, lutein, and zeaxanthin. *β*-carotene has high provitamin A activity, while lutein and zeaxanthin play an important role in the prevention of several blinding disorders by absorbing blue light that enters the human eye [3]. Carrots are the most important source of *β*-carotene in the diet, along with green leafy vegetables. Betanin, the most abundant betacyanin pigment in beetroot, have been found to have great antioxidant activity and it is also effective in preventing lipid peroxidation [4]. Other class of phenolic compounds found in fruits, berries or vegetable are anthocyanins. From chemical point of view, they are glycosides of anthocyanidins and it is currently thought that only the following six are of relevance to the human diet (cyanidin, delphinidin, malvidin, pelargonidin, peonidin, petunidin) [5].

Several observational and randomized controlled studies demonstrated that fruit-based diets are important factor for reducing the burden of non-communicable diseases. Diets rich in anthocyanins promote the lowering of cardiovascular disease and are promising candidates in developing anti-obesity therapies [5, 6]. They also bear anti-inflammatory and antimicrobial properties, limit the oxidative stress, and contribute to cellular signaling by interacting with a wide spectrum of molecular targets [7, 8].

Low plasma ascorbic acid content is associated with increased risk of stroke, especially among hypertensive and overweight men aged 42-60 years [9]. Moreover, ascorbic acid is a promising anti-cancer agent [10] and is likely to reduce the risk of coronary heart disease [11].

Beetroot juice protect against cold symptoms in health during periods of psychological stress and suggest particular benefits in asthma [12]. Cranberry based products bear high antioxidant and antiradical properties [13] and might improve augmentation index in obese men [20]. Clinical trials have demonstrated that pomegranate juice has benefit effect on polycystic ovarian syndrome [14], blood pressure and lipid profile [15, 16], and increases glutathione activity reducing lipid and protein oxidation [17]. Pomegranate is also important in nanotechnology for biosynthesizing different nanoparticles [18].

Composition, bioavailability, and antioxidant activity of phytochemicals are significantly influenced by plant processing and other post-harvest technologies [19-24]. Thus, these steps should be designed with caution in order to preserve or enhance the quality of products. When fruits and vegetables are made into fresh-squeezed juices, several bacteria might be present in the final product. Pasteurization is the most common way to remove bacteria and other potentially harmful microorganisms [25], however, it usually leads to degradation of biologically active compounds. Ultrasound treatment might be a reliable, innovative alternative of pasteurization that could effectively improve the health-related compounds and other quality parameters of fruit juices [26-30].

Herein, we assessed the carotenoid content of several, unpasteurized and pasteurized carrot and apple juices and anthocyanins respectively betalains content of commercially available beetroot, cranberry, and pomegranate juices. Ascorbic acid content was evaluated using titrimetric method and antioxidant potential of the samples were determined through spectrophotometric methods.

RESULTS AND DISCUSSION

Carotenoid content of the carrot and apple juices

Carotenoids were extracted, underwent a saponification process and were separated and analyzed by HPLC (**Figure 1** and Experimental section). In all tested samples, *β*-carotene and *cis*-*β*-carotene were identified as the major carotene compounds (**Table 1**). In accordance with the literature data [2], significantly higher concentrations of total carotenoids were observed in carrot juice samples as compared to apple juices. More surprisingly, no carotenoid compound was identified in commercial apple juice.

Similar concentrations of total carotenoids were obtained in samples of the same species (50.00–54.00 mg/100g in carrot samples, 24.00 mg/100g and 29.00 mg/100g in apple samples) (**Table 1**). Apparently, pasteurization process has no significant adverse effect on the total carotenoid concentration in carrot and apple samples, but it might induce or accelerate several isomerization reactions. Naturally, *β*-carotene is found as all-*trans* isomers in plants. However, these isomers are very unstable and can easily undergo transformation into *cis*-isomers when exposed to heat and light [31]. It has been demonstrated that commercial carrot juices might contain from 4% to 17% *cis*-*β*-carotene [32]. Marx et al have also revealed that 13-*cis*-β-carotene was formed during the pasteurization and sterilization of carrot juice [25]. Similar conclusions were obtained by Chen et al, who reported 62.5 μg/mL *β*-carotene together with 1.1– 3.4 μg/mL *cis*-isomer for untreated carrot juice.

When different pasteurization conditions were applied (temperature up to 121°C), the *β*-carotene content decreased steadily along with increasing temperature and heating time, while *cis*-isomers increased significantly [33]. In accordance with these findings, we also observed higher *cis*-*β*-carotene concentrations in all tested sample as compared to *β*-carotene content.

Nevertheless, significant (P <0.05) increases in total carotenoids were observed in thermo-sonicated carrot and apple juices as compared to non-sonicated samples (1.37 and 1.55 µg/mL, respectively, compared to 1.22 µg/mL) [29, 34].

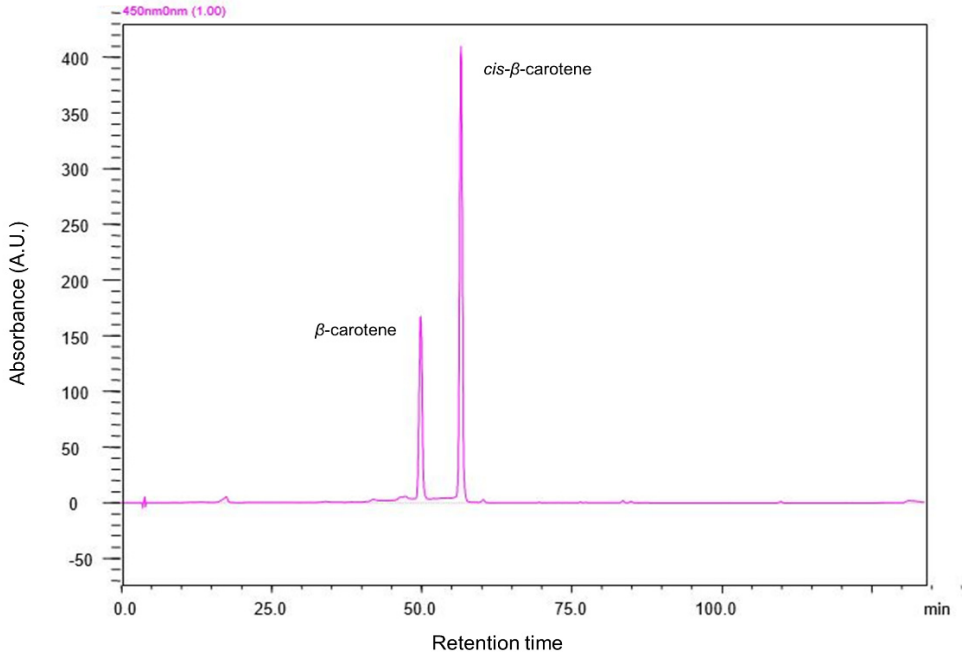

Figure 1. Carotenoids separation for saponified sample of unfiltered carrot juice

Table 1. Carotenoid content of carrot and apple juices

Sample	Total carotenoids (±SD) mg/100g	*β*-Carotene mg/100g	*cis*-*β*-Carotene mg/100g
Unfiltered carrot juice	54.00±6.34[a]	16.74	37.26
Pasteurized carrot juice	50.00±5.22[a]	15.5	34.5
Unpasteurized carrot juice	53.40±4.13[a]	16.55	36.84
Commercial apple juice	–	–	–
Pasteurized apple juice	24.00±3.56[b]	7.44	16.56
Unpasteurized apple juice	29.00±2.87[b]	8.99	20.01

SD, standard deviation. Different letters within a column denote significant differences (P<0.05).

Anthocyanins content of red juices

Anthocyanins from beetroot, cranberry, and pomegranate juices were extracted with acidified methanol and further analyzed by HPLC-DAD or HPLC-ESI-MS techniques (**Figure 2** and Experimental Section).

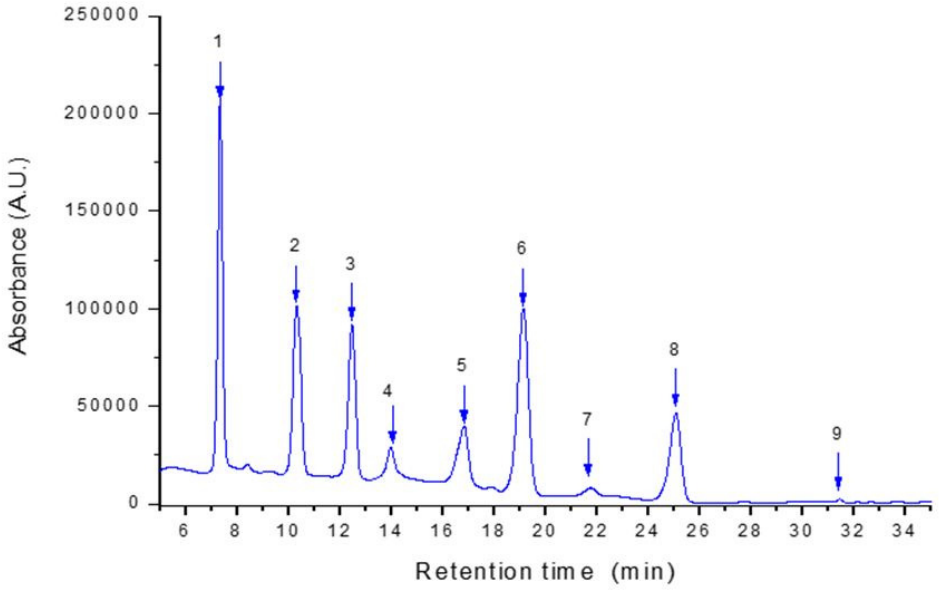

Figure 2. Illustrative HPLC chromatogram of the anthocyanins from cranberry juice. Peak assigment: 1. delphinidin 3-*O*-galactoside; 2. delphinidin 3-O-glucoside; 3. cyanidin 3-*O*-galactoside; 4. delphinidin 3-*O*-arabinoside; 5. cyanidin 3-*O*-glucoside; 6. petunidin 3-*O*-galactoside; 7. cyanidin 3-O-arabinoside; 8. peonidin-3-*O*-galactoside; 9. petunidin 3-*O*-arabinoside

In beetroot juice, betanin and isobetanin were identified as the major components (>80% of total concentration). Betanidin and neo-betanidin-5-glucoside were also detected (**Table 2**). These findings are in accordance with those reported in other studies [35]. In red beet concentrate, betanin and isobetanin were detected in similar quantity (40.6% and 40.2%, respectively of total betalains), while betanidin yielded 8.4% and neo-betadinin-5-glucoside 3.9% [36]. The two latter compounds are likely to result from thermal degradation of beetroot juice [37].

Total betacyanin content obtained in this study was 656.21 mg/100 mL. Wruss et al determined the total betalain content of beetroot juices prepared from 7 varieties. They results shows concentrations which varied between 789 mg/L and 1309 mg/L, approximately 60% being betacyanins [38].

In cranberry juice, a total of 9 anthocyanins were identified (**Table 2**). Delphinidin 3-*O*-galactoside was identified in the highest concentration (24.63 mg/100mL), followed by petunidin 3-*O*-galactoside, delphinidin 3-*O*-glucoside, and cyanidin3-*O*-galactoside (17.28 mg/100mL, 16.83 mg/100mL, and 14.68 mg/100mL, respectively). Amongst peonidin derivatives, peonidin 3-*O*-galactoside was found in relatively high amount (8.73 mg/100mL). Previous studies conducted on cranberry extracts reported glycosylated cyanidins and their derivatives (peonidins) as one of the most prevalent anthocyanins [23, 39, 40].

In terms of sugar moieties attached to aglycone, galactosides were predominant in our samples, followed by glucosides (expect for peonidin and petunidin moieties, where glucosides were not detected) (**Table 2**). This might be explained with the stability of anthocyanins. When changes in anthocyanin content were evaluated throughout juice processing, it has been demonstrated that anthocyanin stability is determined by the type of sugar attached to aglycones. The order of anthocyanin stability during pasteurization was glucosides> galactosides> arabinosides [41].

Available literature data on the total anthocyanin content of cranberries are heterogeneous. Herein, we detected 99.23 mg/100mL total anthocyanin. Other researchers reported 18.8 mg/100mL [42] or 11.36 mg/L [43] total anthocyanins in cranberry juice and 725 nmol/g [39] or 117 mg/g [8] in cranberry extract.

The amount of total identified anthocyanin in pomegranate juice was 70.52 mg/100mL (**Table 2**). Mono- and diglucosides of delphinidins, cyanidins, and pelargonidins were identified at different quantity. Highest concentration was detected for cyanidin 3,5-*O*-diglucoside (31.25 mg/100mL, 44.31% of the total content). Significantly lower, but similar values were obtained for delphinidin 3,5-*O*-diglucoside and cyanidin 3-*O*-glucoside. The total anthocyanins content reported in pomegranate cultivars ranged between 5.56 mg/100g and 30.11 mg/100g [44]. Though total anthocyanin content differs significantly among pomegranate varieties, the typical anthocyanin profile of pomegranate juice includes 3-*O*-glucoside and 3,5-*O*-diglucosides of delphinidin, cyanidin, and pelargonidin as major components [45-47]. Our findings are in accordance with these reports.

In freshly prepared juices of 15 Iranian pomegranate juices delphinidin 3,5-*O*-diglucoside, delphinidin 3-*O*-diglucoside, cyanidin 3,5-*O*-diglucoside, cyanidin 3-*O*-glucoside, pelargonidin 3,5-*O*-diglucoside, and pelargonidin 3-*O*-glucoside were identified [20]. Very similar results were obtained by Fabroni et al, cyanidin 3,5-*O*-diglucoside and cyanidin 3-*O*-glucoside accounting for more than 85% of total anthocyanins [48]. It is also known that anthocyanin content of pomegranate juice decreases upon thermal treatment. Non-thermal processing methods are used to maximize quality and enhance shelf stability of juices [27]. While the use of pulsed electric field did not alter [49], pasteurization

processes significantly influenced the anthocyanin content of the pomegranate juice [50-52]. As anthocyanins are also sensible to environmental conditions, juice composition might be changed during storage. The higher the storage temperature, the more pronounced is the anthocyanin degradation and polymeric color formation [53]. Additionally, diglucosides were demonstrated to be more stable than monoglucosides during storage.

Table 2. Betacyanin and anthocyanin content of red juices

Compound	Concentration* mg/100mL(±SD)	Percentage %
Beetroot juice		
Betanin	281.40±15.36[a]	42.88
Isobetanin	274.40±16.35[a]	41.81
Betanidin	43.19±1.25[b]	6.58
Neo-betanidin-5-glucoside	57.21±2.00[b]	8.71
Total	**656.21**	**100**
Cranberry juice		
Delphinidin 3-*O*-galactoside	24.63±0.94[a]	24.82
Delphinidin 3-*O*-glucoside	16.83±1.17[b]	16.96
Delphinidin 3-*O*-arabinoside	5.02±0.52[d]	5.05
Cyanidin 3-*O*-galactoside	14.68±0.48[b]	14.79
Cyanidin 3-*O*-glucoside	7.63±0.82[c]	7.68
Cyanidin 3-*O*-arabinoside	2.98±0.35[e]	3.00
Peonidin-3-*O*-galactoside	8.73±1.19[c]	8.79
Petunidin 3-*O*-galactoside	17.28±1.31[b]	17.41
Petunidin 3-*O*-arabinoside	1.45±0.40[e]	1.46
Total	**99.23**	**100**
Pomegranate juice		
Delphinidin 3,5-*O*-diglucoside	19.3±6.07[b]	27.36
Delphinidin 3-*O*-glucoside	2.35±0.95[c]	3.33
Cyanidin 3,5-*O*-diglucoside	31.25±9.82[a]	44.31
Cyanidin 3-*O*-glucoside	12.32±2.56[b]	17.47
Pelargonidin 3-*O*-glucoside	5.30±1.10[c]	7.51
Total	**70.52**	**100**

SD, standard deviation. Different letters within a column denote significant differences ($P<0.05$). *values are mean of triplicate measurements.

Ascorbic acid content

The ascorbic acid concentrations of the analyzed samples are presented in **Table 3**. Of the yellow fruit juices, higher ascorbic acid contents were observed in carrot samples as compared to apple juice samples. No statistically significant differences were found among carrot samples and apple samples, respectively. However, pasteurization process is likely to negatively influence the ascorbic acid content of carrot juice (3.52 mg/100mL in unpasteurized versus 2.40 mg/100mL in pasteurized sample). Similar trend was not observed in apple juice samples.

Table 3. Ascorbic acid content of juices

Sample	Ascorbic acid (±SD) mg/100mL
Unfiltered carrot juice	3.50±0.86^{b}
Pasteurized carrot juice	2.40±0.92^{c}
Unpasteurized carrot juice	3.52±1.05^{b}
Commercial apple juice	2.11±0.71^{c}
Pasteurized apple juice	2.34±0.64^{c}
Unpasteurized apple juice	2.81±0.54^{c}
Beetroot juice	3.52±0.19^{b}
Cranberry juice	4.57±0.15^{a}
Pomegranate juice	2.11±0.08^{c}

SD. standard deviation. Different letters within a column denote significant differences ($P<0.05$).

Values detected in our study are slightly lower than those reported in literature. In a study analyzing the effect of branching and sonication on the ascorbic acid content of carrot juice, 6.36 mg/100mL ascorbic acid was reported in untreated juice, 4.31 mg/100 mL in water-blanched and 4.27 mg/100mL in acid-blanched juices. These values were significantly increased after submitting carrot juice to sonication (7.07 mg/100mL, 5.37 mg/100mL, and 5.56 mg/100mL, respectively) [30]. Sonication could recover the loss of ascorbic acid by the removal of dissolved oxygen that is a major cause of ascorbic acid degradation. Similarly, ascorbic acid from fresh apple juice was reported at a concentration of 5.27 mg/100mL [28] and 4.20 mg/mL [54], which were subsequently increased by sonication up to 6.07 and 5.63 mg/100 mL, respectively. It has also been demonstrated, that thermo-sonicated juices retain their ascorbic acid content up to 20 days [34]. In another study conducted at

Timisoara, remarkably higher amount of ascorbic acid has been reported for fresh-squeezed “Golden auriu” apple juice (7.02 mg/100g) and beetroot juice (33.84 mg/100g) compared to our results [55].

Amongst red juices, highest ascorbic acid concentration (4.57 mg/100mL) was obtained in cranberry juice, followed by beetroot (3.52 mg/100mL) and pomegranate (2.11 mg/100mL) juices (**Table 3**). In a study conducted by Borges et al, 1107 nmol/g ascorbic acid has been detected in cranberries [39]. In pomegranate juice prepared from halved fruit, ascorbic acid concentration was 500 µg ascorbic acid equivalent/mL [46].

Antioxidant activity

Highest radical scavenging activity was observed in unprocessed carrot juices (23 mg TE/100g in unfiltered carrot juice, 21 mg TE/ 100g in unpasteurized carrot juice). The loss of activity was significant following pasteurization of the carrot juice (**Table 4**). Apparently, pasteurization process had no significant effect on the antioxidant capacity of apple juices, though slight decrease was observed in the pasteurized compared to unpasteurized juice.

Table 4. Antioxidant activity of juices

Sample	ORAC mg TE/100 g (±SD)	Percent of inhibition (%)
Unfiltered carrot juice	23.00±1.87^{a}	-
Pasteurized carrot juice	18.89±1.69^{b}	-
Unpasteurized carrot juice	21.00±2.14^{a}	-
Commercial apple juice	10.00±0.86^{d}	-
Pasteurized apple juice	13.00±1.54^{c}	-
Unpasteurized apple juice	14.7±1.20^{c}	-
Beetroot juice	-	43±2.71^{a}
Cranberry juice	-	37±1.89^{b}
Pomegranate juice	-	24±1.65^{c}

SD, standard deviation; **TE**, Trolox equivalent. Different letters within a column denote significant differences ($P<0.05$).

According to the data's presented in **Tabel 4**, beetroot juice exhibited the highest inhibitory potential during the first 30 min, followed by cranberry juice and pomegranate juice.

In the study conducted in the United States, authors detected 6.52 μmol Trolox equivalent (TE)/mL scavenging activity for untreated carrot juice. After 10 days of storage, it has been increased up to 7.07 μmol TE/mL, probably due to the increase in phenolic compounds [34]. The research group led by Zeng reported 32.40% and 32.87% DPPH activity for untreated carrot and apple juices, respectively, which were significantly improved by sonication [30, 54].

It has been shown that beetroots possess strong antioxidant capacity [56] and this capacity is dependent on the betalain concentration [38]. Guldiken et al have analyzed several home-processed beetroot products and detected a total antioxidant capacity of 110 mg TE/100g beetroot juice using DPPH assay, significantly lower than that measured for fresh, unprocessed beetroot (137 mg TE/100g) [35].

Juice processing was found to influence significantly the free radical scavenging activity of cranberry [24]. Is has been postulated, that anthocyanins are the major contributor to the antioxidant activity in cranberries, contributing 39% of the total antioxidant capacity. Ascorbic acid was responsible for 22.6% of antioxidant activity [39]. A strong negative correlation ($r = –0.92$) was found between anthocyanin level and relative antioxidant potential in cranberries, while ascorbic acid content was positively correlated ($r = 0.84$) [40]. On the other hand, correlation analysis indicated close association between total phenolic content and antioxidant activity [57].

In case of pomegranate, linear relationship was observed between radical scavenging potential and total monomeric anthocyanins, suggesting that these compounds contributed greatly to the antioxidant capacity in pasteurized pomegranate fruit [58]. In a study comparing eight innovative fruit beverages, pomegranate juice presented the highest DPPH radical scavenging activity (539.87 g gallic acid equivalent/mL), total carotenoids (3.18 μg β-carotene equivalent/mL), and total phenolic content (3766.33 μg/mL) even after 20 days of storage at 4°C. Interestingly, antioxidant activity increased during storage [19]. This might be explained by the susceptibility of polyphenols to polymerization reaction [59]. As Iran controls approximately 47% of the world pomegranate production, the Iranian pomegranate juice has been the subject of numerous studies. However, miscellaneous data were reported on the antioxidant potential of these varieties. While Derakhshan et al reported 9–10% scavenging potential [60], significantly higher values (15.59–40.72%) have also been reported [44]. Pomegranate fractions used for juices could also determine the antioxidant activity of juice. A study conducted by Mphahlele et al demonstrated that halved fruit juice has the highest antioxidant activity as compared to arils, arils and seeds, and whole fruit [46].

CONCLUSIONS

Although we had limited information about the source of the fruits and vegetables and post-harvest regimen, the present analysis revealed that the phytochemical composition and quality of marketed beverages are fairly different and strongly related to processing techniques. All carrots juices analyzed herein contains approximately 2-fold higher carotenoids than apple juices. Betanin and isobetanin were identified as the major betacyanins in beetroot juice, while the anthocyanin profile of cranberry and pomegranate juices consists of 3-*O*-glucosides, 3-*O*-galactosides, and 3-*O*-arabinosides of malvidin, delphinidin, cyanidin, and petunidin. Ascorbic acid content ranged between 2.11 mg/100 mL (commercial apple juice and beetroot juice) and 4.57 mg/100 mL (cranberry juice). DPPH scavenging capacity was highest in the unprocessed carrot juice and lowest in Commercial apple juice. Amongst red juices, beetroot juice exhibited a percentage of inhibition higher than cranberry or pomegranate juices.

EXPERIMENTAL SECTION

Pasteurized and unpasteurized carrot and apple juices were obtained from a local producer. All other juices were purchased from the local market.

Methanol, ethyl acetate, petroleum ether, diethyl ether, triethylamine, sodium chloride, anhydrous sodium sulphate were purchased from Sigma Chemical Co. The purity of carotenoid standards (98 % for *β*-cryptoxanthin, 96 % for *β*-carotene, 97.5 % for lutein) was estimated by UV-VIS spectra and by an individual HPLC. Solvents used for carotenoid analysis (ethyl acetate, ethanol, hexane) were purchased from Merck.

Carotenoid separation, identification, and statistical methods

Carotenoids were extracted from 15 ml juice with a mixture of ethanol/ ethyl acetate/hexane (*ϕ*r = 1:0.5:0.5) containing butylated hydroxytoluene as anti-oxidant, following the procedure described by [61]. The sample was centrifuged, and extraction was repeated until the residue became colorless. The extracts were combined and partitioned in a separation funnel, successively with water, diethyl ether, and saturated saline solution. The ether phase was evaporated to dryness at 35°C under diminished pressure using a rotary evaporator. The samples were kept under nitrogen, at –20°C until further use. A proportion of the oleoresin obtained was dissolved in diethyl ether and saponified with 30 % methanolic KOH at room temperature in the

dark. For the removal of soaps and alkalis, the solution was washed several times with a sodium chloride saturated solution and distilled water. The organic layer containing carotenoids was dried with anhydrous sodium sulphate and evaporated to dryness. The samples were kept under nitrogen, at –20°C until further utilization. HPLC–PDA was performed using a system of Shimadzu LC20 AT with Waters 990 PDA detector, Kontron pumps and controller, and a reversed phase C18 column Hibar 250-4 Lichrosorb C18 (250 x 4,6 mm), 5 µm. The mobile phases used were acetonitrile/water (ϕr = 9:1) with 0.25% of triethylamine (A), and ethyl acetate with 0.25% of triethylamine (B). The gradient started with 15% of B at 0 min and increased to 50% of B at 16 min. The program continued isocratically with 50% of B up to 30 min. The flow-rate was 1 mL min^{-1}.The chromatograms were monitored at 450 nm.

Anthocyanins extraction and determination

Ten ml of juice was centrifuged at 3500 rpm for 10 min, filtered and directly injected to the HPLC. Analyses were performed on a Shimadzu HPLC system equipped with a binary pump delivery system LC-20 AT (Prominence), a degasser DGU-20 A3 (Prominence), diode-array SPD-M20 A UV–VIS detector and a Luna Phenomenex C18 column (5µm, 25 cm x 4.6 mm) was used. The mobile phase consisted in: solvent A - formic acid (4.5%) in bidistilled water and solvent B - acetonitrile. The gradient elution system was: 10% B, 0-9 min; 12% B, 9-17 min; 25% B 17-30 min; 90% B, 30-50 min; 10% B, 50-55 min. The flow rate was 0.8 ml/min and the analyses were performed at 35°C. The chromatograms were monitored at 520 and 580 nm respectively for betalains.

Ascorbic acid determination

Ascorbic acid content was quantitatively determined according to the titrimetric method described by Moldovan et al., based on the oxidation of ascorbic acid with iodine [62].

Antioxidant activity

The antioxidant activity of juice samples was measured and calculated by the oxygen radical absorbance capacity assay, as described previously [64]. ORAC values were expressed as mg TE/100 g reported on fresh weight. The 2,2-Diphenyl-1-picrylhydrazyl (DPPH) radical is one of the few stable organic nitrogen radicals, which bears a deep purple color. 50 µL of extracts

were added with 1.0 mL of 0.4 mM methanolic - DPPH and brought up with methanol to 5.0 mL. The mixture was shaken vigorously using a vortex and left to stand for 15 min, at room temperature, in the dark. The scavenging effect on the DPPH radical was read using a spectrophotometer at 517 nm. The radical scavenging activity was expressed using the following equation: percentage (%) of DPPH radical scavenging:

$$\%DPPH \cdot scavenging\ activity = \left(1 - \left[\frac{Asample}{Acontrol\ t = 0)}\right]\right) 100$$

where: Asample - Absorbtion of test extract solution (t=15 min)
Acontrol t=o Absorbtion of blank sample (t=o min)

DPPH solution was used as control.

ACKNOWLEDGMENTS

This project is funded by the Ministry of Research and Innovation through Program 1 - Development of the National Research and Development System, Subprogram 1.2 - Institutional Performance - Projects for Financing the Excellence in CDI, Contract no.37PFE/06.11.2018.

REFERENCES

1. M. Rodriguez-Concepcion, J. Avalos, M.L. Bonet, A. Boronat, L. Gomez-Gomez, D. Hornero-Mendez, M.C. Limon, A.J. Meléndez-Martínez, B. Olmedilla-Alonso, A. Palou, J. Ribot, M.J. Rodrigo, L. Zacarias, C. Zhu. *Progress in Lipid Research*, **2018**, *70*, 62.
2. R.K. Saini, S.H. Nile, S.W. Park. *Food Research International*, **2015**, *76*, 735.
3. P.S. Bernstein, F. Khachik, L.S. Carvalho, G.J. Muir, D.Y. Zhao, N.B. Katz. *Experimental eye research*, **2001**, *72*, 215.
4. N. Chhikara, K. Kushwaha, P. Sharma, Y. Gat, A. Panghal. *Food Chemistry*, **2019**, *272*, 192.
5. A. Cassidy. *Molecular Aspects of Medicine*, **2018**, *61*, 76.
6. L. Xie, H. Su, C. Sun, X. Zheng, W. Chen. *Trends in Food Science & Technology*, **2018**, *72*, 13.
7. M.J. Kruger, N. Davies, K.H. Myburgh, S. Lecour. *Food Research International*, **2014**, *59*, 41.

8. R. Puupponen-Pimia, L. Nohynek, C. Meier, M. Kahkonen, M. Heinonen, A. Hopia, K.M. Oksman-Caldentey. *Journal of Applied Microbiology*, **2001**, *90*, 494.
9. S. Kurl, T.P. Tuomainen, J.A. Laukkanen, K. Nyyssönen, T. Lakka, J. Sivenius, J.T. Salonen. *Stroke*, **2002**, *33*, 1568.
10. N. Shenoy, E. Creagan, T. Witzig, M. Levine. *Cancer Cell*, **2018**, *34*, 700.
11. S.K. Osganian, M.J. Stampfer, E. Rimm, D. Spiegelman, F.B. Hu, J.E. Manson, W.C. Willett. *Journal of the American College of Cardiology*, **2003**, *42*, 246.
12. T. Ritz, C.A. Werchan, J.L. Kroll, D. Rosenfield. *Physiology & Behavior*, **2019**, *202*, 45.
13. S. Caillet, J. Côté, G. Doyon, J.F. Sylvain, M. Lacroix. *Food Research International*, **2011**, *44*, 1408.
14. Z. Esmaeilinezhad, S. Babajafari, Z. Sohrabi, M. H. Eskandari, S. Amooee, R. Barati-Boldaji. *Nutrition, Metabolism and Cardiovascular Diseases*, **2019**, 29, 201.
15. A. Sahebkar, C. Ferri, P. Giorgini, S. Bo, P. Nachtigal, D. Grassi. *Pharmacological Research*, **2017**, *115*, 149.
16. G. Sohrab, H. Roshan, S. Ebrahimof, O. Nikpayam, G. Sotoudeh, F. Siasi. *Clinical Nutrition ESPEN*, **2019**, *29*, 30.
17. C.M. Matthaiou, N. Goutzourelas, D. Stagos, E. Sarafoglou, A. Jamurtas, S.D. Koulocheri, S.A. Haroutounian, A.M. Tsatsakis, D. Kouretas. *Food and Chemical Toxicology*, **2014**, *73*, 1.
18. M. Karimi, R. Sadeghi, J. Kokini. *Trends in Food Science & Technology*, **2017**, *69*, 59.
19. C. Castro-López, E.J. Sánchez-Alejo, S. Saucedo-Pompa, R. Rojas, J. Aranda-Ruiz, G.C.G. Martínez-Avila. *Heliyon*, **2016**, *2*, e00152.
20. H. Alighourchi. *European Food Research & Technology*, **2008**, *v. 227*, pp. 881.
21. M. Zielinska, D. Zielinska. *LWT-Food Science and Technology*, **2019**, *104*, 202.
22. F. Weber, L.R. Larsen. *Food Research International*, **2017**, *100*, 354.
23. G.M. Cătunescu, A.M. Rotar, C.R. Pop, Z. Diaconeasa, F. Bunghez, M.-I. Socaciu, C.A. Semeniuc. *LWT-Food Science and Technology*, **2019**, *102*, 385.
24. J. Côté, S. Caillet, G. Doyon, D. Dussault, S. Salmieri, G. Lorenzo, J. F. Sylvain, M. Lacroix. *Food Research International*, **2011**, *44*, 2907.
25. M. Marx, M. Stuparic, A. Schieber, R. Carle. *Food Chemistry*, **2003**, *83*, 609.
26. F. Chemat, H. Zill e, M. K. Khan. *Ultrasonics Sonochemistry*, **2011**, *18*, 813.
27. P. Putnik, Ž. Kresoja, T. Bosiljkov, A. Režek Jambrak, F.J. Barba, J.M. Lorenzo, S. Roohinejad, D. Granato, I. Žuntar, D. Bursać Kovačević. *Food Chemistry*, **2019**, *279*, 150.
28. M. Abid, S. Jabbar, B. Hu, M.M. Hashim, T. Wu, S. Lei, M.A. Khan, X. Zeng. *Ultrasonics Sonochemistry*, **2014**, *21*, 984.
29. M. Abid, S. Jabbar, T. Wu, M.M. Hashim, B. Hu, S. Lei, X. Zeng. *Ultrasonics Sonochemistry*, **2014**, *21*, 93.
30. S. Jabbar, M. Abid, T. Wu, M.M. Hashim, B. Hu, S. Lei, X. Zhu, X. Zeng. *Int J Food Science & Nutrition*, **2014**, *65*, 28.
31. L.Q. Zepka, A.Z. Mercadante. *Food Chemistry*, **2009**, *117*, 28.
32. M. Marx, A. Schieber, R. Carle. *Food Chemistry*, **2000**, *70*, 403.

33. B.H. Chen, H.Y. Peng, H.E. Chen. *Journal of Agricultural and Food Chemistry*, **1995**, *43*, 1912.
34. H.E. Martínez-Flores, M.G. Garnica-Romo, D. Bermúdez-Aguirre, P.R. Pokhrel, G.V. Barbosa-Cánovas. *Food Chemistry*, **2015**, *172*, 650.
35. B. Guldiken, G. Toydemir, K. Nur Memis, S. Okur, D. Boyacioglu, E. Capanoglu. *International Journal of Molecular Sciences*, **2016**, *17*.
36. F.C. Stintzing, J. Trichterborn, R. Carle. *Food Chemistry*, **2006**, *94*, 296.
37. K.M. Herbach, F.C. Stintzing, R. Carle. *Journal of Food Science*, **2004**, *69*, C491.
38. J. Wruss, G. Waldenberger, S. Huemer, P. Uygun, P. Lanzerstorfer, U. Müller, O. Höglinger, J. Weghuber. *Journal of Food Composition and Analysis*, **2015**, *42*, 46.
39. G. Borges, A. Degeneve, W. Mullen, A. Crozier. *Journal of Agricultural and Food Chemistry*, **2010**, *58*, 3901.
40. P.N. Brown, C.E. Turi, P.R. Shipley, S.J. Murch. *Planta Medica*, **2012**, *78*, 630.
41. B.L. White, L.R. Howard, R.L. Prior. *Journal of Agricultural Food Chemistry*, **2011**, *59*, 4692.
42. J.D. Wightman, R.E. Wrolstad. *Journal of Food Science*, **1995**, *60*, 862.
43. I.M. Caminiti, F. Noci, A. Muñoz, P. Whyte, D.J. Morgan, D.A. Cronin, J.G. Lyng. *Food Chemistry*, **2011**, *124*, 1387.
44. A. Tehranifar, M. Zarei, Z. Nemati, B. Esfandiyari, M. R. Vazifeshenas. *Scientia Horticulturae*, **2010**, *126*, 180.
45. G. Borges, A. Crozier. *Food Chemistry*, **2012**, *135*, 1863.
46. R.R. Mphahlele, O.A. Fawole, L.M. Mokwena, U.L. Opara. *South African Journal of Botany*, **2016**, *103*, 135.
47. U.A. Fischer, R. Carle, D.R. Kammerer. *Food Chemistry*, **2011**, *127*, 807.
48. S. Fabroni, G. Ballistreri, M. Amenta, F.V. Romeo, P. Rapisarda. *Journal of Scince Food Agriculture*, **2016**, *96*, 4713.
49. M. Guo. *Food and Bioprocess Technology*, **2013**, *v. 6*, 2013 v.6 no.11.
50. U.A. Fischer, R. Carle, D.R. Kammerer. *Food Chemistry*, **2013**, *138*, 1800.
51. P. Mena, S. Vegara, N. Martí, C. García-Viguera, D. Saura, M. Valero. *Food Chemistry*, **2013**, *141*, 2122.
52. Ö. Turfan, M. Türkyılmaz, O. Yemiş, M. Özkan. *Food Chemistry*, **2011**, *129*, 1644.
53. Ö. Turfan, M. Türkyilmaz, O. Yemİş, M. Özkan. *Journal of Food Quality*, **2012**, *35*, 272.
54. M. Abid, S. Jabbar, T. Wu, M.M. Hashim, B. Hu, S. Lei, X. Zhang, X. Zeng. *Ultrasonics Sonochemistry*, **2013**, *20*, 1182.
55. D.G. Dumbravă, N.G. Hădărugă, C. Moldovan, D.N. Raba, M.V. Popa, B. Rădoi. *Journal of Agroalimentary Processes and Technologies*, **2011**, *17*, 163.
56. P.C. Wootton-Beard, L. Ryan. *Journal of Functional Foods*, **2011**, *3*, 329.
57. M. Fidelis, J.S. Santos, A.L.K. Coelho, O.Y. Rodionova, A. Pomerantsev, D. Granato. *Food Control*, **2017**, *73*, 796.
58. S. Vegara, P. Mena, N. Martí, D. Saura, M. Valero. *Food Chemistry*, **2013**, *141*, 1630.

59. M. Pinelo, L. Manzocco, M.J. Nuñez, M.C. Nicoli. *Journal of Agricultural and Food Chemistry*, **2004**, *52*, 1177.
60. Z. Derakhshan, M. Ferrante, M. Tadi, F. Ansari, A. Heydari, M. S. Hosseini, G.O. Conti, E.K. Sadrabad. *Food and Chemical Toxicology*, **2018**, *114*, 108.
61. D.E. Breithaupt, W. Schwack. *European Food Research and Technology*, **2000**, 211, 52.
62. P. Moldovan, M.I. Toşa, D. Leţ, C. Majdik, C. Paizs, F.D. Irimie. Aplicaţii pentru laboratorul de biochimie, Editura Napoca Star, **2006**, p. 110-115.
63. D. Huang, B. Ou, M. Hampsch-Woodill, J.A. Flanagan, R.L. Prior. *Journal of Agricultural and Food Chemistry,* **2002**, 50(*16)*:4437.

STUDIA UBB CHEMIA, LXIV, 2,Tom I, 2019 (p. 127-138)
(RECOMMENDED CITATION)
DOI:10.24193/subbchem.2019.2.11

Dedicated to Professor Florin Dan Irimie on the Occasion of His 65th Anniversary

COMPARATIVE STUDY ON ESSENTIAL OILS OF SELECTED APIACEOUS SEEDS CULTIVATED IN TRANSYLVANIA

VASILICA MICLEA[a], IOANA DONCA[a], MONICA CULEA[b] NICODIM FIŢ[c], PAULA PODEA[a*]

ABSTRACT. A comparative study for analysis of essential oils obtained from plants grown in Transylvania, plants belonging to *Apiaceae* family, was achieved. Five types of plants seeds from *Coriandrum sativum L*. (coriander), *Anethum graveolens L.* (dill), *Pimpinella anisum L.* (anise), *Carum carvi L*. (caraway) and *Foeniculum vulgare L.* (fennel) were hydrodistilled to yield essential oils. The chemical composition of the obtained essential oils was determined; also the antioxidant, antimicrobial and tyrosinase inhibitory activities were investigated. The major constituent of coriander essential oil were linalool (73%), for dill (52.7%) and caraway (67.55%) was carvone and for anise (95.2%) and fennel (89.64%) was trans-anethole. The anise seeds essential oils provide the highest antioxidant activity while the coriander essential was the lowest. The fennel essential oils proved to be a potent tyrosinase inhibitor. All studied essential oils exhibited considerable antimicrobial activity, but coriander essential oil proved to have a very high antibacterial activity on gram-negative bacteria *E. Coli* and *Klebsiella pneumonia.*

Keywords: *essential oils, antioxidant activity, tyrosinase inhibitors, antimicrobial activity, GC/MS*

INTRODUCTION

Because of growing population concern about using unhealthy synthetic additives, consumers are increasing interests in ingredients from natural sources [1,2]. Essential oils are complex, combination of volatile compounds

[a] *Babes-Bolyai University, Faculty of Chemistry and Chemical Engineering*
[b] *Babes-Bolyai University, Faculty of Physics, Kogalniceanu str. No. 1, RO-400084 Cluj-Napoca, Romania*
[c] *University of Agricultural Sciences and Veterninary Medicine, Faculty of Veterinary Medicine, Calea Mănăştur str. No. 3-5, RO-400372 Cluj-Napoca, Romania*
**Corresponding author: mpaula@chem.ubbcluj.ro*

from natural sources, with potent medicinal beneficial properties which make them perfect ingredients in cosmetic, pharmaceutical and food industries. Presently, it is mandatory, to investigate plants essential oils compositions and biological activities for understanding and fasten the use of essential oils in practical application. Based on several studies, many essential oils, constituents of plants, herbs, spices, seeds are an excellent source of bioactive compounds with powerful antioxidant and antimicrobial activities [3].

Apiaceae (or *Umbelliferae***)** are a family of mostly aromatic plants, spread in regions with a temperate clime used as culinary herbs and spices. Due to the high concentration of secondary metabolites such as essential oils, in seeds and herbs, the apiaceae are used as flavouring agents and also for medical purposes and are known as nutraceutical plants [4].

For our study we have chosen from this class, five aromatic plants, coriander (*Coriandrum sativum*), dill (*Anethum graveolens*), fennel (*Foeniculum vulgare*), caraway (*Carum carvi*) and anise (*Pimpinella anisum*) due to the fact that there are indigenously available raw materials/oilseeds, they have a high concentrations of essential oils, are very aromatic and intensely used in our cuisine for their flavour, so are good potential candidates as food additives. It has been reported that essential oils from apiaceous fruits have some medicinal properties [5,6]. Coriander seeds essential oil proved to be antimicrobial and has insecticidal effects [7]. Dill essential oil is used for antispasmodic effects [8]. It has been reported that fennel oil essential have antifungal, antioxidant and hypoglycemic properties [9] while caraway essential is antimicrobial, antioxidant and have cytotoxic activities [10]. Anise seed essential oil can be used as antibacterial, antifungic, antiviral, and antispasmodic agents [11].

Due to the influence of climatic conditions, growth region, on qualitative composition and biological activities of plants, in this paper we propose the investigation of antioxidant, antimicrobial and antityrosinasic activity of essential oils extracted from fruits of *Coriandrum sativum L*. (coriander), *Anethum graveolens L.* (dill), *Pimpinella anisum L.* (anise), *Carum carvi L*. (caraway) and *Foeniculum vulgare L.* (fennel), cultivated in Transylvania, Romania. Also, identification and comparison of isolated essential oils chemical components by GC/MS was investigated.

RESULTS AND DISCUSSION

The aim of this work was to achieve a comparative study for analysis of coriander, dill, fennel, caraway and anise seeds by comparing the chemical composition, the antioxidant, antimicrobial activity and tyrosinase inhibitory activities of the obtained essential oils. The essential oils were obtained by

hydrodistillation of selected seeds plant using Clevenger apparatus. The seeds used were collected from plants from Botanical Garden of Târgu Mures, Transylvania, Romania.

The essential oils yield and the chemical composition of the essential oil analyzed by GC–MS

The yields of the obtained essential oils are provided in table 1. Comparing the obtained essential oils from selected *Apiaceae*, the highest yield was obtained for Anise seeds (2.4±0.2 (%v/w)), followed by Caraway seeds (2.1±0.1 (%v/w)). The lowest essential oils yield was obtained in case of Coriander seeds (0.9±0.1 (%v/w)). The obtained dill seeds essential oil yields 1.2±0.1 (%v/w) and fennel seeds essential oil yield is 1.7±0.2 (%v/w).

There are some reports about the influence of many factors like geographic growth region, type of cultivar, climatic conditions, stage of plant maturity, soil fertilizer on the yield and on chemical composition of *Apiaceae* seeds essential oils from different countries [12,13,14].

The reported coriander seeds essential oils yields, cultivated in different countries, is between 0.3-1.2% [15,16], but also higher yields were reported [6], 1.9-3%, even in a different geographical area in Romania (2%) [17].

The reported dill seeds essential oil yield gave similar yields [6,18,19] with our results, but also really high yields were reported [20].

The fennel seeds essential oil gave similar yields with yields reported in literature (1.6-2%) [6,21], but also difference in yield comparative with plants from others geographical regions were reported (2.81-7.1%) [22,23,24].

Caraway essential oil obtained yield was higher than some literature results (0.48-1.41)[25], but also comparable with other results obtained from literature[6]. The literature reported yields for anise seed essential oils vary from 1.4% to 6% [6,24,26,27].

Table 1. Essential oils yields

Yield(%v/w)	Essential oil
0.9±0.1	Coriander
1.2±0.1	Dill
1.7±0.2	Fennel
2.1±0.1	Caraway
2.4±0.2	Anise

The main components of the essential oils obtained from five plants from *Apiaceae* family plants are presented in Table 2. Identification of the constituents was based on comparison with mass fragmentation pattern and spectral comparison using NIST and Wiley mass spectra libraries of standards.

The major constituents of coriander essential oil obtained were linalool (73%), camphor (6.7%), p-cymene (6.02%), α-pinen (4.57%) and limonene (1.8%). In dill essential oil, carvone (52.7%) was the main constituent identified, followed by dillapiole (22.05%) and limonene (15.89%). In fennel essential oil the main components were identified as trans-anethole (89.64%), limonene (7.37%), fenchone (1.73%), estragole (1.26%). Caraway essential oil composition had as a main components carvone (67.55%) and limonene (26.06%). In addition, various minor components were identified. Anise essential oil contain trans-anethole (95.2%) and p-anisealdehyde (4.8%). It is known that anise flavor it is very similar with fennel flavor, the high concentration of trans-anethole found in both analyzed essential oils proved that the smell and taste can be very similar.

Table 2. Chemical composition of the obtained essential oils analysed by GC-MS

Component	M	Rt	Coriander %	Dill %	Fennel %	Caraway %	Anise %
alpha-pinene	136	6.0	4.57	<0.1	<0.1	<0.1	-
camphene	136	6.3	1.53	-	<0.1	-	-
sabinene	136	6.7	1.12	<0.1	<0.1	<0.1	-
beta-pinene	136	6.82	1.03	-	-	-	-
p-cymene	136	7.63	6.02	<0.1	<0.1	-	-
γ-terpinene	136	7.68	<0.1	<0.1	<0.1	<0.1	-
limonene	136	7.72	1.7	15.29	7.27	26.06	-
cis-linalool oxide	170	8.36	1.88	-	-	-	-
trans-linalool oxide	170	8.62	1.45	-	-	-	-
linalool	154	8.85	73	-	-	-	-
fenchone	152	9.28	-	-	1.33	-	-
cis, limonene oxide	152	9.46	-	<0.1	-	0.3	-
trans,limonene oxide	152	9.53	-	-	-	0.19	-
camphor	152	9.77	6.7	-	-	-	-
cis-dihydrocarvone	152	10.54	-	4.53	-	2.49	-
trans-dihydrocarvone	152	10.64	-	4.23	-	-	-
dihydrocarveol	154	10.83	-	<0.1	-	0.6	-
cis-carveol	152	10.86	-	<0.1	-	0.32	-
cis-dihydrocarveol	154	11.05	-	-	-	1.52	-
trans-anethole	148	11.16	-	-	89.64	-	95.1
carvone	150	11.33	<0.1	52.7	-	67.5	-
carvone oxide, cis	166	11.72	-	-	-	3.43	-
estragole	148	12.35	-	-	1.26	-	-
geranyl acetate	198	12.77	0.8	-	-	-	-
p-anisealdehyde	136	14.33	-	-	<0.1	-	4.8
caryophyllene oxide	200	15.77	-	-	-	0.72	-
cis-isopiolle	222	16.22	-	-	-	0.12	-
dillapiole	222	16.77	-	22.05	-	-	-

The main components, in all analyzed essential oils, were similar with literature data [21,28,29,30,31]. Differences appear in compounds relative concentration. This variation in composition might be connected with climatic conditions, geographic position of the growth region also with plant stage of development and metabolism. The volatile compounds classes percentages are provided in Table 3.

Table 3. Compound classes classification in studied essential oils

Component	Coriander %	Dill %	Fennel %	Caraway %	Anise %
Monoterpene hydrocarbons	16.07	15.89	7.37	26.06	-
Oxygenated monoterpenes	83.93	83.61	92.63	76.77	100
Sesquiterpene hydrocarbons	-	-	-	0.72	-

Antioxidant activity

Antioxidant activities of essential oils extracted from five plants from *Apiaceae* family plants were investigated using DPPH scavenging method. DPPH percent scavenging activities of volatile oils were measured at different concentrations between 0.01 and 0.25 mg/ml. EC50% is a parameter used for quantification of antioxidant activity and is giving by the amount of plant extract used for decreasing the initial DPPH concentration by 50%. A lower EC50% indicates a higher antioxidant activity. All tested essential oil present antioxidant and free radical scavenging activities. Comparing the antioxidant activity, measuring EC50%, we can conclude that anise seeds volatile oils provide the highest antioxidant activity comparable with vitamin E's activity used as standard. Fennel essential oils, which major component is also trans-anethole, exhibit also a high antioxidant activity. The results obtained were comparable with literature data [22]. Dill and caraway essential oil have a similar medium persistent antioxidant activity. Coriander seeds essential oil proved to have a weak antioxidant potential, comparative with the other obtained essential oils. The small antioxidant activity of essential oil from Coriander seeds was also found in literature data from plants grown on different geographic regions [15]. The results obtained in this study, showed that high antioxidant activity may be correlated with the presence of anethole, carvone and limonene in essential oils, but further research has to be made.

Table 4. Antioxidant capacity parameters

Sample	EC50%(µL/mL)	Equiv. µLVit E/mL essential oil
Vitamine E	2.68±0.13	-
Dill (*Anethum graveolens*)	80.28±0.52	73.09±6.13
Coriander (*Coriandrum sativum*)	175.45±0.43	57.35±7.9
Anise (*Pimpinella anisum*)	16.31±0.45	125.63±6.40
Fennel (*Foeniculum vulgare*)	34.06±0.25	99.68±2.39
Caraway (*Carum carvi*)	85.19±0.27	62.25±4.26

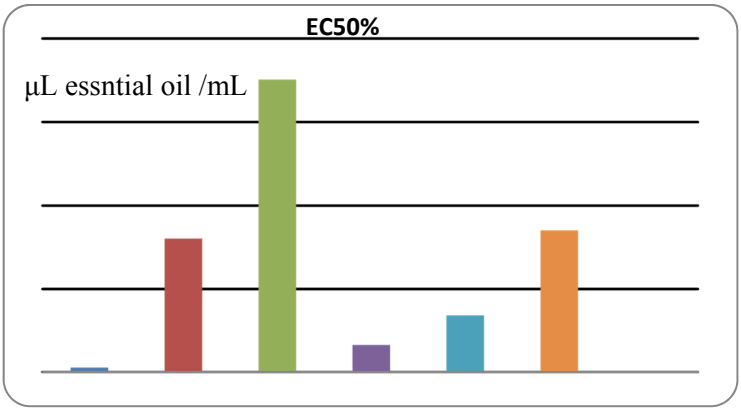

Figure 1. Efective concentration of studied essential oils (EC50%)

Tyrosinase inhibitory activity

Tyrosinase is an important enzyme involved in melanin biosynthesis [32] in animals and enzymatic browning in fruits [33]. Single compounds and plants extracts with anti-tyrosinasic inhibitory activity can be used as whitening agents in cosmetics or as additives in food industry to prevent fruits enzymatic browning phenomenon [34]. Tyrosinase inhibitory activity assay was followed spectrophotometrically using L-tyrosine as the substrate. Anti-tyrosinase inhibitory activity of studied essential oils was evaluated. All studied essential oils showed an inhibitory activity, the reaction rate of standard reaction was lowered with different percents 93% (fennel essential oil), 78%(caraway essential oil), 69%(anise essential oil), 61%(dill essential oil), 46% (coriander essential oil). The studied essential oil proved to be potent tyrosinase inhibitors, which make them good candidates for cosmetic use.

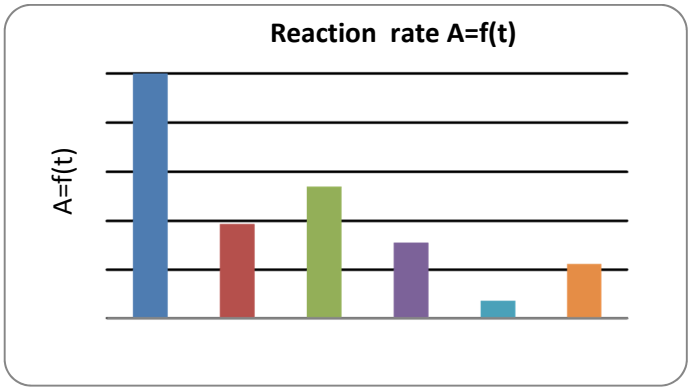

Figure 2. Comparation of reaction rates for tyrosinase enzyme inhibitory activity of studied essential oils

Antimicrobial activity

The antimicrobial activity of the obtained essential oils was examined against a panel of six microorganisms by the application of agar disc diffusion method. The data expressed as diameter of growth inhibition zone (mm). The results are illustrated in Table 5. All samples of volatile oils exhibited considerable antimicrobial activity. Coriander essential oil proved to have a very high antimicrobial activity on gram-negative bacteria *E. Coli* and *Klebsiella pneumonia* and a high antifungal activity on *Candida albicans,* fennel essential oil has a high antimicrobial activity on *Staphylococcus aureus, Pseudomonas aeruginosa* and *Candida albicans,* while caraway essential oils proved to be more effective on *Bacillus cereus* and on *Pseudomonas aeruginosa*. Dill essential oil proves to have the higher activity of all studied essential oils on *Staphylococcus aureus* and a high activity on *Candida albicans*. Anise essential oils proved to have the smallest inhibition zones from all studied essential oils, but still active on all studied microorganisms. The standard used proved to be not effective on gram-negative bacteria *Pseudomonas aeruginosa, Klebsiella pneumonia* and *E Coli,* while our studied essential oils exhibited all antibacterial activity. The antimicrobial activity of our studied essential oils is in agreement with other literature results [6,15,22,29,31] differences in activity appear due to the geographical and climatical grown region. The high revealed antimicrobial activity of our essential oils, make them an important source of new therapeutic and antimicrobial preparates.

Table 5. Antimicrobial activity of studied essential oils

	Inhibition diameter (mm)					
Microbial species	**Anise**	**Fennel**	**Coriander**	**Caraway**	**Dill**	**M CFR30**
Staphylococcus aureus	10±1	13±1	12±1	10±1	15±1	26±1
Bacillus cereus	7±1	10±1	9±1	12±1	8±1	15±1
E. coli	9±1	8±1	23±1	10±1	9±1	-
Klebsiella pneumoniae	7±1	9±1	13±1	9±1	9±1	-
Pseudomonas aeruginosa	8±1	12±1	7±1	9±1	12±1	-
Candida albicans	9±1	17±1	15±1	6±1	15±1	17±1

CONCLUSIONS

A comparative study for analysis of five plants from *Apiaceae* family was achieved. The essential oils seeds were compared in terms of chemical composition, antioxidant, antimicrobial and tyrosinasic inhibitors activities. The indigenously available *Apiaceae* plants fruits proved to have a high concentration of essential oil. The chemical composition of the obtained essential oils showed us that major constituents were similar with data obtained from other essentials oils obtained from plants cultivated in different geographic regions. Differences still appear in compounds relative concentration. This variation in composition might be connected with climatic conditions, geographic position of the growth region also with plant stage of development and metabolism. The anise seeds essential oils provide the highest antioxidant activity, followed by fennel and caraway. Fennel essential oils proved to be a very potent inhibitor of tyrosinase activity, which make it a very good candidate as a whitening agent for cosmetic use. Coriander essential oil proved to have a very high antimicrobial activity on gram-negative bacteria.

All studied essential oils exhibited considerable antioxidant, antimicrobial and antityrosinasic activity, proving that essential oils can be a good indigenous resources for natural food additives, new pharmaceutical preparates and also natural additives in cosmetic industry.

EXPERIMENTAL SECTION

MATERIAL AND METHODS

Five plants from *Apiaceae* family plants, *Coriandrum sativum L*. (coriander), *Anethum graveolens L.* (dill), *Pimpinella anisum L.* (anise), *Carum carvi L*. (caraway) and *Foeniculum vulgare L.* (fennel), were procured from Botanical Garden of Târgu Mures, Transylvania, Romania. The fruits were dried and grounded. All reactive and standards were purchased from Merck (Darmstadt, Germany). Antioxidant and antityrosinasic activities were determined using a Varian Cary 50 Spectrophotometer in a kinetic mode.

GC–MS apparatus

A Trace DSQ Thermo Finnigan quadrupole mass spectrometer coupled with a Trace GC was used. The Rtx-5MS capillary column, 30m x 0.25mm, 0.25µm film thickness was used in a temperature program from 50^{o}C, 2 min, then 8^{o}C /min to 250^{o}C, with 30^{o}C /min at 310^{o}C (10min) for essential oils compounds analysis. Helium was used as carrier gas at a flow rate of 1 mL/min. 1µL of each sample was injected into the GC-MS using the split mode (10:1) using a TriPlus autosampler(Proanalysis, Bucharest, Romania). The mass spectrometer was operated in EI mode at 70 eV, emission current was 100µA and mass spectra mass range 50-500 a.m.u. Transfer line temperature was set at 250^{o}C, injector at 250^{o}C and ion source at 250^{o}C.

EXTRACTION PROCEDURE FOR ESSENTIAL OILS

100 g of dried and grounded coriander, dill, fennel, caraway and anise seeds were submitted to hydrodistilation in a Clevenger type apparatus for 4h. The collected essential oils were dried over anhydrous Na_2SO_4. For the GC-MS analysis samples were diluted 100µL/mL in ethanol.

DETERMINATION OF ANTIOXIDANT ACTIVITY

For determination of antioxidant activity, DPPH antioxidant assay was used. Samples essential oils were used to decolorize an ethanolic solution of 40µM DPPH. The monitoring of DPPH reduction was followed at 517nm. The percentage of DPPH scavenging activity is expressed using following formula: $DPPH_{inhibition}\% = [(A_i-A_t)/A_i] \times 100$. For determination of effective concentration (EC_{50}), different concentration of essential oils 10, 20, 40, 80, 160 µL/mL were used. The EC_{50} was determined by plotting the $DPPH_{inhibition}\%$ against used extract concentration. Vitamine E was used as standard for the calibration curve and was plotted at 2, 4, 6, 8, and 10 µL/mL, prepared in ethanol.

DETERMINATION OF TYROSINASE INHIBITION ACTIVITY

For determination of antyrosinasic activity of essential oils, a spectrophotometric method was used. To 897 µL sodium phosphate buffer solution (20mM, pH= 6.8), 4µL L-tyrosine water solution (4mM) and 3µL phosphate buffer solution of tyrosinase (≥0.2 unit/mg solid in 1µL) 5µL of ethanol diluted essential oil sample (100µL/mL) was added. The enzymatic reaction was followed at 475nm for 15 minutes. The reaction rates were calculated from regression curve slope.

DETERMINATION OF ANTIMICROBIAL ACTIVITY

The antimicrobial activity of the essential oils were tested using Agar Diffusion Test (ADT). For testing the antibacterial activity of the obtained essential oils, five species of bacteria were chosen, two gram-positive bacteria *Staphylococcus aureus, Bacillus cereus,* three gram-negative species *Escherichia coli, Klebsiella pneumonia* and *Pseudomonas aeruginosa* and a fungi specie *Candida albicans.* The discs (6 mm in diameter) were impregnated with 5 µL essential oils placed on inoculated agar. As standard antibiotic the Cefadroxil (M CFR30), 30µg/disc was used. Antimicrobial activity was evaluated by measuring the inhibition zone.

REFERENCES

1. D.W. Reische, D.A. Lillard, R.R. Eitenmiller, “Chemistry, nutrition and biotechnology”, C. C. Ahoh & D. B. Min (Eds.) New York, **1998,** 423–448.
2. R. S. Farag, M. N. Ali, S. H. Taha, *Journal of American Oil Chemists Society*, **1990**, *67,* 188–191.
3. P. Tongnuanchan, S. Benjakul *Journal of Food Science*, **2014**, *79(7)*, 1231-1249.
4. M. Olle, I. Bender, *Agronomy Research*, **2010**, *8 (III)*, 687–696.
5. H.J.D. Dorman, S.G. Deans, *Journal of. Applied Microbiology*, **2000**, *88,* 308-316; D. Kalemba, A. Kunicka, *Current Medicinal Chemistry*, **2003**, *10*, 813-829; L. Brkovi_ C. Ljiljana, S. Slavica, *Kragujevac Journal of Science*, **2006**, *28*, 65-72.
6. N. Khalil, M. Ashour, S. Fikry, A. N. Singab, O. Salama, *Future Journal of Pharmaceutical Sciences*, **2018**, *4*, 88-92.
7. I. Kubo, K. Fujita, A. Kubo, K. Nihei, T. Ogura, *Journal of Agricultural Food Chemistry,* **2004***, 52,* 3329-3332; U.R. Pathipati, *Journal of biopesticides*, **2012**, *5*, 120-128.
8. N. Gharib, A. Heidari, *International Journal of Pharmacology*, **2007**, *3*, 260-264.

9. M.T. Ghanem, H.M. Radwan, S.M. Mahdy, Y.M. Elkholy, H.D. Hassanein, A.A. Shahat, *Pharmacognosy Research*, **2012**, *4*, 104-108; N.A. El-Soud, N. El-Laithy, G. El-Saeed, M.S. Wahby, M. Khalil, F. Morsy, N. Shaffie, *Macedonian Journal of Medical Science*, **2011**, *4*, 139-146.
10. S. Deb Roy, S. Thakur, A. Negi, M. Kumari, N. Sutar, G.K. Jana, *International Journal of Chemical and Analytical Science*, **2010**, *1*, 149-150; M. Kamaleeswari, N. Nalini, *Journal of Pharmacy and Pharmacology*, **2006**, *58*, 1121-1130.
11. A. Shojaii, M. A. Fard, *International Scholarly Research Notice Pharmaceutics*, **2012**, 2012-2020.
12. E. Beyzia, K. Karamanb, A. Gunesc, S. B. Beyzid, *Industrial Crops and Products*, **2017**, *109*, 74–78.
13. K. Msaada, K. Hosni, M. B. Taarit, T. Chahed, M. E. Kchouk, B. Marzouk, *Food Chemistry*, **2007,** *102,* 1131–1134.
14. M. Rostaei, S. Fallah, Z. Lorigooini, A. A. Abbasi Surki, *Journal of Cleaner Production* **2018**, *199*, 18-26.
15. B. Laribi, K. Kouki, M. M. Hamdi, T. Bettaieb, *Fitoterapia*, **2015**, *103*, 9–26.
16. M. Khodadadi, H. Dehghani, M. J. Javarana, J. T. Christopher, *Industrial Crops and Products* **2016**, *94,* 72–81;
17. A. Tsagkli, M.Hancianu, C. Aprotosoaie, O.Cioanca, O.Tzakou, *Records of Natural Products,* **2012**, *6(2)*, 156-160.
18. S. Nanasombat, P. Wimuttigosol, *Food Science and Biotechnology*, **2011**, *20(1)*, 45-53.
19. H.Y. Sintim, A. Burkhardt, A. Gawdea, C.L. Cantrell, T. Astatkie, A.E. Obour, V.D. Zheljazkov, V. Schlegel, Industrial Crops and Products, **2015**, *63*, 190–196.
20. V. Rădulescu, M.L. Popescu, D.C. Ilieş, *Farmacia*, **2010**, *58*, 594-600.
21. W.R. Diao, Q.P. Hu, H.Zhang, J.G. Xu, *Food Control*, **2014**, *35*, 109-116.
22. F. Anwara, M. Alia, A.I. Hussain, M. Shahid, *Flavour and Fragrance Journal*, **2009**, *24*, 170–176.
23. M. Abdellaoui, E.T. Bouhlali, A.Kasrati, L.El Rhaffari, *Journal of the Association of Arab Universities for Basic and Applied Sciences*, **2017**, *24*, 107–114.
24. M. Acimovic, V. Tesevic, M. Todosijevic, J. Djisalov, S. Oljaca, *Botanica Serbica*, **2015**, *39 (1)*, 09-14.
25. B. Laribi, K. Kouki, T. Bettaieb, A. Mougou, B. Marzouk, *Industrial Crops and Products*, **2013**, *41*, 312– 318.
26. A. Orav, A. Raal, E. Arak, *Natural Product Research*, **2008**, *22(3*), 227–232.
27. M.B. Embong, D. Hadziyev, S. Molnar, *Canadian Journal of Plant Science*.
28. N. Peerakam, J. Wattanathorn, S. Punjaisee, S. Buamongkol, P. Sirisaard, S. Chansakaow, *Journal of Natural Sciences Research*, **2014**, *4(16)*, 34-41.
29. B. Laribi, K. Kouki, T. Bettaieb, A. Mougou, B. Marzouk, *Industrial Crops and Products*, **2013**, *41*, 312–318.
30. U. Topal, M. Sasaki, M. Goto, S. Otles, *International Journal of Food Sciences and Nutrition*, **2008**, *59(7-8),* 619-634.
31. S. Mandal, M. Mandal, *Asian Pacific Journal of Tropical Biomedicine*, **2015**, *5(6),* 421–428.

32. S.Y Seo, V.K. Sharma, N.Sharma, *Journal of Agricultural Food Chemistry* **2003**, *51*, 2837-2853.
33. N. Alam, K.N. Yoon, K.R. Lee, P.G. Shin, J.C. Cheong, Y.B. Yoo, M.J. Shim, M.W. Lee, U.Y. Lee, T.S. Lee, *Mycobiology*, **2010**, *38(4)*, 295-301.
34. M.R. Loizzo, R. Tundis, F. Menichini, Comprehensive Reviews in Food Science and Food Safety, **2012**, *11*, 378-398.

STUDIA UBB CHEMIA, LXIV, 2,Tom I, 2019 (p. 139-157)
(RECOMMENDED CITATION)
DOI:10.24193/subbchem.2019.2.12

Dedicated to Professor Florin Dan Irimie on the Occasion of His 65th Anniversary

MATHEMATICAL MODELLING AND PREDICTION OF CONGO RED ADSORPTION ON CHERRY STONES ACTIVATED CARBON

ANDREI SIMION[a], CRISTINA GRIGORAȘ[a*], LIDIA FAVIER[b], LUCIAN GAVRILĂ[a*]

ABSTRACT. The present paper was aimed to establish mathematical models useful to reduce the time required to discover the appropriate adsorption conditions of Congo Red (an intensively used organic dye) on an activated carbon prepared from cherry stones through calcination. To this purpose, various values of three parameters known as influencing the process, namely dye initial concentration (200 mg/L to 1000 mg/L), *p*H (2 to 12) and contact time (10 to 180 minutes) between the adsorbent and the adsorbate were variated. The recorded results of the adsorption process were used as data for Response Surface Methodology and Artificial Neural Network and several mathematical equations were generated. The conducted statistical analyses revealed that these equations can accurately express the Congo Red elimination from aqueous solutions. Moreover, the developed procedure is able to predict the process evolution in different conditions than those experimentally tested.

Keywords: *Adsorption, Artificial Neural Network, cherry stone, Congo Red, mathematical modelling, Response Surface Methodology, water treatment*

INTRODUCTION

Colored wastewater coming from various industries is considered a major source of environmental concerns. Besides being responsible for the unwanted visual effect, due to their chemical structures, dyes are often characterized by a reduced biodegradability being difficult to remove by classical wastewater treatments [1]. Moreover, most of the dyes can also negatively affect

[a] *"Vasile Alecsandri" University of Bacău; Faculty of Engineering; Department of Food and Chemical Engineering; Calea Mărășești 157, RO-600115, Bacău, România*
[b] *Univ. Rennes, Ecole Nationale Supérieure de Chimie de Rennes; CNRS, UMR 6226; 11 Allée de Beaulieu, CS 50837, 35708 Rennes Cedex 7, France*
**Corresponding authors: cristina.grigoras@ub.ro, lgavrila@ub.ro*

the human and animals state of health causing severe skin irritations [2, 3], respiratory problems [4], liver damages or central nervous system injuries [5].

Therefore, many procedures directed to treat dye containing effluents are tested and the interest in developing and adapting other techniques increases continuously.

One of these methods is represented by the adsorption process. Recognized as an efficient, inexpensive and simple to manage procedure [6], the adsorption can be conducted even by using low cost materials such as biomass prepared from flower spikes [7], alginate [8], chitosan [9, 10], clays [11, 12] composites [13-15], adsorbents obtained from vegetal wastes [16, 17] including olive cake [18], date wastes [19], seeds [20], coffee grounds [21] etc.

The adsorption mechanism relies on different interactions (van der Waals forces, hydrogen bonding, polarity, static interactions, dipole-dipole interactions etc.) occurring between the adsorbent and the adsorbate [22] and on the chemical attractions taking place between them [23]. Its efficiency is strongly influenced by a series of factors related to dye (class type, molecular structure etc.), characteristics of the material possessing adsorbing properties (surface area, regenerating capacity etc.) and to the parameters affecting the process (dye solution pH, its initial concentration, temperature, length of the contact time, adsorbent amount - dye solution volume ratio etc.). These aspects have been the subject of many researches [24-27] which revealed that dyes adsorption represent a very attractive alternative to the costlier other techniques of wastewater treatment [28-30] such as those employing for example immobilized enzymes [31], nanofiltration [32], Fenton oxidation [33], photosynthetic bacteria [34] or biogenic nanomaterials [35]. The already conducted investigations show also that the steps to be followed for establishing the appropriate dye adsorption conditions are time-consuming and require multiple experimental tests.

Based on these considerations, in this work, we have used an absorbent material obtained from cherry stones (CS) by physical activation to eliminate Congo Red (CR) (a frequent anionic azo dye in textile, paper, cosmetic, printing industries) from aqueous solutions. The effect of pH, dye initial concentration and contact time was primarily explored. Then, the acquired data were introduced in computer specific software. Mathematical modeling and simulation were tested for predicting the adequate parameters to be utilized in order to obtain the best results in terms of CR removal. Two different approaches: the Response Surface Methodology (RSM) and the Artificial Neural Network (ANN) were applied. Their choice was based on the fact that they have been reported as procuring precise results for dye adsorption modeling. RSM takes into account the interactions of the involved parameters being helpful for designing the experiments. It fits linear or polynomial functions to the collected data [36-38]. ANN is known as a simple and highly reliable artificial intelligence technique which can connect large sets of variables with the purpose of offering trustful nonlinear mathematical equations [39, 40]. Both methodologies return models verified by statistical tests [41, 42].

RESULTS AND DISCUSSION

Congo Red adsorption process onto cherry stones activated carbon

Table 1. Congo Red dye final concentrations after adsorption on cherry stones activated carbon in different working conditions

Initial dye concentration	200 mg/L	400 mg/L	600 mg/L	800 mg/L	1000 mg/L
Time (min)	Final dye concentration (mg/L) at pH 2				
10	11.172	20.007	26.994	39.812	55.184
20	5.858	7.591	16.007	27.044	37.148
30	3.578	5.448	8.333	15.628	18.621
40	2.022	3.612	5.757	7.911	8.788
55	1.075	2.336	3.212	4.911	6.012
60	0.827	1.272	1.896	2.435	3.312
80	0.803	1.146	1.728	2.045	2.873
90	0.791	1.083	1.644	1.850	2.654
100	0.738	1.018	1.526	1.807	2.496
120	0.631	0.888	1.290	1.722	2.181
150	0.588	0.833	1.272	1.678	2.109
180	0.488	0.779	1.178	1.622	1.899
Time (min)	Final dye concentration (mg/L) at pH 4.5				
10	18.177	29.580	43.797	60.602	78.919
20	11.031	19.930	30.755	45.305	57.978
30	8.390	14.616	20.745	31.961	42.375
40	5.503	9.100	13.129	20.372	25.439
55	3.575	4.879	6.873	10.133	13.208
60	1.822	2.112	2.913	4.054	5.251
80	1.436	1.870	2.686	3.519	4.946
90	1.243	1.750	2.572	3.251	4.794
100	1.210	1.677	2.441	3.111	4.684
120	1.144	1.531	2.179	2.832	4.464
150	0.891	1.169	1.705	2.599	3.693
180	0.594	1.052	1.607	1.998	2.500
Time (min)	Final dye concentration (mg/L) at pH 7				
10	29.782	40.271	57.168	71.181	90.788
20	20.181	30.123	40.01	52.571	70.644
30	11.746	18.205	30.25	41.200	54.707
40	7.101	13.137	20.274	29.786	37.331
55	5.588	8.370	10.774	15.333	21.58
60	2.474	3.273	4.662	6.970	7.981
80	2.050	2.676	4.153	5.690	6.823
90	1.838	2.377	3.899	5.050	6.244
100	1.628	2.298	3.819	4.928	6.014
120	1.207	2.141	3.660	4.683	5.555
150	0.599	1.216	2.638	4.282	5.350
180	0.516	1.178	2.452	3.500	4.210

The results of the adsorption process of Congo Red dye on activated carbon prepared from the cherry stones are represented in Table 1. For all the initial concentrations tested in the experiments, more than 90 % of the pollutant was retained after only 10 minutes of contact between the adsorbent material and the dye solutions. After 180 minutes the adsorption efficiency reached over 99 %. Similar observations were reported by other researches which have studied the CR elimination from aqueous effluents by the help of different adsorbing materials made from biowastes [43] or wood sawdust [44]. These researches explain that CR exists in its cationic form at acidic *p*H. The experiments showed that a *p*H between 2 and 7 favors the adsorption. Therefore, it can be concluded that the adsorbent surface is able to retain the pollutant due to the electrostatic attraction caused by its positively charged surface. On the contrary, when the experimental program was conduced at higher *p*H (10 and 12) (data not shown here) a very low CR retention was observed confirming the above hypothesis since at alkaline *p*H CR is in anionic form. In this case, HSO_3^- ion will turn into $–SO^3–Na^+$. As consequence, the CR negative charge density will decrease inducing an electrostatic repulsion between the pollutant and the adsorbent surface with unfavorable repercussions on the adsorption process.

RSM modelling

Models fitting

As stated before, RSM is a powerful tool containing multiple designs. The most frequently employed ones, Central composite and Box-Behnken, present limitations in considering the extent of the investigation ranges and/or the inability of including key experimental extreme points. Moreover, the generated equations present unsatisfactory correlation coefficients (with rather reduced values). Due to these facts and in order to characterize the entire adsorption process, it seemed adequate to create a custom central composite design (CCCD). Therefore, a three-factors with three variation levels CCCD consisting of 135 experimental runs (data not showed but retrieved from Table 1), including replications at the center point, was adopted to optimize the experimental data. The response function (the final CR concentration) was expressed by the linear and polynomial equations (1), (2) and (3).

Linear $$Y = 13.9211 + 9.622351A + 5.094307B - 19.0636C \quad (1)$$

Quadratic $$Y = 5.523482 + 9.157365A + 5.690574B - 19.5703C + 3.011641AB - 12.5546AC - 6.83729BC + 1.826601A^2 - 0.849685B^2 + 18.124092C^2 \quad (2)$$

Cubic $$Y = 5.808814 + 5.542864A + 3.895732B - 15.1419C + 2.908154AB - 12.8594AC - 6.94087BC + 1.73932A^2 - 0.79793B^2 + 17.91289C^2 - 2.79414ABC + 0.298217A^2B - 2.35658A^2C - 1.14011AB^2 + 10.96966AC^2 + 1.397214B^2C + 3.728796BC^2 - 0.54938A^3 - 5.6188C^3 \quad (3)$$

where *Y* represent the final dye concentration and *A*, *B* and *C* are the coded values of the initial dye concentration, *p*H and adsorption time, respectively.

The sequential model sum of squares (Table 2) can be viewed in the reduction of the sum of squares error (SSE). A predictor added to a model explains some of the response variability and thereby reduces the error. A sequential sum of squares quantifies how much variability could be explained (increase in regression sum of squares) or alternatively how much error could be reduced (reduction in the error sum of squares). In this study, the sequential model shows a value of 1648.202 for the sum of squares and therefore it favors the selection of the cubic polynomial equation instead of the quadratic model even though this last one is intensively used when RSM is applied.

Table 2. Sequential model sum of squares

Model	Sum of Squares	Degree of freedom	Mean Square	F-value	p-value Prob > F
Mean vs Total	28883.77	1	28883.77	-	-
Linear vs Mean	30965.47	3	10321.82	90.34611	< 0.0001
2FI* vs Linear	6925.197	3	2308.399	36.74498	< 0.0001
Quadratic vs 2FI	6024.829	3	2008.276	124.4959	< 0.0001
Cubic vs Quadratic	1648.202	9	183.1336	57.69459	< 0.0001
Residual	368.2059	116	3.174189	-	-
Total	74815.68	135	554.1902	-	-

*2FI – two factor interaction

The quality of the models (Table 3) was statistically evaluated firstly based on the coefficient of determination (R^2) and by graphical comparison of the predicted vs. measured values (Figure 2).

Table 3. Models summary statistics

Model	Standard deviation	R^2	Adjusted R^2	Predicted R^2	PRESS*
Linear	10.68867	0.67416	0.666698	0.650026	16074.99
Quadratic	4.016374	0.9561	0.952939	0.946682	2448.981
Cubic	1.781625	0.991984	0.99074	0.988706	518.758

*PRESS – Predicted residual error sum of square

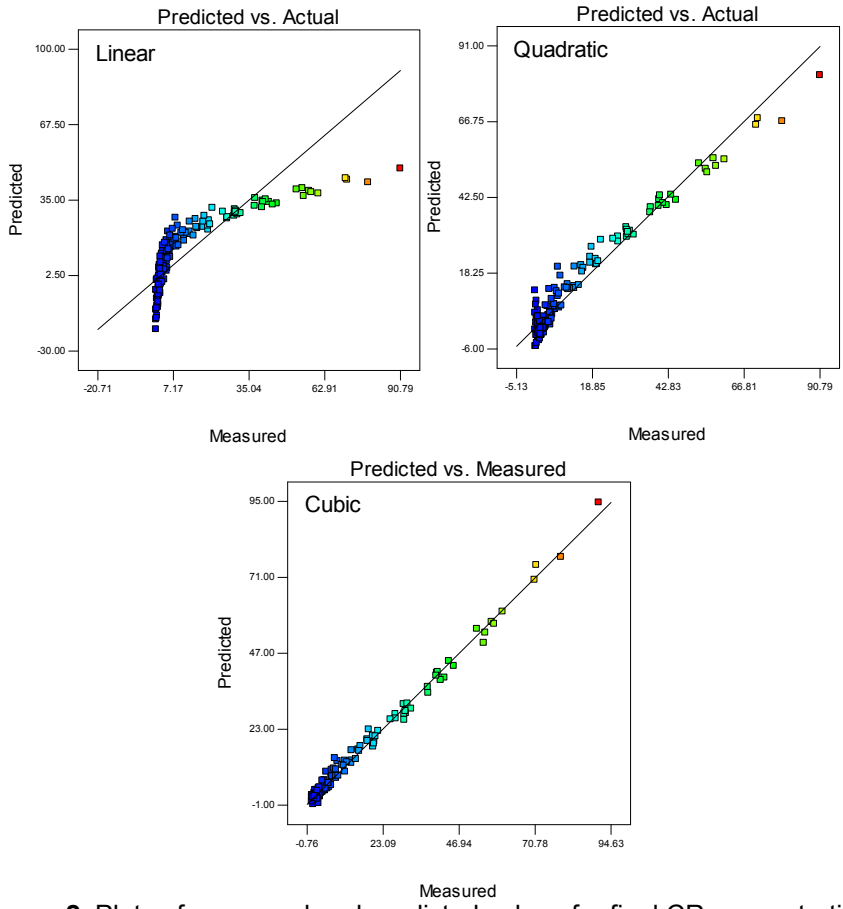

Figure 2. Plots of measured and predicted values for final CR concentration

R^2 is the ratio of the explained variation versus the total variation. It verifies the reliability of an established model. Values of R^2 closer to 1 will better fit the experimental data while a smaller R^2 implies a more reduced similarity between the predicted and the measured records. As noted in Table 3, R^2 is 0.674 for the linear equation, 0.956 for the quadratic model and 0.992 for the cubic one. This means that 32.6 %, 4.4 % and respectively 0.8 % of the total variables for the analyzed response function were not explained by the models. The adjusted R^2 value also explains the accuracy of the model. The important difference between R^2 and adjusted R^2 is that the latter increases only with the addition of input (independent) variables recognized as significant. If non-significant variables are added into the model, the value of adjusted R^2 will decrease, whereas the R^2 will continually

increase. Thus, the smaller gap between R^2 and the adjusted R^2 is desirable for the judgement of a model adequacy. The values of adjusted R^2 of the response show that only 35.0 %, 5.3 % and respectively 1.1 % of the total models variation could not explained.

R^2 values were comparable with those of the predicted R^2 indicating that the models almost perfectly explain the studied experimental range and they can be successfully used to predict the final dye concentration.

Taking into consideration these aspects, it can be concluded that the linear model is the less precise from all and the cubic model has a slight higher degree of confidence then the quadratic one.

The analysis of variance (ANOVA), detailed in Table 4, shows that the generated mathematical equations models were highly significant, because the F-values are greater than 0.001. The *p*-values inferior to 0.0001 means that there are only 0.01 % of the total variation that could not be explained by the model and are attributed to the noise signal.

Table 4. ANOVA results of the RSM models

Source	Sum of Squares	Degree of freedom	Mean Square	F-value	p-value
Linear					
Model	30965.47	3	10321.82	90.34611	< 0.0001
Residual	14966.43	131	114.2476	-	-
Corrected Total	45931.91	134	-	-	-
	Standard deviation	Mean	Coefficient of variance, %	Adequate precision	
	10.68867	14.62716	73.0741	37.64376	
Quadratic					
Model	43915.5	9	4879.5	302.4872	< 0.0001
Residual	2016.408	125	16.13126	-	-
Corrected Total	45931.91	134	-	-	-
	Standard deviation	Mean	Coefficient of variance, %	Adequate precision	
	4.016374	14.62716	27.45833	79.30854	
Cubic					
Model	45563.7	18	2531.317	797.4688	< 0.0001
Residual	368.2059	116	3.174189	-	-
Corrected Total	45931.91	134	-	-	-
	Standard deviation	Mean	Coefficient of variance, %	Adequate precision	
	1.781625	14.62716	12.18025	142.7195	

Adequate precision measures the range in predicted response and its associated error (i.e., a signal-to-noise ratio). Its values were higher than 4 implying desirable fitness of the equations. The coefficient of variance (CV) presents the reproducibility of the models. Expressed as the percent ratio between the standard error of the estimate and the mean value of the observed response, when it is under 10 %, it states that the model can be considered as reasonably reproducible. The cubic and the quadratic models presented the closest values (12.18 % and 27.45 % respectively) to the targeted 10 % of CV while the linear mathematical model has a CV of 73.07 %. Therefore, it was not submitted to more advanced statistical analyses.

Table 5 shows the ANOVA of the quadratic model coefficients for the response indicating that eight terms, namely A, B, C, AB, AC, BC, A^2 and C^2 were found out to be statistically significant ($p < 0.0001$) for the studied response function. The quadratic term A^2, was less significant based on a 95 % confidence level ($p < 0.05$). The lowest importance was attributed to the quadratic term B^2 ($p < 0.2488$).

The sum of squares (SS) of model components was used to calculate the percentage contributions (PC) for each individual term. For the final dye concentration, the time (C) has the highest level of significance with a contribution of 51.29 % as compared to the other components.

Table 5. ANOVA results for the quadratic model coefficients

Factor	Coeffi-cient	95% Confidence interval		Standard error	F-value	p-value	Sum of squares	Contri-bution (%)
		Low	High					
Y, Final pollutant concentration								
Intercept	5.523482	3.860511	7.186453	0.840256	-	-	-	-
A	9.157365	8.188344	10.12639	0.489621	349.8013	< 0.0001	5642.736	12.78
B	5.690574	4.851378	6.529771	0.424024	180.1073	< 0.0001	2905.358	6.58
C	-19.5703	-20.6042	-18.5364	0.522412	1403.36	< 0.0001	22637.97	51.29
AB	3.011641	1.826688	4.196593	0.598726	25.30174	< 0.0001	408.1491	0.92
AC	-12.5546	-14.0149	-11.0943	0.737855	289.5119	< 0.0001	4670.192	10.58
BC	-6.83729	-8.10195	-5.57263	0.639001	114.4892	< 0.0001	1846.856	4.18
A^2	1.826601	0.191211	3.461991	0.82632	4.886419	0.0289	78.82412	0.18
B^2	-0.84968	-2.30095	0.601582	0.733286	1.342661	0.2488	21.65882	0.05
C^2	18.24092	16.35712	20.12471	0.951833	367.2586	< 0.0001	5924.346	13.42

Table 6 points the ANOVA applied for the cubic model coefficients of the response function indicating that sixteen terms A, B, C, AB, AC, BC, A^2, B^2, C^2, ABC, A^2C, AB^2, AC^2, B^2C, BC^2 and C^3 were found out to be statistically significant ($p < 0.0001$) for the adsorption process. The other terms of the model as the quadratic term B^2 and his interaction with initial concentrations and time (A^2B, AB^2, B^2C) and the cubic term A^3 were highly significant based on a 95 % confidence level ($p < 0.05$), meaning that the variable *p*H did not have an intense influence on dye removal in the tested experimental range. For the final dye concentration, the time and his interactions (C) showed the highest level of significance.

Table 6. ANOVA results for the cubic model coefficients

Factor	Coefficient	95% Confidence interval		Standard error	F-value	P-value	Sum of squares	Contri-bution (%)
		Low	High					
Y, Final pollutant concentration								
Intercept	5.808814	0.375201	5.065681	6.551948	-	-	-	-
A	5.542864	0.766931	4.023861	7.061866	52.23436	< 0.0001	165.8017	1.02
B	3.895732	0.371286	3.160353	4.631111	110.0932	< 0.0001	349.4566	2.15
C	-15.1419	0.776783	-16.6804	-13.6034	379.9809	< 0.0001	1206.131	7.41
AB	2.908154	0.266004	2.3813	3.435008	119.5252	< 0.0001	379.3956	2.33
AC	-12.8594	0.327725	-13.5085	-12.2103	1539.635	< 0.0001	4887.093	30.04
BC	-6.94087	0.283819	-7.50301	-6.37873	598.0615	< 0.0001	1898.36	11.67
A^2	1.73932	0.36712	1.012193	2.466447	22.44621	< 0.0001	71.24851	0.44
B^2	-0.79793	0.325787	-1.4432	-0.15267	5.998842	0.0158	19.04146	0.12
C^2	17.91289	0.424883	17.07135	18.75442	1777.43	< 0.0001	5641.899	34.68
ABC	-2.79414	0.400866	-3.58811	-2.00018	48.58463	< 0.0001	154.2168	0.95
A^2B	0.298217	0.448927	-0.59094	1.187374	0.441278	0.5078	1.4007	0.01
A^2C	-2.35658	0.553247	-3.45236	-1.2608	18.14369	< 0.0001	57.59152	0.35
AB^2	-1.14011	0.460014	-2.05122	-0.22899	6.142595	0.0146	19.49776	0.12
AC^2	10.96966	0.597115	9.786999	12.15232	337.4976	< 0.0001	1071.281	6.59
B^2C	1.397214	0.490958	0.424809	2.369619	8.099099	0.0052	25.70807	0.16
BC^2	3.728796	0.517117	2.704581	4.75301	51.99484	< 0.0001	165.0415	1.01
A^3	-0.54938	0.722842	-1.98106	0.882299	0.577642	0.4488	1.833547	0.01
C^3	-5.6188	0.812954	-7.22896	-4.00864	47.76998	< 0.0001	151.631	0.93

Figures 3 and 4 illustrate the influence of two factors while maintaining the other constant at coded value of 0 for the quadratic and the cubic mathematical models. Dye initial concentration has negative effect on the adsorption process. On the contrary, the *p*H showed a positive impact but its influence extent passes from slightly less to highly inferior than that of the adsorption time once that initial dye concentrations increase. The adsorption time is the most important parameter and showed a positive effect on dye removal. The major differences between models are the number of negative values generated on the final dye concentrations, the quadratic model being inferior in the data prediction at low level of initial concentrations and *p*H than the cubic one.

Coefficients used for the cubic mathematical model are given in Table 7.

Table 7. Final equation in terms of actual factors

Final dye concentration =		
Quadratic coefficients	Cubic coefficients	Actual parameters
4.141866292	-1.90961894	-
0.034002923	0.016535466	* Init. dye conc.
5.035463556	4.799626589	* *p*H
-0.733780548	-0.089280881	* Time
0.003011641	0.00953296	* Init. dye conc.* *p*H
-0.00069748	-0.001531938	* Init. dye conc.* Time
-0.060775911	-0.150172977	* pH * Time
1.14163E-05	4.09688E-05	* Init. dye conc.^{2}
-0.135949235	-0.12727603	* *p*H^2
0.009007859	0.00757967	* Time^2
-	-6.2092E-05	* Init. dye conc.* *p*H * Time
-	7.45542E-07	* Init. dye conc.^{2} * *p*H
-	-3.27303E-07	* Init. dye conc.^{2} * Time
-	-0.000456044	* Init. dye conc.* *p*H^2
-	1.35428E-05	* Init. dye conc.* Time^2
-	0.004967872	* *p*H^2 * Time
-	0.000736552	* *p*H * Time^2
-	-8.58406E-09	* Init. dye conc.^{3}
-	-6.16604E-05	* Time^3

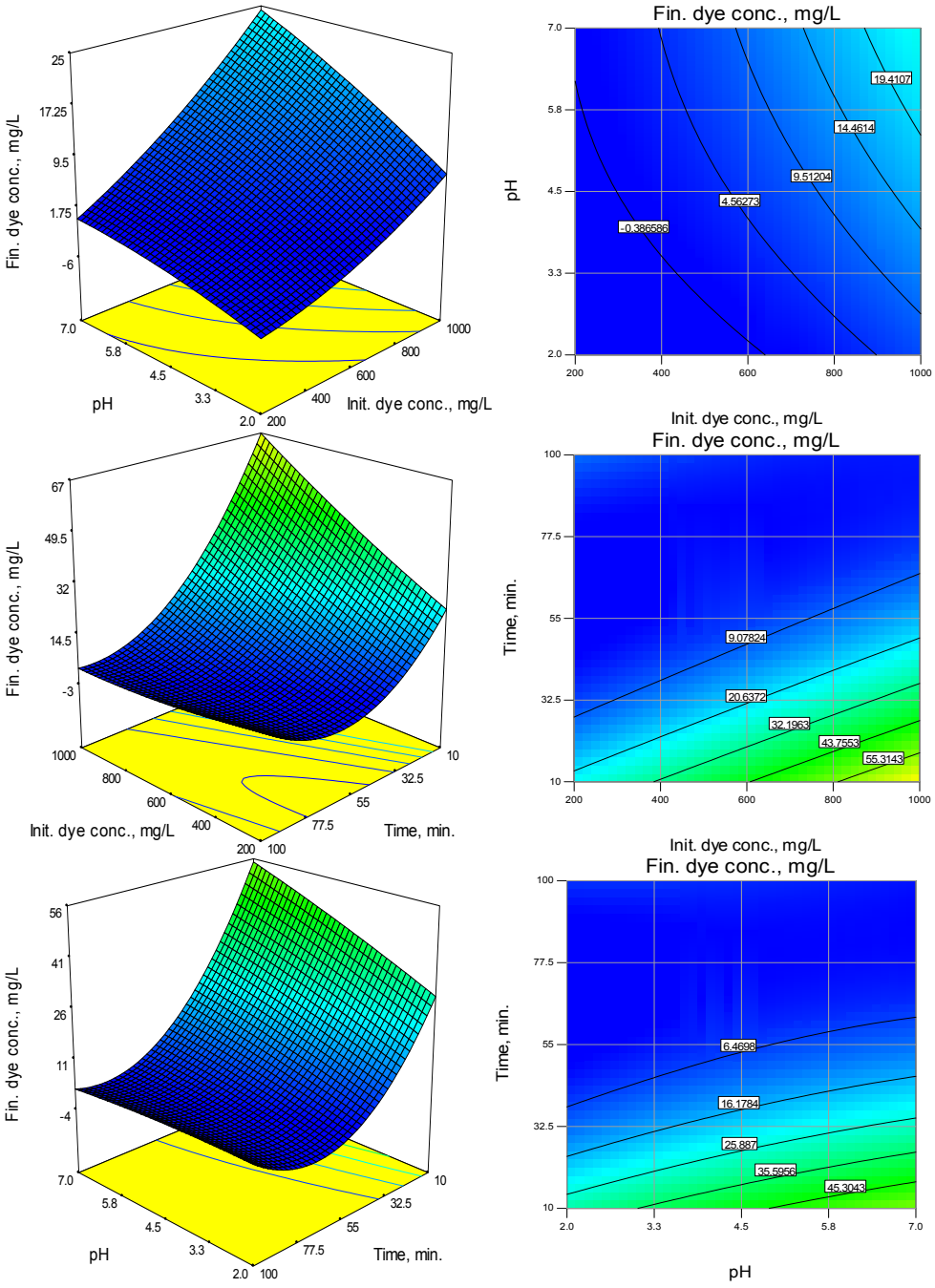

Figure 3. Response surface graphs and contour plots of final dye concentration: the effect of initial dye concentration, *p*H and adsorption time for the quadratic model

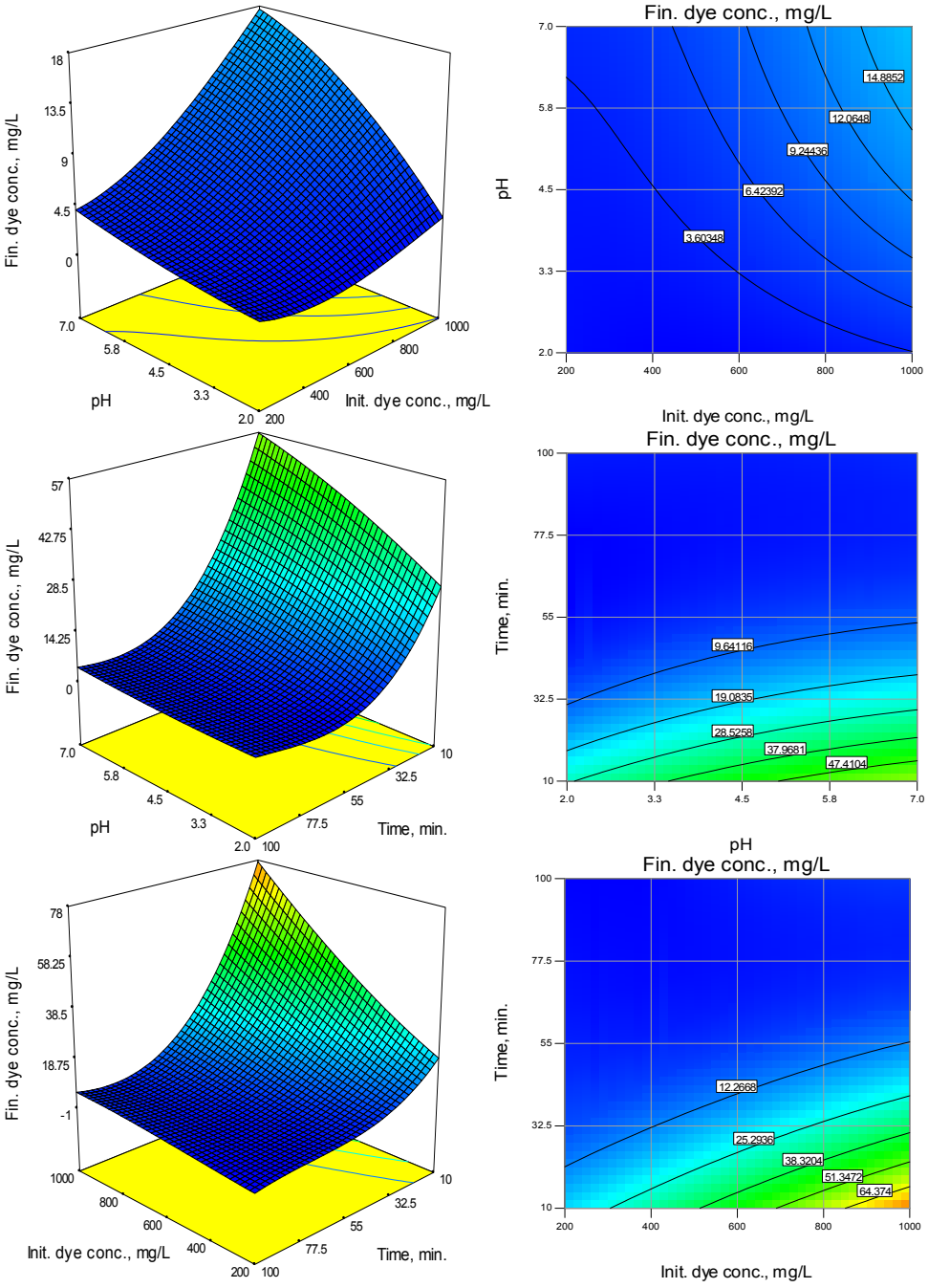

Figure 4. Response surface graphs and contour plots of final dye concentration: effect of initial dye concentration, *p*H and adsorption time for the cubic model

Testing the model

The adopted mathematical model was tested in the conditions planed in the experimental setup A comparison of measured Congo Red final concentrations when dye adsorption from solutions with initial concentrations varying between 200 mg/L and 1000 mg/L was conducted at *p*H 4.5 for 10 to 100 minutes and data predicted by the cubic model is reported in Table 8 as an example. Only minor differences were distinguished. These outcomes along with the similar results registered for runs carried out at *p*H 2.0 and 7.0 (data not shown) sustain also the model adequacy.

Table 8. Measured final dye concentrations at *p*H 4.5 vs predicted by cubic model

Initial dye conc.	**200 mg/L**		**400 mg/L**		**600 mg/L**		**800 mg/L**		**1000 mg/L**	
Time (min)	Final dye concentration, mg/L									
	M	P	M	P	M	P	M	P	M	P
10	18.177	19.756	29.580	30.889	43.797	44.482	60.602	60.124	78.919	77.401
20	11.031	13.007	19.930	20.937	30.755	31.066	45.305	42.980	57.978	56.269
30	8.390	8.238	14.616	13.508	20.745	20.713	31.961	29.443	42.375	39.285
40	5.503	5.081	9.100	8.230	13.129	13.055	20.372	19.141	25.439	26.078
55	3.575	3.164	4.879	4.736	6.873	7.720	10.133	11.705	13.208	16.279
60	1.822	2.117	2.112	2.653	2.913	4.340	4.054	6.765	5.251	9.517
80	1.436	1.157	1.870	1.246	2.686	1.962	3.519	2.893	4.946	3.627
90	1.243	0.503	1.750	1.181	2.572	2.224	3.251	3.221	4.794	3.758
100	1.210	-0.760	1.677	1.049	2.441	2.961	3.111	4.565	4.684	5.448

*M – measured value, P – predicted value

ANN modelling

A selection of data presented in Table 1 was employed for building a feed forward multilayer perceptron's ANN. The values of the three parameters influencing the adsorption procedure (initial dye concentration, *p*H and time) were used as inputs while the final dye concentration was considered as output. The network was trained on 70 % of the input data. The cross validation and the final testing were each managed on 15 % of the inputs. After various trials, a 3 neurons hidden layer with then process elements on the first layer, five process elements on the second and four process elements on the third layer lead to the best results.

At 10000 epochs, the training and the cross validation mean squared errors (MSE) overlay almost perfectly. The MSE insignificant values of 0.000430891 and of 0.000365063 respectively allow to consider that the developed network defines with high confidence the adsorption process evolution.

The analysis of experimental recorded final dye concentrations and of those predicted by ANN (Table 9) discloses as well no significant dissimilarities. Thus, the chosen ANN can offer a correct fact sustained by the high value of the correlation coefficient (0.9926) and by the low value of the minimum square error (13.61).

Table 9. Measured final dye concentrations vs predicted by ANN model

Run	Initial dye concentration, mg/L	*p*H	Time, min.	Final dye concentration, mg/L	
				Measured	Predicted
1	200	2	10	11.172	11.196
2	200	2	20	5.858	6.949
3	200	2	40	2.022	2.785
4	200	2	50	1.075	1.021
5	400	2	30	5.448	6.869
6	400	2	90	1.083	1.147
7	600	2	60	1.896	1.467
8	600	2	80	1.728	1.446
9	800	2	50	4.911	3.771
10	800	2	60	2.435	2.040
11	800	2	80	2.045	1.861
12	800	2	90	1.85	2.183
13	1000	2	20	37.148	36.641
14	1000	2	30	18.621	20.792
15	1000	2	50	6.012	4.550
16	400	4.5	50	4.879	4.548
17	400	4.5	90	1.7495	2.022
18	800	4.5	30	31.961	29.506
19	800	4.5	40	20.372	17.766
20	800	4.5	60	4.054	5.106
21	1000	4.5	10	78.919	69.129
22	1000	4.5	50	13.208	12.197
23	1000	4.5	100	4.684	4.495
24	200	7	30	11.746	12.720
25	400	7	20	30.123	29.439
26	400	7	40	13.137	12.952
27	400	7	50	8.37	7.506
28	600	7	20	40.01	42.683
29	600	7	30	30.25	30.035
30	600	7	40	20.274	19.401
31	600	7	90	3.899	3.613
32	800	7	80	5.69	4.557
33	1000	7	10	90.788	72.717
34	1000	7	90	6.244	5.214

Figure 5 shows the measured values versus the predicted responses indicating that the ANN model almost perfectly explains the studied experimental range and can be successfully used to predict the dye final concentration.

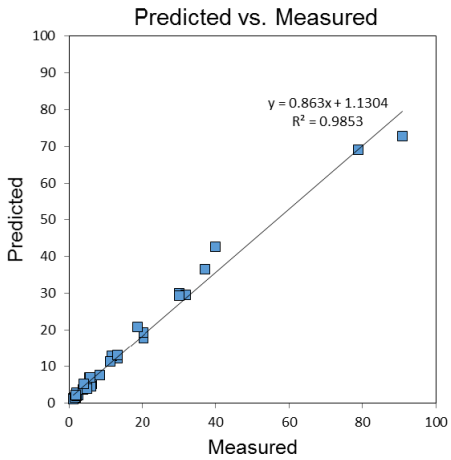

Figure 5. Plot of measured and predicted values for final CR concentration

CONCLUSION

The present research reveals that Congo Red dye is adsorbed on activated carbon obtained by physical activation method from cherry stones, in acidic and neutral media, more than 99 % of the existing dye being removed after 180 minutes.

Even though there were drawbacks in finding the appropriate mathematical models for describing the adsorption of Congo Red dye when influenced by multiples process parameters, this paper emphasizes the successful possibility of using Response Surface Methodology (RSM) and Artificial Neural Network (ANN) for generate adequate equations that fit the recorded experimental data and illustrate their behavior with a high confidence level.

The third-degree polynomial (cubic) model obtained with RSM can be efficiently employed to predict the residual dye concentrations all over the established parameters ranges: initial concentration from 200 mg/L to 1000 mg/L, *p*H from 2 to 7 and contact time between the pollutant and the adsorbent material from 10 minutes to 180 minutes. ANN modelling conducted also to reliable results but contrary to the cubic model, it cannot be emulated in usual computer software's such as Excel spreadsheet requiring only dedicated professional programs which represent a limiting factor for the interested users.

EXPERIMENTAL SECTION

Reagents

Congo Red (CR) dye (Sigma Aldrich, France) solutions with concentrations of 200 mg/L, 400 mg/L, 600 mg/L 800 mg/L and 1000 mg/L were obtained with distilled water.

Sodium hydroxide 0.1 N or hydrochloric acid 0.1 N, procured from Chemical Company (Iasi, Romania), were added in order to insure specific *p*H values of 2, 4.5, 7, 10 and 12.

Adsorbent preparation

Cherry stones used for the adsorbent material preparation were firstly washed then dried at room temperature and crushed.

The resulted powder was calcinated at 600 °C for 4 h in a Caloris L1003 laboratory furnace (Caloris Group, Romania) and the product (abbreviated as CS) was kept at 20 °C in closed vessels until further use.

Adsorption setup

0.1 g of CS were introduced in 50 mL Erlenmeyer flasks. 20.0 mL of CR solution having the anteriorly mentioned concentrations and pH were added.

The adsorption experiments were executed at room temperature on Nahita Blue 692 heating plates (Auxilab, Spain) for 10, 20, 30, 40, 55, 60, 80, 90, 100, 120, 150 and 180 minutes.

The solid phase was eliminated with the help of a Nahita 2615/1 digital centrifuge (Auxilab, Spain) set at 3000 rpm for 5 minutes.

The CR concentration was determined by UV-VIS spectrometry (Zuzi 4201 UV-VIS spectrophotometer, Auxilab, Spain) at specific maximum absorbance wavelengths (570 nm for *p*H 2; 530 nm for *p*H 4.5 and 500 nm for *p*H 7, 10 and 12).

The adsorption efficiency was calculated with the equation (4):

$$Adsorption\ efficiency\ (\%) = \frac{C_0 - C_e}{C_0} \times 100 \quad (4)$$

where C_0 and C_e are the initial and final dye concentration, respectively.

RSM modelling

All data recorded from the experimental program were introduced in two computer software's with the special aim of finding mathematical models able to describe the adsorption process.

Response Surface Methodology (RSM) with custom central composite design (CCCD) based on a three factors and three levels of variation setup was performed using Design-Expert 7.0 software. The regression procedure fitted the polynomial models represented by the equations (5), (6) and (7).

Linear $$Y = \beta_0 + \sum_{i=1}^{k} \beta_i X_i + e_0 \quad (5)$$

Quadratic $$Y = \beta_0 + \sum_{i=1}^{k} \beta_i X_i + \sum_{i=1}^{k} \beta_{ii} X_i^2 + \sum_{i=1}^{k} \sum_{j=i+1}^{k} \beta_{ij} X_i X_j + e_0 \quad (6)$$

Cubic $$Y = \beta_0 + \sum_{i=1}^{k} \beta_i X_i + \sum_{i=1}^{k} \beta_{ii} X_i^2 + \sum_{i=1}^{k} \beta_{iii} X_i^3 + \sum_{i=1}^{k} \sum_{j=i+1}^{k} \beta_{ij} X_i X_j + \sum_{i=1}^{k} \sum_{j=i+1}^{k} \beta_{iij} X_i^2 X_j + + \sum_{i=1}^{k} \sum_{j=i+1}^{k} \beta_{ijj} X_i X_j^2 + \sum_{i=1}^{k} \sum_{j=1+1}^{k} \sum_{j=i+1}^{k} \beta_{ijk} X_i X_j X_k + e_0 \quad (7)$$

Herein, Y is the predicted response (final dye concentration); X_i and X_j are variables; β_0 is the constant coefficient; β_i is the coefficient that determines the influence of parameter i in the response (linear term), β_{ij}, β_{ijk}, β_{iij}, β_{ijj} are the cross-products, coefficient β_{ii} is the quadratic coefficient and β_{iii} is the cubic coefficient, which refer to the effects of the interaction among independent variables. The multiple regression analysis can be applied to obtain the coefficient, and the equation can be used to predict the response.

The coded values (Table 9) of the parameters can be determined from the following equation:

$$x_i = \frac{X_i - X_o}{\delta X} \quad (8)$$

X_0 is the real value of the independent variable at the center point, X_i is the real value of the independent variable, and δX is the step change values between low (−1) and high (+1) levels.

Table 9. Experimental ranges and levels of the independent test variables

Variables	Unit	Symbol	Coded variable level		
			-1	0	1
Initial dye concentration	mg/L	A	400	600	800
*p*H	-	B	2.0	4.5	7.0
Time	min.	C	10	55	100

ANN modelling

Data employed for the Response Surface Methodology design were chosen as inputs and outputs in an Artificial Neural Network three-layered feed forward momentum type. Hidden layers with two to twelve neurons were tried with NeuroSolutions 6.0 software. Three input and one output node with 10000 epochs were used for ANN training.

REFERENCES

1. N. Ribeiro de Mattos; C. Rodrigues de Oliveira; L.G. Brogliato Camargo; R.S. Rocha da Silva; R. Lassarote Lavall; *Sep. Purif. Technol.*, **2019**, *209*, 806-814
2. H. Park; J.-H. Hwang; J.-S. Han; B.-S. Lee; Y.-B. Kim; K.-M. Joo; M.-S. Choi; S.-A. Cho; B.-H. Kim; K.-M. Lim; *Food Chem. Toxicol.*, **2018**, *121*, 360-366
3. C. Goebel; T.L. Diepgen; B. Blomeke; A.A. Gaspari; A. Schnuch; A. Fuchs; K. Schlotmann; M. Krasteva; I. Kimber; *Regul. Toxicol. Pharm.*, **2018**, *95*, 124-132
4. K.B. Tan; M. Vakili; B.A. Horri; P.E. Poh; A.Z. Abdullah; B. Salamatinia; *Sep. Purif. Technol.*, **2015**, *150*, 229-242
5. Y. Gao; S.-Q. Deng; X. Jin; S.-L. Cai; S.-R. Zheng; W.-G. Zhang; *Chem. Eng. J.*, **2019**, *357*, 129-139
6. D. Jiang; M. Chen; H. Wang; G. Zeng; D. Huang; M. Cheng; Y. Liu; W. Xue; Z. Wang; *Coordin. Chem. Rev.*, **2019**, *380*, 471-483
7. Z. Jia; Z. Li; T. Ni; Z. Li; *J. Mol. Liq.*, **2017**, *229*, 285-292
8. A. Oussalah; A. Boukerroui; A. Aichour; B. Djellouli; *Int. J. Biol. Macromol.*, **2019**, *124*, 854-862
9. G.L. Dotto; J.M.N. Santos; E.H. Tanabe; D.A. Bertuol; E.L. Foletto; E.C. Lima; F.A. Pavan; *J. Clean. Prod.*, **2017**, *144*, 120-129
10. H. Ma; A. Kong; Y. Li; B. He; Y. Song; J. Li; *J. Clean. Prod.*, **2019**, *214*, 89-94
11. I. Chaari; E. Fakhfakh; M. Medhioub; F. Jamoussi; *J. Mol. Struct.*, **2019**, *1179*, 672-677
12. W. Hamza; N. Dammak; H.B. Hadjltaief; M. Eloussaief; M. Benzina; *Ecotox. Environ. Safe.*, **2018**, *163*, 365-371
13. M. Tanzifi; M.T. Yaraki; M. Karami; S. Karimi; A.D. Kiadehi; K. Karimipour; S. Wang; *J. Colloid. Interf. Sci.*, **2018**, *519*, 154-173
14. A.M. Herrera-Gonzalez; M. Caldera-Villalobos; A.-A. Pelaez-Cid; *J. Environ. Manage.*, **2019**, *234*, 237-244
15. D.P. Dutta; S. Nath; *J. Mol. Liq.*, **2018**, *269*, 140-151
16. J. Mo; O. Yang; N. Zhang; W. Zhang; Y. Zheng; Z. Zhang; *J. Environ. Manage.*, **2018**, *227*, 395-405
17. K.A. Adegoke; O.S. Bello; *Water Res. Ind.*, **2015**, *12*, 8-24
18. K.H. Toumi; M. Bergaoui; M. Khalfaoui; Y. Benguerba; A. Erto; G.L. Dotto; A. Amrane; S. Nacef; B. Ernst; *J. Mol. Liq.*, **2018**, *271*, 40-50

19. M. Wakkel; B. Khiari; F. Zagrouba; *J. Taiwan. Inst. Chem. E.*, **2019**, *96*, 439-452
20. N.K. Soliman; A.F. Moustafa; A.A. Aoud; K.S.A. Halim; *J. Mater. Res. Technol.*, **2018**, https://doi.org/10.1016/j.jmrt.2018.12.010
21. X. Wen; H. Liu; L. Zhang; J. Zhang; C. Fu; X. Shi; X. Chen; E. Mijowska; M.-J. Chen; D.-Y. Wang; *Bioresource Tehnol.*, **2019**, *272*, 92-98
22. S. Dawwod; T.K. Sen; *J. Chem. Proc. Eng.*, **2014**, *1*, 1-11
23. T. Ngulube; J.R. Gumbo; V. Masindi; A. Maity; *J. Environ. Manage.*, **2017**, *191*, 35-57
24. K. Vikrant; B.S. Giri; N. Raza; K. Roy; K.-H. Kin; B.N. Rai; R.S. Singh; *Bioresource Technol.*, **2018**, *253*, 355-367
25. M.C. Collivignarelli; A. Abba; M.C. Miino; S. Damiani; *J. Environ. Manage.*, **2019**, *236*, 727-745
26. E. Li; B. Mu; Y. Yang; *Bioresource Technol.*, **2019**, *277*, 157-170
27. H.N. Tran; S.-J. You; A. Hosseini-Badegharaei; H.-P. Chao; *Water Res.*, **2017**, *120*, 88-116
28. C.X.-H. Su; L.W. Low; T.T. Teng; Y.S. Wong; *J. Environ. Chem. Eng.*, **2016**, *4*, 3618-3631.
29. M.M. Hassan; C.M. Carr; *Chemosphere*, **2018**, *209*, 201-219
30. C.R. Holkar; A.J. Jadhav; D.V. Pinjari; N.M. Mahamuni; A.B. Pandit; *J. Environ. Manage.*, **2016**, *182*, 351-366
31. L.Y. Jun; L.S. Yon; N.M. Mubarak; C.H. Bing; S. Pan; M.K. Danquah; E.C. Abdullah; M. Khalid; *J. Environ. Chem. Eng.*, **2019**, *7*, 1-14
32. M.A. Abdel-Fatah; *Ain Shams Eng. J.*, **2018**, *9*, 3077-3092
33. M.-H. Zhang; H. Dong; L. Zhao; D.-E. Wang; D. Meng; *Sci. Total Environ.*, **2019**, *670*, 110-121
34. A. Talaiekhozani, S. Rezania; *J. Water Process Eng.*, **2017**, *19*, 312-321
35. P.K. Gautam; A. Singh; K. Misra; A.K. Sahoo; S.K. Samanta; *J. Environ. Manage.*, **2019**, *231*, 734-748
36. S. Karimifard; M.R.A. Moghaddam; *Sci. Total Environ.*, **2018**, *640-641*, 772-797
37. S. Khamparia; D. Jaspal; *J. Environ. Manage.*, **2017**, *201*, 316-326
38. A.K.S. Priya; B.S. Kaith; N. Sharma; J.K. Bhatia; V. Tanwar; S. Panchal; S. Bajaj; *Int. J. of. Biol. Macromol.*, **2019**, *124*, 331-345
39. A.M. Ghaedi; A. Vafaei; *Adv. Colloid Interfac.*, **2017**, *245*, 20-39
40. M.R. Gadekar; M.M. Ahammed; *J. Environ. Manage.*, **2019**, *231*, 241-248
41. A. Simion; C.G. Grigoraş; A. Chiriac; N.C. Tâmpu; L. Gavrilă; *Environ. Eng. Manag. J.*, **2018**, *17*, 771-781
42. A.I. Simion; I. Ioniţă; C.G. Grigoraş; L. Favier-Teodorescu; L. Gavrilă; *Environ. Eng. Manag. J.*, **2015**, *14*, 277-288
43. S. Kaur; S. Rani; K. Mahajan; *J. Chem.*, **2013**, http://dx.doi.org/10.1155/2013/628582
44. C. Tian; C. Feng; M. Wei; Y. Wu; *Chemosphere*, **2018**, *208*, 476-483

STUDIA UBB CHEMIA, LXIV, 2,Tom I, 2019 (p. 159-174)
(RECOMMENDED CITATION)
DOI:10.24193/subbchem.2019.2.13

Dedicated to Professor Florin Dan Irimie on the Occasion of His 65th Anniversary

METABOLIC ENGINEERING OF *E. COLI*: INFLUENCE OF GENE DELETIONS AND HETEROLOGOUS GENES ON PHYSIOLOGICAL TRAITS

RÉKA SINKLER[a], MÁRTA BOTH-FODOR[a], EMŐKE ANTAL[a], HUNOR BARTOS[b], SZABOLCS LÁNYI[c], ILDIKÓ MIKLÓSSY[c*]

ABSTRACT. 1,4-butanediol (BDO) is an important commodity molecule that is used as a platform chemical for the production of polybutylene terephthalate (PBT), elastic fibres (Spandex) and other materials. The homologous enzyme of *E. coli*, *succinyl-CoA synthetase* (*sucCD*) and the heterologous *malonyl-CoA reductase* from *Chloroflexus aurantiacus* (*mcr*) are key enzymes in a heterologous pathway leading to BDO production, which were introduced into a genome-engineered *E. coli* MG1655(DE3) Δ*ldhA*, Δ*pflB* strain. Knowing that the expression of recombinant proteins and gene deletions can significantly influence cellular viability, the present study was carried out to investigate the impact of the two key enzyme expression on deletion strains, helping us to analyze the physiological changes of *E. coli* strains and providing directions for further optimizations in order to achieve satisfying target product yields.

Keywords: *1,4-butanediol, heterologous enzyme, Escherichia coli, metabolic engineering*

[a] *Politehnica University of Bucharest, Faculty of Applied Chemistry and Materials Science, 1-7 Gheorghe Polizu str., RO-011061, Bucharest, Romania*
[b] *University of Pécs, Faculty of Natural Sciences, Doctoral School of Chemistry, 6 Ifjúság str., Hu-7624, Pécs, Hungary*
[c] *Sapientia Hungarian University of Transylvania, Faculty of Economics, Socio-Human Science and Engineering, Department of Bioengineering, 1 Libertatii sqr., RO-530104, Miercurea Ciuc, Romania*
** Corresponding author: miklossyildiko@uni.sapientia.ro*

INTRODUCTION

Over the last decade, the necessity of alternative bio-based processes for currently petro chemistry-derived bulk chemicals demand has emerged [1,2]. The global production of BDO is currently manufactured almost entirely from petroleum-based, non-renewable feedstock such as acetylene, butane or butadiene resulting in 1,4-butanediol (BDO) to became listed on the NICNAS High Volume Industrial Chemicals List (HVICL) [3]. A native BDO pathway does not exist in any known organism, therefore developing a bio-based production system for 1,4-butanediol (BDO) through metabolic engineering methods, utilizing *E. coli* MG1655 as host strain is considered a good alternative to classical syntheses. However, to achieve a high yield of BDO with genetic engineering tools some technical challenges have to be met, mainly concerning the metabolic performance of host cells [4-10]. In metabolic engineering projects, altering the cellular metabolism with increased substrate uptake, reduction of carbon flux leading to undesirable by-products or the extracellular export of the target product may occur in order to shift the equilibrium towards product formation [11]. These modifications and additionally, the expression of heterologous proteins/enzymes can inflict a significant metabolic burden that can lead to decrease in biomass yield and cellular viability [10].

Carneiro et. al. discusses about several physiological stresses affecting bacterial strains during recombinant protein production, while the over-expression of heterologous proteins provokes a reduction in the synthesis of biomass-related proteins, due to the unequal competition for the translation apparatus by the mRNA species synthesized from the high-level expression of recombinant material. This can be explained by different amino acid composition of the recombinant protein relative to the average composition of biomass related proteins, which causes increased metabolic imbalance in the host cells [10].

Moreover, heterologous expression of even non-toxic proteins under strong promoter control (e.g. T7) causes competition for ribosomes from the exogenous mRNAs and decreases free ribosome concentration, which can lead to cell death. Moderate overexpression can affect the cellular environment by modifying the redox equilibrium, potentially resulting in growth inhibition, toxic accumulation of acetate, reduction of carbon flux via the oxidative branch of the pentose phosphate pathway, reduced expression of housekeeping genes, and inducing of various stress responses [12]. For example, overexpressing membrane proteins can decrease cellular fitness, presumably by saturating the protein translocation system and reducing respiratory chain complex formation, which eventually leads to respiratory stress [12].

There are phenomenological, empirical models describing linear correlations between growth rate and RNA/protein ratio, and predicting an overall linear effect on protein overproduction on cellular fitness [13]. Alternatively, it has been shown by modeling supported by wet experiment data that a strongly nonlinear fitness landscape associates with the *lac* pathway of *E. coli* depending on protein yield and activity [13].

Regardless, consequences of cellular stress on population dynamics at macro and molecular levels are not well understood. The picture is even less clear in cases, where the heterologously introduced gene products require ATP or/and make use of the host redox coenzymes or they interact with the host core metabolism [12]. This is the case in our present work, where we investigate the effect of an overexpressed two-step biosynthetic pathway requiring NADH, on a genome-edited deletion mutant *E. coli* strain.

In 2011 Yim et al. reported for the first time de novo biosynthesis of 1,4-BDO via a biological platform, which constituted the base for the bio-manufacturing of 1,4-butanediol, established by Genomatica [14]. Our aim was to build a simpler biosynthetic pathway of BDO in *E. coli*, able to use and convert renewable feedstock such as glucose and glycerol. As a by-product of biodiesel industry, glycerol is considered a very attractive carbon source [15-17]. To our knowledge, our group is the first to consider glycerol as a sustainable substrate for BDO production.

In our previous work [18], we reported construction of an *E. coli* strain with knocked-out genes for ethanol, lactate and formate production (Δ*adhE,* Δ*ldhA* and Δ*pflB*), able to produce a limited quantity of 1,4-BDO (.89 mg/L BDO under microaerobic conditions and .82 mg/L under anaerobic conditions), using glycerol as carbon source [18].

Here we present physiological assessment of a designed alternative biosynthetic pathway, using a different enzyme combination leading to the target product. The pathway contains the two-subunit native enzyme of *E. coli*, succinyl-CoA synthetase (sucCD) and the heterologous malonyl-CoA reductase from *Chloroflexus aurantiacus* (mcr) under the control of a strong T7 promoter, introduced and expressed in a genome-engineered MG1655(DE3) ΔldhA, ΔpflB strain.

RESULTS AND DISCUSSION

Given that genetic modifications, in our case gene inactivation and expression of recombinant proteins can significantly influence cellular viability, our present study tackled to investigate how expression of the two key enzymes impact cellular fitness and population stability of deletion strains, helping us to analyze physiological changes of *E. coli* strains and providing directions for further optimizations in order to achieve robust cultures with satisfying target product yields.

In the first phase of our study selection of putative enzymes (*mcr* EC 1.2.1.75 and *sucCD* EC 6.2.1.5) to our alternative heterologous pathway was carried out based on relevant literature. We considered the less studied *Chloroflexus aurantiacus* hydroxipropanoate cycle enzyme as extremely interesting due to its double specificity, with high potential also in other biosynthetic pathways.

1,4-butanediol production strains were obtained by model-driven metabolic optimization of the *E. coli* MG1655 host strain, identification of target genes for deletions was performed by metabolic flux balance analysis. The metabolic optimization was achieved by deletion of key genes *(ΔldhA* and *ΔpflB)* of the metabolic routes being competitive with the new heterologous pathway. Gene deletions were carried out using the λ-Red recombination method [19]. Expression of BDO-pathway enzymes under the control of T7 promoter was achieved after (DE3) lysogenization of the knocked-out strains. The vectors were checked by sequencing and their functionality tested by chemical transformation into the metabolically optimized strains [20]. Protein production of the strains was investigated in comparation with a specialized protein production strain. Strain optimizations were followed by examination of culture conditions of the optimized and the heterologous strains under anaerobic (oxygen-restricted) conditions. For carbon source glucose and glycerol was used providing an insight into the glycerol-utilization potential of these strains.

Pathway design. Heterologous reactions for 1,4-butanediol formation were selected based on literature sources and specific databases (KEGG; ECOCYC; BRENDA; PDB; NCBI). Thereafter we analyzed the key enzymatic parameters like substrate specificity, k_{cat}, molecular weight, subunits and genetic properties (GC content, phylogenetic distance from the host) as well. The new biosynthetic pathway employs the 4-carbon TCA cycle intermediate *succinyl-CoA*, which, in three enzymatic reduction/CoA activation steps is converted into 1,4-butanediol (Fig.1).

The designed biochemical pathway leading to BDO production is starting from succinyl-CoA, which can be converted into 4-hydroxybutyrate by a heterologous enzyme, *malonyl-CoA reductase* from *Chloroflexus aurantiacus* (*mcr*). The carboxylic group of 4-hydroxybutyrate can be activated by the native enzyme of *E. coli*, *succinyl-CoA synthetase* (*sucCD*) and in the final step the 4-hidroxybutyryl-CoA will be converted to 1,4-butanediol by the *malonyl-CoA reductase* from *Chloroflexus aurantiacus* (*mcr*).

The constraint-based models work well in the design of strains for the improved production of chemicals that belong to the central carbon metabolism, but the recombinant processes are far more complex, since the expression of recombinant proteins is generally plasmid-based, meaning that

the interaction with the central carbon metabolism is not straightforward to understand and to model. The combination of dynamic and stoichiometric models can be useful for the simulation of cell growth and metabolite and/or product formation [10].

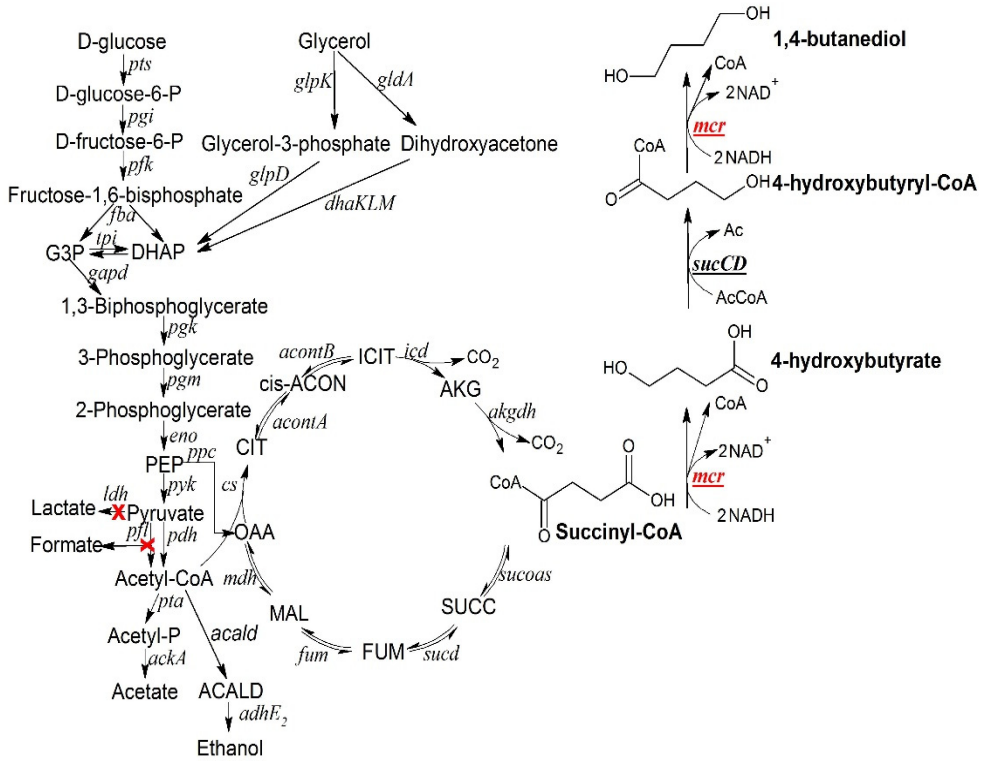

Fig. 1. Proposed biosynthesis pathway for 1,4-butanediol formation

Significant carbon metabolism pathways with relevant reactions of *E. coli* are depicted, the proposed BDO pathway starting from the TCA intermediate succinyl- CoA. Genetic modifications of the strain are marked in red, overexpressed endogenous ***sucCD*** gene is marked in bold letters. The image was created in ChemSketch

Plasmid construction. As the designed biosynthetic pathway requires the presence of two or more parallel heterologous enzymes, we decided to use the pETDuet system capable for the simultaneous expression of two genes with a strong promoter. Based on the literature these expression plasmids are currently applied successfully in several metabolic engineering applications for example butanol [21] acetoin, 2,3-butanediol [22, 23] and 3-hydroxypropionic acid biosynthesis [24].

For gene amplifications, the conventional PCR-directed molecular cloning methods were used with gene-specific primers, resulting in vectors used for protein production experiments (pGS2) and vectors, which contain two heterologously expressed genes of the BDO-production pathway (pGS2.1).

On the below gel electrophoresis images, we were able to detect the expected gene-specific PCR products as shown in Fig. 2, panel A, and the correct assembly of (pGS2) plasmid, examined by restriction digestion, and separated on a 1% agarose gel (panel B).

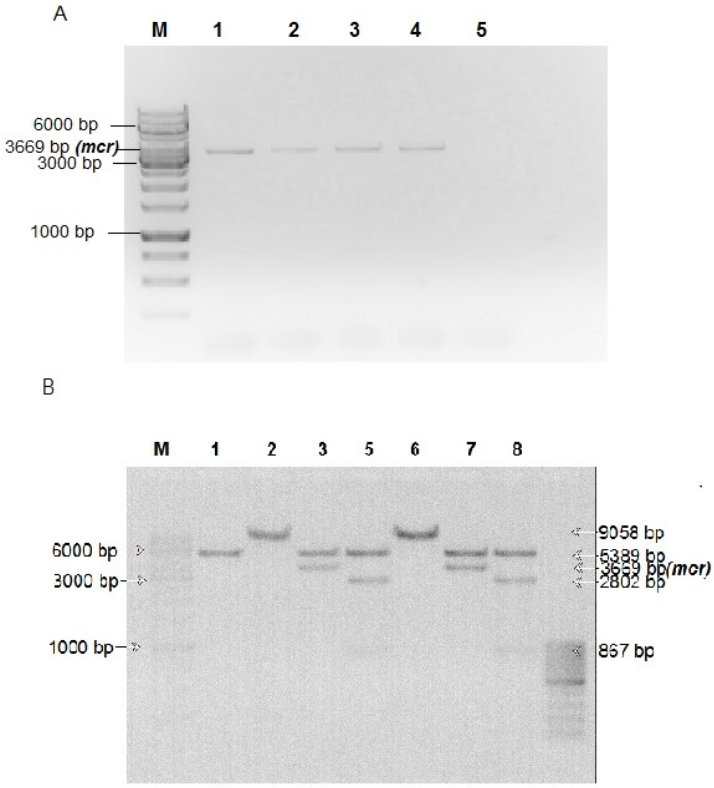

Fig. 2. PCR reaction products for isolation of *mcr* (A) and restriction verification of the pGS2 construct (B)

(Panel A: M- Molecular weight marker GeneRuler 1kb Thermo, Lanes: 1-5: PCR products of cloning reactions for *mcr*, the 3669 bp band corresponds to the *mcr* coding sequence, 6: no template control

Panel B: M- Molecular weight marker GeneRuler 1kb Thermo, Lanes: 1- Non-digested pGS2 vector; 2- pGS2 vector digested with *EcoRI*; 3-7: pGS2 digested with *EcoRI* and *HindIII* enzymes, the 3669 bp band corresponds to the *mcr* gene, 5,6,7,8-digestion of pGS2 with *EcoRI*, *SalI* and *HindIII* restriction enzymes, with the expected DNA fragment sizes).

In silico design of the vectors was carried out by the trial version of Snapgene. The restriction map of the pETDuet1-mcr-sucCD (pGS2.1) co-expression plasmid, presenting the main features is shown in Fig. 3.

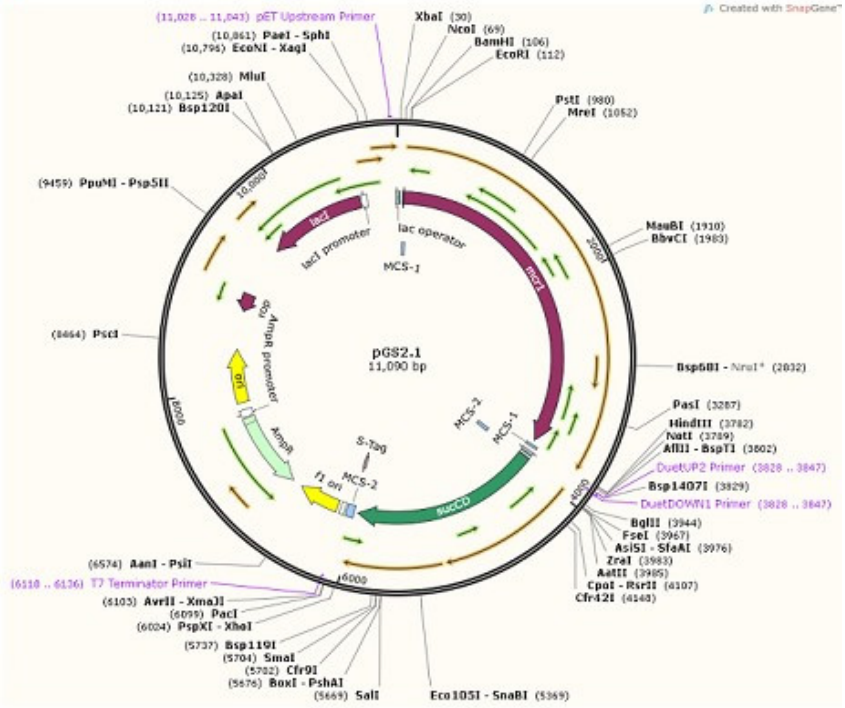

Fig. 3. *In silico* design of pGS2.1 vector containing the heterologous enzymes for 1,4-butanediol pathway

Genome engineering. To delete the key genes of metabolic routes competitive with the new heterologous pathway chromosomal gene deletions were carried out using the λ-Red recombination system [19]. Blocking off the competing metabolic pathways with the integrated biosynthetic pathway is one of the promising strategies for optimizing the yield of the target product. Redirection of the carbon flux to the BDO biosynthesis firstly was analyzed by OptKnock algorithm, after which we identified *ldhA* gene deletion to inhibit lactic acid production and deletion of the *pflB* gene for suppression of formic acid production in our previous work. Verification of genomic regions for *pflB* and *ldhA* of the wild-type MG1655(DE3) and double mutant MG14D2(DE3) was carried out by gene-specific PCR, whereas products separated on 1% agarose gel are shown in Fig. 4.

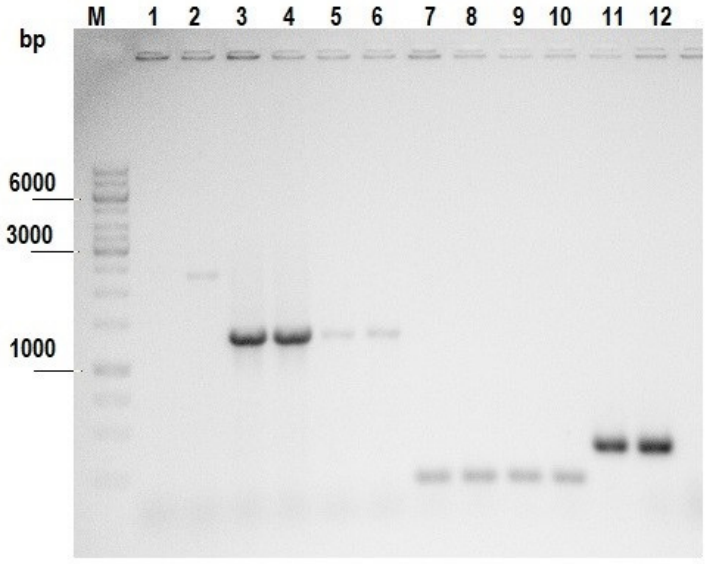

Fig. 4. Genotype analysis of wild-type and mutant *E.coli* strains with *pflB* and *ldhA* specific primers in PCR reactions.

(M: Molecular Weight Marker GeneRuler 1kb (Thermo); 2: *pflB* region of MG1655(DE3); 3.4: *ldhA* region of MG1655(DE3); 5.6: *ldhA* region of MG14D1(DE3), 7-9: *pflB* region of MG14D1(DE3), MG14D2(DE3) strains, 11: *ldhA* region of MG14D2(DE3) strain.) PCR products were separated by 1% AGE and visualized by RedSafe (Chembio).

Heterologous expression. In order to define protein production potential correlated to genomic modifications, mcr protein expression of the wild-type and double mutant strains was monitored in comparison to a specialized protein production strain. The target protein (*mcr*) expression was investigated in MG1655(DE3), MG14D2(DE3) and *Escherichia coli* BL21 Star (DE3), where chemically competent mutant strains were transformed by heat-shock with co-expression vector pGS2. Expression was induced by isopropyl β-D-1-thio-galacto-pyranoside (IPTG) in a final concentration of 0.5 mM and the cultures were maintained for 3h. Protein production was monitored after 0, 1, 2 and 3 hours of expression, by electrophoresis performed under denaturing conditions starting from samples with equal biomass (OD_{595} values) of expression cultures.

Based on the results presented in the gel electrophoresis image (Fig. 5), the apparent size of the protein produced by all the studied different strains was around 130 kDa. This value agrees well with the theoretical molecular weight of *mcr,* calculated at 131.978 kDa.

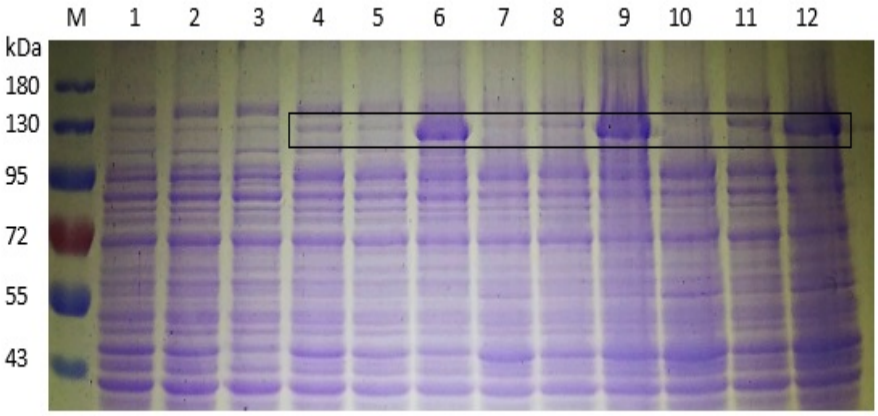

Fig. 5. Heterologous expression of the *mcr* enzyme in different *E. coli* strains. (M: PageRuler™ Prestained Protein Ladder, 10 to 180 kDa (Thermo); 1: MG1655(DE3)pGS2 before induction; 2. MG14D2(DE3)pGS2 before induction; 3: *E.Coli* BL21 Star (DE3)pGS2 before induction; 4,7,10: MG1655(DE3)pGS2 after 1,2 and 3 hours of induction; 5,8,11: MG14D2(DE3)pGS2 after 1,2 and 3 hours of induction; 6,9,12: *E.Coli* BL21 Star (DE3) after 1,2 and 3 hours of induction. Cellular proteins were separated by tris-glycine SDS-PAGE and stained by Commassie.

In case of pGS2-transformed, wild type MG1655(DE3) strain, protein production is less significant in all three sampling time-points, and based on the gel image, we can observe even a higher quantity of heterologous protein after the 1st hour of expression compared to samples after two and three hours of expression, respectively. In case of the double mutant strain, a slightly elevated protein production was registered in all three samples (Fig. 5, lanes 5,8,11), and a small increase in protein quantity over the time course of expression can be noted, based on the intensity of the specific protein bands.

The highest yield of produced heterologous protein was observed, as anticipated, in case of *E. coli* BL21 Star (DE3), in which case after just one hour of induction a notable quantity of *mcr* appeared, increasing with the time of expression, based on protein band intensity (Fig. 5, lanes 6,9,12).

However, in case of a similar experimental setup, studying expression of a smaller molecular weight protein of around 94 kDa (*adhE* from *Clostridium acetobutylicum*), even a triple deletion mutant strain showed comparable levels of protein expression to the same specialized *E. coli* strain (data not shown). Based on these results, we can hypothesize, that heterologous protein size has a significant influence over expression levels in non-specialized *E. coli* strains, especially if these strains harbor genomic modifications as well.

Furthermore, amino-acid composition, and presumably, phylogenetic distance of the source organism for non-codon-optimized heterologous coding sequences can be taken into account in order to further investigate and clarify this question.

Growth dynamics investigation. Population dynamics studies were carried out by comparing the optimized MG14D2 (DE3) strain, the production strain MG14D2(DE3)pGS2.1, as well as the MG1655(DE3) and MG14D2(DE3)pC control strains under oxygen-limited conditions in terms of maximal OD values, growth rates and phases of bacterial dynamics. In small-scale experiments, minimal media was inoculated in triplicates to an initial OD_{595} of 0.1 with genetically homogeneous inoculum of the above strains, containing as carbon source glucose or glycerol at 5 g/L concentration and cultivated for 12 hours. Growth curves were compiled based on blank-corrected OD_{595} values, and the data comparing the four studied strains in case of glucose and glycerol substrates, respectively, are presented in Figure 6.

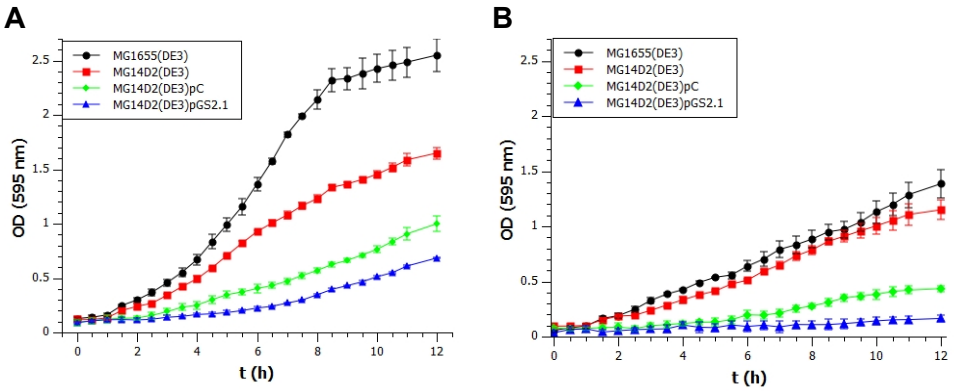

Fig. 6. Growth dynamics profile of the investigated strains using as sole carbon source glucose (panel A) and glycerol (panel B).

Analysis of the data presented above shows that, using glucose as carbon source, the duration of the exponential growth stage for MG1655(DE3), the lysogenized wild-type strain reached around 5 hours, while the estimated growth rate was ~0.26/h with a generation time of 2.6 hours. The recorded OD_{595} values depict a standard growth dynamics profile, where individual phases can be clearly separated.

In turn, for the knock-out mutant MG14D2(DE3), a higher 3.2 hour generation time was calculated, whereas presence of an even empty plasmid required a 3.5 hour generation time for population maintenance, in case of MG14D2(DE3)pC. The generation time reflects pretty fairly, in our view

the metabolic burden of several genetic modifications, as in case of MG14D2(DE3)pGS2.1, a double mutant harboring two plasmid-borne overexpressed genes, the generation time reaches 4.1 hours, by 1.5 hours longer than in case of the initial, wild-type strain. These differences should be significant especially from the point of view of process engineering. The calculated generation times reflect the maximal optical density values reached by each strain, as well as the growth dynamics.

In similar fashion, in case of using glycerol as the sole carbon source an elongated growth dynamic profile can be distinguished in case of all four strains. The strain MG14D2(DE3)pC containing the empty plasmid was hardly able to adapt to the culture conditions in the studied timeframe, the estimated growth rate being only ~0.15/h. In comparison, the double deletion mutant MG14D2(DE3) showed a ~ 0.23/h value with a generation time of 2.79 hours, comparable to that of the wild-type strain.

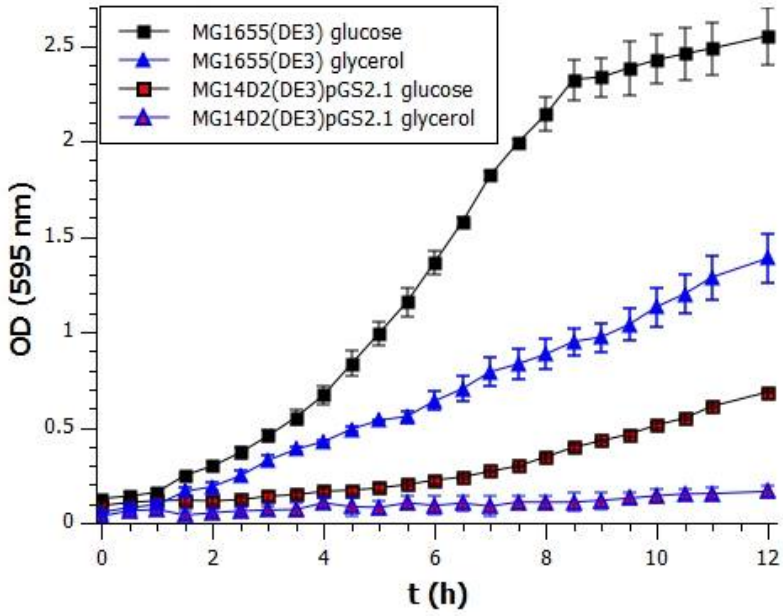

Fig. 7. Comparison of growth dynamics of the control MG1655(DE3) and the production strain MG14D2(DE3)pGS2.1 using glucose or glycerol as carbon source

Comparing the control MG1655(DE3) to the double mutant and heterologous enzyme (*mcr, sucCD*) expressing MG14D2(DE3)pGS2.1 strains, a significant difference in the population growth dynamics can be observed. According to the results shown in figure 7, even in conditions of highly

assimilated glucose carbon source, genetic interventions greatly influence growth profiles, cause a significant decrease in biomass production due to competition for cellular resources and create a prolonged generation time in order for the cells to function in altered intracellular metabolic environment. Nevertheless, in order to approach the theoretical growth rate (0.59/h) obtained during *in silico* simulations, further long-term adaptation experiments are foreseen in order to investigate adaptability and robustness of these *E. coli* strains.

CONCLUSIONS

The main biomass precursors are generally associated in the carbon metabolism with glycolytic activities and the tricarboxylic acids (TCA) pathway, which are diverted during recombinant protein production, causing metabolic imbalance in protein producing bacterial cells. The redox equilibrium and carbon flux diversion can be further enhanced by genomic modifications directed to the central carbon metabolism. However, the two modifications can complement each other in terms of rebalancing the redox equilibrium with carefully selected heterologous genes.

Our study subjects were genetically modified *E. coli* strains in various stages of genetic modifications designed to produce BDO; the production strain being a metabolically optimized double mutant derived from *E. coli* MG1655 harboring a two-gene heterologous biosynthetic pathway.

Taken in consideration the above, we considered essential to investigate cell behavior in case of multiple genetic modifications in our strains. Consequently, we tried to focus on the extent of adverse effects (physiological stresses) of gene deletions and heterologous genes on biomass production and strain fitness. We investigated protein production potential as well as the growth profiles of the original, gene deleted and heterologous pathway-bearing *E. coli* strains. We consider our experimental data obtained from the population dynamics and fitness testing of bacterial cultures under various carbon sources (glucose and glycerol) as being a good basis for process design and optimization in biosynthesis of valuable chemicals. Moreover, they provide a good starting point for further scale-up experiments and deeper physiological investigations (gene expression, transcriptomics) for such bacterial strains.

EXPERIMENTAL SECTION

The list of bacterial strains used in this study is presented in Tab. 1.

Table 1. Bacterial strains, plasmids and oligonucleotides used in this study

Strain	Relevant genotype	Purpose	Source
MG1655	K-12 F– λ– ilvG– rfb-50 rph-1	Original *E. coli* strain for gene deletions and *sucCD* cloning	DSMZ
BL21 STAR (DE3)	F^-ompThsdSB(r_B^-, m_B^-) *galdcmrne*131(DE3)	*E. coli* strain for routine T7 expression	Novagen
MG1655(DE3)		Wt strain with DE3-lysogenization	This study
MG14D1(DE3)	MG1655 (DE3) Δ*pflB*	Lysogenized *pflB* deletional mutant	This study
MG14D2(DE3)	MG1655 (DE3) Δ*pflB*Δ*ldhA*	Lysogenized *pflB*, *ldhA* double deletional mutant	This study
MG14D2(DE3)pC	MG1655 (DE3) Δ*pflB*Δ*ldhA* pETDuet1	Control strain	This study
MG14D2(DE3)pGS2	MG1655 (DE3) Δ*pflB*Δ*ldhA* harbouring pGS2	Production strain	This study
MG14D2(DE3)pGS2.1	MG1655(DE3) Δ*pflB*Δ*ldhA* harbouring pGS2.1	Production strain	This study
Chloroflexus aurantiacus	WT	Strain for *mcr* cloning	DSMZ
E. coli (Top10F')	F', mcrA Δ(mrr-hsdRMS-mcrBC), recA1 araD139 galU galK rpsL endA1 nupG	Replication host	Invitrogen

The list of plasmids and oligonucleotides is presented in Tab. 2. Coding sequences were obtained by gene-specific PCR reactions using as templates genomic DNA from *Chloroflexus aurantiacus (DSMZ)* and *E. coli* MG1655, followed by standard restriction cloning and ligation techniques (Table3).

Subcloning the sequences into pETDuet1 was performed by cleaving the vector and PCR products with restriction enzymes *EcoRI-HindIII* in case of *mcr* and with *AatI-XhoI* in case of *sucCD*, followed by isolation and purification of the bands of the vector fragments (GeneJET Gel Extraction Kit, Thermo Fisher Scientific), respectively of the insert (see digestion and ligation details of *mcr* in Table 4).

Table 2. Plasmids and oligonucleotides used in this study

Plasmid			
pETDuet-1	Ampr, lacI, T7lac	Coexpression vector	Merck - Millipore
pGS2	pETDuet-1 harbouring *mcr*	Expression vector for *mcr*	This study
pGS2.1	pETDuet-1 harbouring *mcr* and *sucCD*	Coexpression vector for *mcr* and *sucCD*	This study
Oligonucleotide			
SucCD1AatIFor	5′gccacagacgtcatgaacttacatgaatatcag	Cloning primers for *sucCD*	
SucCD1XhoIRev	5′cgatatctcgagtttcagaacagttttcagtgc		
Mcr1EcoRIFor	5’gagaattcaatgagcggaacaggacgactg	Cloning primers for *mcr*	
Mcr1HindIIIRev	5’ccaagcttttacacggtaatcgccccgtcc		
ΔpflB3	5′aaatccacttaagaaggtaggtg	Verification primers for *pflB*	
ΔpflB4	5′tcgtggagcctttattgtac		
ΔldhA3	5′gcacaaagcgatgatgctgtag	Verification primers for *ldhA*	
ΔldhA4	5′ccgttcagttgaaggttgcg		

Table 3. PCR reaction for *mcr* amplification

		PCR Protocol	
Template DNA	20 ng	Initial denaturation	98ºC
HF buffer	1×	Denaturation	98ºC
Forward primer	0.5 µM	Annealing	63ºC
Reverse primer	0.5 µM	Extension	72ºC
dNTP	200 µM each	Final extension	72ºC
Phusion polymerase	2 U	Hold	4ºC
upH2O			

Ligation was carried out with T4 DNA ligase (Thermo Fisher Scientific), thereafter the products were test digested and verified by sequencing (UDGenomed, Hungary). All buffers, restriction and ligase enzymes used were obtained from Thermo Scientific. DE3-lysogenization was applied (λDE3 Lysogenization Kit, Novagen, Merck Millipore) for expression of heterologous genes under the control of T7 promoter, according to the manufacturer’s instructions.

Table 4. Digestion and ligation reactions used for the pETDuet-*mcr* construct

Digestion with *EcoRI* + *HindIII*		Ligation pETDuet-*mcr*	
Template DNA	100 ng	Digested pETDuet-1	1×
R buffer	1×	*mcr* gene	3×
EcoRI	10 U	T4 buffer	1×
HindIII	10 U	T4 DNA ligase	10 U
upH2O		upH2O	
Incubation 2 hours at 37°C			

Cultures for protein expression were obtained by transformation of chemically competent mutant strains by heat-shock with co-expression vectors pGS2 and pGS2.1. Transformed colonies were selected on LB plates containing 100 μg/mL ampicillin (Sigma). Starter cultures from a single colony were grown overnight at 37°C in LB medium containing 100 μg/mL ampicillin. To produce the target protein, a volume of 50 mL LB medium supplemented with 100 μg/ml ampicillin was inoculated from the starter culture to OD_{595}=0.05 and was grown at 37°C until OD_{600}=0.6. Expression was induced by isopropyl β-D-1-thiogalactopyranoside (IPTG, Sigma) in a final concentration of 0.5 mM. The culture was maintained at 37°C in a shaking incubator at 250 rpm for 3h, and samples were harvested by centrifugation (12000 rpm for 5 minutes). Separation of cellular proteins was performed by SDS-PAGE.

For growth dynamics experiments inoculum cultures were set up starting from a single colony, cells were grown in complex media (Luria-Bertoni media supplied with 50 μg/mL ampicillin) at 37°C and 160 rpm until reaching the mid-log phase. Minimal media were inoculated to an initial OD_{595} of 0.1, containing as carbon source glucose or glycerol at 5 g/L, and 0.5 mM IPTG was added (M9 mineral medium, 25 mM Na_2HPO_4, 25 mM KH_2PO_4, 50 mM NH_4Cl, 2 mM $MgSO_4 \times 7H_2O$, 0.05 mM $FeCl_3 \times 6H_2O$, 0.02 mM $CaCl_2 \times 4H_2O$, 0.01 mM $MnCl_2$, 0.01 mM $ZnSO_4 \times 7H_2O$, 0.002 Mm $CoCl_2$, 0.002 mM $CuCl_2$, 0.002 mM $NiCl_2$, 0.002 mM $Na_2MO_4 \times 2H_2O$, 0.002 mM H_3BO_3). Cultivation was carried out in microtiter plates (200 μL) covered with adhesive foils as well in hermetically sealed glass bottles (50 mL). Small volume cultures in triplicates were maintained and determination of optical density at 595 nm was performed with the BMG Fluostar Optima microplate reader, at 37°C and 160 rpm shaking. Growth dynamics were investigated for 12 hours with measurements of OD_{595} values in every 30 minutes.

REFERENCES

1. T.M. Carole, J. Pellegrino, M.D. Paster, *Appl. Biochem. Biotechnol.*, **2004**, *115*, 871–885.
2. J.J, Straathof, *Chem. Rev.*, **2014**, *114*, 1871-1908**.**
3. S. Zeng*, Curr. Opin. Biotechnol.*, **2011**, *22*, 749-757.
4. P.K. Ajikumar, K. Tyo, S. Carlsen, O. Mucha, T.H. Phon, G. Stephanopoulos, *Mol. Pharm.*, **2008**, *5,* 167-190.
5. J.D. Keasling, *Science*, **2010**, *330*, 1355-1358.
6. J. Kirby, J.D. Keasling, *Annu. Rev. Plant. Biol.*, **2009**, *60*, 335–55.
7. D.K. Marcuschamer, P.K. Ajikumar, G. Stephanopoulos, *Trends Biotechnol.,* **2007**, *25,* 417-424.
8. R. Muntendam, E. Melillo, A. Ryden, O.Kayser, *Appl. Microbiol. Biotechnol.,* **2009,** *84*,1003-1019.
9. V.G. Yadav, G. Stephanopoulos, *Curr. Opin. Microbiol.*, **2010,** *13*, 371-376.
10. S. Carneiro, E.C. Ferreira, I. Rocha, *J. Biotechnol.,* **2013,** *164,* 396– 408.
11. V.G. Yadav, M.D. Mey, C.G. Lim, P.K. Ajikumar, G. Stephanopoulos, *Metab. Eng.*, **2012,** *14*, 233-241.
12. J.T. Kittleson, G.C. Wu, J.C. Anderson, Curr. Opin. *Chem. Biol.*, **2012,** *16*, 329–336.
13. M. Scott, C.W. Gunderson, E.M. Mateescu, Z. Zhang, T. Hwa, *Science*, **2010**, *330*,1099-1101.
14. H. Yim, R. Haselbeck, W. Niu, C. Pujol-Baxley, A. Burgard, J. Boldt, J. Khandurina, J.D. Travick, R.E. Osterhout, R. Stephen, J. Estadilla, S. Teisan, H.B. Schreyer, S. Andrae, T.H. Yang, S.Y. Lee, M.J. Burk, S. Van Dien, *Nat. Chem. Biol.*, **2011**, *7*, 445–452.
15. G.P. da Silva, M. Mack, J. Contiero, *Biotechnol. Adv.*, **2009**, *27*, 30-39.
16. S.S. Yazdani, R. Gonzalez, *Metab. Eng.*, **2008**, *10*, 340– 351.
17. V.F Wendisch, S.N. Lindner, T.M. Meiswinkel, *Biodiesel- Quality, Emissions and By-Products*, IntechOpen, London, **2011**, 305–339.
18. I. Miklóssy, Zs. Bodor, K.Cs. Orbán, R. Sinkler, Sz. Lányi, B. Albert, *J. Biomol. Struct. Dyn.,* **2016**, *35*, 1874-1889.
19. K.A. Datsenko, B.L. Wanner, *Proc. Natl. Acad. Sci.,* **2000***97*, 6640-6645.
20. J.F. Sambrook, D.W. Russell, *Molecular Cloning: A Laboratory Manual* 3rd ed., *Cold Spring Harbor Laboratory Press*, New York, **2001**
21. P. Zhou, Y. Zhang, P. Pixiang, J. Xie, Q. Ye, *Ann. Microbiol.*, **2014***64*, 219-227.
22. C. Gao, L. Zhang, Y. Xie, C. Hu, Y. Zhang, L. Li, Y. Wang, C. Ma, P. Xu, *Bioresour. Technol.*, **2013**137,111-115.
23. D.R. Nielsen, S.H. Yoon, C.J. Yuan, K.L.J. Prather, *Biotechnol. J.*, **2010**, *5*, 274-284.
24. W.S. Jung, J.H. Kang, H.S. Chu, I.S. Choi, K.M. Cho, *Metab. Eng.,* **2014**, *23*, 116-122.

STUDIA UBB CHEMIA, LXIV, 2,Tom I, 2019 (p. 175-188)
(RECOMMENDED CITATION)
DOI:10.24193/subbchem.2019.2.14

Dedicated to Professor Florin Dan Irimie on the Occasion of His 65th Anniversary

SYNTHESIS OF 3-AMINO-7-ARYL-8-AZACHROMANS: VALIDATION OF A SYNTHETIC ROUTE WITH ENANTIOSELECTIVE POTENTIAL

EDUARD BADARAU[a,b,c], FRANCK SUZENET[b], ADRIANA-LUMINITA FINARU[c], AND GERALD GUILLAUMET[b,*]

ABSTRACT. A potential enantioselective access to 3-amino-7-aryl-8-azachromans is described. The reported multi-step synthesis involved the use of aspartic acid as the building block that could induce chirality. The azachroman scaffold was obtained *via* a key intramolecular inverse Diels-Alder cycloaddition between a 1,2,4-triazine and a judiciously functionalized alkyne. This class of compounds are hetero-isosteres of previously reported ligands of the histaminergic H_3 receptor.

Keywords: *8-azachroman, inverse Diels-Alder cycloaddition, H_3R ligands*

INTRODUCTION

Inspired by their naturally occurring benzene analogues, the aza-chromans constitute a class of compounds of high interest in medicinal chemistry. Their interaction with the biological targets have the advantage of generating additional strong interactions (*e.g.* hydrogen bonding) compared to their benzene analogues, which finally translates to better biological activities. From a chemical point of view, the "CH" to "N" isosterism induce regioselectivity patterns, which allows a better control on the pharmaco-modulation output.

[a] *University of Bordeaux, Institute of Chemistry & Biology of Membranes & Nano-objects (CBMN), Allée Geoffroy Saint Hilaire, Bat B14, 33600, Pessac, France*

[b] *Institut de Chimie Organique et Analytique, Université d'Orléans, UMR-CNRS 6005, UFR Sciences, BP 6759, Rue de Chartres, 45067 Orléans Cedex 2, France*

[c] *Centrul de Cercetare "Chimie Aplicata si Inginerie de Proces", Universitatea din Bacau, Calea Marasesti, nr. 157, 600115 Bacau, Romania*

** Corresponding author: gerald.guillaumet@univ-orleans.fr*

One of the medicinal chemistry projects developed by our group focuses on the lastly discovered serotoninergic receptor: 5-HT_7R. Among the different series of compounds that we designed and synthesized as serotoninergic ligands, 8-azachromans was a class of compounds we developed using a Diels-Alder cycloaddition strategy. We already described in the past the synthesis of 8-azachromans [1], decorated on the oxane ring with an amine moiety, while the pyridine incorporated an aliphatic or aromatic substituent in the 7-position. Unfortunately, compared to the 8-substituted chromans, which were described as highly potent serotoninergic 5-HT_7 ligands [2], the 7-substituted-azachromans did not show a promising binding to the same receptors, most probably because of the shape mismatch between the reference and the newly synthesized molecules.

However, 7-arylchromans were reported as bioactive molecules for another CNS-involved target: the histaminergic H_3 receptor (H_3R) [3]. Because of the perfect 2D and shape similarity between the reported H_3 antagonist and our series of azachromans (*Scheme 1*), we continued investigating this class of compounds. We were particularly interested in developing an enantioselective access to the 3-amino-7-aryl-8-azachromans.

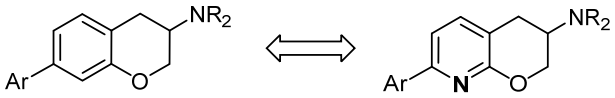

previously reported H3R ligand new hetero-isosteric analogues

Scheme 1

The synthesis of the desired isosters was designed on an intramolecular Diels-Alder cycloaddition approach between a 1,2,4-triazine (as electron-poor diene partner) and a terminal alkyne (as electron-rich dienophile partner). We validated in the past this inverse-electron demand Diels-Alder methodology [1], however, in the case of 8-aza-3-aminochromans, our previous strategy involved a fast access to the desired molecules without chiral discrimination on the C_3 center. As a next step of our research program, we were interested in developing a synthetic route with an enantioselectivity potential. Because of the optimization phase required by such a multistep synthesis (which should be devoided of any racemization steps), racemic starting materials were used, and, when all the synthetic issues would be solved, enantiopure starting materials could be used instead. The present paper exposes only the first *validation step* of the designed synthetic route and was conducted on racemic mixtures.

The retrosynthetic plan was constructed on a key Diels-Alder cycloaddition step: the desired compounds **I** would be obtained *via* an intramolecular [4+2] cycloaddition conducted on the triazines **II**. The acetylenic intermediate **II** would be synthesized from the alcohol **III** (after its activation, as a sulfonate for example). Finally, the intermediate **III** would be the result of the sulfone substitution from triazine **IV** by the alcohol intermediate **V** (*Scheme 2*).

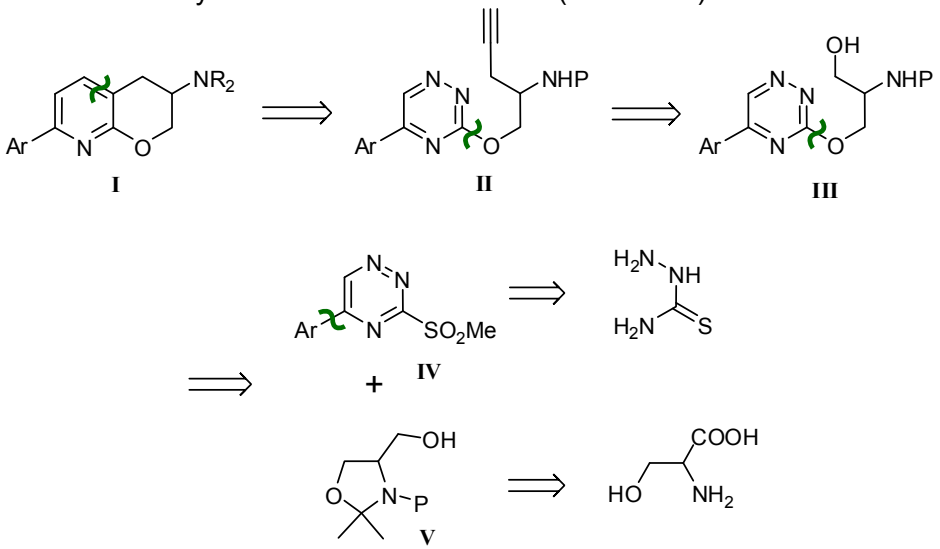

Scheme 2

RESULTS AND DISCUSSION

The synthesis started by obtaining the triazine intermediate **1**, using the previously published protocols [1], in 5 consecutive steps, starting from the commercially available thiosemicarbazide (*Scheme 3*).

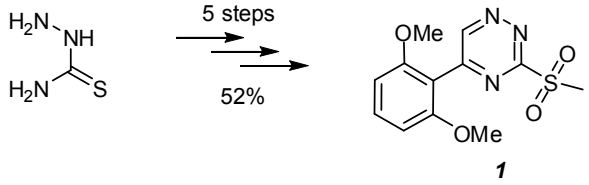

Scheme 3

The alcohol **V** was obtained after 4 steps starting from D,L-serine, and involved the synthesis originally described by Garner [4], with further improvements. Briefly, the starting amino-acid was reacted with di-*tert*-butyl-dicarbonate under basic conditions, and subsequently with iodomethane to

give the ester **2** in 78% yield. Subsequently, the alcohol and the amine moieties were protected with an isopropylidene using dimethoxypropane and *para*-toluenesulfonic acid in refluxing toluene. The ester **3** was reduced to the corresponding alcohol **4** by lithium aluminum hydride in refluxing diethyl ether (*Scheme 4*).

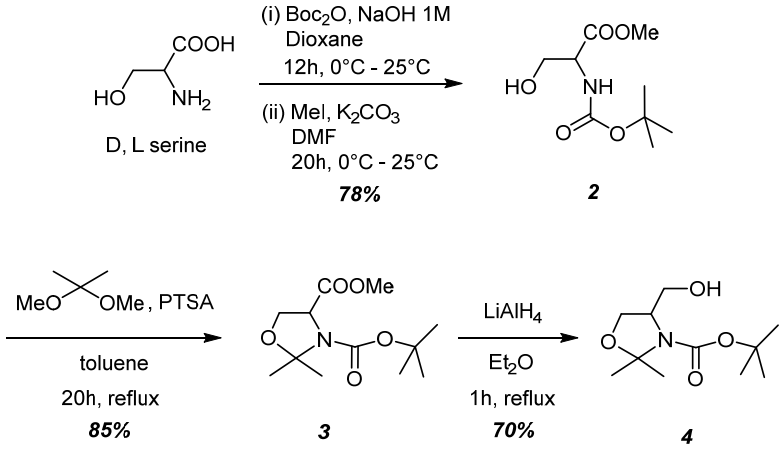

Scheme 4

With both intermediates **1** and **4** available, the synthesis continued by sulfone substitution with the alkoxide **4**, followed by the isopropylidene cleavage under acidic conditions. The resultant alcohol **6** was subsequently activated as a methyl-sulfonate (**7**) and used for the next step as a crude product, because of its instability during the flash-chromatography purification step. (*Scheme 5*).

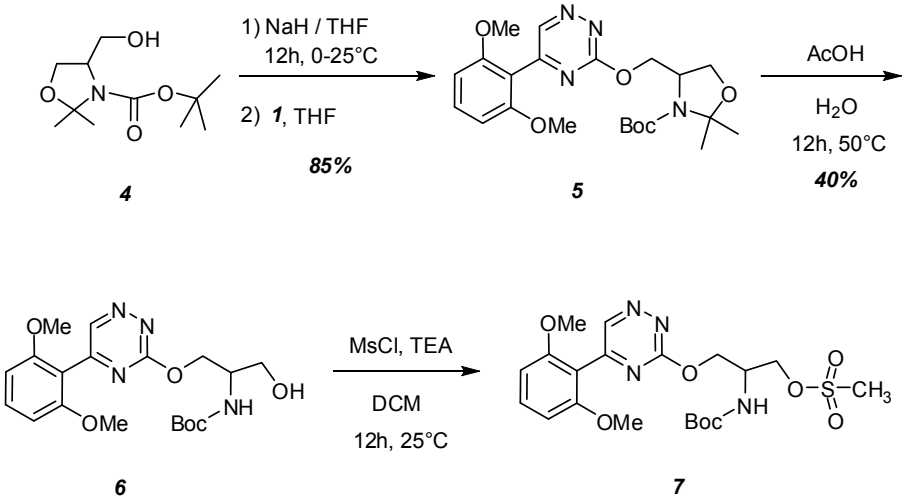

Scheme 5

Several trials of substitution of the methylsulfonate (OMs) with different acetylene sources (phenyl or trimethylsilyl acetilydes) were unsuccessful, in all cases only the degradation of the starting material **7** was observed (*Scheme 6*). It should also be mentioned that the same synthetic strategy of activating the alcohol moiety as different sulfonates (methylsulfonate, *para*-toluenesulfonate or trifluoromethylsulfonate) was tested directly on the intermediate **4**, but the subsequent substitution with various acetylides were also unsuccessful (results not presented).

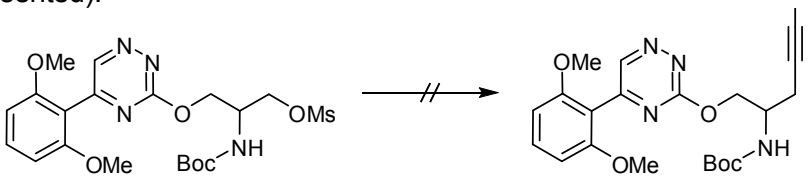

7

Scheme 6

As the activated alcohol failed to deliver the desired alkyne, a backup strategy was subsequently used. Starting from the aspartic acid, we decided to generate the acetylene feature of the aminoalcohol **VI,** before its insertion on the triazinic intermediate **IV** (*Scheme 7*).

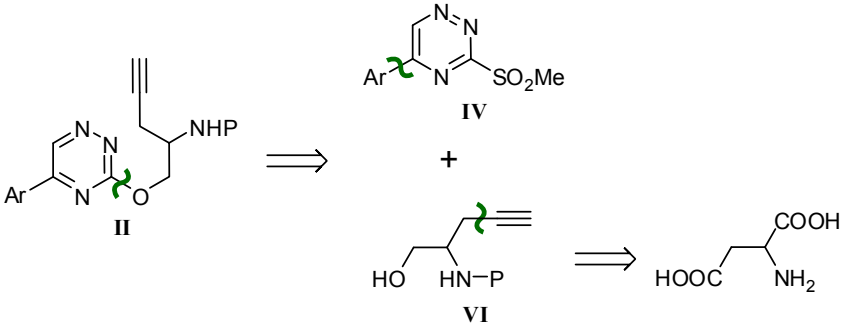

Scheme 7

The commercially available D,L-aspartic acid was submitted to a synthetic sequence following the protocols previously described in the literature [5, 6]. The higher homologue of the Garner's aldehyde **8** was obtained with an excellent 43% yield, over 5 steps. Subsequently, the terminal alkyne could be generated *via* the 2-steps Corey-Fuchs method [7]: (i) reacting the aldehyde with triphenylphosphine and carbon tetrabromide conducted to the dibromoalkene intermediate **9**, and (ii) reacting 2 eq. of *n*-butyl lithium at low temperature generated, one-pot, a first bromide elimination step followed by a second halogen-metal exchange to conduct to the desired alkyne. Finally, the aminoacetal **10** was cleaved under acidic conditions and the amine moiety

reprotected as the benzyl carbamate **11** (*Scheme 8*). The choice of the aromatic carbamate for the amine protection proved essential for the success of the Diels-Alder cycloaddition step (*vide infra*), contrarily to the thermally instable *tert*-butyl analogue.

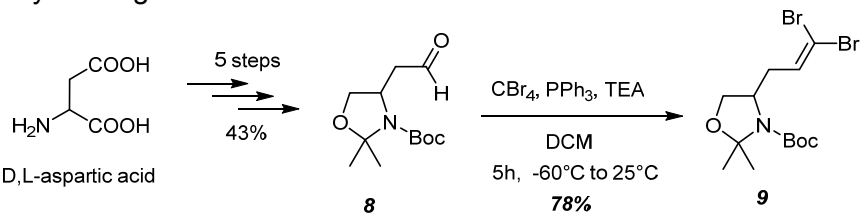

Scheme 8

Subsequently, the sulfone **1** was substituted by the alcoholate **11** to conduct to the desired Diels-Alder precursor **12** in good yield (88%). This intermediate smoothly generated the [4+2] cycloadduct under microwaves irradiation at 220°C. The carbamate was submitted to hydrogenolysis using a palladium catalyst. A final reductive amination step with formaldehyde conducted to the desired model compound **14** (*Scheme 9*).

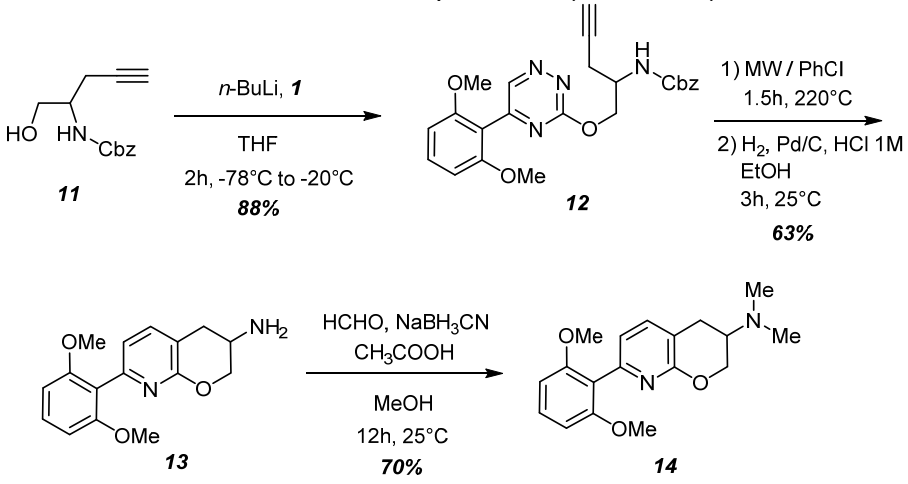

Scheme 9

CONCLUSIONS

In conclusion, we present herein a general procedure for the synthesis of 3-amino-7-aryl-8-azachromans. This multi-step approach involved 12 linear steps, and was optimized to deliver the desired compounds in an overall 11% yield. One key step was particularly challenging: generation of the alkyne moiety. Our initial sulfonates substitutions assays by various acetylides proved unsuccessful. Unfortunately, no side-products could be isolated to explain a specific reactivity pattern. The back-up solution was to generate the alkyne moiety from an aldehyde precursor. The Corey-Fuchs method was successfully applied and allowed the synthesis of the key alkyne intermediate.

This synthetic route opens a window for subsequent SAR studies, as it allows modulations of the: (1) aryl substituent on the azachroman scaffold, (2) amine moiety and (3) potentially the C3 stereochemistry, by using enantiopure aspartic acid as starting material. Several pharmaco-modulations are currently investigated by our group with the final goal of identifying a new class of ligands targeting the histaminergic H_3 receptor.

EXPERIMENTAL SECTION

^{1}H-NMR and ^{13}C-NMR were recorded with Bruker Avance DPX250 (250.131 MHz) and Bruker Avance II (400 MHz) spectrometers in CDCl3, using tetramethylsilane as an internal standard. Multiplicities were determined by the DEPT135 sequence; chemical shifts are reported in parts per million (ppm).

Coupling constants are reported in units of Hertz [Hz]. Infrared (IR) spectra were recorded with a Perkin–Elmer Paragon 1000 PC FTIR using NaCl films or KBr pellets. Low-resolution mass spectra (MS) were recorded with a Perkin–Elmer SCIEX AOI 300 spectrometer. High-resolution mass spectra were recorded with a Q-Tof micro Waters spectrometer. Melting points were determined in open capillary tubes and are uncorrected. Flash chromatography was performed on Merck 40–70 nM (230–400 mesh) silica gel under nitrogen pressure. Thin-layer chromatography (TLC) was carried out on Merck silica gel 60 F254 precoated plates. Visualization was made with ultraviolet light (λ = 254 nm) and, if necessary, an ethanolic solution of potassium permanganate. Reactions requiring anhydrous conditions were performed under nitrogen. Toluene and tetrahydrofuran were freshly distilled from sodium / benzophenone under argon prior to use.

Methyl 2-[(tert-butoxycarbonyl)amino]-3-hydroxypropanoate (**2).** D,L-serine (35 g, 333.05 mmol, 1 eq.) was disolved in sodium hydroxide (1M aq. soln. 666 mL, 666.10 mmol, 2 eq.) and dioxane (340 mL). The mixture was cooled to 0°C and di-*tert*-butyldicarbonate was subsequently added (87 g,

399.66 mmol, 1.2 eq.). The mixture was stirred for 12 h at room temperature. During the reaction time, the pH was corrected to 9-10 by addition of sodium hydroxide (1M aq.soln.). The organic solvent was evaporated and the aqueous phase was washed with diethyl ether to remove unreacted di-*tert*-butyldicarbonate. Then, the pH of the recovered aqueous phase was adjusted to 2-3 by addition of sulfuric acid (1M aq. soln.), before extraction of organic materials with ethyl acetate (3 x 400 mL). The combined organic layers were dried over magnesium sulfate, filtered and the solvent was removed under vacuum to give the crude carbamate as a viscous yellow oil. The obtained Boc-serine (44 g, 214.41 mmol, 1 eq.) was dissolved in 350 mL DMF and the mixture was cooled to 0°C. Under nitrogen atmosphere, potassium carbonate (32.60 g, 235.85 mmol, 1.1 eq.) and methyl iodide (26.7 ml, 428.83 mmol, 2 eq.) were subsequently added. After 20 h of stirring at room temperature, the solvent was evaporated and the crude product was dissolved in ethyl acetate (200 mL) and washed with water and brine. The organic phase was dried over magnesium sulfate, filtered and the solvent was removed under vacuum to conduct to a yellow viscous oil, used as a crude product for the next step. Yield 78%; ^{1}H-NMR ($CDCl_3$, 250 Hz) : δ (ppm) 1.39 (s, 9H, 3C**H**$_3$), 3.35 (ls, 1H, O**H**), 3.71 (s, 3H, C**H**$_3$), 3.78-3.92 (m, 2H, C**H**$_2$OH), 4.7-4.49 (m, 1H, C**H**NH), 5.61 (d, 1H, N**H**, *J* = 7.8 Hz); ^{13}C-NMR ($CDCl_3$, 62.9 Hz) : δ (ppm) 28.3 (**C**H$_3$), 52.6 (**C**H$_3$), 55.8 (**C**H), 63.2 (**C**H$_2$), 80.3 (**C**$_q$), 155.9 (**C**$_q$), 171.6 (**C**$_q$); IR (ATR-Ge) : ν (cm^{-1}) 3391, 2977, 1692, 1507, 1366, 1210, 1159, 1058, 1029; SM (ESI): *m/z* = 242.0 [M+Na]$^+$.

3-Tert-butyl 4-methyl 2,2-dimethyl-1,3-oxazolidine-3,4-dicarboxylate (**3**). Under inert atmosphere, 2,2-dimethoxypropane (42.4 mL, 341.85 mmol, 2.5 eq.) and monohydrated *para*-toluenesulfonic acid (0.52 g, 2.74 mmol, 0.02 eq.) were added to a solution of compound **2** (30 g, 136.74 mmol, 1 eq.) in 600 mL dry toluene. After 30 min of refluxing, 190 ml of co-solvents were distilled using a Dean-Stark trap. A new portion of 2,2-dimethoxypropane (17 mL, 138.74 mmol, 1 eq.) and monohydrated PTSA (0.26 g 1.37 mmol, 0.01 eq.) were added, and the mixture was refluxed for 30 more minutes. Additional 190 mL of reaction mixture were distilled using a Dean-Stark trap and the remaining reaction mixture was refluxed for 20 h. The volatiles were evaporated, the crude product was dissolved in ethyl acetate (150 mL) and washed with sodium bicarbonate (satd. aq. soln., 150 mL). The organic materials were extracted from the aqueous phase with ethyl acetate (2 x 200 mL). The combined organic layers were washed with brine, dried over magnesium sulfate and concentrated under vacuum. The crude product was purified by flash chromatography (PE/EtOAc 9/1) to conduct to the desired aminoacetal **3** as a light-yellow oil. Yield 85%; Mixture of conformers (A/B ~6/4, as resulted from the integration of the two ^{1}H-NMR signals corresponding to the C**H**$_3$-C-NBoc substituents): ^{1}H-NMR ($CDCl_3$, 250 Hz): δ (ppm) 1.32 (s, 5H), 1.41 and 1.44 (2 x s, 7H), 1.55 and 1.57 (2 x s, 3H), 3.66 (s, 3H, C**H**$_3$), 3.91-4.10 (m, 2H, C**H**$_2$O), 4.27-4.41

(m, 1H, C**H**NH). ^{13}C-NMR ($CDCl_3$, 62.9 Hz): δ (ppm) 24.3, 24.9, 25.1, 26.0 (**C**H_3), 28.2 (**C**H_3), 28.3 (**C**H_3), 52.2 (**C**H_3), 52.3 (**C**H_3), 59.2 (**C**H), 59.2 (**C**H), 66.0 (**C**H_2), 66.2 (**C**H_2), 80.2 (**C**$_q$), 80.8 (**C**$_q$), 94.3 (**C**$_q$), 95.0 (**C**$_q$), 151.1 (**C**$_q$), 152.0 (**C**$_q$), 171.2 (**C**$_q$), 171.6 (**C**$_q$); IR (ATR-Ge): ν (cm^{-1}) 2976, 1762, 1711, 1393, 1255, 1199, 1168; SM (ESI): *m/z* = 282.0 $[M+Na]^+$.

Tert-butyl 4-(hydroxymethyl)-2,2-dimethyl-1,3-oxazolidine-3-carboxylate (**4**). In a 100 mL round bottom flask, under inert atmosphere, a solution of the previously purified ester **3** (3 g, 11.58 mmol, 1 eq.) in dry diethyl ether (30 mL) was added to a suspension of lithium aluminum hydride (0.44 g, 11.58 mmol, 1 eq.) in dry diethyl ether (30 mL). The mixture was refluxed for 1 h, and subsequently cooled to room temperature. The excess of hydride was hydrolyzed by slow successive addition of water (0.44 mL), sodium hydroxide (15% aq. soln., 0.44 mL) and finally water (1.32 mL). The precipitate was filtered on a Celite pad and was washed with diethyl ether. The filtrate was dried over magnesium sulfate, filtered and concentrated under vacuum. The crude product was purified by flash-chromatography PE/EtOAc 7/3) to give the desired alcohol **4**. Yield: 70%; ^{1}H-NMR ($CDCl_3$, 250 Hz): δ (ppm) 1.42 (as, 12H, 4C**H**$_3$), 1.48 (s, 3H, C**H**$_3$), 3.49-3.93 (m, 5H, C**H**NH, C**H**$_2$O, C**H**$_2$OH); ^{13}C-NMR ($CDCl_3$, 62.9 Hz): δ (ppm) 24.5, 27.2 (2**C**H_3), 28.4 (3**C**H_3), 59.4 (**C**H), 64.4, 65.3 (2**C**H_2), 81.1 (**C**$_q$), 94.0 (**C**$_q$), 153.8 (**C**$_q$); IR (ATR-Ge): ν (cm^{-1}) 3458, 2983, 1665, 1401, 1365, 1247, 1072, 1102, 1048, 885; MS (ESI) : *m/z* = 232.0 $[M+H]^+$, 254 $[M+Na]^+$.

Tert-butyl-4-[[5-(2,6-dimethoxyphenyl)-1,2,4-triazin-3-yl]oxymethyl]-2,2-di-methyl-oxa-zolidine-3-carboxylate (**5**). Under nitrogen atmo-sphere, a solution of the alcohol **4** (3.30 g, 14.22 mmol, 1.2 eq.) in dry THF (10 mL) was added to a suspension of sodium hydride (60% dispersion in mineral oil, 0.57 g, 14.22 mmol, 1.2 eq.) in dry THF (80 mL). After 30 min of stirring at 0°C, a solution of sulfone **1** (3.5 g, 11.85 mmol, 1 eq.) in dry THF (30 mL) was added dropwise. The reaction mixture was allowed to come back to room temperature overnight under stirring, and subsequently quenched by addition of water (100 mL). The organics were extracted with dichloromethane (3 x 100 mL). The combined organic layers were dried over magnesium sulfate, filtered and the solvent was evaporated under reduced pressure. The crude product was purified by flash chromatography (PE/EtOAc 6/4) to give the desired compound **5** as a yellow oil. Yield: 85%; ^{1}H-NMR ($CDCl_3$, 250 Hz) : δ (ppm) 1.41-1.58 (m, 15H, 5C**H**$_3$), 3.71 (s, 6H, 2C**H**$_3$), 3.96-4.00 (m, 1H), 4.11-4.15 (m, 1H), 4.32-4.39 (m, 2H), 4.64-4.76 (m, 1H, C**H**$_2$OC=N), 6.60 (d, 2H, 2C**H**, *J* = 8.0 Hz), 7.35 (t, 1H, C**H**, *J* = 8.0 Hz), 8.89 (s, 1H, C**H**); ^{13}C-NMR (DMSO, 62.9 Hz, 80°C): δ (ppm) 26.2 (**C**H_3), 27.6 (3**C**H_3), 30.0 (**C**H_3), 55.1 (**C**H), 55.8 (**C**H_3O), 64.5 (**C**H_2O), 66.3 (**C**H_2O), 79.1 (**C**$_q$), 93.0 (**C**$_q$), 104.6 (2**C**H), 112.3 (**C**$_q$), 131.9 (**C**H), 146.7 (**C**H), 150.9 (**C**$_q$), 157.2 (**C**$_q$), 157.6 (**C**$_q$), 164.7 (**C**$_q$); IR (NaCl) : ν (cm^{-1}) 2977, 1692, 1598, 1472, 1364, 1251, 1169, 1107, 1085, 1021, 730; MS (ESI) : *m/z* = 447.5 $[M+H]^+$.

Tert-butyl N-[1-[[5-(2,6-dimethoxyphenyl)-1,2,4-triazin-3-yl]oxymethyl]-2-hydroxy-ethyl]carba-mate (**6**). The previously obtained compound **5** (3 g, 6.719 mmol, 1 eq.) was added to an acetic acid/water mixture (60 mL / 15 mL) and the reaction was stirred for 12 h at 50°C. The solvents were subsequently co-evaporated with toluene, the residue was diluted with water (50 mL) and was extracted with ethyl acetate (3 x 50 mL). The combined organic layers were dried oved magnesium sulfate, filtered and the solvent was evaporated under vacuum to conduct to the desired aminoalcohol **6** as a highly viscous yellow oil. Yield: 40%; ^{1}H-NMR ($CDCl_3$, 250 Hz): δ (ppm) 1.41 (s, 9H, 3C**H**$_3$), 3.69–3.87 (m, 8H, 2C**H**$_3$O, C**H**$_2$OH), 4.03–4.10 (m, 1H, C**H**NH), 4.58–4.77 (m, 2H, C**H**$_2$OC=N), 5.31 (d, 1H, N**H**, *J* = 7.5 Hz), 6.63 (d, 2H, 2C**H**, *J* = 8.3Hz), 7.39 (t, 1H, C**H**, *J* = 8.3 Hz), 8.94 (s, 1H, C**H**). ^{13}C-NMR ($CDCl_3$, 62.9 Hz): δ (ppm) 28.5 (3**C**H$_3$), 51.5 (**C**H), 56.0 (2**C**H$_3$O), 61.8 (**C**H$_2$), 67.0 (**C**H$_2$OC=N), 79.9 (**C**$_q$), 104.2 (2**C**H), 112.2 (**C**$_q$), 132.6 (**C**H), 147.7 (**C**H), 155.9 (**C**$_q$), 158.3 (**C**$_q$), 165.3(**C**$_q$); IR (NaCl): v (cm^{-1}) 3432, 2984, 1697, 1600, 1514, 1255, 1110, 1022, 755; MS (ESI): *m/z* = 407.5 [M+H]$^+$.

[2-(Tert-butoxycarbonylamino)-3-[[5-(2,6-dimethoxyphenyl)-1,2,4-triazin-3-yl]oxy]propyl] methanesulfonate (**7**). Under inert atmosphere, methane-sulfonyl chloride (0.05 mL, 0.59 mmol, 1.2 eq.) was added to a solution of alcohol **6** (0.2 g, 0.49 mmol, 1 eq.) and triethylamine (0.08 mL, 0.59 mmol, 1.2 eq.) in dry DCM (5 mL). The mixture was stirred for 12 h at room temperature, and after complete consumption of the starting material, the reaction was quenched by addition of water (20 mL). The organics were extracted with ethyl acetate (3 x 30 mL), the combined organic layers were dried over magnesium sulfate, filtered and the solvent was evaporated under reduced pressure. The obtained moisture-sensitive product was subsequently used without further purification. ^{1}H-NMR ($CDCl_3$, 250 Hz) : δ (ppm) 1.451 (s, 9H, 3C**H**$_3$), 3.04 (s, 3H, C**H**$_3$S), 3.79 (s, 6H, 2C**H**$_3$O), 4.36-4.48 (m, 1H, C**H**NH), 4.57-4.59 (m, 2H, C**H**$_2$OS), 4.61-4.68 (m, 2H, C**H**$_2$OC=N), 6.63 (d, 2H, 2C**H**, *J* = 8.3 Hz), 7.43 (t, 1H, C**H**, *J* = 8.3 Hz), 8.99 (s, 1H, C**H**); ^{13}C-NMR ($CDCl_3$, 62.9 Hz) : δ (ppm) 28.4 ($3CH_3$), 37.5 (CH_3S), 48.8 (CH), 56.2 ($2CH_3O$), 66.8 (CH_2OS), 67.7 ($CH_2OC=N$), 80.4 (C_q), 104.3 (2CH), 112.0 (C_q), 133.2 (CH), 147.7 (CH), 155.7 (C_q), 158.6 (C_q), 165.5(C_q).

Tert-butyl 4-(3,3-dibromoallyl)-2,2-dimethyl-oxazolidine-3-carboxylate (**9**). Under inert atmosphere, a solution of carbon tetrabromide (17.45 g, 52.61 mmol, 3.2 eq.) in dry DCM (50 mL) was added at -40°C to a solution of triphenylphosphine (27.60 g, 105.22 mmol, 6.4 eq.) in dry DCM (400 mL). After 15 min of vigorous stirring at low temperature, dry trimethylamine was subsequently added (28.6 mL, 205.5 mmol, 12.5 eq.) and the mixture was cooled to -78°C before adding a solution of aldehyde **8** (4 g, 16.44 mmol, 1 eq.), synthesized as previously described in the literature)[5] in dry DCM (50 mL). After 10 min of stirring at -78°C, the reaction was continued for 2 h at 0°C.

After the complete consumption of the starting material, the reaction was quenched by addition of water (150 mL) and hydrogen peroxide (30% aq. soln., 40 mL) and further stirring for 20 min at room temperature. Subsequently, the organic layer was separated, and the remaining organic materials from the water phase were further extracted with DCM (2 x 200 mL). The combined organic layers were dried over magnesium sulfate, filtered and the solvent was evaporated under reduced pressure. The crude product was purified by flash-chromatography (PE / EtOAc 8/2) to give a white solid. Yield 78%; ^{1}H-NMR ($CDCl_3$, 250 Hz) (1/1 mixture of two conformers): δ (ppm) 1.43-1.59 (m, 15H, 5C**H**$_3$), 2.40-2.49 (m, 2H, C**H**$_2$C=C), 3.71 (d, 1H, C**H**$_2$O, *J* = 8.0 Hz), 3.90-4.05 (m, 2H, C**H**N), 6.38-6.45 (m, 1H, C**H**=C); ^{13}C-NMR ($CDCl_3$, 62.9 Hz) (1/1 mixture of two conformers): δ (ppm) 23.2, 24.5 (**C**H$_3$), 26.8, 27.5 (**C**H$_3$), 28.5, 28.6 (3**C**H$_3$), 36.6, 37.4 (**C**H$_2$C=C), 55.6, 55.9 (**C**HN), 66.7, 67.1 (**C**H$_2$O), 80.1, 80.5 (**C**$_q$), 91.0 (**C**$_q$Br), 93.8, 94.4 (**C**$_q$N), 134.8, 135.0 (**C**H=C), 151.7, 152.3 (**C**$_q$); IR (ATR-Ge): ν (cm^{-1}) 2971, 1685, 1396, 1383, 1086; MS (ESI): *m/z* = 420.0 [M+Na]$^+$, 422.0 [M+Na]$^+$, 424 [M+Na]$^+$; Melting point: 96-98°C.

Tert-butyl 2,2-dimethyl-4-prop-2-ynyl-oxazolidine-3-carboxylate (**10**). *n*-butyl lithium (2.1 M in THF, 10 mL, 21.05 mmol, 2.1 eq.) was added at -78°C to a solution of the previously isolated dibromide **9** (4 g, 10.02 mmol, 1 eq.) in dry THF (100 mL). After 40 min of stirring at -78°C, the bath temperature was adjusted to -15°C and the mixture was stirred 15 additional minutes. The reaction was subsequently quenched by addition of sodium hydroxide (0.01M aq. soln., 50 mL). The organic materials were extracted with ethyl acetate (3 x 100 mL), the combined organic layers were dried over magnesium sulfate and the solvent was evaporated under reduce pressure. The crude product was purified by flash-chromatography (DCM) to give the desired alkyne **10** as a colorless oil. Yield: 90%; ^{1}H-NMR ($CDCl_3$, 250 Hz): δ (ppm) 1.44 (s, 12H, 4C**H**$_3$), 1.51-1.55 (m, 3H, C**H**$_3$), 1.92-1.95 (m, 1H, CH), 2.30-2.70 (m, 2H, C**H**$_2$CHN), 3.91-3.96 (m, 3H, C**H**$_2$O, C**H**N); ^{13}C-NMR ($CDCl_3$, 62.9 Hz) : δ(ppm) (two conformers) 22.3, 23.1 (**C**H$_2$CHN), 23.4, 24.6 (**C**H$_3$), 26.8, 27.6 (**C**H$_3$), 28.5 (3**C**H$_3$), 56.4, 56.6 (**C**HN), 66.5, 66.7 (**C**H$_2$O), 70.0, 70.2 (**C**H), 80.0, 80.4 (**C**$_q$), 80.9, 81.0 (**C**$_q$), 93.8, 94.4 (**C**$_q$), 151.5, 152.1 (**C**$_q$); IR (ATR-Ge): ν (cm^{-1}) 3304, 2976, 2129, 1696, 1399, 1260, 1102; MS (ESI): *m/z* = 262.0 [M+Na]$^+$.

Benzyl N-[1-(hydroxymethyl)but-3-ynyl]carbamate (**11**). A solution of compound **10** (2 g, 10.04 mmol, 1 eq.) in methanol (10 mL) was added to trifluoroacetic acid (40 mL). After 2 h of reaction at room temperature, the solvents were co-evaporated (never to dryness !) with diethyl ether (3 x 50 mL). Another co-evaporation with dioxane (40 mL) allowed removal of residual solvents. The crude product was dissolved in sodium bicarbonate (satd. aq. soln., 40 mL) and the pH was corrected to 8 by addition of trace amounts of pure sodium bicarbonate. Potassium carbonate (1.8 g, 13.05 mmol, 1.3 eq.)

and benzyl chloroformate (1.7 mL, 12.05 mmol, 1.2 eq.) were subsequently added, and the reaction mixture was stirred for 12 h at room temperature. After the complete consumption of the starting material, water was added (60 mL) and the organics were extracted with ethyl acetate (3 x 100 mL). The combined organic layers were dried over magnesium sulfate, filtered and the solvent was removed under vacuum. The crude product was purified by flash-chromatography (PE / EtOAc 5/5) to conduct to the desired carbamate **11**, isolated as a white solid. Yield: 84%; ^{1}H-NMR ($CDCl_3$, 250 Hz): δ (ppm) 2.02 (t, 1H, C**H**, *J* = 2.6 Hz), 2.48 (d, 2H, C**H**$_2$C≡C, *J* = 3.77 Hz), 3.03 (ls, 1H, O**H**), 3.63-3.78 (m, 2H, C**H**$_2$OH), 3.82-3.90 (m, 1H, C**H**N), 5.09 (s, 2H, C**H**$_2$OC=O), 5.43 (d, 1H, N**H**, *J* = 8.3 Hz), 7.34 (s, 5H, 5C**H**) ; ^{13}C-NMR ($CDCl_3$, 62.9 Hz): δ (ppm) 21.1 (**C**H$_2$C≡C), 51.2 (**C**HN), 63.4 (**C**H$_2$OH), 67.0 (**C**H$_2$OC=O), 71.1 (**C**H), 80.1 (**C**$_q$), 128.2 (**C**H), 128.3 (**C**H), 128.6 (**C**H), 136.2 (**C**$_q$), 156.4 (**C**$_q$) ; **IR** (NaCl) : ν (cm^{-1}) 3409, 3300, 2950, 2128, 1714, 1536, 1232, 1061, 741 and 698 ; **MS** (ESI) : *m/z* = 256.5 $[M+Na]^+$; Melting point: 66–68 °C.

Benzyl {1-[5-(2,6-Dimethoxyphenyl)-1,2,4-triazin-3-yloxy]pent-4-yn-2-yl}car-bamate (**12**). Under nitrogen atmosphere, *n*-butyllithium (1.5 M in THF, 5.78 mmol, 1.05 eq.) was slowly added at –78 °C to a solution of the alcohol **11** (1.3 g, 5.5 mmol, 1 eq.) in anhydrous THF (60 mL). After 40 min at –78 °C, a solution of triazine **1** (1.98 g, 6.70 mmol, 1.2 eq.) in anhydrous THF (25 mL) was added. The mixture was stirred for 45 min at –78 °C and 1 h at –30 °C, before it was quenched at low temperature with 5% $NaHCO_3$. The aqueous layer was separated and extracted with AcOEt (3 x 100 mL). The combined organic layers were dried with magnesium sulfate, the solvent was evaporated, and the crude product was purified by flash chromatography (PE / EtOAc, 5:5) to give compound **12** as a viscous yellow oil. Yield 88 %; IR (NaCl) : ν (cm^{-1}) 3298, 2946, 2118, 1718, 1599, 1515, 1255, 1110. ^{1}H-NMR ($CDCl_3$, 250 Hz) : δ (ppm) 2.01 (t, 1H, **H**C≡C, *J* = 2.6 Hz), 2.67-2.70 (m, 2H, C**H**$_2$-C≡C), 3.75 (s, 6H, OC**H**$_3$), 4.28-4.37 (m, 1H, C**H**NH), 4.57-4.64 (m, 1H, C**H**$_2$CHNH), 4.76-4.82 (m, 1H, C**H**$_2$CHNH), 5.09 (s, 2H, C**H**$_2$OC=O), 5.44 (d, 1H, N**H**, *J* = 8.7 Hz), 6.63 (d, 2H, 2C**H**, *J* = 8.5 Hz), 7.30-7.34 (m, 5H, 5C**H**), 7.39 (t, 1H, C**H**, *J* = 8.5 Hz), 8.96 (s, 1H, C**H**C=N). ^{13}C-NMR ($CDCl_3$, 62.9 Hz): δ (ppm) 21.6 (**C**H$_2$-C≡C), 48.9 (**C**HNH), 56.0 (2O**C**H$_3$), 67.0 (**C**H$_2$OC=O), 68.0 (**C**H$_2$CHNH), 71.3 (CH$_2$-C≡**C**), 79.7 (CH$_2$-**C**≡C), 104.2 (2**C**H), 112.3 (**C**$_q$), 128.1, 128.2, 128.6 (5**C**H), 132.5 (**C**H), 136.3 (**C**$_q$), 147.9 (**C**H=N), 155.8 (**C**$_q$), 158.4 (**C**$_q$), 165.0 (**C**$_q$). IR (NaCl) : ν (cm^{-1}) 3298, 2946, 2118, 1718, 1599, 1515, 1255, 1110; MS (ESI) : *m/z* = 449.5 $[M+H]^+$, 471.5 $[M+Na]^+$; HRMS (ESI): calcd. for $C_{24}H_{24}N_4O_5$ 471.1644, found 471.1643.

7-(2,6-Dimethoxyphenyl)-3,4-dihydro-2H-pyrano[2,3-b]pyridin-3-amine (**13**). A solution of compound **12** (0.5 g1.11 mmol, 1 eq.) in chlorobenzene (5 mL) was heated at 220 °C under microwaves irradiation for 1.5 h. The solvent

was removed in vacuo, and the residue was purified by flash chromatography (PE / EtOAc, 4:6) to afford the corresponding cycloadduc as a white solid, in a 88% yield. ^{1}H-NMR ($CDCl_3$, 250 Hz) : δ (ppm) 2.84 (d, 1H, C**H**$_2$CHNH, *J* = 16.6 Hz), 3.11 (d, 1H, C**H**$_2$CHNH, *J* = 16.6 Hz), 3.70 (s, 6H, OC**H**$_3$), 4.27 (ls, 3H, C**H**$_2$C**H**NH), 5.10 (s, 2H, C**H**$_2$OC=O), 5.39 (d, 1H, N**H**, *J* = 6.4 Hz), 6.59 (d, 2H, 2C**H**, *J* = 8.4 Hz), 6.91 (d, 1H, C**H**, *J* = 7.5 Hz), 7.27 (t, 1H, C**H**, *J* = 8.4 Hz), 7.33 (ls, 5H, 5C**H**), 7.41 (d, 1H, C**H**, *J* = 7.5 Hz). ^{13}C-NMR ($CDCl_3$, 62.9 Hz): δ (ppm) 31.0 (**C**H$_2$CHNH), 43.7 (**C**HNH), 56.0 (O**C**H3), 66.9 (**C**H$_2$OC=O), 68.8 (**C**H$_2$OCHNH), 104.0 (2**C**H), 112.2 (**C**$_q$), 118.4 (**C**$_q$), 120.5 (**C**H), 128.2 (3**C**H), 128.6 (2**C**H), 129.6 (**C**H), 136.3 (**C**$_q$), 139.6 (**C**H), 152.0 (**C**$_q$), 155.8 (**C**$_q$), 158.1 (**C**$_q$), 159.7 (**C**$_q$); IR (ATR-Ge) : ν (cm^{-1}) 3338, 2942, 1715, 1602, 1472, 1248, 1111, 755; MS (ESI) : *m/z* = 421.5 $[M+H]^+$; HRMS (ESI): Calcd. for $C_{24}H_{24}N_2O_5$ 421.1763, found 421.1778; Melting point: 167–169 °C. To a solution of the previously obtained cycloadduct (0.2 g, 0.5 mmol, 1 eq.) in ethanol (10 mL) was added 10% Pd/C (0.02 g), and hydrogen was bubbled through the suspension for 15 min at room temperature. 1*N* HCl (0.5 mmol) was added, and the reaction mixture was stirred under hydrogen atmosphere until the complete consumption of the starting material (10 h). The mixture was filtered through Celite, diluted with satd. K_2CO_3 (25 mL), and extracted with DCM (3 x 50 mL). The separated organic layers were dried with magnesium sulfate, and the solvent was evaporated to give the amine **13** as a light yellow solid, subsequently used without further purification. Yield: 71%; ^{1}H-NMR ($CDCl_3$): δ (ppm) 2.63(dd, 1H, C**H**$_2$CHNH$_2$, *J* = 7.4 Hz, *J* = 16.1 Hz), 3.07 (dd, 1H, C**H**$_2$CHNH$_2$, *J* = 5.1 Hz, *J* = 16.1 Hz), 3.38-3.47 (m, 1H, C**H**NH$_2$), 3.71 (s, 6H, OC**H**$_3$), 3.98 (dd, 1H, C**H**$_2$O, *J* = 7.4 Hz, *J* = 10.5 Hz), 4.27-4.33 (m, 1H, C**H**$_2$O), 6.60 (d, 2H, 2C**H**, *J* = 8.4 Hz), 6.89 (d, 1H, C**H**, *J* = 7.5 Hz), 7.26 (dd, 1H, C**H**, *J* = 7.8 Hz, *J* = 9.0 Hz), 7.43 (d, 1H, C**H**, *J* = 7.5 Hz). ^{13}C-NMR($CDCl_3$): δ (ppm) 34.4 (**C**H$_2$CHNH$_2$), 44.0 (**C**HNH$_2$), 56.1 (2O**C**H$_3$), 72.1 (**C**H$_2$O), 104.1 (2**C**H), 113.1 (**C**$_q$), 118.8 (**C**$_q$), 119.9 (**C**H), 129.5 (**C**H), 139.3 (**C**H), 151.6 (**C**$_q$), 158.2 (2**C**$_q$), 160.1 (**C**$_q$); IR (ATR-Ge): ν (cm^{-1}) 3358, 2942, 1602, 1471, 1248, 752; MS (ESI) : *m/z* = 287.0 $[M+H]^+$; HRMS (ESI): Calcd. for $C_{16}H_{18}N_2O_3$ 287.1396, found 287.1405.

7-(2,6-Dimethoxyphenyl)-3-(dimethylamino)-3,4-dihydro-2H-pyrano-[2,3-b]-pyridine (**14**): To a solution of amine **13** (0.08 g, 0.28 mmol, 1 eq.) in methanol (5 mL) was added formaldehyde (37% aq. soln., 0.167 ml, 2.32 mmol, 8 eq.) and sodium borohydride (0.088 g, 1.40 mmol, 5 eq.). The pH of the mixture was adjusted to 6 by addition of acetic acid, and the mixture was stirred for 24 h at room temperature, then subsequently poured into 1 M NaOH (10 mL). The aqueous phase was extracted with DCM (3 x 30 mL), the combined organic layers were dried with magnesium sulfate, and the solvents were evaporated *in vacuo*. The final compound **14** was isolated by

flash chromatography (DCM/MeOH, 95:5) as a light yellow viscous oil. Yield : 70% ; ^{1}H-NMR ($CDCl_3$, 250 Hz): δ (ppm) 2.41 (s, 6H, NC**H**$_3$), 2.77-3.02 (m, 3H, C**H**N, C**H**$_2$CHN), 3.71 (s, 6H, C**H**$_2$CHN), 3.99-4.09 (m, 1H, C**H**$_2$O), 4.48-4.54 (m, 1H, C**H**$_2$O), 6.60 (d, 2H, 2C**H**, *J* = 8.4 Hz), 6.89 (d, 1H, C**H**, *J* = 7.5 Hz), 7.27 (t, 1H, C**H**, *J* = 8.4), 7.45 (d, 1H, C**H**, *J* = 7.5 Hz); ^{13}C-NMR ($CDCl_3$, 62.9 Hz): δ (ppm) 29.2 (**C**H$_2$CHN), 42.8 (2**C**H$_3$), 56.0 (2O**C**H$_3$), 57.1 (**C**HN), 68.2 (**C**H$_2$O), 104.1 (2**C**H), 113.4 (**C**$_q$), 118.8 (**C**$_q$), 119.8 (**C**H), 129.5 (**C**H), 139.1 (**C**H), 151.5 (**C**$_q$), 158.2 (**C**$_q$), 160.4 (**C**$_q$); IR (ATR-Ge): ν (cm^{-1}) 2938, 1606, 1471, 1248, 1110, 749; MS (ESI) : *m/z* = 315.5 $[M+H]^+$; HRMS (ESI): Calcd. for $C_{18}H_{22}N_2O_3$ 315.1471, found 315.1460

REFERENCES

1. E. Badarau, F. Suzenet, A.L. Fînaru, G. Guillaumet, *European Journal of Organic Chemistry*, **2009**, *21*, 3619.
2. P. Holmberg, D. Sohn, R. Leideborg, P. Caldirola, P. Zlatoidsky, S. Hanson, N. Mohell, S. Rosqvist, G. Nordvall, A.M. Johansson, R. Johansson., *Journal of Medicinal Chemistry*, **2004**, *47*, 3927.
3. T.W. Butler, T.T. Wager, International Patent WO2007/088450, 9 Aug **2007**
4. P. Garner, J.M. Park, *Journal of Organic Chemistry*, **1987**, *52*, 2361.
5. D.R. Hou, J.H. Reibenspies, K. Burgess, *Journal of Organic Chemistry*, **2001**, *66*, 206.
6. G.M. Ksander, R. de Jesus, A. Yuan, R.D. Ghai, A. Trapani, C. McMartin, R. Bohacek, *Journal of Medicinal Chemistry*, **1997**, *40*, 495.
7. E.J. Corey, P.L. Fuchs, *Tetrahedron Letters*, **1972**, *13*, 3769.

STUDIA UBB CHEMIA, LXIV, 2,Tom I, 2019 (p. 189-196)
(RECOMMENDED CITATION)
DOI:10.24193/subbchem.2019.2.15

Dedicated to Professor Florin Dan Irimie on the Occasion of His 65th Anniversary

HETEROCYCLES 50. SYNTHESIS AND CHARACTERIZATION OF NEW 2-PHENYLAMINOTHIAZOLE DERIVED MANNICH BASES BY BIOCATALYTIC MULTICOMPONENT REACTIONS

DENISA LEONTE[a], ROBERT TŐTŐS[b], VALENTIN ZAHARIA[a,*]

ABSTRACT. In this work we describe the synthesis and characterization of new Mannich bases derived from 2-phenylaminothiazole, by applying the trimolecular condensation of thiazole aldehydes with aniline and acetone, catalyzed by lipase B from *Candida antarctica*. The target compounds were obtained with 68-76% yields, in mild and eco-friendly reaction conditions. The new heterocyclic Mannich bases were characterized by melting points, ^{1}H NMR, ^{13}C NMR and MS spectrometry.

Keywords: *thiazole, Mannich base, lipase, multicomponent reactions*

INTRODUCTION

Multicomponent reactions have a great synthetic value because of their practical simplicity, rapidity and high atom economy. In particular, the three component Mannich reaction has become a versatile tool in drug discovery and modern synthetic chemistry, as a key step for new C-C and C-N bond forming. The classical procedure is based on the use of formaldehyde as carbonyl component, a secondary amine as nucleophile and an enolisable carbonyl compound as CH-acidic substrate. Other variants of the Mannich reaction have been reported, most part being focused on the variation of the component with mobile hydrogen or the nucleophilic component [1],[2].

[a] *"Iuliu Haţieganu" University of Medicine and Pharmacy, Department of Organic Chemistry,41 Victor Babeş str., RO-400012 Cluj-Napoca, Romania*

[b] *Babeş-Bolyai University, Faculty of Chemistry and Chemical Engineering, Biocatalysis and Biotransformations Research Group, 11 Arany Janos str., RO-400028, Cluj-Napoca, Romania*

** Corresponding author: vzaharia@umfcluj.ro*

In the pharmaceutical field, Mannich reaction allows the assembly of different pharmacophore units in the same molecule, with the possibility of structural modulation by varying the carbonyl moiety, the nucleophilic component as well as the component with mobile hydrogen [2].

Beta-amino carbonyl compounds, the products of the Mannich reaction, are recognized to present different biological activities such as antibacterial, antifungal, antiviral, anti-inflammatory and anticancer properties [3]. New β-amino ketones obtained by a three-component coupling Mannich reaction were reported to present antifungal activity against *Candida albicans*, as well as good antibacterial activity against *Bacillus subtilis*, *Escherichia coli*, *Staphylococcus aureus* and *Pseudomonas aeruginosa* strains [4]. Pharmacophore prediction studies revealed similar interactions and orientation of the active molecules with a potential protein-binding site and confirmed the important role of the hydrophilic moieties (NH group), the hydrophobic ones (the aryl rings) and their relative distance. It was found that the minimal structural requirements for the antimicrobial activity of β-amino ketones consist of an aromatic ring (hydrophobic region) attached to the NH group (H-bonding donor area) and a carbonyl fragment, as H-bonding acceptor region [4].

The 2-aminothiazole system is an important pharmacophore present in the structure of many therapeutic agents, such as the anti-inflammatory drug meloxicam, the dopamine agonist pramipexole and the cephalosporin antibiotic cefdinir. In particular, the 2-phenylaminothiazole scaffold can be found in the structure of new bioactive compounds with antitubercular [5] and antileishmanial properties [6].

Enzyme catalyzed reactions are of great value in organic synthesis because they offer multiple possibilities to perform difficult transformations under mild reaction conditions and with high selectivity. Lipases offer efficient routes towards variously functionalized compounds, such as alcohols [7],[8], esters [9],[10], amines [11], amides [12], amino acids [13] and β-hydroxyacids. [14] Moreover, lipases proved to be effective biocatalysts for the formation of novel C-C and C-N bonds in Mannich-type multicomponent reactions [15],[16]. In previous researches, we have applied the Mannich type enzymatic reaction starting from 2-arylthiazole aldehydes as carbonyl substrates, with *Candida antarctica* lipase B as biocatalyst [17].

In the continuation of these researches and being aware of the biological potential of the 2-phenylaminothiazole scaffold, we decided to extend the lipase catalyzed multicomponent Mannich type reaction in the series of aldehydes derived from 2-phenylaminothiazole, in order to access new Mannich bases for medicinal applications.

RESULTS AND DISCUSSION

The aim of this study was to obtain new heterocyclic compounds with biological potential, bearing the 2-phenylaminothiazole scaffold, by mild and ecofriendly reaction conditions. In this sense, we oriented us researches to the investigation of the enzyme catalyzed trimolecular Mannich type condensation of different 2-phenylaminothiazole derived aldehydes with aniline and acetone.

The first step was the synthesis of 2-arylaminothiazole aldehydes **1a–c**, necessary as substrates in the Mannich type condensation. Their synthesis was performed as previously described by us, starting from the corresponding aryl isothiocyanates, by addition of ammonia, followed by Hantzsch condensation of arylthioureas with 1,3-dichloroacetone, N-acetylation and Sommelet reaction (Scheme 1) [18].

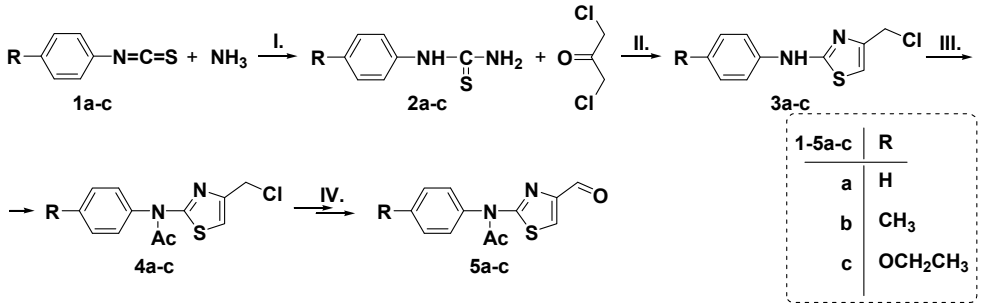

Scheme 1. Synthesis of thiazole aldehydes **5a-c**. Reaction conditions: **I.** NH_4OH 20%, r.t. 24 h, **II.** ethanol, reflux 1h, **III.** Acetic anhydride, reflux 10 min, **IV.** 1. urotropin, $CHCl_3$, reflux 1h, 2. urotropin, CH_3COOH 50%, reflux 1h. [18]

First enzymatic experiments were performed at analytical scale, in order to find the optimal reaction conditions. Various lipases (lipase from *Burkholderia cepacia*, lipase from *Candida rugosa*, lipase from *Pseudomonas fluorescens*, lipase B from *Candida antarctica*) have been evaluated as biocatalysts for the direct Mannich condensation between the obtained thiazole aldehydes, aniline and acetone, in aqueous media. Control experiments were also performed, in the absence of the enzyme and in the presence of bovine serum albumin. It is known that the presence of water in the reaction media strongly influence the activity of lipases in the Mannich type condensation, the optimal water concentration being between 40% and 50%. [15],[16] Consequently, in our experiments we choose an acetone/water 1:1 *v*/*v* mixture as the reaction media, taking into account also the low solubility in water of the used thiazole aldehydes. The enzymatic reactions were conducted at room temperature, under continuous shaking at 1200 rpm.

TLC analysis of preliminary experiments at analytical scale revealed that lipases from *Candida rugosa*, *Pseudomonas fluorescens* and lipase B from *Candida antarctica* presented good catalytic activity in the transformation of the substrates. In the absence of the enzyme or in the presence of bovine serum albumin, the formation of Mannich bases was not detected. Lipase B from *Candida antarctica* (CaL-B, Novozym 435) was chosen for further studies, because in this case total conversion was achieved.

In further experiments, we opted for the use of aniline sulfate instead of aniline, because of its better stability, easier manipulation and storage. Good results were also obtained when aniline sulfate was used in the enzymatic reactions, in the presence of sodium acetate.

The preparative scale enzymatic synthesis of Mannich bases **6a-c** was performed in the presence of CaL-B (Novozym 435) as biocatalyst (Scheme 2). Aniline was added in excess (1.1 eq.) in order to ensure the total consumption of the heterocyclic aldehyde. The Mannich bases **6a-c** were obtained with 68-76% yields, starting from the corresponding N-acetylated 2-arylaminothiazole aldehydes (0.08 mol/L), aniline sulphate (0.088 mol/L), sodium acetate (0.088 mol/L), in the presence of CaL-B, in acetone/water 1/1 *v*/*v* mixture.

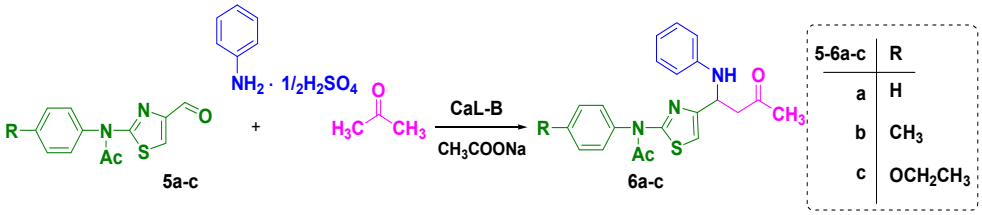

Scheme 2. Synthesis of 2-phenylaminothiazole derived Mannich bases **6a-c.** Reaction conditions: Novozym 435 (10 mg/mL), CH_3COONa (0.088 mol/L), acetone/water 1:1 *v/v*, r.t., 24 h

The newly synthesised Mannich bases were purified, physically and chemically characterized by melting point, ^1H NMR, ^{13}C NMR and MS spectroscopy.

In the ^1H NMR spectra of Mannich bases **6a-c**, the CH proton located in the 4th position of the butanone chain appears as a triplet (t) at 4.87-4.88 ppm and the CH_2 protons located in the 3th position of the butanone chain are appearing as a doublet of doublets of doublets (ddd), at chemical shifts of 2.76-2.79 ppm. The proton located in the 5th position of the thiazole ring appears as a singlet (s) at 6.80-6.81 ppm. All signals corresponding to the protons located on the benzene rings are present in the aromatic region.

In the ^{13}C NMR spectra of compounds **6a-c**, a characteristic signal between 207.70 and 207.76 ppm indicates the presence of the carbonyl group of the butanone chain. The presence of the amide group is confirmed by a characteristic signal at 169.89–170.40 ppm corresponding to the CO-NH carbon. All aromatic and aliphatic signals are also present, thus confirming the chemical structures of the products.

The LC-MS spectra of the obtained Mannich bases confirm their structures by the presence of the $[M+H]^+$ peak.

CONCLUSIONS

New 2-phenylaminothiazole derived Mannich bases were obtained by a three component biocatalytic reaction, starting from N-acetylated 2-arylaminothiazole aldehydes, aniline and acetone, in acetone/water mixture as reaction media, at room temperature.

The results of the presented study reveal that N-acetylated 2-arylaminothiazole aldehydes are novel substrates in the Cal-B catalyzed Mannich type condensation. The enzymatic reactions occurred without affecting the amide group present in the structure of the aldehydes used as substrates.

The applied biocatalytic method allowed us to obtain in good yields new pharmacologically useful Mannich bases containing the 2-phenylaminothiazole system, in mild and eco-friendly reaction conditions.

Spectral analyses MS, ^1H NMR and ^{13}C NMR confirm the structures of the newly obtained compounds.

EXPERIMENTAL SECTION

The ^1H NMR and ^{13}C NMR spectra were recorded on a Brucker Avance DPX-300 spectrometer operating at 600 and 150 MHz, respectively. Chemical shifts on the δ scale are expressed in ppm values from TMS as internal standard. MS spectra were recorded on Agilent 6410 Triple Quadrupole LC/MS mass spectrometry system.

Thin layer chromatography (TLC) was performed with Merck Kieselgel 60F254 sheets. Spots were visualized in UV light at 254 nm. The purification of compounds was performed by column chromatography on Merck Kieselgel 60Å (63–200 μm).

Melting points were determined on open glass capillaries using an Electrothermal IA 9000 digital apparatus.

The reagents and solvents necessary for the synthesis and purification of the target compounds and intermediates were purchased from Sigma Aldrich and Alfa Aesar. Aniline was purified by distillation under reduced pressure

before use in the enzymatic reactions. Lipase B from *Candida antarctica* (CaL-B, Novozym 435) was purchased from Novozymes. Lipases from *Pseudomonas fluorescens* and *Burkholderia cepacia* were from Amano, England. Lipase from *Candida rugosa* (CrL) was purchased from Fluka.

Lipase screening for the biocatalytic Mannich reaction. Analytical scale experiments

To a solution of N-acetyl-2-phenyaminothiazol-4-carbaldehyde **5a** (0.05 mmol, 12.3 mg) dissolved in acetone (0.4 mL), aniline (5 µL, 0.055 mmol), deionized water (0.4 mL) and different lipases (10 mg of lipase from *Burkholderia cepacia*, lipase from *Candida rugosa*, lipase from *Pseudomonas fluorescens*, lipase B from *Candida antarctica*) were added in this order. The reaction mixtures were shaken at 1200 rpm for 24 h and then analyzed by TLC using a mixture of petroleum ether: ethyl acetate 4:1 *v/v* as mobile phase.

Enzymatic Synthesis of Thiazole Mannich Bases 6a-c

To a solution of heterocyclic aldehyde **5a–c** (1.6 mmol) dissolved in acetone (10 mL), aniline sulphate (1.76 mmol, 250 mg), deionized water (10 mL), sodium acetate (1.76 mmol, 144 mg) and CaL-B (200 mg) were added in this order. The reaction mixtures were shaken at 1200 rpm until complete consumption of aldehydes **5a–c** (36 h, checked by TLC using a mixture of petroleum ether: ethyl acetate 4:1 *v*/*v* as eluent). The formed Mannich bases precipitated in the reaction media and these were isolated by filtration. The enzyme was washed three times with acetone for the quantitative recovery of the reaction product. The crude product was purified by column chromatography, using as mobile phase a mixture of petroleum ether: ethyl acetate 4:1 *v*/*v*.

4-(Phenylamino)-4-(2-(N-phenylacetamido)thiazol-4-yl)butan-2-one (**6a**) yellow solid, m.p. 143-144°C, yield: 70%. ^{1}H NMR (600 MHz, $CDCl_3$) δ 7.60 – 7.47 (m, 3H, Ar-H), 7.34 – 7.22 (m, 2H, Ar-H), 7.15 – 7.07 (m, 2H, Ar-H), 6.81 (s, 1H, CH-5 thiazole), 6.69 (t, J = 7.3 Hz, 1H, Ar-H), 6.57 (d, J = 8.5 Hz, 2H, Ar-H), 4.87 (t, J = 6.1 Hz, 1H, C*H*-CH_2-C=O), 2.76 (ddd, J = 22.6, 15.9, 6.2 Hz, 2H, CH-C*H*$_2$-C=O), 2.03 (s, 3H, >N-CO-C*H*$_3$), 1.85 (s, 3H, -CO-C*H*$_3$). ^{13}C NMR (151 MHz, $CDCl_3$) δ 207.69, 169.89, 160.20, 151.35, 146.81, 140.51, 130.00, 129.38, 129.18, 128.98, 118.19, 113.98, 110.24, 51.09, 47.85, 30.70, 23.93. LC-MS: m/z found: 380.10 (M calculated for [$C_{21}H_{21}N_3O_2S$+H^+]: 380.14);

4-(Phenylamino)-4-(2-(N-p-tolylacetamido)thiazol-4-yl)butan-2-one (**6b**) white solid, m.p. 149-150°C, yield: 68%. ^{1}H NMR (600 MHz, $CDCl_3$) δ 7.33 (d, J = 8.0 Hz, 2H, Ar-H), 7.17 – 7.11 (m, 4H, Ar-H), 6.80 (s, 1H, CH-5 thiazole), 6.69 (t, J = 7.3 Hz, 1H, Ar-H), 6.58 (d, J = 7.9 Hz, 2H, Ar-H), 4.88 (t, J = 6.1 Hz, 1H, C*H*-CH_2-C=O), 2.78 (ddd, J = 22.5, 15.9, 6.2 Hz, 2H, CH-C*H*$_2$-C=O), 2.47 (s, 3H, Ar-C*H*$_3$), 2.03 (s, 3H, >N-CO-C*H*$_3$), 1.87 (s, 3H, -CO-C*H*$_3$). ^{13}C NMR (151 MHz, $CDCl_3$) δ 207.70, 170.12, 160.37, 151.31, 146.85,

139.17, 137.90, 130.59, 129.36, 128.63, 118.17, 113.98, 110.20, 51.14, 47.91, 30.66, 23.90, 21.38. LC-MS: m/z found: 394.10 (M calculated for [$C_{22}H_{23}N_3O_2S+H^+$]: 394.15);

4-(Phenylamino)-4-(2-(N-p-ethoxyphenylacetamido)thiazol-4-yl)butan-2-one (**6c**) white solid, m.p. 152-153°C, yield: 76%. ^{1}H NMR (600 MHz, $CDCl_3$) δ 7.16 (d, J = 8.8 Hz, 1H, Ar-H), 7.12 (t, J = 7.9 Hz, 2H, Ar-H), 7.02 (d, J = 8.8 Hz, 2H, Ar-H), 6.80 (s, 1H, CH-5 thiazole), 6.69 (t, J = 7.3 Hz, 1H, Ar-H), 6.58 (d, J = 7.9 Hz, 2H, Ar-H), 4.88 (t, J = 6.1 Hz, 1H, C*H*-CH_2-C=O), 4.11 (q, J = 7.0 Hz, 2H, OCH_2CH_3), 2.79 (ddd, J = 22.5, 15.9, 6.2 Hz, 2H, CH-CH_2-C=O), 2.04 (s, 3H, >N-CO-CH_3), 1.90 (s, 3H, -CO-CH_3), 1.48 (t, J = 7.0 Hz, 3H, OCH_2CH_3). ^{13}C NMR (151 MHz, $CDCl_3$) δ 207.76, 170.40, 160.54, 159.33, 151.27, 146.86, 132.99, 129.91, 129.37, 118.17, 115.54, 114.00, 110.24, 63.97, 51.15, 47.96, 30.74, 23.90, 14.93. LC-MS: m/z found: 424.10 (M calculated for [$C_{23}H_{25}N_3O_3S+H^+$]: 424.16).

REFERENCES

1. A. Toma, D. Hapău, M. Naghi, L. Vlase, C. Mogoşan, V. Zaharia, *Studia UBB Chemia*, **2013**, *2*, 93-104.
2. V.M. Patel, N.B. Patel, M.J. Chan-Bacab, G. Rivera, *Comput. Biol. Chem.*, **2018**, *76*, 264-274.
3. S. Bala, N. Sharma, A. Kajal, S. Kamboj, V. Saini, *Int. J. Med. Chem*. **2014**, ID 191072.
4. A.M. El-Bayouki, W.M. Basyouni, A.S. El-Sayed, W.M. Tohamy, A.A. El-Henawyb, *Croat. Chem. Acta,* **2012**, *85 (3),* 255–268.
5. M. Pieroni, B. Wan, S. Cho, S.G. Franzblau, G. Costantino, *Eur. J. Med. Chem.*, **2014**, *72*, 26-34.
6. D. Bhuniya, R. Mukhhavilli, R. Dhivhare, D. Launay, R. Dere, A. Deshpandey, A. Verma, P. Vishwakarma, M. Moger, A. Pradhan, H. Pati, V. S. Gopinath, S. Gupta, S. Puri, D. Martin, *Eur. J. Med. Chem.*, **2015**, *102*, 582–593.
7. M.E. Moisă, L. Poppe, C.A. Gal, L.C. Bencze, F.D. Irimie, C. Paizs, M.I. Toşa, *Reaction Chemistry & Engineering*, **2018**, *3(5)*, 790-798.
8. D. Hapău, J. Brem, V. Zaharia, *Tetrahedron: Asymmetry*, **2011**, *22(24)*, 2165-2171.
9. D. Hapău, J. Brem, M. Moisă, M.I. Toşa, F.D. Irimie, V. Zaharia, *J. Mol. Cat. B: Enzym.*, **2013**, *94*, 88-94.
10. M.A. Lăcătuş, L.C. Bencze, M.I. Toşa, C. Paizs, F.D. Irimie, ACS *Sustainable Chemistry & Engineering*, **2018**, *6 (9)*, 11353-11359.
11. J. Brem, L.C. Bencze, A. Liljeblad, M.C. Turcu, C. Paizs, F.D. Irimie, L.T. Kanerva, *Eur. J. Org. Chem.*, **2012**, *17*, 3288-3294.

12. E. Farkas, M. Oláh, A. Földi, J. Kóti, J. Éles, J. Nagy, C.A. Gal, C. Paizs, G. Hornyánszky, L. Poppe, *Org. Lett.*, **2018**, *20 (24)*, 8052–8056.
13. D. Leonte, L. Bencze, C. Paizs, M. Toşa, V. Zaharia, F. Irimie, *Molecules*, **2016**, *21 (1)*, 25.
14. M.A. Naghi, L.C. Bencze, J. Brem, C. Paizs, F.D. Irimie, M.I. Toşa, *Tetrahedron: Asymmetry*, **2012**, *23 (2)*, 181-187.
15. K. Li, T. He, C. Li, X. W. Feng, N. Wang, X. Q. Yu, *Green Chemistry*, **2009**, *11*, 777–779.
16. T. He, K. Li, M. Y. Wu, X. W. Feng, N. Wang, H. Y. Wang, C. Li, X. Q. Yu, *J. Mol. Catal. Enzym.*, **2010**, *67*, 189–194.
17. D. Leonte, L.C. Bencze, C. Paizs, F.D. Irimie, V. Zaharia, *Molecules*, **2015**, *20(7),* 12300-12313.
18. I. Simiti, M. Farkas, S. Silberg, *Chem. Ber.*, **1962**, *95*, 2672-2679.

STUDIA UBB CHEMIA, LXIV, 2,Tom I, 2019 (p. 197-206)
(RECOMMENDED CITATION)
DOI:10.24193/subbchem.2019.2.16

Dedicated to Professor Florin Dan Irimie on the Occasion of His 65th Anniversary

ESTERS OF DIPHENYLPHOSPHINOSELENOTHIOIC AND DIPHENYLPHOSPHINODISELENOIC ACIDS WITH POTENTIAL FOR RAFT POLYMERIZATION

NORA CHIOREAN, ALEXANDRA POP, CRISTIAN SILVESTRU, ANCA SILVESTRU*

ABSTRACT. Compounds of type $Ph_2P(E)SeR$ [E = S, R = 2-MeC_6H_4 (**1**), 2-$(Me_2NCH_2)C_6H_4$ (**2**); E = Se, R = 2-$(Me_2NCH_2)C_6H_4$ (**3**)], were prepared and structurally characterized in solution by multinuclear NMR (^1H, ^{31}P, ^{77}Se). The attempts to obtain the derivative $Ph_2P(S)SeC_6H_4(CH_2NMePr^i)$-2 (**4**) resulted in a complex mixture. The attempts to separate the components resulted in further decomposition and hydrolysis and the isolated crystals were investigated by single-crystal X-ray diffraction when proved to be the ammonium salt $[MePr^iBnNH]^+[Ph_2P(S)O]^-$ (Bn = benzyl) (**4a**).

Keywords: *organophosphorus(V) compounds, organoselenium compounds; intramolecular coordination; solution behavior, solid state structure.*

INTRODUCTION

Radical polymerization is largely used in organic synthesis and different methods were employed during last years, *e.g*. reversible addition fragmentation transfers polymerization (RAFT) [1-3], nitroxide-mediated polymerization (NMP) [4,5], or atom transfer radical polymerization (ATRP) [6,7], in order to realize a better control of both the polymerization process and the characteristic properties of the obtained polymers. Among these methods, RAFT proved to be

Babeş-Bolyai University, Faculty of Chemistry and Chemical Engineering, Department of Chemistry, Supramolecular Organic and Organometallic Chemistry Centre (SOOMCC), 11 Arany Janos str., RO-400028 Cluj-Napoca, Romania
** Corresponding author: ancas@chem.ubbcluj.ro*

a very efficient one in living polymerization and it was observed that for best efficiency it is essential to design an appropriate RAFT agent. For this purpose esters of carboxydithioic [8] and phosphinodithioic [9,10] acids (Scheme 1, **A** and **B**) were used as RAFT agents. At a lesser extent esters of the phosphinodiselenoic acid (Scheme 1, **C**) were also investigated as RAFT agents for the polymerization of styrene [11,12].

Our research comprised in the last years several studies regarding organophosphorus [13,14] and organochalcogen [15,16] compounds bearing aromatic groups with pendant arms capable for intramolecular N→E (E = P, S, Se) intramolecular interactions. As a continuation of our work, we report here about several esters of the diphenylphosphinoselenothioic and the diphenylphosphinodiselenoic acids, namely compounds of type $Ph_2P(E)SeR$ [E = S, R = 2-MeC_6H_4 (**1**), 2-$(Me_2NCH_2)C_6H_4$ (**2**); E = Se, R = 2-$(Me_2NCH_2)C_6H_4$ (**3**)], which might be used as RAFT agents. Our attempts to isolate in pure form the related ester $Ph_2P(S)SeC_6H_4(CH_2NMePr^i)$-2 (**4**) were unsuccessful due to very fast decomposition in solution.

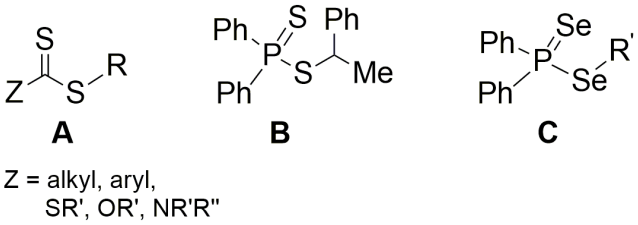

Scheme 1

RESULTS AND DISCUSSION

Synthesis and solution behavior

The new compounds were obtained by a succession of reactions, as depicted in Scheme 2, based on the *in situ* prepared organomagnesium (for compound **1**) or organolithium (for compounds **2** and **3**) reagents, subsequent selenium insertion in the new formed metal-carbon bond and further metal halide elimination between the as formed metal organoselenolate and the appropriate thio- or selenophosphinyl halide.

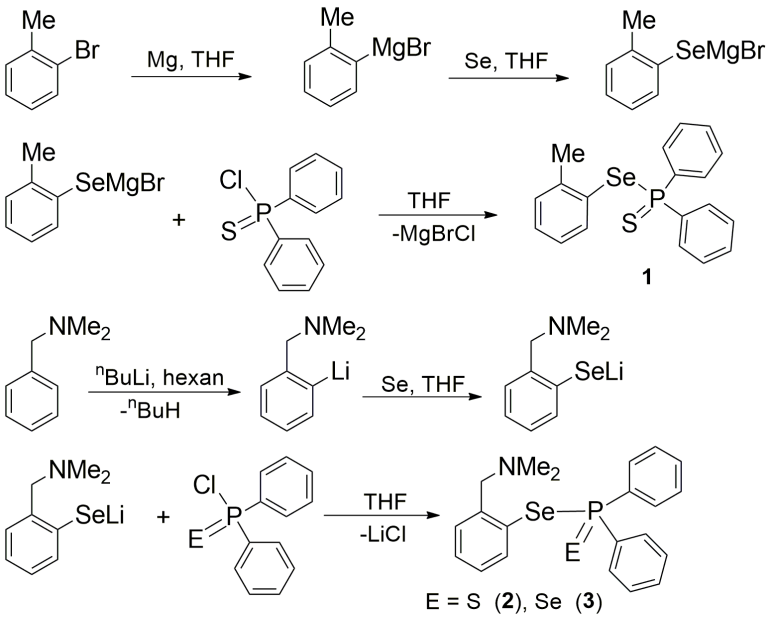

Scheme 2

The reaction between the lithium organoselenolate 2-($MePr^iNCH_2$)C_6H_4SeLi and $Ph_2P(S)Cl$ resulted in a complex mixture and our attempts to separate the ester $Ph_2P(S)SeC_6H_4(CH_2NMePr^i)$-2 (**4**) only allowded to isolate the ammonium salt $[MePr^iBnNH]^+[Ph_2P(S)O]^-$ (Bn = benzyl) (**4a**), formed by hydrolysis/decomposition processes.

Compound **1** was isolated as a slightly brown oil, while compounds **2** and **3** as yellowish solids, soluble in organic solvents. The new species were investigated in solution by multinuclear NMR (^1H, ^{31}P and ^{77}Se). The ^1H NMR spectra show the expected resonances for the aliphatic and the aromatic organic groups, with multiplicities due to ^1H-^1H and ^{31}P-^1H couplings. The room temperature ^1H NMR spectra of compounds **2** and **3**, which contain a 2-$Me_2NCH_2C_6H_4$ group attached to selenium, show no evidence for an intramolecular N→Se interaction. In the aliphatic region they show singlet resonances for the CH_2N and the N(CH_3)$_2$ protons of the pendant arm. For all these three compounds the $^{31}P\{^1H\}$ NMR resonances appear as singlets, accompanied by satellites due to ^{31}P-^{77}Se coupling, as shown in Figure 1 for **2** and **3**. One pair of satellites due to the coupling with the single bonded Se atom was observed for **2**, while couplings with both single and double bonded Se atoms in **3** resulted in two pairs of satellites.

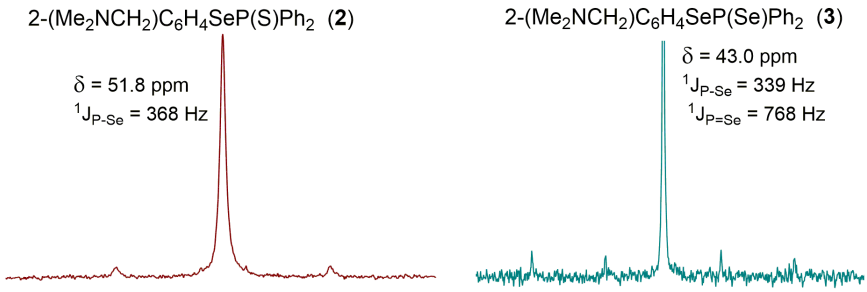

Figure 1. $^{31}P\{^{1}H\}$ resonances for compounds **2** and **3**

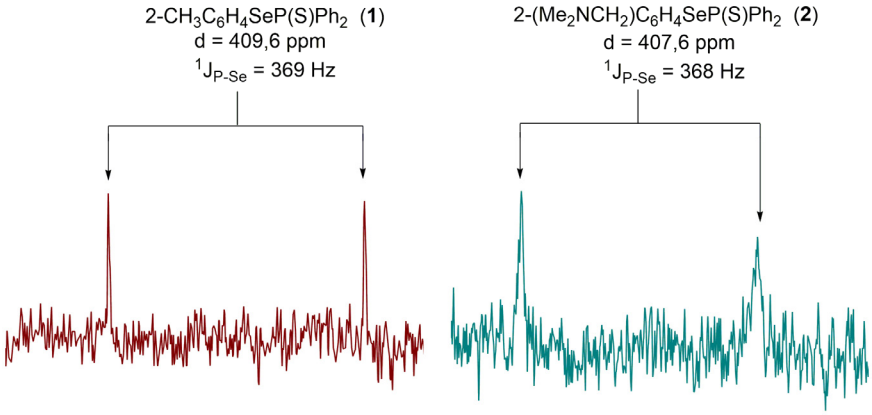

Figure 2. $^{77}Se\{^{1}H\}$ resonances for compounds **1** and **2**.

The $^{77}Se\{^{1}H\}$ NMR spectra of compounds **1** and **2** exhibit doublet resonances due to ^{31}P-^{77}Se couplings, as shown in Figure 2. For compound **3** the $^{77}Se\{^{1}H\}$ resonances could not be observed.

Single-crystal X-ray diffraction studies

The ORTEP-like diagram of **4a** with the atom numbering scheme is depicted in Figure 3, while selected interatomic distances and angles are given in Table 1.

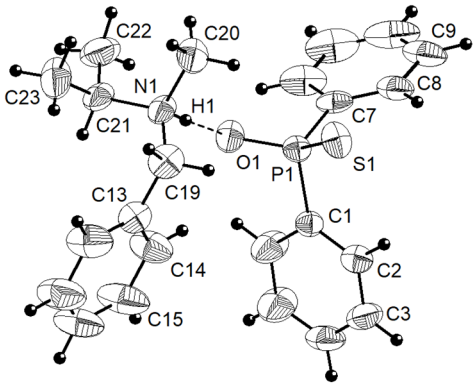

Figure 3. ORTEP-like diagram at 30% probability ellipsoids for **4a**.

The coordination geometries about phosphorus and nitrogen are distorted tetrahedral, with angles in the range 102.5(2)-118.1(2)º and 106.4-114.1(5)º, respectively. The phosphorus-oxygen and phosphorus-sulfur interatomic distances are characteristic for single P–O and double P=S bonds, close to the values found in the diphenylphosphinomonothioic acid [P–O 1.582(2) Å, and P=S 1.956(1) Å] [17].

Table 1. Selected interatomic distances [Å] and angles [°] in **4a**

P1−C1	1.805(7)	C1−P1−C7	102.5(2)
P1−C7	1.818(6)	C1−P1−S1	110.0(2)
P1−S1	1.967(2)	C7−P1−S1	110.0(2)
P1−O1	1.507(4)	C1−P1−O1	107.2(2)
N1−C19	1.484(8)	S1−P1−O1	118.1(2)
N1−C20	1.501(7)	C7−P1−O1	107.9(3)
N1−C21	1.504(8)	C19−N1−C20	109.6(5)
N1−H1	0.980	C19−N1−C21	114.1(5)
H1···O1	1.650	C20−N1−C21	113.4(5)
N1···O1	2.624(6)	C19−N1−H1	106.4
N1–H1···O1	176	C20−N1−H1	106.4
P1−O1···H1	125	C21−N1−H1	106.4

The ammonium cation and the diorganophosphinomonothioato anion are connected in the crystal through hydrogen bonding: N1−H1 0.980 Å, H1···O1 1.650 Å, N1···O1 2.624(6) Å [cf Σr_{vdW}(O,H) 2.60 Å; Σr_{vdW}(N,O) 2.94 Å] [18].

EXPERIMENTAL SECTION

Starting materials were prepared according to literature procedures: $Ph_2P(S)Cl$, $Ph_2P(Se)Cl$ [19], $MePr^iNCH_2C_6H_5$ [20] or were commercially available and used as purchased. Solvents were dried and distilled under argon prior to use. Elemental analysis was performed on a Flash EA 1112 analyzer and melting points were measured on an Electrothermal 9200 apparatus. ^1H, $^{31}P\{^1H\}$ and $^{77}Se\{^1H\}$ NMR spectra were recorded on a BRUKER Avance 400 instrument in $CDCl_3$ solutions. The chemical shifts are reported in δ units (ppm) relative to TMS (ref. $CHCl_3$: ^1H 7.26 ppm), H_3PO_4 85% and Me_2Se_2, respectively. The NMR data were processed using the MestReNova software [21].

Synthesis of 2-$MeC_6H_4SeP(S)Ph_2$ (1)

Selenium powder (2.303 g, 29.16 mmol) was added at 0 °C to a THF solution of a Grignard reagent *in situ* prepared from 2-bromotoluen (3.6 mL, 4.988 g, 29.16 mmol) and magnesium span (0.815 g, 29.16 mmol). The reaction mixture was stirred for 30 min until all selenium was reacted. Subsequently, $Ph_2P(S)Cl$ (7.37 g, 29.16 mmol) was added and stirring continued for other two hours. THF was removed under reduced pressure and the desired product was extracted in CH_2Cl_2. After removing the solvent and washing with 3 x 10 mL of n-hexane, the title compound resulted as a slightly brown oil. Yield: 5.86 g (52%). ^1H NMR: *δ* 1.73 (s, 3H, CH_3), 6.52 (t, 1H, C_6H_4, $^3J_{HH}$ 7.9 Hz), 6.63-6.79 (m, 2H, C_6H_4), 6.90-7.04 (m, 6H, C_6H_5-*meta+para* + 1H, C_6H_4), 7.40 (ddd, 4H, C_6H_5-*ortho*, $^3J_{HH}$ 7.4, $^4J_{HH}$ 1.5, $^3J_{PH}$ 14.3 Hz). $^{31}P\{^1H\}$ NMR: *δ* 53.14 (s, $^1J_{PSe}$ = 368 Hz, $^1J_{PC}$ 75.4 Hz). $^{77}Se\{^1H\}$ NMR: *δ* 409.6 (d, $^1J_{PSe}$ = 369 Hz).

Synthesis of [2-(Me_2NCH_2)C_6H_4]$SeP(S)Ph_2$ (2)

Selenium powder (0.547g, 6.93 mmol) was added under stirring to a solution of [2-(Me_2NCH_2)C_6H_4]Li (0.978 g, 6.93 mmol) in 20 mL THF. After two hours a solution of $Ph_2P(S)Cl$ (1.75 g, 6.93 mmol) in 20 mL THF was added dropwise and stirring continued for other two hours. THF was removed under reduced pressure and the reaction mixture was worked up with toluene (40 mL). From the clear toluene solution, after removing the solvent and washing with n-hexane (3 x 10 mL), the title compound was obtained as a yellowish solid. Yield: 2.98 g (50%). M.p. 66 °C. ^1H NMR: *δ* 2.15 (s, 6H, NCH_3), 3.35 (s, 2H, CH_2N), 7.04 (t, 1H, C_6H_4, $^3J_{HH}$ 6.9 Hz), 7.22-7.37 (m, 3H, C_6H_4), 7.40-7.57 (m, 6H, C_6H_5-*meta+para*), 7.96 (dd, 4H, C_6H_5-*ortho*, $^3J_{HH}$ 6.4, $^3J_{PH}$ 14.1 Hz). $^{31}P\{^1H\}$ NMR: *δ* 51.78 (s, $^1J_{PSe}$ = 367 Hz). $^{77}Se\{^1H\}$ NMR: *δ* 407.6 (d, $^1J_{PSe}$ = 368 Hz).

Synthesis of [2-(Me$_2$NCH$_2$)C$_6$H$_4$]SeP(Se)Ph$_2$ (3)

Compound **3** was prepared similarly with compound **2**, from [2-(Me$_2$NCH$_2$)C$_6$H$_4$]Li (0.524 g, 3.71 mmol), selenium powder (0.293 g, 3.71 mmol) and Ph$_2$P(Se)Cl (1.11 g, 3.71 mmol), as a yellowish solid. Yield: 0.91 g (51%). M.p. 75 °C. ^{1}H NMR: δ 2.75 (s, 6H, NC*H*$_3$), 4.41 (s, 2H, C*H*$_2$N), 7.04 (t, 1H, C$_6$H$_4$, $^3J_{HH}$ 6.9 Hz), 7.22-7.37 (m, 6H, C$_6$H$_5$-*meta+para* + 1H C$_6$H$_4$), 7.42-7.54 (m, 2H, C$_6$H$_4$), 7.84 (dd, 4H, C$_6$H$_5$-*ortho*, $^3J_{HH}$ 7.4, $^4J_{HH}$ 1.8, $^3J_{PH}$ 13.7 Hz), 7.97 (d, 1H C$_6$H$_4$). ^{31}P{^{1}H} NMR: δ 42.93 (s, $^1J_{P\text{-}Se}$ 339, $^1J_{P=Se}$ 768 Hz).

Formation of [MePr^{i}BnNH]$^+$[Ph$_2$P(S)O]$^-$ (4a)

The lithium organoselenolate *[2-(MePr^{i}NCH$_2$)C$_6$H$_4$]SeLi* was prepared *in situ* from a 1.6 M solution of ^{n}BuLi in hexane (4.1 mL, 5.91 mmol) and *N,N*-methylisopropylbenzylamine (0.97 g, 5.91 mmol) in hexane (20 mL). Selenium powder (0.47 g, 5.91 mmol) was inserted in the C–Li bond and the synthesis continued as described for compound **2**. The obtained oil was layered with hexane and left overnight at –20 °C, when a beige powder was formed. Yield: 1.72 g (64%). ^{1}H and ^{31}P{^{1}H} NMR suggested a complex mixture. Further attempts to separate the components by recrystallization resulted in the hydrolysis title product, as a colorless solid. M.p. 112-114 °C. ^{1}H NMR: δ 1.31 [s, br., 3H, NCH(C*H*$_3$)$_2$], 1.40 (s, br., 3H, NCH(C*H*$_3$)$_2$), 2.55 (s, 3H, NC*H*$_3$), 3.69 [m, br, 1H, NC*H*(CH$_3$)$_2$], 4.20 (s, br, 2H, C*H*$_2$N), 7.25-7.30 (m, 1H, C$_6$H$_4$), 7.32-7.39 (m, 6H, C$_6$H$_5$-*meta+para* + 2H, C$_6$H$_4$), 7.63 (d, 1H, C$_6$H$_4$, $^3J_{HH}$ 7.4 Hz), 7.99 (ddd, 4H, C$_6$H$_5$-*ortho*, $^3J_{HH}$ = 7.3, $^4J_{HH}$ = 2.3, $^3J_{PH}$ = 12.6 Hz). ^{31}P{^{1}H} NMR: δ 56.8 (s).

X-ray structure determination

The details of the crystal structure determination and refinement for **4a** are given in Table 2. Data were collected on a Bruker SMART APEX diffractometer by using graphite-monochromated Mo-K_α radiation (λ = 0.71073 Å). The crystals were attached with paraton/N oil on cryoloops and the data were collected at room temperature (293 K). The structure was refined with anisotropic thermal parameters. The hydrogen atoms were refined with a riding model and a mutual isotropic thermal parameter. For structure solving and refinement the software package SHELX-97 was used [22]. The drawings were created with the Diamond program [23].

Table 2. Crystallographic data for **4a**

	4a
Empirical formula	$C_{23}H_{28}NOPS$
Formula weight	397.49
Temperature (K)	293(2) K
Wavelength (Å)	0.71073
Crystal system	monoclinic
Space group	P21/c
a (Å)	9.0645(17)
b (Å)	19.403(4)
c (Å)	13.339(2)
α (°)	90
β (°)	106.335(4)
γ (°)	90
Volume, (Å^3)	2251.4(7)
Z	4
Density (calculated) (g/cm^3)	1.173
Absorption coefficient (mm^{-1})	0.227
F(000)	848
Crystal size, mm	0.25 x 0.32 x 0.40
θ range for data collections, °	1.91 to 25.00
Reflections collected	21394
Independent reflections	3963 [R(int) = 0.099]
Refinement method	Full-matrix least-squares on F^2
Data / restraints / parameters	3963 / 0 / 247
Goodness-of-fit on F^2	1.144
Final *R* indicies [I>2sigma(I)]	R1 = 0.1114, wR2 = 0.2330
R indicies (all data)	R1 = 0.1745, wR2 = 0.2648
Largest diff. peak and hole, eÅ^{-3}	0.30 and -0.35

CONCLUSIONS

The reactions between 2-$MeC_6H_4SeMgBr$ or 2-$(Me_2NCH_2)C_6H_4SeLi$ with diphenylthio- or diphenylselenophosphinyl chloride allowed the isolation of stable esters **1** - **3**, while the reaction between 2-$(MePr^iNCH_2)C_6H_4SeLi$ and $Ph_2P(S)Cl$ resulted in a complex mixture of products, from which the ammonium salt $[MePr^iBnNH]^+[Ph_2P(S)O]^-$ (Bn = benzyl) (**4a**), formed during a hydrolysis/decomposition process, could be isolated and structurally characterized. The ^{1}H NMR spectra for compounds **2** and **3**, which contain

the 2-(Me_2NCH_2)C_6H_4 group attached to selenium, brought no evidence for the intramolecular N→Se interaction in solution at room temperature. This observation might be consistent with the absence of any intramolecular interaction or it might suggest a dynamic behavior involving de-coordination, inversion at nitrogen and re-coordination, too fast at room temperature to be observed at the NMR time scale.

ACKNOWLEDGMENTS

Financial support from the Ministry of Education and Research of Romania (Research Project No. PN-II-ID-PCE-2011-3-0659) is greatly appreciated.

SUPPLEMENTARY DATA

CCDC 1902133 contain the supplementary crystallographic data for **4a**. These data can be obtained free of charge *via http://www.ccdc.cam.ac.uk/conts/retrieving.html*, or from the Cambridge Crystallographic Data Centre, 12 Union Road, Cambridge CB2 1EZ, UK; fax: +44 1223 336 033; or e-mail: deposit@ccdc.cam.ac.uk.

REFERENCES

1. X. Tian, J. Ding, B. Zhang, F. Qiu, X. Zhuang, Y. Chen, *Polymers*, **2018**, *10*, 318.
2. C. Barner-Kowollik, T.P. Davis, J.P. A. Heuts, M.H. Stenzel, P. Vana, M. Whittaker, *J. Polym. Sci., Part A: Polym. Chem.*, **2003**, *41*, 365.
3. D.J. Keddie, G. Moad, E. Rizzardo, S.H. Thang, *Macromolecules*, **2012**, *45*, 5321.
4. C. Konn, F. Morel, D.L. Beyou, P. Chaumont, E. Bourgeat-Lami, *Macromolecules*, **2007**, *40*, 7464.
5. J. Nicolas, Y. Guillaneuf, C. Lefay, D. Bertin, D. Gigmes, B. Charleux, *Prog. Polym. Sci.*, **2013**, *38*, 63.
6. N.V. Tsarevsky, K. Matyjaszewski, *Chem. Rev.*, **2007**, *107*, 2270.
7. J. Ran, L. Wu, Z. Zhang, T. Xu, *Prog. Polym. Sci.*, **2014**, *39*, 124.
8. A. Alberti, M. Benaglia, M. Laus, K. Sparnacci, *J. Org. Chem.*, **2002**, *67*, 7911.
9. D. Gigmes, D. Bertin, S. Marque, O. Guerret, P. Tordo, *Tetrahedron Lett.*, **2003**, *44*, 1227.
10. J.L. Hodgson, K.A. Green, M.L Coote, *Org. Lett.*, **2005**, *7*, 4581.
11. J. Moon, H. Nam, S. Kim, J. Ryu, C. Han, C. Lee, S. Lee, *Tetrahedron Lett.*, **2008**, *49*, 5137.

12. T. Kimura, T. Murai, *J. Org. Chem.*, **2005**, *70*, 952.
13. R. Şuteu, S. Shova, A. Silvestru, *Inorg. Chim. Acta*, **2018**, *475*, 105.
14. A. Covaci, R. Mitea, I. Hosu, A. Silvestru, *Polyhedron*, **2014**, 72, 157.
15. A. Pop, A. Silvestru, E.J. Juárez-Pérez, M. Arca, V. Lippolis, C. Silvestru, *Dalton Trans.*, **2014**, *43*, 2221.
16. R.A. Popa, E. Licarete, M. Banciu, A. Silvestru, *Appl. Organomet. Chem.*, **2018**, *32*, e4252.
17. R. Mattes, D. Rühl, *Acta Crystallogr., Sect. C: Struct. Chem.*, **1984**, *C40*, 106.
18. J. Emsley, "Die Elemente", Walter de Gruyter, Berlin, **1994**.
19. M.W. Schmidt, P.H. Truong, M.S. Gordon, *J. Am. Chem. Soc.*, **1987**, *109*, 5217.
20. H. Ahlbrecht, J. Harbach, R.W. Hoffmann, T. Ruhland, *Liebigs Ann.,* **1995**, 211.
21. *MestReC and MestReNova*, Mestrelab Research S.L., Feliciano Barrera 9B, Bajo, 15706 Santiago de Compostela, Spain, **2015**.
22. G.M. Sheldrick, *Acta Crystallogr., Sect. A: Found. Crystallogr.*, **2008**, *A64*, 112.
23. *DIAMOND*, Visual Crystal Structure Information System, Crystal Impact, Postfach 1251, 53002 Bonn, Germany, **2015**.

STUDIA UBB CHEMIA, LXIV, 2,Tom I, 2019 (p. 207-216)
(RECOMMENDED CITATION)
DOI:10.24193/subbchem.2019.2.17

Dedicated to Professor Florin Dan Irimie on the Occasion of His 65th Anniversary

FEATURES OF INFECTED VERSUS UNINFECTED CHEMICAL PROFILES RELEASED FROM HUMAN EXUDATES

ILEANA-ANDREEA RATIU[a,b*], TOMASZ LIGOR[a], FERNANDA MONEDEIRO[a,c], HOSSAM AL-SUOD[a], VICTOR BOCOS-BINTINTAN[d], JACEK SZELIGA[e], MAREK JACKOWSKI[e], BOGUSLAW BUSZEWSKI[a*]

ABSTRACT. Detection of bacterial volatile metabolites produced by human pathogenic bacteria is gaining continuous interest in both scientific and medical fields. Solid-phase microextraction (SPME) is a sampling technique that gained increasing attention in the last years due to its simplicity to implement and sensitivity. Volatile organic compounds (VOCs) released in the headspace over exudates infected with different bacteria were investigated in this work. GC-MS was involved for analysis. The above mentioned VOCs resulted from bacterial metabolism and the afferent processes that occur inside the biological samples. However, we identified 14 compounds emitted by the infecting pathogens, which can be assumed as bacterial markers.

Keywords: *bacterial markers, exudates, headspace profiles, diagnostic tool.*

[a] *Department of Environmental Chemistry and Bioanalytics, Faculty of Chemistry, Interdisciplinary Centre of Modern Technologies, Nicolaus Copernicus University,7 Gagarina Str., 87-100 Torun, Poland*
[b] *Faculty of Chemistry and Chemical Engineering, Babeş-Bolyai University, 11 Arany Janos, RO-400028, Cluj-Napoca, Romania*
[c] *Department of Chemistry, Faculty of Philosophy, Science and Letters of Ribeirão Preto, University of São Paulo, CEP 14040-901 Ribeirão Preto, Brazil*
[d] *Faculty of Environmental Science and Engineering, Babeş-Bolyai University, 30 Fântânele ,RO-400294 Cluj-Napoca, Romania*
[e] *Dept. of General, Gastroenterologic and Oncologic Surgery Collegium Medicum, Nicolaus Copernicus University, Torun, Poland*
** Corresponding authors email: busz@chem.umk.pl; andreea_ratiu84@yahoo.com*

INTRODUCTION

Typical microbiological methods for bacteria identification are usually expensive and time consuming. This whole necessary procedure is a great burden for the health care system. Therefore, having the possibility of identifying bacterial biomarkers directly from clinical samples may offer a valuable opportunity for developing rapid and inexpensive diagnostic tools [1,2]. An in situ methodology that is non-invasive, rapid and sensitive will definitely facilitate timely and effective diagnosis which is highly desired. In vitro studies have been carried out in attempt to create bacterial fingerprint data bases for relevant human pathogens [3,4]. VOCs emitted by human biological samples (e.g. breath, urine, tissue) were analysed and proposed to be used as a diagnostic tool for various diseases or for bacterial infection, because it does not require invasive procedures, reagents usage or complex sample preparation methods [5,6]. SPME is widely used for VOCs analysis since it is a simple and effective sampling technique, combining the sampling, selective isolation, and pre-concentration in a single step. Gas chromatography coupled with mass spectrometry (GC-MS) provides detailed analytical information and identifies the analyses with the highest certainty, when compared to other techniques. [7].

Different other analytical techniques, for example SIFT-MS (selected ion flow tube-mass spectrometry), PTR-MS (proton transfer reaction mass spectrometry), SESI-MS (secondary electrospray ionization mass spectrometry) were involved in direct measurements of bacterial biomarkers [8]. Ion mobility spectrometry (IMS), and multi-capillary GC columns coupled to an ion mobility spectrometer (MCC-IMS) were used for detection of pathogenic bacteria by sniffing their characteristic emitted volatiles [9,10]. Sensors and e-noses can be used for detection and monitoring of target components, but as standalone instrumentation they do not have have the potential for chemical identification of complex VOCs profiles [11-14]. Identification and classification of bacteria can be achieved by MALDI MS (matrix-assisted laser desorption and ionization coupled with mass spectrometry) [15]. In spite of its capabilities, MALDI MS does not detect VOCs and is a more expensive instrumentation compared with GC-MS.

The aim of this research was to analyse samples of infected exudates and to identify the presence of the bacterial colonization and pathogens themselves. The advantage of this approach consists in the simplicity of the method and in getting closer with real scenario of clinical samples. To detect pathogen-specific signals in the context of an infection remains a challenge, however, 14 compounds were assumed as bacterial markers in this study.

RESULTS AND DISCUSSIONS

Uninfected samples were used as controls. The identity of each component in chromatograms was assigned using the NIST data base. The peaks with a Match Factor value >850 were only considered. The VOCs emitted by infected samples resulted in 46 compounds.

Table 1 presents the identified substances coming from the 15 patients (P), together with the infecting pathogen. The identity of infecting pathogens was provided by the behind microbiological clinical trials realized in the hospital. Finally, 8 bacterial species named*: Escherichia coli (E. coli), Enteroccus faecalis (E. faecalis), Citrobacter freundii (C. freundii), Staphylococcus aureus (S. aureus), Proteus mirabilis (P. mirabilis), Pseudomonas aeruginosa (P. aeruginosa), Morganella morganii (M. morganii)* and *Stenotrophomonas maltophilia (S. maltophilia)* were identified as infecting pathogens of investigated samples. We assume that some of compounds presented in Table 1 are metabolism products of bacteria, while others are degradation products of mammalian and bacterial cells. The compounds identified in infected samples and confirmed to be similar with those detected in headspace of in vitro cultivated bacteria (confirmation with literature, reference presented in Table 1) were considered bacterial markers and they are bold highlighted. By visual inspection of chromatograms, we noticed that samples infected with *P. mirabilis* presented higher peaks intensities compared with others. Less intensive peaks were observed for P 2, 3 and 6. Chromatograms of samples coming from P 7, 8, 9 and 10 present more components compared with others. Generaly, highest signals were observed for indole, dimethyl disulfide, dimethyl trisulfide and benzoic acid ethyl ester. Uninfected profiles were significantly different of infected profiles. The presence of markers like indole, volatile sulfur components, butanoic acid, acetic acid and alcohols (1-butanol, 3-methyl, phenylethyl alcohol) was not observed in the blanks.

Bacterial markers emitted from investigated strains

Biological samples, like exudates, are complex mixtures containing huge number of substances. Phospholipids, proteins, amino acids, fatty acids, etc are indispensable to living cells. Microorganisms, can degrade organic material according with their metabolisms, resulting in a variety of VOCs. When we talk about volatiles emitted from infected clinical samples, they can be bacterial volatile metabolites, also they may reflect the pathogen-induced host responses, [21], endogenous enzymes produced compounds [22], as well as putrefaction products. Comparing the components from Table 1 with those detected from cultivated bacteria, it was noticed that the profiles of cultivated bacteria and samples collected from human patients are

different. However, 14 compounds observed in clinical samples were common with those produced by bacteria grown in vitro. We assume that they were produced by pathogens, and can be considered bacterial markers. We present them in Figure 1, with the connection between producing bacteria and patient in which were detected.

Table 1. Compounds detected in infected and uninfected samples

Patient ID	Detected components	Infecting pathogen	Ref
Patient 1	**1-pentanol**, 2-nonanone, **acetoin,** benzyl alcohol, decane, dimethyl trisulfide**, dimethyl disulfide, ethanol**, **indole**, limonene, octanal, phenylethyl alcohol	*E. coli*	4
Patient 2	**1-pentanol, acetoin**, benzaldehyde, benzyl alcohol, biphenyl, dodecanal, **ethanol**, **hexanal**, limonene, undecane.	*E. coli* + *E. faecalis*	4, 16
Patient 3	1-octanol, **1-pentanol, acetoin,** benzoic acid ethyl ester, biphenyl, decane, **hexanal.**	*E. coli*	4
Patient 4	1-butanol, 1-octanol, **1-pentanol**, 2-methyl-butanoic acid, 3-methyl butanoic acid, benzeneacetaldehyde, benzoic acid ethyl ester, benzyl alcohol, biphenyl, butanoic acid, **dimethyl disulfide**, **hexanal, indole**, methyl-thiolacetate, **phenol,** tetradecane.	*C. freundii* + *S. aureus*	17, 18
Patient 5	1-hexanol, 1-nonanol, **1-octanol,** 2-methyl-butanoic acid, **3-methyl-1-butanol**, 3-methyl-butanoic acid, **acetic acid, acetophenone**, benzeneacetaldehyde, benzoic acid ethyl ester, benzyl alcohol, biphenyl, **dimethyl disulfide, dimethyl trisulfide,** dodecane, **indole**, limonene, naphthalene, tetradecane.	*P. mirabilis*+ *P. aeruginosa*	9, 19
Patient 6	**acetic acid**, benzaldehyde, benzoic acid ethyl ester, benzyl alcohol, biphenyl, naphthalene, nonanal, tetradecane, toluene.	*P. aeruginosa*	20
Patient 7	1-hexanol, **3-methyl-1-butanol,** acetophenone, **dimethyl disulfide**, dimethyl tetrasulfide, **dimethyl trisulfide,** dodecane, ethanol, hexanal, indole, naphthalene, octanal, phenol, **phenylethyl alcohol**.	*P. mirabilis*	9, 19
Patient 8	1-hexanol, 2-nonanone, 2-tridecanone, **3-methyl-1-butanol,** benzoic acid ethyl ester, biphenyl, **dimethyl disulfide**, dimethyl tetrasulfide, **dimethyl trisulfide,** dodecane, ethanol, hexanal, indole, limonene, naphthalene, **phenol**, tetradecane,	*M. morganii* + *S. maltophilia*	15, 19
Patient 9	**1-octanol**, 2-methyl- butanoic acid, **2-nonanone, 3-methyl-1-butanol,** 3-methyl-butanoic acid, acetophenone, benzyl alcohol, butanoic acid, chloroaniline, **dimethyl disulfide, dimethyl trisulfide,** dodecane, ethanol, indole, octanoic acid, pentanoic acid, phenol, **phenylethyl alcohol,** tetradecane.	*P. mirabilis*	9, 19
Patient 10	1-hexanol, 1-nonanol, **1-octanol**, 1-pentanol, 2-methyl-butanoic acid, **2-nonanone**, **3-methyl-1-butanol,** 3-methyl-butanoic acid, acetophenone, butanoic acid, dimethyl tetrasulfide, **dimethyl disulfide**, **dimethyl trisulfide,** dodecane, indole, nonanal, pentanoic acid, phenol, **phenylethyl alcohol**,tetradecane.	*P. mirabilis*	9, 19
Patient 11	1-decene, 1-dodecene, 4-methyl-octane, dodecane, eicosane, limonene, octadecanal, octane, pentadecane, undecane.	Uninfected	
Patient 12	1-decene, 1-dodecene, 4-methyl-decane, 4-methyl-octane, decane, dodecane, eicosane, octane, propofol, tetradecane, undecane.	Uninfected	
Patient 13	1-decene, 1-dodecene, 2-methyl-dodecane, decane, dodecane, eicosane, limonene, octane, propofol, tetradecane, undecane.	Uninfected	
Patient 14	1-decene, 1-dodecene, 4-methyl-decane, 4-methyl-octane, decane, dodecane, eicosane, octane, propofol, tetradecane, undecane.	Uninfected	
Patient 15	1-decene, 1-dodecene, 4-methyl-octane, decane, dodecane, eicosane, limonene, octane, propofol, tetradecane, undecane.	Uninfected	

Figure 1 denotes discrimination among some strains as well. For example, *E. coli*, having as markers acetoin, 1-pentanol, ethanol, indole and hexanal, could not be confused with *P. mirabilis* or *M. morganii*, which are represented by 1-octanol, phenylethyl alcohol, 3-methyl-1-butanol, dimethyl trisulfide and phenol, although if all three have dimethyl disulfide as a common metabolite. In the same time *E. coli* can be confused with *E. faecalis*, because the first one include the markers generated by the second one, however, never the opposite due mostly to the indole occurrence. Moreover, considering that the metabolites emitted by each bacteria are coming together in a particular combination of components like a fingerprint, statistical approaches were used in order to check the differences between profiles emitted by samples infected with different pathogens and controls.

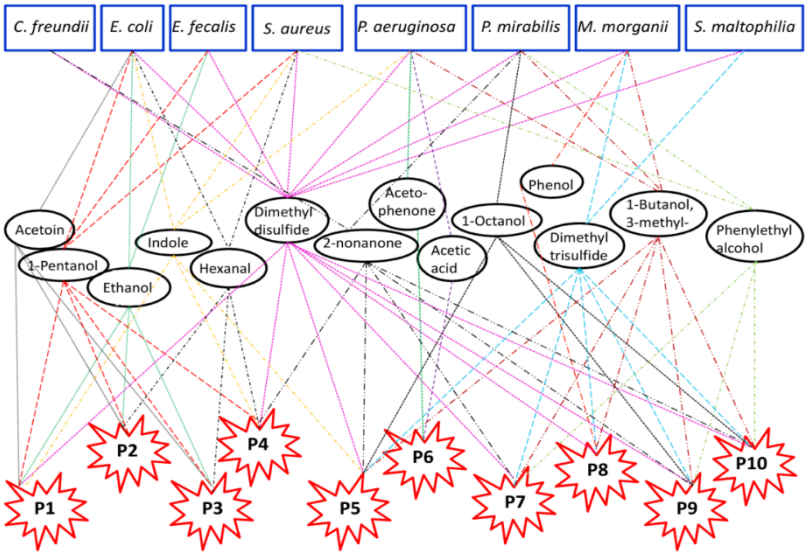

Figure 1. Detected bacterial markers and the links between infecting pathogens and the donor patients.

Discrimination between infected and uninfected profiles

A dendrogram using Ward linkage (created in IBM SPSS Statistics 21) is presented in Figure 2. The formation of two separated categories of clusters: coming from infected and uninfected patients respectively was observed. Infected group is presented again different cluster modeling, according with infecting pathogens. Thus, separated clusters were obtained for P1 to P3 infected or coinfected with *E. Coli*, while the sample infected with

P. Aeruginosa clustered close with the previously mentioned three. All the samples infected or coinfected with *P. Mirabilis* clustered nearby and separately the samples coinfected with *C. freundii* + *S. aureus* and *M. morganii* + *S. maltophilia* were positioned. In contrast with in vitro cultivated samples, in case of biological samples, the grouping of clusters can be sometimes disturbed, for some reasons listed below. Microbial density is difficult to control in a biological sample. If the number of bacterial cell is too high, the metabolic pathways can be influenced, due to intra-specific interactions. If samples are infected with more bacterial strains, ecological interactions can occur. Considering that our exudates samples were collected from post-operative patients, previously cured with antibiotics, under anaesthesia or treated with bactericide or bacteriostatic agents, is possible that all this agents together can change the bacterial metabolism, resulting in some new or atypical compounds.

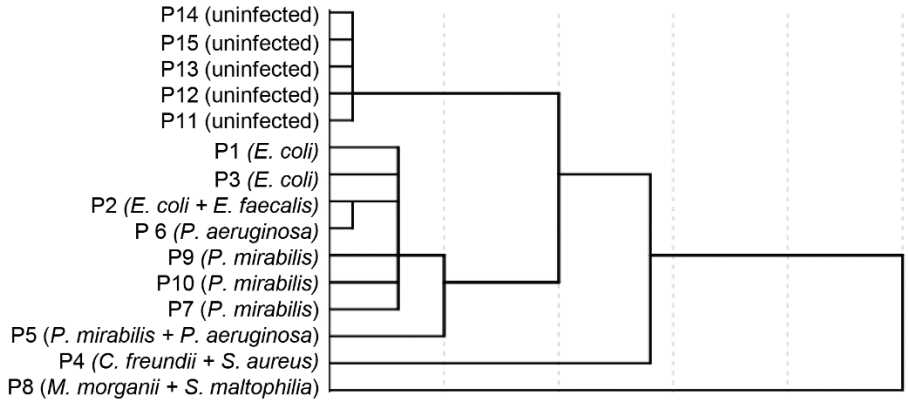

Figure 2. Discrimination between infected and uninfected group enrolled in the study, as well as between patients infected with different pathogens.

Emitted VOCs as a diagnostic tool for bacterial infections

The using of VOCs emitted by bacteria in attempt to create screening tools which has the ability to confirm or deny the presence of a bacterial infection, or moreover to predict the infecting pathogen identity is a tempting and bright perspective. ROC curves (receiver-operating characteristic) offer the possibility to test between two states of health and are a suitable choice to test the performance of analytical and clinical application. This model can be used for prediction of a diagnostic in absence of knowledge of true disease

status. Thus ROC curves were used to test the diagnostic ability based on detected VOCs. We tested four types of infected profiles (those with *E. coli*, with *P. mirabilis*, with *P. aeruginosa* and all the co-infected samples together) versus uninfected profiles. A binary algorithm classifier was used, where the volatiles coming from infected samples were assumed as positive, while those received from uninfected samples as negative. The obtained results show that the area under the receiver-operating characteristic (95% probability interval) was 0.830 in case of samples infected with *E. coli*, 0.907 for samples infected with *P. mirabilis*, and 0.856 for those infected with *P. aeruginosa*. The AUC in case of co-infected samples was 0.875, and 0.522 for uninfected samples, as seen in Figure 3. The positioning of control value (of uninfected samples) in the middle of the range between 0 and 1, confirm that the diagnosis predictability worked correct, once 0.522 value predict nothing; giving the same accuracy like when you roll up a coin. However, this finding indicates a good predictability of infection (more that 80%) and the possibility to apply this methodology as a new diagnostic tool of bacterial infection.

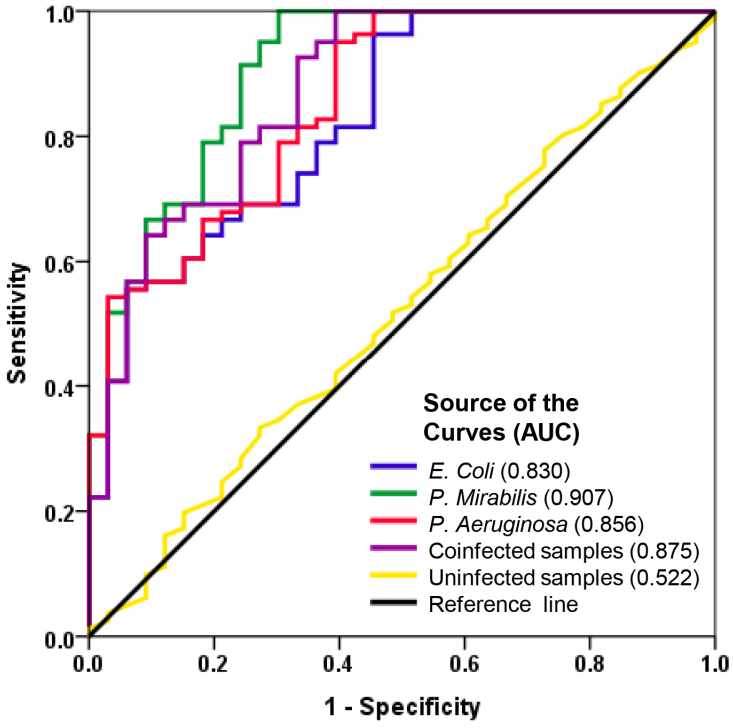

Figure 3. ROC presenting the ability of VOCs to predict bacterial infections.

CONCLUSIONS

The possibility of using volatile metabolites emitted by bacteria as a diagnostic tool is a promising perspective. The potential of discrimination between volatiles emitted by infected and uninfected exudates was proven through this study; infected samples presented a different cluster modelling, according with the infecting pathogens. Each bacterial strain relieved a characteristic fingerprint of components, which was reflected in different combinations of VOCs, as highlighted in Table 1. A good predictability of diagnosis accuracy, (between 83% and 90%) for infected patients, was achieved when ROC curves were generated. Nevertheless, additional fast and on-site spectrometry techniques can be used for the detection of biomarker compounds specific to bacteria, once they are known and confirmed by GC-MS. Starting from the key biomarkers detected, instrumentation used for fast screening of bacterial infection from various matrixes can be develop.

EXPERIMENTAL SECTION

A mass spectrometer Agilent 5975 Inert XL MSD coupled with a gas chromatograph Agilent 6890 N (Agilent, Waldbronn, Germany) with split-splitless injector were used for analysis. The operating conditions and characteristics for the GC/MS system are presented in Table 2. The chromatographic data achisition was performed by means of Chemstation software package (Agilent). The mass spectrum library NIST 2005 (Gaithersburg, USA) was used for identification. PDMS/DVB coated fiber was used for sampling. Screw top headspace glass vials (20mL) with silicon/ PTFE septa and caps were provided by Supelco.

Table 2 Operating conditions and characteristics for the GC/MS system

SPME desorption	Agilent GC 6890 N	Agilent-5975 Mass Selective Detector
Desorption flow: 35 cm^3 min^{-1} Desorption temperature: 240°C Desorption time: 2 min	Column: 30 m x 0.25 mm x 0.25 µm RTX-5MS Velocity : He @ 1.1 cm^3 min^{-1} Initial oven temperature: 40°C (5 min) Initial hold time: 5 min Oven temperature program: 10°C min^{-1} to 300°C - hold for 5 min	Scan type: Full Scan Mass range: 30 to 300 m/z Ionization type: EI 70 eV Scan rate: 3.4 scan/s Ion source temperature: 280°C Transfer line temperature: 250°C Total run time: 33 min

All biological infected samples were collected from surgical wounds, under aseptic conditions in the Department of General, Gastroenterological and Oncological Surgery of Collegium Medicum of Nicolaus Copernicus University, according with the agreement KB 730/2016, signed on 13 December 2016 by Ethical Committee Collegium Medicum, in Bydgoszcz. A number of 10 volunteers, diagnosed with surgical-site infection based on typical clinical symptoms were included into the study. Apart of those, 5 more patients undergoing surgery, without bacterial infection, were enrolled into the study to collect the control samples. Local anesthesia with 1-2% lignocaine (Lignocaine hydrochloride) infiltration was used. Prior to sample collection, water solution of “Octanisept” were used for wound cleaning.

When samples were collected, the identity of infecting pathogens was unknown. At the same time a classic wound smear using a microbiological swab was collected and transferred for routine identification (classical methods of bacteriological diagnostics). For the chromatographic analyses, the exudates were collected in sterile container, transported into the laboratory and analyzed in maximum 4 hours. In the laboratory each sample was transferred to in a 20 mL glass vials crimped with silicon septa and incubated at 37 °C for 30 min. In the next step, the SPME was inserted into the glass vial over sample, through the septum, for a period of 45 min. After extraction the volatiles were desorbed in hot GC injector in splitless mode for 2 min.

ACKNOWLEDGMENTS

The financial resources for conducting the scientific research was obtained under the research grant for young researchers from abroad awarded by the Rector of the Nicolaus Copernicus University pursuant to Order no. MNZ/01/1029.

REFERENCES

1. Y. Kim, K. Park, K. Lee, Y.J. Park. *Annals of Laboratory Medicine*, **2015**, *35*, 422.
2. I.A. Ratiu, T. Ligor, V. Bocos-Bintintan, J. Szeliga, K. Machała, M. Jackowski, B. Buszewski, *Journal of Breath Research* **2019**, *13*, 026003 https://doi.org/10.1088/1752-7163/aaf708.
3. B. Buszewski, I.A. Ratiu, M. Milanowski, P. Pomastowski, T. Ligor, *Journal of Breath Research*, **2018**, *12*, 027105.

4. I.A. Ratiu, V. Bocoş-Bintintan, M. Turner, V. Moll, C.L.P. Thomas, *Current Analitical Chemistry*, **2014**, *10*, 488.
5. D. Chan, C. Leggett, K. Wang, *World Journal of Gastroenterology*, **2016**, *2,* 1639.
6. C.S.J. Probert, I. Ahmed, T. Khalid, E. Johnson, S. Smith, N. Ratcliffe, *Journal of Gastrointestinal and Liver Diseases,* **2009**, *18*, 337.
7. I.A. Ratiu, T. Ligor, V. Bocos-Bintintan, H. Al-Suod, T. Kowalkowski, K. Rafińska, B. Buszewski, *Journal of Breath Research*, **2017**, *11*, 036012.
8. I.A. Ratiu, T. Ligor, V. Bocos-Bintintan, B. Buszewski, *Bioanalysis*, **2017**, *9*, 1069.
9. M. Jünger, W. Vautz, M. Kuhns, L. Hofmann, S. Ulbricht, J.I. Baumbach, M. Quintel, T. Perl, *Applied Microbiology and Biotechnology.* **2012**, *93*:2603.
10. I.A. Ratiu, V. Bocos-Bintintan, A. Patrut, V. Moll, M. Turner, C.L.P. Thomas, *Analitica Chimica Acta*, **2017**, *982*, 209.
11. R. Huo, A. Agapiou, V. Bocos-Bintintan, L.J. Brown, C. Burns, C.S. Creaser, N.A. Devenport, B. Gao-Lau, C. Guallar-Hoyas, L. Hildebrand, A. Malkar, H.J. Martin, V.H. Moll, P. Patel, I.A. Ratiu, J.C. Reynolds, S. Sielemann, R. Slodzynski, M. Statheropoulos, M.A. Turner, W. Vautz; V.E. Wright, C.L.P. Thomas, *Journal of Breath Research*, **2011**, *5*, 046006.
12. V. Bocos-Bintintan, A. Smolenschi, I.A. Ratiu, *Studia UBB Chemia*, **2016***,* LXI, 203.
13. G.B. Ghira, I.A. Ratiu, V. Bocoş-Binţinţan, *Environmental Engineering and Management Journal,* **2013**, *12 (2),* 251.
14. V. Moll, V. Bocoş-Binţinţan, I.A. Ratiu, D. Ruszkiewicz, C.L.P. Thomas, *Analyst*, **2012**, 137(6), 1458
15. J.L. Narayana, J. Gopal, H.F. Wu, *Analyst*, **2012**, 137, 3372.
16. R.S.M. Thorn, d.m. Reynold, J. Greenman, *Journal of Microbiological Methods*, **2011**, *84*, 258.
17. G. Preti, E. Thaler, C.W. Hanson, M. Troy, J. Eades, A.J. Gelperin, *Journal of Chromatography* B, **2009**, *877*, 2011.
18. A.b. DeMilo, C.J. Lee, D.S. Moreno, A.J. Martinez, *Journal of Agricultural and Food Chemistry*, **1996**, *44*, 607.
19. E. Tait, J.D. Perry, S.P. Stanforth, J.R. Dean, *Trends in Analitical Chemistry,* **2014**, *53*, 117.
20. R.a. Quinn, K. Whiteson, Y.W. Lim, J. Zhao, D. Conrad, J.J.L. Puma, F. Rohwer, S. Widder. *Biofilms Microbiomes,* **2017**, *2*, 11.
21. S. Sethi, R. Nanda, T. Chakraborty, *Clinical Microbiology Review*, **2013**, *26*, 462.
22. S. Paczkowski, S. Schütz, *Applied Microbiology & Biotechnology*, **2011**, *91,* 917.

STUDIA UBB CHEMIA, LXIV, 2,Tom I, 2019 (p. 217-229)
(RECOMMENDED CITATION)
DOI:10.24193/subbchem.2019.2.18

Dedicated to Professor Florin Dan Irimie on the Occasion of His 65th Anniversary

IN VITRO – IN VIVO CORRELATION FOR GLICLAZIDE 60 MG MODIFIED RELEASE TABLETS

DIANA IOANA POP[a,b], ADRIANA MARCOVICI[b], MONICA OROIAN[a,b], ANA-MARIA GHELDIU[c*], LAURIAN VLASE[a]

ABSTRACT. The objective of the study was to determine *in vitro – in vivo* correlations for Gliclazide 60 mg modified release tablets developed by Ranbaxy Laboratories Limited, now Sun Pharmaceutical Industries Limited, India, based on the data obtained in two bioequivalence clinical trials and in *in vitro* dissolution tests. Each clinical trial was designed as an open-label, randomized, single-dose, crossover study that consisted of two periods. The first bioequivalence study was performed under the fasting state of the subjects, while the second bioequivalence study was carried out under the fed state of the subjects. During each study period, venous blood samples were taken pre-dose and post-dose up to 96 hours. Afterwards, individual plasma profiles were obtained and mathematical deconvolution was applied to obtain the relative fraction absorbed of gliclazide. These data were correlated with the *in vitro* dissolution data obtained after performing dissolution tests in three different dissolution media, at pH 4.5, 6.8 and 7.2, with Gliclazide 60 mg modified release tablets (EvoluPharm, France). All calculation were performed by Phoenix WinNonlin® version 6.3. For each *in vivo* data set from the bioequivalence studies (under fasting and fed conditions), three level A *in vitro-in vivo* correlations were obtained for Gliclazide 60 mg modified release tablets, for *in vitro* tests performed at pH 4.5, 6.8, and 7.2. Good correlation coefficients were found for each established correlation (R2=0.98-0.99). In

[a] *University of Medicine and Pharmacy 'Iuliu Hatieganu', Faculty of Pharmacy, Department of Pharmaceutical Technology and Biopharmaceutics, 8 Victor Babes str., RO-400012, Cluj-Napoca, Romania*

[b] *Terapia SA – a Sun Pharma Company, Department of Clinical Pharmacology and Pharmacokinetics, 124 Fabricii str., RO-400632, Cluj-Napoca, Romania*

[c] *University of Medicine and Pharmacy 'Iuliu Hatieganu', Faculty of Pharmacy, Department of Pharmaceutical Botany, 23 Marinescu str., RO-400337, Cluj-Napoca, Romania*

** Corresponding author: anamaria.gheldiu@yahoo.com*

conclusion, six level A *in vitro-in vivo* correlations were obtained for Gliclazide 60 mg modified release tablets manufactured by Ranbaxy Laboratories Limited, now Sun Pharmaceutical Industries Limited, India.

Keywords: *gliclazide, in vitro-in vivo correlations, clinical trial, healthy Caucasian subjects*

INTRODUCTION

The oral absorption, and therefore the bioavailability of a drug, is determined by the extent of drug aqueous solubility and permeability along the gastro-intestinal tract. The Biopharmaceutical Classification System (BCS) is the guiding tool used for the prediction of a drug's *in vivo* performance and development of drug delivery system that suits this performance [1]. It consists of four classes, which categorizes the drug substances based on the previously mentioned properties as it follows: class I – high solubility and high permeability, class II – low solubility and high permeability, class III – high solubility and low permeability, class IV – low solubility and low permeability [1]. Because of its application in early drug development and afterwards in the management of product post-approval changes, the interest in this BCS is high [2].

Bioequivalent drug products are pharmaceutical equivalents or pharmaceutical alternatives whose rate and extent of absorption are comparable, without statistically significant differences, when administered at the same molar dose of the therapeutic moiety under similar experimental conditions, either single dose or multiple dose [3]. Bioequivalence clinical studies conducted on healthy volunteers are requested for pharmaceutically equivalent drugs (generics), but which may be different in terms of the nature and quantity of excipients and manufacturing process [4]. In the last years, different approaches were developed to reduce the need for *in vivo* bioequivalence studies, considering that the costs for such trials are high [4,5]. Regulatory authorities adopted several guidelines on biowaivers that could be accepted by application of the BCS based scheme or by establishing an *in vitro-in vivo* correlation (IVIVC) [4,6,7,8]. A biowaiver represents the permission given by the regulatory authorities to use dissolution test as a surrogate of pharmacokinetic data obtained in bioequivalence studies, in cases when scale-up and post-approval (SUPAC) related changes occur.

An *in vitro-in vivo* correlation (IVIVC) was defined by the U.S. Food and Drug Administration (FDA) as "a predictive mathematical model describing the relationship between an *in-vitro* property of a dosage form and an *in-vivo* response" [7]. In addition, IVIVCs are also defined in the United States Pharmacopoeia (USP) [16]. *In vitro* property refers to dissolution rate, dissolution profile, mean dissolution time (MDT), and percent dissolved at a

certain time point ($t_{x\%}$) [3]. *In vivo* response is the plasma drug profile, the amount absorbed at a certain time (Q_{abs}), the mean absorption time (MAT), or other pharmacokinetic (PK) parameters such as peak plasma concentration (C_{max}) or observed area under the plasma concentration versus time curve (AUC_{0-t}) [3]. Currently, four distinct IVIVC levels were established: level A, level B, level C and multiple level C. Level A is a point to point correlation between *in vitro* dissolution and *in vivo* absorption rate of a drug from the dosage form [3,7,16]. Level A IVIVC is of highest regulatory value as its purpose is to define a direct relationship such that measurement of *in vitro* dissolution rate is a surrogate for *in vivo* performance. Hence, this level of IVIVC is an excellent quality control procedure since it is predictive of the dosage forms *in vivo* performance and can be used to apply for a biowaiver [3]. Usually, biowaiver is not possible for level B, C and multiple C [3,4,7,9].

Currently, the IVIVC based biowaiver is recommended by regulatory authorities for modified release dosage forms with extended release and recently it was suggested that this type of waiver could be also applied to Class II BCS drugs, as long as the dissolution process is complete during the gastro-intestinal (GI) passage [4,6,7,8,10]. In case of BCS class II drugs, an IVIVC is expected if *in vitro* dissolution rate is similar to *in vivo* dissolution rate, which is correlated with *in vivo* absorption rate [1].

Gliclazide (see Figure 1) is an oral hypoglycemic agent for the treatment of type 2 diabetes mellitus (T2DM), which belongs to BCS Class II. It presents high permeability and an intermediate solubility, as it is an ampholyte which solubility is pH-dependent in the GI pH range. After oral administration, it was reported that gliclazide displays a non-solubility-limited absorption. The absorption rate and the onset of action is delayed after oral administration [6,11,12,13]. Gliclazide has a wide therapeutic index and displays linear profile for doses up to 120 mg [19,20]. Although its pre-systemic metabolism has not been thoroughly studied, the low plasma clearance of 13 mL/min (0.78 L/h) suggests this elimination pathway is not significant [18]. Considering the pharmacological and pharmaceutical profile, gliclazide is eligible for assessment of level A IVIVC.

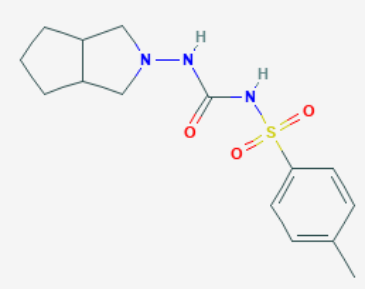

Figure 1. Chemical structure of gliclazide (IUPAC name: 1-(3,3a,4,5,6,6a-hexahydro-1H-cyclopenta[c]pyrrol-2-yl)-3-(4-methylphenyl)sulfonylurea) [22]

For establishing level A IVIVC, the most common process is to develop formulations with different release rates (slow, medium and fast) and then to obtain for these formulation *in vitro* dissolution profiles and *in vivo* plasma concentration profiles [7]. Afterwards, an appropriate deconvolution method is applied to each formulation in order to estimate the *in vivo* absorption [7]. The purpose of developing such an IVIVC is to prove that *in vitro* dissolution characteristics are predictable for *in vivo* performance of a drug product and are maintained over a range of *in vitro* dissolution release rates, used to define the IVIVC relationship and manufacturing changes [7].

The aim of this study was to evaluate the possibility of establishing level A IVIVC for gliclazide 60 mg modified release tablets from *in vitro* studies at different pH (4.5, 6.8 and 7.2) with *in vivo* bioequivalence studies, under fasting and fed conditions of subjects. The current research is a preliminary study whose objective was not to develop an industrial IVIVC, but to support additional studies to this purpose. Therefore, the *in vitro* studies were performed for a single modified release formulation of gliclazide.

RESULTS AND DISCUSSION

In vivo data

The *in vivo* data that were used for determination of IVIVC for gliclazide were obtained by mathematical deconvolution. This approach considers the available output function, the mean plasma concentrations, for determining the input function, the absorption results of gliclazide. Thus, the relative fraction absorbed of gliclazide from the site of administration over time was obtained and is depicted in Figure 2. The data of the bioequivalence studies were previously reported [11,14,15].

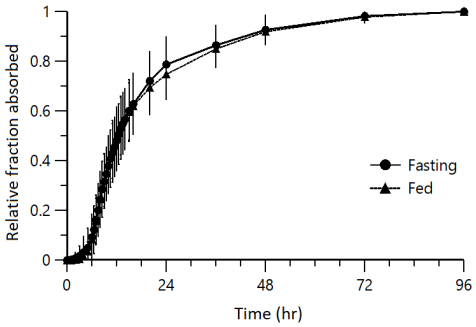

Figure 2. The relative fraction absorbed of gliclazide (60 mg, p.o.) in the systemic circulation from the site of administration over time in subjects under fasting (n=41) or fed conditions (n=23) [11]

In vitro studies

By using the methodology and sample preparation described in the experimental section, the percent of dissolved gliclazide from the 60 mg modified release generic tablets were obtained, in three distinct dissolution media. The first *in vitro* test was performed in pH 4.5 sodium acetate buffer, the second test was carried out in pH 6.8 phosphate buffer and the third *in vitro* dissolution test was realized in pH 7.2 phosphate buffer. The results are summarized in Table 1. The *in vitro* release profiles over 24 hours of gliclazide 60 mg generic modified release tablets in three different dissolution media are depicted in Figure 3. Data are shown as mean ± standard deviation (n=6).

Table 1. *In vitro* dissolution profiles of 60 mg generic gliclazide modified release tablets in three different dissolution media (pH 4.5, 6.8 and 7.2)

Time (hr)	% Drug release								
	pH 4.5			pH 6.8			pH 7.2		
	Mean[1]	SD[2]	CV%[3]	Mean[1]	SD[2]	CV%[3]	Mean[1]	SD[2]	CV%[3]
0.5	0.8	1.3	173.2	1.8	0.2	12.9	2.6	0.5	18.1
1	3.9	0.5	13.9	4.8	1.4	29.4	5.3	0.1	2.6
1.5	6.7	3.1	46.3	5.6	0.2	3.2	8.2	0.9	11.1
2	9.5	3.3	34.2	8.6	1.6	18.4	11.2	1.5	13.6
2.5	14.6	0.9	6.3	10.9	1.8	17.0	13.5	0.7	5.3
3	18.2	1.2	6.4	13.8	1.2	8.7	16.8	0.8	4.8
3.5	19.7	2.0	10.3	15.4	1.6	10.2	19.2	0.5	2.5
4	22.7	2.8	12.2	18.1	1.7	9.3	21.8	1.7	7.8
5	26.3	4.6	17.5	22.8	2.9	12.7	27.2	3.3	12.2
6	30.5	2.5	8.2	28.6	2.2	7.6	33.6	1.3	3.7
7	35.5	1.5	4.3	33.7	2.6	7.7	37.8	2.8	7.3
8	41.9	1.3	3.2	38.3	3.0	7.9	42.8	2.6	6.1
9	45.9	0.6	1.4	43.9	2.4	5.4	50.2	3.8	7.5
10	49.7	2.1	4.2	49.6	4.8	9.6	54.3	3.4	6.2
12	55.7	1.4	2.6	59.2	4.4	7.3	64.7	5.1	7.9
14	60.4	2.0	3.3	67.4	4.0	5.9	73.7	5.8	7.9
16	63.4	0.3	0.4	76.2	3.1	4.0	80.5	5.8	7.2
24	69.3	3.7	5.3	94.2	2.5	2.6	94.1	3.2	3.4

[1]Data are shown as mean of n=6; [2]SD – standard deviation; [3]CV% - coefficient of variation

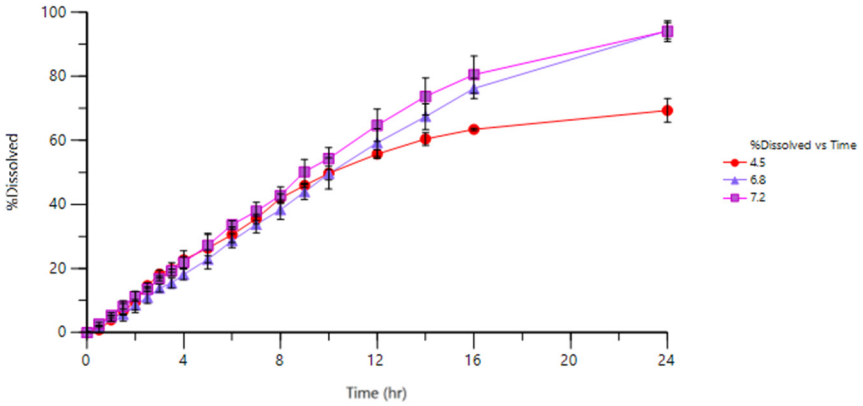

Figure 3. The 24 hours in vitro release profiles of Gliclazide 60 mg generic modified release tablets in various dissolution media with different pH (data are shown as mean ± SD, n=6)

In vitro – in vivo correlation

The *in vitro–in vivo* correlations (IVIVCs) were evaluated for level A correlation. Hence, the absorption profiles of Gliclazide 60 mg modified release tablets manufactured by Ranbaxy Laboratories Limited, now Sun Pharmaceutical Industries Limited, India, were obtained from the individual plasma drug concentration versus time profiles from the bioequivalence trials [11,14,15]. The absorption profiles were determined for both clinical trials performed under fasting or fed conditions. Therefore, the percent of *in vivo* absorbed gliclazide was correlated with the *in vitro* dissolved percent. Figures 4 and 5 illustrate the IVIVCs without time scaling, while figures 6 and 7 depict the IVIVCs that took into consideration a time scaling factor, which was the observed lag time in the *in vivo* data, in order to obtain a meaningful IVIVC. The obtained slopes, intercepts, and correlation coefficients of the regression lines for IVIVCs are shown in Table 2.

Table 2. Results of the *in vitro-in vivo* correlation (IVIVC) of Gliclazide 60 mg modified release tablets and the statistical evaluation of the obtained IVIVC for the fasting and fed clinical trials (deconvolution approach)

Clinical trial type						
Dissolution media pH	**Fasting**			**Fed**		
	Slope	**Intercept**	**Correlation**	**Slope**	**Intercept**	**Correlation**
4.5	0.855	4.781	0.990	0.826	1.327	0.994
6.8	0.927	1.720	0.993	0.884	-1.614	0.984
7.2	1.002	3.329	0.993	0.959	-0.401	0.988

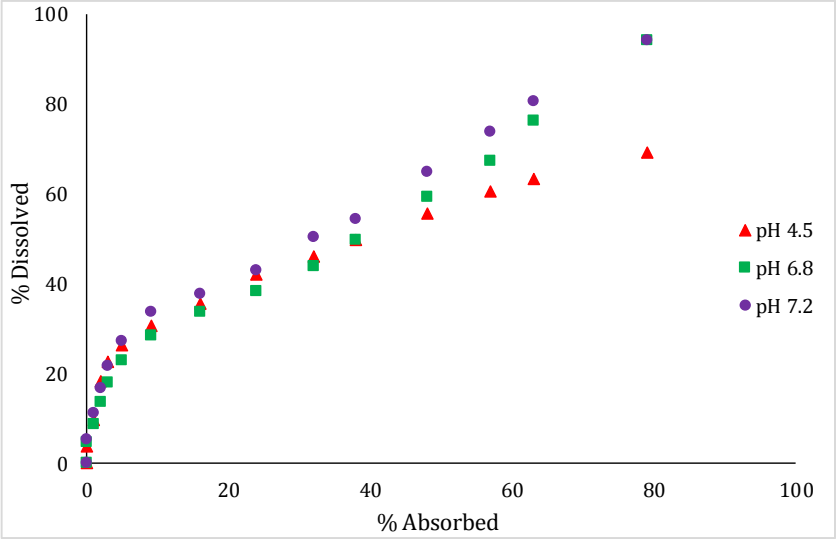

Figure 4. *In vitro – in vivo* correlation plot for Gliclazide 60 mg modified release tablets (deconvolution approach) at various pH of the dissolution media of *in vitro* tests (no time scaling factor), under the fasting state of the *in vivo* clinical trial

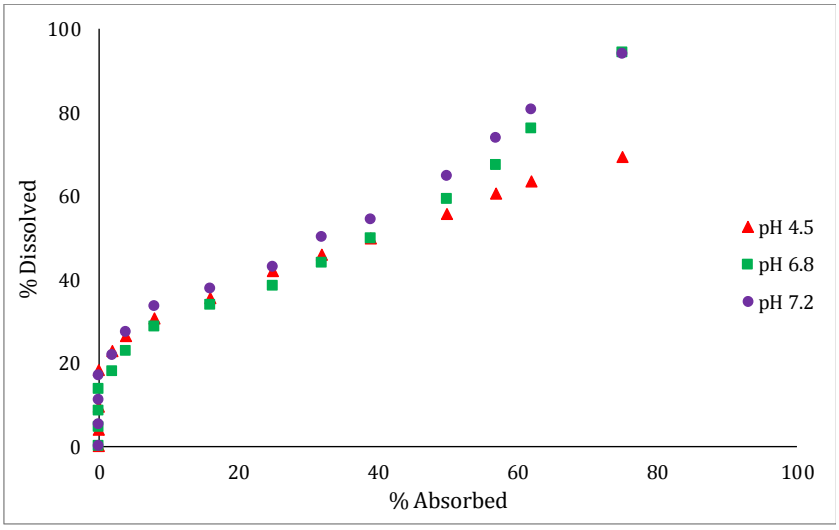

Figure 5. *In vitro – in vivo* correlation plot for Gliclazide 60 mg modified release tablets (deconvolution approach) at various pH of the dissolution media of *in vitro* tests (no time scaling factor), under the fed state of the *in vivo* clinical trial

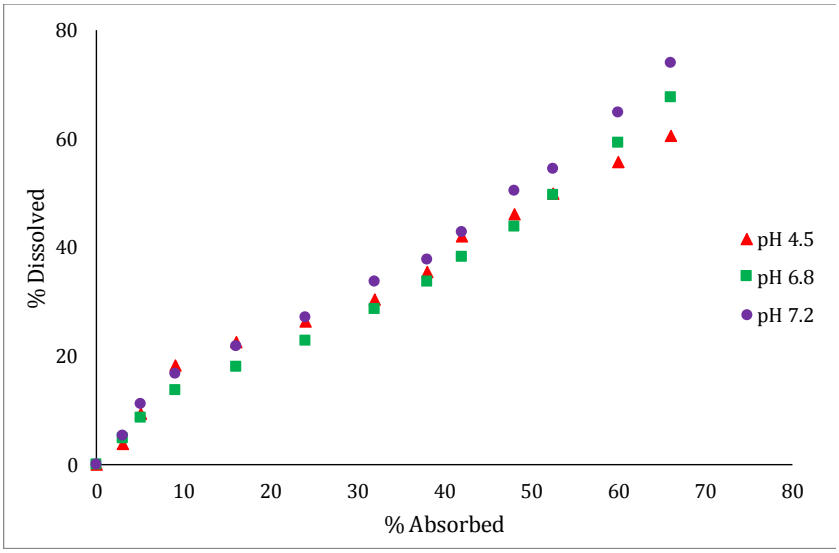

Figure 6. *In vitro – in vivo* correlation plot for Gliclazide 60 mg modified release tablets (deconvolution approach) at various pH of the dissolution media of *in vitro* tests (with time scaling factor), for the fasting state of the subjects of the *in vivo* clinical trial

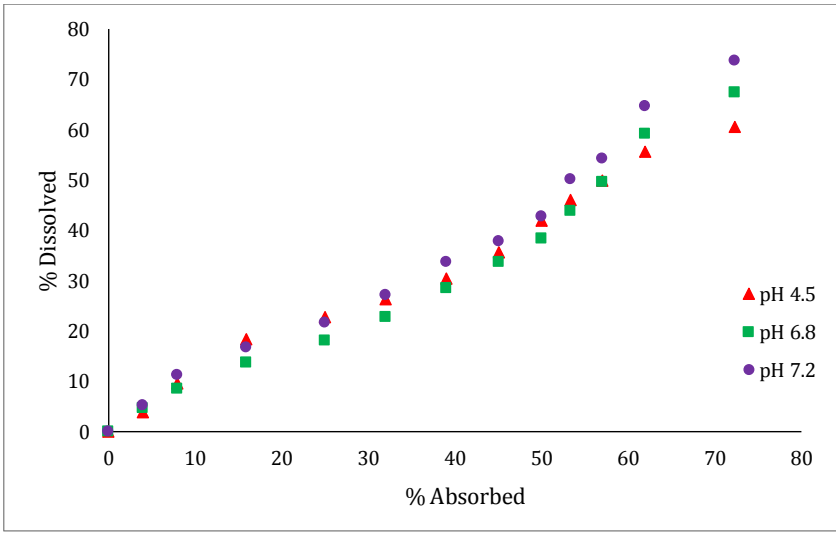

Figure 7. *In vitro – in vivo* correlation plot for Gliclazide 60 mg modified release tablets (deconvolution approach) at various pH of the dissolution media of *in vitro* tests (with time scaling factor), for the fed state of the subjects of the *in vivo* clinical trial

In order to establish an IVIVC, the factor controlling the appearance of the active pharmaceutical ingredient (API) in the blood stream should be linked with the formulation or characteristics of the API. In this case, any physiological factor should not be a limiting factor for drug absorption. Thus, IVIVC are probable in practice for API belonging to BCS class II (low solubility, high permeability) in drug dosage forms with slow release [18]. The newly developed generic tablet of gliclazide 60 mg was designed as a modified release (MR) formulation for which the tablet's hydration leads to formation of a gel layer through which the API is slowly released in time [11,14,15]. Hence, the drug dosage type controls the absorption of gliclazide and its low solubility is not a rate-limiting step for absorption. Gliclazide MR was shown to have predictable and reproducible release of the API and effective plasma concentrations over a 24 hours' period taken as a single daily dose (30 -120 mg), thus assuring a hypoglycemic effect for a longer time-period [14,15,19,20].

In order to produce a meaningful IVIVC for gliclazide, it was assumed that the *in vivo* profile and the *in vitro* profile should not be different in their morphology (shape). In the case of MR tablets, the *in vitro* dissolution profiles of gliclazide ran ahead the *in vivo* profiles, which were obtained by using the mathematical deconvolution approach. This was probably due to slow release of the API, additionally to the biphasic gastric emptying. Another possible explanation would be the absorption of gliclazide from two distinct sites within the upper gastrointestinal tract [11]. The time-lapse between the administration of the drug and the start of the absorption process is highlighted by the lag time, which is approximately 3 hours and can be observed in figures 3 and 4. Thus, the rescaling of the time by considering a time scaling factor of 3 hrs was necessary, this being the latency time observed for *in vivo* absorption in both clinical trials [14,15,17]. Afterwards, the IVIVCs were established by taking into account the *in vitro* data that corresponded to the *in vivo* data after rescaling the time axis (time-adjustment), for the dissolution tests performed under different pH conditions.

The *in vitro* dissolution profile for the test performed at pH 4.5 revealed a lower release of the drug from the pharmaceutical formulation or instability of gliclazide at acidic pH. [21]. However, for this *in vitro* profile the IVIVC, a good correlation coefficient was observed, as illustrated by the statistical parameters in Table 2. For the *in vitro* dissolution profiles obtained by working at pH of 4.5, 6.8 and 7.2, a linear correlation was found with the absorption *in vivo* data. Hence, six level A IVIVCs were established for these conditions and they are given in figures 5 and 6. Three level A IVIVCs were established for the *in vivo* clinical trial performed under fasting condition, while 3 level A IVIVCs were determined for the *in vivo* clinical trial carried out under the fed condition.

Even though the established correlations were not meant to be scaled-up at industrial level, the preliminary results of this study are promising and could be a good predictor of a possible IVIVC to be further developed in order to apply for a biowaiver. Thus, the costs of the manufacturing company for additional studies consecutive to post-approval changes would be lower as the drug product could benefit from a biowaiver given by the regulatory authorities on the basis of a level A IVIVC.

CONCLUSIONS

Six level A IVIVCs were established for gliclazide 60 mg modified release tablets. The in vivo studies were two bioequivalence studies for newly developed gliclazide 60 mg modified release tablet, under fasting and fed conditions. The in vitro studies were carried out in three different dissolution media, at pH 4.5, 6.8 and 7.2. The calculated point-to-point IVIVCs (R^2>0.98) could be further used for developing IVIVCs at industrial level which are useful from a regulatory point of view. The knowledge of the BCS class of a drug substance is essential for biowaivers, thus reducing the costs in terms of both time and money. Gliclazide belongs to class II of the BCS, characterized by low solubility and high permeability, thus level A IVIVCs were possible to establish with the in vivo data from the clinical trial of the new generic Gliclazide 60 mg modified release formulation, developed by Ranbaxy Laboratories Limited, now Sun Pharmaceutical Industries Limited, India.

EXPERIMENTAL SECTION

In vivo data

The clinical study data (plasma concentration versus time profile) were obtained from two bioequivalence trials that took place at the Clinical Unit of Clinical Pharmacology and Pharmacokinetics Department of Terapia S.A. The study protocols were approved by the Ethics Committee of the University of Medicine and Pharmacy “Iuliu Hatieganu”, from Cluj-Napoca (Romania) and by the National Agency for Medicines and Medical Devices, Romania. The first study took place under the fasting state and the second clinical trial was carried out under the fed state [14,15]. The clinical trials were conducted in accordance with all applicable regulatory requirements. These data were further used for *in vitro-in vivo* correlation purpose.

In vitro studies

Dissolution studies were performed on 60 mg generic gliclazide modified release tablets (EvoluPharm, France). The dissolution test was carried out in a rotating paddle apparatus (USP apparatus II) (Pharma Test, type PT WS100S, serial number 20208, D-63512 Hainburg, Germany) at 37±0.5°C and rotational speed of 50 rpm, using 900 ml of various dissolution media (media pH 4.5, 6.8 and 7.2).

The dissolution media were prepared as it follows:

• pH 4.5 sodium acetate buffer – 2.99 g of sodium acetate ($NaC_2H_3O_2*3H_2O$) were weighted and transferred in a volumetric flask of 1000 ml, 14 ml of 2N acetic acid (CH_3COOH) were added and then distilled water was used to made up to volume.

• pH 6.8 phosphate buffer – 250 ml of 0.2M monobasic potassium phosphate solution were transferred in a volumetric flask of 1000 ml, along with 112 ml of 0.2M NaOH and then distilled water was added to the volume.

• pH 7.4 phosphate buffer – 250 ml of 0.2M monobasic potassium phosphate solution were transferred in a 1000 ml volumetric flask, then 195.5 ml of 0.2M NaOH were added and made up to specified volume with distilled water.

All the reagents used for the preparation of the dissolution media buffer were of United States Pharmacopoeia (USP) reagents grade.

The samples (100 µl each) were taken before the release of the tablets in the dissolution media (time 0) and after, at the following times: 1, 2, 3, 4, 5, 6, 7, 8, 9, 10, 12, 14, 16, 24 hours. Withdrawn samples were filtered and assayed for gliclazide content by means of a validated HPLC UV bioanalytical method with detection at 225 nm.

In vitro – in vivo correlation

In order to analyze the level of correlation, the numerical deconvolution method was used. In this approach, the absorption profile was obtained, based on the *in vivo* data from the clinical trials conducted under fasting and fed state of the subjects. Afterwards, the percent of drug absorbed *in vivo* was plotted against the dissolved percent in *in vitro* test [11]. Taking into account the time discrepancies between the *in vivo* absorption profiles and the *in vitro* release profiles for Gliclazide 60 mg modified release tablets, a time scaling factor was considered for the determination of an IVIVC.

ACKNOWLEDGMENTS

Financial disclosures: Ana-Maria Gheldiu and Laurian Vlase are full-time employees of the University of Medicine and Pharmacy "Iuliu Hatieganu", Cluj-Napoca, Romania.

Conflicts of interest: Diana Pop, Adriana Marcovici, Monica Oroian were employees of the Ranbaxy Laboratories Limited, now Sun Pharmaceutical Industries, India, during the conduct of this study.

REFERENCES

1. G.L. Amidon, H. Lennernas, V.P. Shah, J.R. Crison, *Pharmaceutical Research*, **1995**, *12(3)*, 413.
2. B.M. Davit, I. Kanfer, Y.C. Tsang, J.M. Cardot, *The AAPS Journal*, **2016**, *18(3)*, 612.
3. L. Shargel, A.B.C. Yu, "Applied biopharmaceutics and pharmacokinetics, 7th edition", McGraw-Hill Education, Inc., Maryland, 2016, chapter 15**.**
4. International Council for Harmonization of technical; requirements for pharmaceuticals for human use. Biopharmaceutics classification system-based biowaivers. 2018. Available at: https://www.ich.org/fileadmin/Public_Web_Site/ICH_Products/Guidelines/Multidisciplinary/M9/M9EWG_DraftGuideline_Step2_2018_0606.pdf. Accessed January 10, 2019.
5. J.E. Polli, *The AAPS Journal*, **2008**, *10(2)*, 289.
6. S. Grbic, J. Parojcic, S. Ibric, Z. Djuric, *AAPS PharmSciTech*, **2011**, *12(1)*, 165.
7. U.S. Department of Health and Human Services, Food and Drug Administration, Center for Drug Evaluation and Research. Guidance for Industry. Extended Release Oral Dosage Forms: Development, Evaluation, and Application of *In Vitro/In Vivo* Correlations. 1997. Available at: https://www.fda.gov/downloads/drugs/guidances/ucm070239.pdf. Accessed January 10, 2019.
8. U.S. Department of Health and Human Services, Food and Drug Administration, Center for Drug Evaluation and Research. Guidance for Industry. SUPAC-MR: Modified Release Solid Oral Dosage Forms. 1997. Available at: https://www.fda.gov/downloads/Drugs/Guidances/ ucm070640.pdf. Accessed January 10, 2019.
9. U.S. Department of Health and Human Services, Food and Drug Administration, Center for Drug Evaluation and Research. Guidance for Industry. Waiver of *In Vivo* Bioavailability and Bioequivalence Studies for Immediate-Release Solid Oral Dosage Forms Based on a Biopharmaceutics Classification System. 2017. Available at: https://www.fda.gov/downloads/ Drugs/Guidances/ucm070246.pdf. Accessed January 10, 2019.

10. L.X. Yu, G.L. Amidon, J.E. Polli et al., *Pharmaceutical Research*, **2002**, *19(7)*, 921.
11. D.I. Pop, A.M. Gheldiu, M. Oroian, A. Marcovici, S. Bhardwaj, A. Khuroo, R. Kochhar, L. Vlase, *Acta Medica Marisiensis*, **2018**, *64(4)*, 161.
12. M.B.V. Priya, T.E.G.K. Murthy, *Dissolution Technologies*, **May 2012**, 38.
13. K.K.S. Skripnik, M.K. Riekes, B.R. Pezzini, S.G. Cardoso, H.K. Stulzer, *AAPS PharmSciTech*, **2017**, *18(5)*, 1785.
14. D.I. Pop, M. Oroian, S. Bhardwaj, A. Marcovici, A. Khuroo, R. Kochhar, L. Vlase, *Clinical Pharmacology in Drug Development*, **2019**, *8(1)*, 16.
15. D.I. Pop, M. Oroian, S. Bhardwaj, A. Marcovici, A. Khuroo, R. Kochhar, L. Vlase, *Farmacia*, **2018**, *66(4)*, 597.
16. The United States Pharmacopeia, 23rd edition. "In Vitro and In Vivo Evaluation of Dosage form < 1088>". Rockville, Maryland, 1995, 1824.
17. J.M. Cardot, B.M. Davit, *The AAPS Journal*, **2012**, *14(3)*, 491.
18. A. Sarkar, A. Tiwari, P.S. Bhasin, M. Mitra, *Journal of Applied Pharmaceutical Science*, **2011**, *01(09)*, 11.
19. Summary of product characteristics Gliclazida® Terapia 60 mg. Available at: https://www.anm.ro/_/_RCP/RCP_8149_30.09.15.pdf. Accessed January 10, 2019.
20. Product information Diamicron® MR 30 mg. Available at https://www.medicines.org.uk/emc/product/1321/smpc. Accessed January 10, 2019.
21. A Gumieniczek, A Berecka, R Pietras, M Slebioda, *Cent Eur J Chem,* **2014**, 12(1), 80.
22. Chemical structure of gliclazide, available at: https://pubchem.ncbi.nlm.nih.gov/compound/gliclazide#section=2D-Structure. Accessed on the 22nd of May 2019.

STUDIA UBB CHEMIA, LXIV, 2,Tom I, 2019 (p. 231-242)
(RECOMMENDED CITATION)
DOI:10.24193/subbchem.2019.2.19

Dedicated to Professor Florin Dan Irimie on the Occasion of His 65th Anniversary

HPLC-UV METHOD APPROACH FOR THE ANALYSIS AND IMPURITY PROFILING OF CAPTOPRIL

ANCA GABRIELA CÂRJE[a], ALINA BALINT[a*], VALENTIN ION[a], ANCA LUCIA POP[b,c], DANIELA-LUCIA MUNTEAN[a], RALUCA SABĂU[a], SILVIA IMRE[a]

ABSTRACT. The aim of the study was to propose an improved HPLC/UV method for captopril impurity profiling based on forced degradation studies. Material and methods: the HPLC-UV analyses were performed on a Luna C18 column at 50 ^{0}C by using a mobile phase consisting of phosphoric acid 15 mM and acetonitrile at 210 nm. Results and discussions: an HPLC method with superior characteristics to one described in the European Pharmacopoeia for captopril impurities profiling was proposed. The main degradation product of captopril was captopril disulfide (Impurity A), the concentration of which increases in all the conditions of forced degradation, except thermal degradation. UV light has led to the highest number of unknown impurities, but the oxidative degradation presented the highest rate of degradation (>88%). A total of 15 unknown impurities have been observed with significant area (>0.50%), who were not initially present in the captopril sample. Conclusions: The proposed HPLC method can be successfully applied in pharmaceutical analysis laboratories as a stability indicating method of captopril, allowing the separation of official impurities A, B, C, D and E and those formed under forced degradation conditions.

Keywords*: captopril, impurities, stability indicating method, degradation*

[a] *University of Medicine, Pharmacy, Sciences and Technology from Târgu Mureş, Faculty of Pharmacy, Gheorghe Marinescu street no 38, 540139, Târgu Mureş, Romania*
[b] *AC HELCOR, Dr. Victor Babeş street no 50, Baia Mare, 430092, Maramureş, Romania*
[c] *University of Medicine and Pharmacy „Carol Davila", Faculty of Pharmacy, Traian Vuia Street no 6, 020956, Bucharest, Romania*
**Corresponding author: alina.balint@umfst.ro*

INTRODUCTION

Captopril CPT (Figure 1), the first developed angiotensin-converting enzyme (ACE) inhibitor, is a specific inhibitor of angiotensin I discovered in 1977 and it is frequently used for the treatment of hypertension and some types of congestive heart failure. The antihypertensive effect of captopril is enhanced when it is given in combination with a diuretic or after salt depletion [1]. Biotransformation of captopril may involve both enzymatic and non-enzymatic processes. The biotransformation of CPT is predominantly produced at thiol group level: reversible disulfide bonds are formed with albumin and other proteins; other transformations in blood involve formation of disulfide dimer and mixed disulfides of CPT with L-cysteine and glutathione. Due to its pharmacological relevance, but also due to its frequent use in cardiovascular therapy, a significant number of methods for captopril determination from tablets or different biological samples, including chromatographic methods, are proposed [2-7].

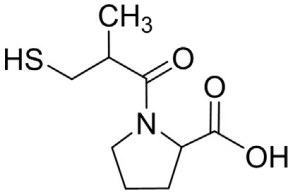

Figure 1. Captopril ((2S)-1-[(2S)-2-Methyl-3-sulfanylpropanoyl]pyrrolidine-2-carboxylic acid).

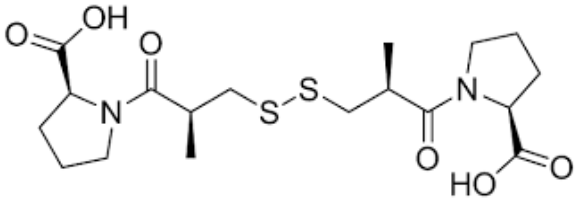

Figure 2. Captopril disulfide (1,1′-[Disulfanediylbis[(2S)-2-methyl-1-oxopropane-3,1- diyl]]bis[(2S)-pyrrolidine-2-carboxylic] acid).

The pharmaceutical impurities may have a significant influence on the effects of a drug or may cause unwanted side-effects, therefore all the possible impurities of an active pharmaceutical ingredient (API) with concentrations above certain value must be detected, identified and quantified [8, 9].

The present study aimed to propose a new HPLC-UV stability indicating method for CPT in the presence of its official impurities and related substances formed under forced degradation conditions: oxidative, acidic/ basic, thermal and natural/UV light exposure, respectively. Due to the presence of the thiol group in the molecular structure of captopril, a very reactive group, a particular attention was done to captopril disulfide formation during the studies (Figure 2) [10]. The analytical performances of the developed method as the linearity, accuracy and precision were determined. Contributions to kinetics of CPT degradation in solution have been made.

RESULTS AND DISCUSSION

A. HPLC stability indication method development and optimization

Firstly, the HPLC method described in the European Pharmacopoeia 9-th Edition for CPT was tested, following the official conditions: column - Luna C18 (Phenomenex) 300x3.9 mm with 10 µm particle size; mobile phase - consisting of 75% phosphoric acid 15 mM and 25% acetonitrile (ACN); flow rate - 1 ml/min [11]. The initial results being unsatisfactory (Figure 3), further tests were performed in order to optimize the method to serve the initial purpose and even to provide better performance characteristics: analysis time as short as possible, higher resolution, symmetrical and narrow peaks.

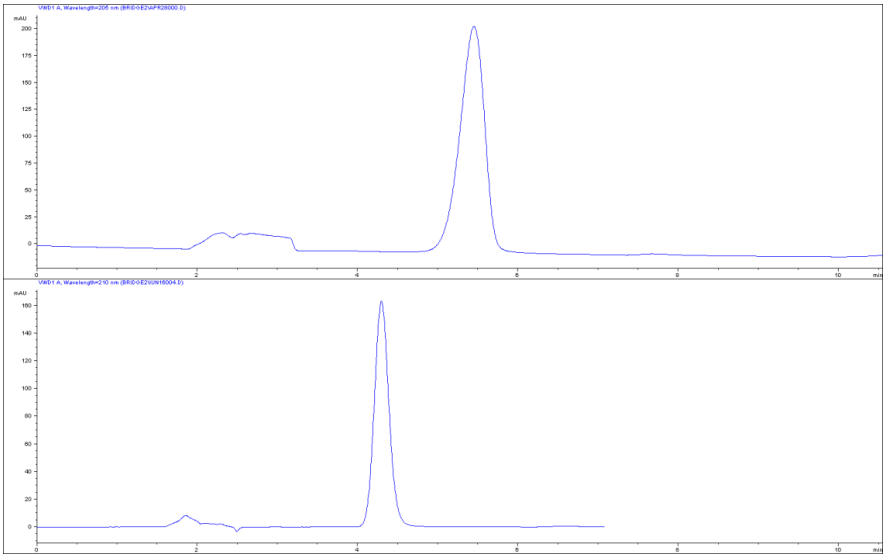

Figure 3. The chromatogram of CPT solution (100 µg/mL). Columns: a) Luna C18, 300 x 3.9 mm, 10 µm (Phenomenex); b) Luna C18 250 X 4.6 mm, 5 µm (Phenomenex). Chromatographic conditions: mobile phase 75% phosphoric acid 15 mM and 25% ACN; flow 1 mL/min; 210 nm; column temperature 50 °C.

Different chromatographic columns were tested and the column Luna C18 250 X 4.6 mm with 5 µm particles, has been shown properties which allowed to attend the goals of the study. For the determination of known chemical-related impurities, identification was made by comparing the retention times determined by individual analysis of each known impurity with the retention times of the peaks in the analyzed samples (control samples and degraded samples). Thus, it was possible to discriminate and identify, as appropriate, the compounds present in the raw material from those formed following the controlled degradation of CPT.

By using a mobile phase consisting of phosphoric acid 15 mM (solvent A) and ACN (solvent B), different isocratic and gradient elution settings were verified due to the fact that the Impurity C has a very similar chromatographic behaviour as Impurity E (Figure 4). Finally, a gradient elution was proposed which solved the interferences between CPT, its known impurities and those formed under forced degradation conditions. The method proposed by us provided the separation of the two impurities with similar chromatographic behaviour (Impurity C and E) with a resolution equal to 1.57.

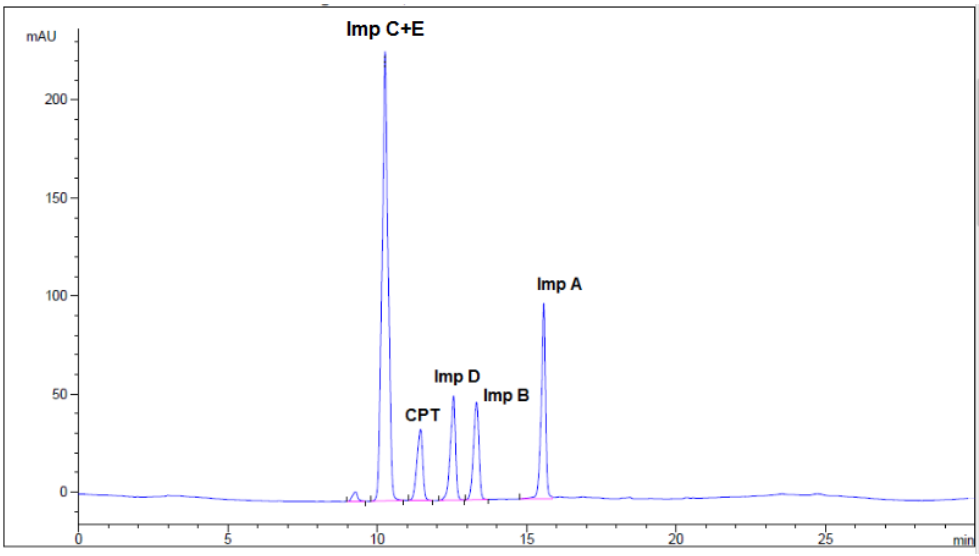

Figure 4. Chromatogram of a mixture of captopril (CPT) and impurities A, B, C, D, E. Chromatographic conditions: column Luna C18 250x4.6 mm, 5 µm, 50°C, gradient elution: 0-1 min: 90%A,10%B; 1-20 min: 90%→50%A, respectively 10%→50%B; flow rate 1.2 ml/min; detection wavelength 210 nm.

Optimal HPLC experimental conditions were established at a column temperature of 50ºC and the aqueous pH modifier component of the mobile phase was phosphoric acid 15 mM. The organic modifier, consisting of ACN, turned to be optimal and the gradient elution was done at a flow rate of 1.2 ml/min. The established chromatographic conditions allowed the separation of all studied impurities of captopril (A, B, C, D and E) in less than 20 minutes. The developed HPLC-UV method allowed the separation of all known impurities of the CPT with good reproducibility of retention times (RSD < 0.5%) and resolution (R>1.5) (Figure 5).

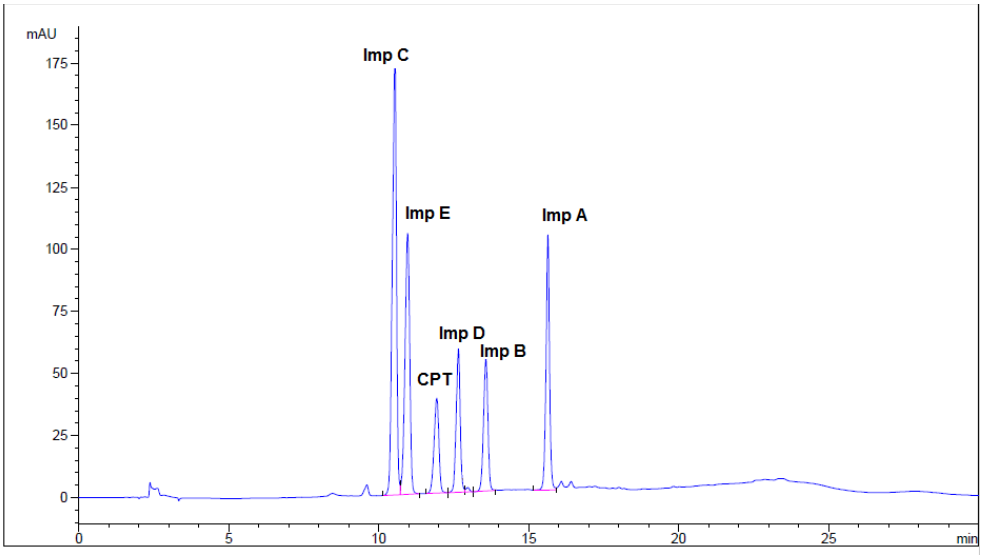

Figure 5. Chromatogram of a mixture of captopril (CPT) and impurities A, B, C, D, E. Chromatographic conditions: column Luna C18 250x4.6 mm, 5 µm; 50°C; gradient elution 0-1 min 95%A-5%B; 1-20 min 95%→50%A; 50%→50%B; flow rate 1.2 ml/min; detection wavelength 210 nm.

B. The analytical performances of the method

The main analytical validation parameters for the developed method were investigated as follows: specificity, linearity, accuracy and precision.

Specificity

Specificity was investigated regarding the interference of any other peak at the retention time of the principal peaks in blank solutions (solvent, extraction samples of the tablets excipients, degradation media). No peaks were detected from blank solutions at the retention time of the known peaks. CPT and its known impurities could be quantified from tablets without any interference from tablet excipients.

Linearity

The linear regression equations (Table 1) were calculated for each impurity and CPT by using six concentration levels and three replicates per concentration level. The linearity range of the each impurity level and CPT has been chosen in order to include the limit of impurities allowed by the European Pharmacopoeia, 9th edition [11].

The linearity domain of CPT was established in the concentration range of 5-50 µg/ml, similar to the main degradation product Impurity A, with the purpose of reporting the areas of possible unknown impurities to the area of CPT. The calibration curves were found to be linear with the correlation coefficient greater than 0.9998 over the ranges of concentrations shown in the table 1.

Table 1. The calibration curves characteristics for the CPT and its known impurities (N=6 levels of concentration, n=3 replicates)

Analyte	Concentration range, µg/ml	The mean equation calibration curve Area = slope (±DSR%) c + intercept	R^2
Impurity A	5.02-50.2	Aria = 29.281x (± 0.675) + 5.8008	0.9999
Impurity B	1.02-10.2	Aria = 56.692x (± 0.695) – 0.6106	>0.9999
Impurity C	0.9-9	Aria = 29.281x(±1.549) + 5.8008	0.9998
Impurity D	5.05-50.5	Aria = 5.377 x(±1.613) - 1.33	0.9989
Impurity E	1-10	Aria = 83.039x(±0.695) - 0.3624	>0.9999
CPT	5.05-50.5	Aria = 40.002x(±0.715) - 4.1780	0.9999

The limit of detection (LOD) and quantification (LOQ) for CPT and its known ipurities was established in terms of peak height to background noise signal ratio. The values obtained for the investigated compounds are found in Table 2.

Table 2. The LOD and LOQ for the CPT and its known impurities

Analyte	LOD (µg/m)	LOQ (µg/m)
Impurity A	0,882	2,648
Impurity B	0,165	0,498
Impurity C	0,345	0,837
Impurity D	0,803	2,413
Impurity E	0,156	0,469
CPT	1,130	3,394

The accuracy and the precision

The accuracy and precision of the method were tested at two concentration levels (QCA and QCB) for each analyte and were expressed as recovery Re% and relative standard deviation (RSD%) of five replicates. As it can be noticed from the data contained in the table 3 the developed HPLC method has a recovery between 98% and 102% and a RSD below 2.0% for all studied analytes, values which are in agreement with pharmacopoeia regulations. For one of the two QC levels of concentration for Impurity D which is the lowest limit of quantification, the accuracy was 95.18% below the lower limit of accuracy. The method was considered proper in terms of accuracy for impurity D taking into consideration the average of the two levels of concentration (98.4%).

Table 3. The intra-series accuracy and the precision of the proposed HPLC method (n=5)

Analyte	QCA				QCB			
	C_T, µ/ml	C_R, µg/ml	Re%	RSD%	C_T, µg/ml	C_R, µg/ml	Re%	RSD%
CPT	25.25	25.15	99.59	0.586	35.35	35.01	99.03	0.165
Imp A	25.10	25.20	100.40	0.579	35.14	35.12	99.94	0.177
Imp B	5.10	5.16	101.09	0.696	7.14	7.15	100.17	0.179
Imp C	4.50	4.58	101.67	0.695	6.30	6.27	99.56	0.197
Imp D	5.00	4.76	95.18*	1.257	7.00	7.11	101.62	1.360
Imp E	5.00	5.05	100.91	0.561	7.00	7.01	100.19	0.154

*below reference lower limit of accuracy

The method was applied for captopril assay from a commercially available product and the recovery was 100.99% with a RSD of 0.21%. The product was in agreement to pharmacopoeia provisions in terms of CPT content.

C. Degradation studies of captopril CPT in solution

Once the optimal conditions have been established and analytical performance were verified, the stability studies of CPT solutions under different stress conditions have been applied. The stability studies of CPT were performed under various pH and temperature conditions, in the presence of strong oxidizing agents, but also under light (natural or UV) exposure to evaluate the potential degradation products and to distinguish it from other types of impurities that may be present in the final product [12].

The amount of remained captopril and the percentage of impurities obtained by degradation were determined by reporting the area obtained after the degradation of captopril under different stress conditions and the peak area obtained by the injection of CPT control (standard solution 0.5 mg/ml). Impurity A, captopril disulfide, was present in all samples subjected to degradation, including in the control sample but in a small concentration, probably formed by the degradation of CPT in the time elapsed between preparation and injection of the solution.

The main degradation product of CPT was captopril disulfide (Impurity A), as it was expected, the concentration of which increased in all the conditions of forced degradation, except thermal degradation [13,14].

Analyzing our results, the amount of captopril degraded in the presence of UV light is 56.04%, which means that more than half of the captopril was degraded within an hour by exposure to the UV lamp. This also explains the presence of 28 other peaks in the sample chromatogram, corresponding to other impurities, besides the main impurity, captopril disulfide. UV light has led to the highest number of unknown impurities for captopril as it can be observed in Figure 6. These unknown impurities have a high hydrophilicity, eluting faster than CPT and the known related impurities. The degradation of CPT under the influence of UV light also leads to formation of related impurities B (2.78 μg/ml), D (5.01 μg/ml) and E (0.97 μg/ml).

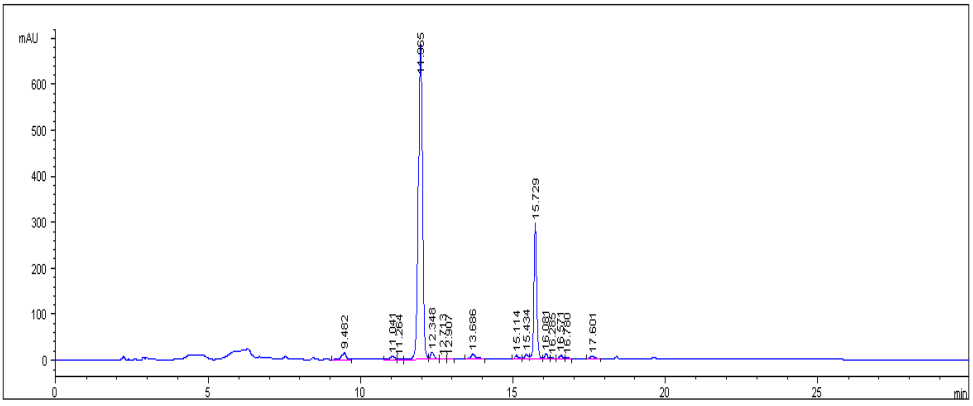

Figure 6. The chromatogram of CPT solution (0.5 mg/ml) after UV degradation.

The highest rate of CPT degradation is due to the presence of the oxidant agent, H_2O_2 3%, with a rate of degradation greater than 88%, the main impurity formed in this case being the captopril disulfide (Impurity A) as it can be seen in the figures 7 and 8.

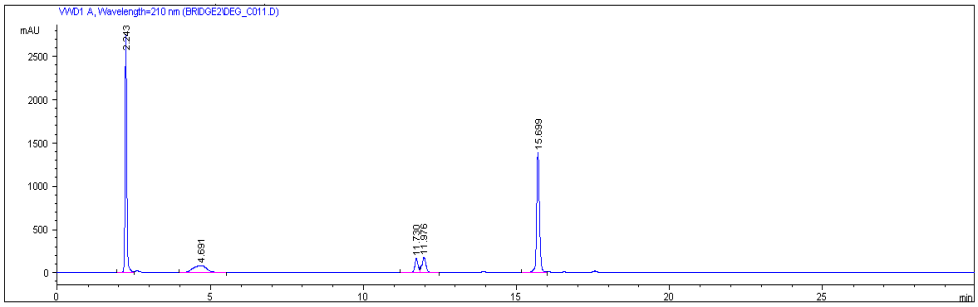

Figure 7. The chromatogram of CPT solution (0.5 mg/ml) after oxidative degradation.

Fifteen unknown impurities have been observed with a significant area (>0.50%) and were not initially present in the analyzed CPT sample.

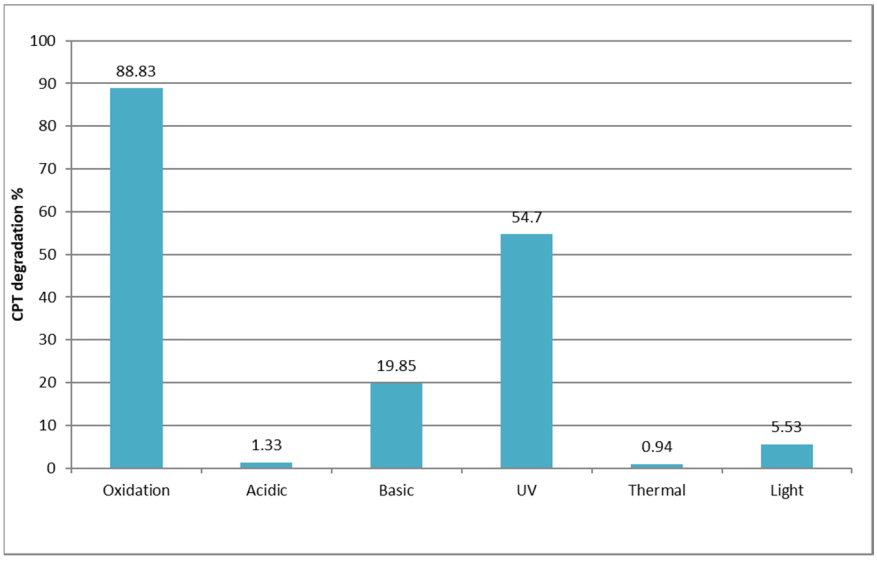

Figure 8. The degradation rate of CPT (%) under different forced degradation conditions.

The study of degradation kinetics under oxidative conditions

The oxidant environment caused the most advanced degradation of all degradation conditions to which the captopril solution was subjected. The analysis of kinetic data has been established a mathematical model of simple zero kinetics in terms of CPT degradation to captopril disulfide (Impurity A) as it can be seen in the figure 9.

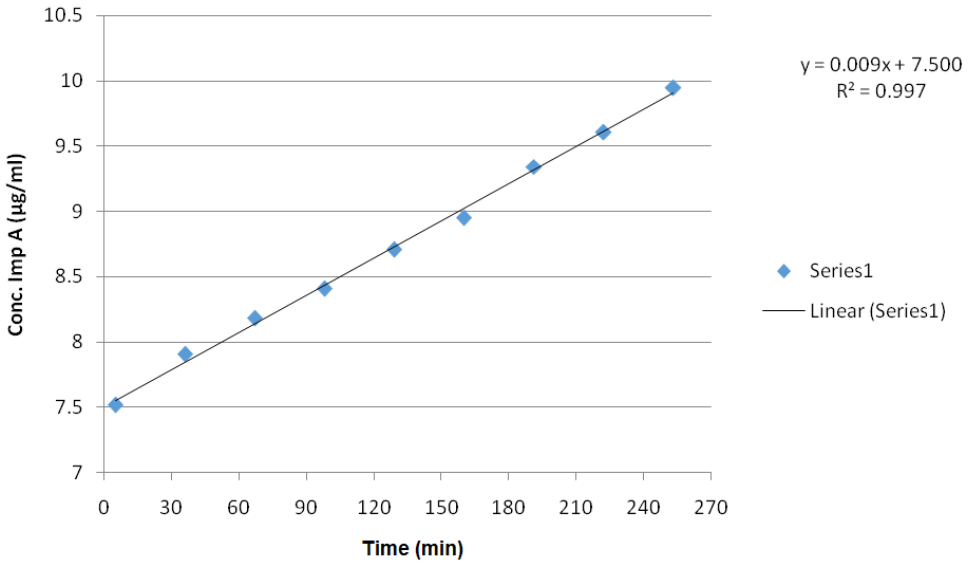

Figure 9. Simulation of zero order kinetics of oxidative degradation of CPT by monitoring the main degradation product captopril disulfide (Impurity A).

CONCLUSIONS

The developed method has superior characteristics in comparison to the official method of European Pharmacopoeia 9-th Edition for captopril related impurities profiling: an analysis time shorter with 15 minutes, very good resolution of the known impurities peaks A, B, C, D and E with excellent resolution and selectivity.

The main impurity formed in all cases of forced degradations, with the exception of thermal degradation, is captopril disulfide (Impurity A). In the presence of an oxidant environment, the CPT exhibits the highest rate of degradation, the main product being impurity A.

A total of 38 unknown impurities were revealed and 15 are present in a significant concentration.

The proposed HPLC method can be successfully applied in pharmaceutical analysis laboratories as a stability indicating method of CPT, allowing the separation of official impurities A, B, D, C and E and those formed under stressful conditions.

EXPERIMENTAL SECTION

The analyses were performed on an Agilent 1100 Series LC system (Agilent Technologies, USA) equipped with a quaternary pump, an autosampler, a thermostated column compartment and a UV-VIS detector. The different types of chromatographic columns have been tested. The optimal separation conditions were obtained on a Luna C18 (2) 250 X 4.6 mm column containing 5 µm size particle (Phenomenex, USA). Overall mobile phase for the LC separation was prepared by mixing different amounts of organic modifier with the variable amounts of aqueous buffer. The mobile phase consisting of phosphoric acid 15 mM and acetonitrile (ACN) (LC Grade, Merck, Germany) was used. Detection was accomplished at 210 nm for captopril (CPT) and its impurities A, B, C, D and E (analytical purity, Sigma Aldrich). Mobile phases and other solutions were submitted to ultrasonication with a ultrasonic bath T700H (Elma Transsonic).

A Direct Q5 (Millipore, France) water purifier dispensing system was used for supplying the purified water and for pH buffer adjustments an InoLab 740 pH-meter (WTW, Germany) was used.

CPT (Sigma Aldrich) and its impurities A 1,1′-[disulfanediylbis[(2S)-2-methyl-1-oxopropane-3,1- diyl]]bis[(2S)-pyrrolidine-2-carboxylic] acid (captopril disulfide, UPS), B (2S)-1-[(2S)-3-bromo-2-methylpropanoyl]pyrrolidine-2-carboxylic acid (EDQM), C (2RS)-2-methyl-3-sulfanylpropanoic acid (EDQM), D (2RS)-3-bromo-2-methylpropanoic acid (EDQM) and E (2S)-1-(2-methylpropanoyl) pyrrolidine-2-carboxylic acid (EDQM) used as reference substances were analytical pure from Sigma Aldrich. All the standard solutions were prepared in methanol (LC Grade, Merck, Germany).

Sample solutions were prepared in methanol due to the low stability of captopril in aqueous solution by weighting an amount corresponding to a concentration of 1 mg/ml CPT for stock solution. The mixture of impurities was similarly processed, the concentrations of solutions for impurities A, B and E being 200 µg/ml, 2 mg/ml for impurity C, and 3 mg/ml for impurity D, respectively. Prior to analysis, the solutions of CPT, impurities and buffer solutions were homogenized and degassed for 10 minutes in the ultrasounds bath. The impurities mixture and captopril stock solution were prepared in methanol and maintained at 15°C during analysis to avoid any possible degradation.

The degradation studies were performed on solutions of CPT 5 mg/ml by subjecting to degradation the same volume of 0.5 ml. The acidic, basic and oxidative stress study consisted of adding 1 mL of the degradative agent (HCl 0.1 N, NaOH 0.1 N and H_2O_2 3%) to the captopril solution sample for 24 hours. The chemical degradation reaction was stopped by adding a suitable neutralizing agent after 24 hours. The thermal degradation consisted of

maintaining the CPT solution for one hour at a temperature of 60 °C. The degradation of CPT under the influence of light was done by maintaining the CPT sample solution for 24 hours at natural light and for 1 hour under the influence of UV light at 254 nm (UV Lamp Vilber Lourmat, 6W with intensity at 710μw/cm^2). After degradation, all the solutions were made up to 5 ml with a mixture of water and ACN 50:50 (v:v).

ACKNOWLEDGMENTS

This work was supported by a grant of the Romanian National Authority for Scientific Research and Innovation, CNCS/CCCDI – UEFISCDI, project number PN-III-P2-2.1-BG-2016-0115, within PNCDI III.

REFERENCES

1. I. Kancirová, M. Jašová, I. Waczulíková, T. Ravingerová, A. Ziegelhöffer, M. Ferko, *Iranian Journal of Basic Medical Science*, **2016**,*19(6)*, 615-623.
2. J. Leanpolchareanchai, J. Suksiriworapong, *Journal of Pharmaceutical Sciences,* **2015**, *42(2),* 85-92.
3. W.M. Mahmoud, K. Kümmerer, *Chemosphere*, **2012**, *88*, 1170–1177.
4. R. Nogueira, W. Wollinger, T.E. Da Silva et al, *Brazilian Journal of Pharmaceutical Sciences*, **2011**, *47(2),* 351-362.
5. S. Imre, S. Vancea, D.L. Muntean, E. Sipos, A. Cociş, V. Avrigeanu, E. Mircia*, Revista Medico-Chirurgicală a Societăţii de Medici şi Naturalişti din Iaşi*, **2008**, *112(3)*, 848-855.
6. N. Rastkari, M. Khoob, A. Shafiee, M.R. Khoshayand, R. Ahmadkhaniha, *Journal of Chromatography B*, **2013**, *932*, 144–151.
7. J.R. Lino e Freitas, F.J Oliveira Quintao, J.C Cardoso da Silva et al, *International Journal of Environmental Analytical Chemistry*, 2017, *1*, 42-55.
8. T. Rawat, I.P. Pandey, *Journal of Pharmaceutical Sciences and Research*, 2015, 7(5), 238-241.
9. M. Blessy, R.D. Patel, P.N. Prajapati, Y.K. Agrawal, *Journal of Pharmaceutical Analysis*, **2014**, 4(3), 159–165.
10. M.R. Pabari, C. McDermott, J. Barlow, Z. Ramtoola, *Clinical Therapeutics*, **2012**, *34*, 2221-2229.
11. ***European Pharmacopoeia 9th edition, **2017**.
12. ICH Expert Working Group – Stability testing of new drug substances and products, ICH Harmonised Tripartite Guideline, **2003**.
13. A. Gindy, M.W. Nassar, K.A. Salam Attia, H.H. Abu-Seada, M. El-Ghandour, *Journal of Liquid Chromatography & Related Technologies*, **2014**, *37*, 696–712.
14. S. Valizadeh, M. Rasekhi, H. Hamishehkar, M. Asadollahi, H. Hamishehka, *Journal of Research Pharmacy Practice*, **2015**, *4(3)*,147–152.

STUDIA UBB CHEMIA, LXIV, 2,Tom I, 2019 (p. 243-254)
(RECOMMENDED CITATION)
DOI:10.24193/subbchem.2019.2.20

Dedicated to Professor Florin Dan Irimie on the Occasion of His 65th Anniversary

MODELING AND PREDICTION OF AMINO ACIDS LIPOPHYLICITY USING MULTIPLE LINEAR REGRESSION COUPLED WITH GENETIC ALGORITHM

ALEXANDRINA GUIDEA[a], COSTEL SÂRBU[a*]

ABSTRACT. Quantitative structure-retention relationships (QSRR) approach was used to model chromatographic lipophilicity of sixteen proteinogenic amino acids using molecular descriptors computed with DRAGON and ALCHEMY software packages. Modeling was performed applying multiple linear regression (MLR) coupled with genetic algorithms (GA) methodology (MLR-GA). The most important descriptors, highly significant in the predictive models of amino acids lipophilicity (R_{M0}), were related to atomic polarizabilities (MATS3p; Ap; H1p), atomic van der Waals volume (MATS3v), Sanderson electronegativity (RDF070e) and Randic molecular profiles (DP11; DP12) calculated with Dragon software. The internal statistical evaluation procedure highlighted some appropriate models for the chromatographic lipophilicity prediction. Moreover, the statistical parameters of regression in order to evaluate the relationship between experimental and predicted values, in case of the test set (four amino acids), revealed three statistically valid models (model A, E and F) that can be successfully used in lipophilicity prediction of amino acids.

Keywords: *chromatographic lipophilicity, amino acids, multiple linear regression, genetic algorithm, molecular descriptors, modeling, prediction*

INTRODUCTION

Quantitative structure-activity/property relationships (QSAR/QSPR) describe how the molecular structure, in terms of descriptors – lipophilic, electronic and steric – affects the biological activity or any other property of

[a] *Babeş-Bolyai University, Faculty of Chemistry and Chemical Engineering, 11 Arany Janos str. No 11, RO-400028, Cluj-Napoca, Romania*
** Corresponding author: csarbu@chem.ubbcluj.ro*

a compound [1-3]. Similarly, a quantitative structure-retention relationship (QSRR) relates these descriptors to chromatographic retention [4, 5]. Finally, the quantitative retention-property relationships (QRPR) imply that conclusions concerning various properties including also a biological activity can be based on chromatographic experiments. Regarding the QRPR approach, it can be considered that the same basic molecular interactions determine the behavior of chemical compounds in both biological and chromatographic environments. As a direct consequence, the chromatographic approach has been quite successful applied, for example, in duplicating lipophilicity data derived by traditional shake-flask technique or other procedures [6-8].

Lipophilicity (hydrophobicity) is a fundamental molecular property defined as the logarithm of the octanol-water partition coefficient ($\log P_{OW}$), which practically reflects the non-ionized compound partition between two phases usually octanol and water [9,10].

Different chromatographic methods were applied and continue to be used with success in order to estimate the physico-chemical characteristics of chemical compounds, of which lipophilicity seems to be the most important [11]. In many cases, this molecular parameter strongly correlates with the biological activity of chemicals, as well as with other important physico-chemical properties. Studies on the relationships between chromatographic retention and the structure are helpful not only for the molecular design/template synthesis of chemical compounds with controlled properties, but also to better understand the biochemical and biophysical processes. In addition, the chromatographic methods have significant advantages in comparison with other physico-chemical methods because (a) they are fast and relatively simple, (b) only small amounts of any compound are needed, (c) the compound should not be very pure because it is purified during the chromatographic process, (d) the process is dynamic and can be very easy modeled [12-15].

The modeling of the lipophilicity for twenty of the proteinogenic amino acids investigated in this study as well as the prediction of this parameter with different molecular descriptors calculated using performant software as Alchemy and Dragon will allow a better understanding of the relationships between the structure and their physico-chemical and biochemical properties. Highly statistical significant multiple linear regression-genetic algorithms (MLR-GA) models were successfully applied to the prediction of chromatographic lipophilicity (R_{M0}) of some amino acids.

RESULTS AND DISCUSSION

A comprehensive investigation was carried out for QSRR of twenty proteinogenic amino acids using MLR-GA methodology. Because the major goal still is to improve the predictive power of the models and the creation of a

''more general'' QSRR model, which can be applied over a wide range of amino acids, a data set of lipophilicity values (R_{M0} indices) obtained in previous determinations for some amino acids (Alanine-**Ala**, Arginine-**Arg**, Asparagine-**Asn**, Aspartic Acid-**Asp**, Cysteine-**Cys**, Glutamic acid-**Glu**, Glycine-**Gly**, Histidine-**His**, Leucine-**Leu**, Lysine-**Lys**, Methionine-**Met**, Phenylalanine-**Phe**, Proline-**Pro**, Serine-**Ser**, Tyrosine-**Tyr**, Valine-**Val**) [16], was used in our investigations. Because at that time, the R_{M0} of four amino acids (Glutamine-**Gln**, Isoleucine-**Ile**, Threonine-**Thr**, Tryptophan-**Trp**) were not been determined they were used here as a test set and also for the external validation of the obtained models. The descriptors that generated the most statistically significant MLR models were selected using GA methodology. The best predictive models for lipophilicity estimation were chosen considering the following regression parameters (goodness of fit): the determination coefficient (R^2), Fisher function (F), residual sum of squares (RSS), standard error of estimate (s), and leave-one-out cross-validation coefficient (Q^2), predictive error sum of squares ($PRESS$) and standard deviation error of prediction ($SDEP$) obtained in the cross-validation process. The retained descriptors from both used software packages are summarized in Table 1. The models obtained using descriptors retained from Dragon and Alchemy with the highest predictive ability and related statistical parameters are shown below in Table 2**.**

The statistical parameters corresponding to the all regression models retained with three, four, and respectively five independent variables (descriptors) illustrate a high to moderate statistically significant prediction power. Furthermore, it is easy to observe that the most powerful models contain four or five descriptors. The „goodness of model" is given by its robustness, prediction ability, and the applicability domain. The determination coefficient of fitting power (R^2) was higher than 89% in the case of Alchemy models and higher than 99% in the case of Dragon models, respectively. By a careful examination, one may be observed that the most informative Alchemy descriptors were molecular polarizability (Polar) and specific polarizability (Sp.Pol), the sum of absolute values of the charges on the nitrogen and oxygen atoms in the molecule ($ABSQ_{ON}$), and Wiener index (WienI) (Table 2). All these retained descriptors appeared to be important in describing the chromatographic lipophilicity. The molecular polarizability increases the lipophilicity, but the charges decrease it [17].

The most significant descriptors calculated with Dragon are related to atomic polarizability (MATS3p, Ap, H1p), atomic van der Waals volume (MATS3v), atomic Sanderson electronegativity (RDF070e) and Randic molecular profiles (DP11/12).

Table 1. Descriptors of amino acids calculated with Alchemy[2000] and Dragon Plus 5.4 software packages and selected by GA methodology

Abv.	Exp. Data*	Descriptor																
		ALCHEMY							DRAGON									
	R_{M0}	Volume	ABSQon	MaxQ-	Polar	Sp.Pol	$^{0}\chi_{v}$	Wienl	MATS3p	MATS3v	DP11	DP12	RDF070e	Mor12u	Ap	HATS2u	SP13	H1p
Ala	-1.14	164.62	1.92	-0.35	17.49	0.11	6.73	247.00	-0.27	-0.34	0.02	0.01	0.00	-0.55	2.66	0.61	0.002	0.40
Arg	-0.60	165.16	1.92	-0.36	17.87	0.11	6.71	247.00	-0.06	-0.06	6.73	6.42	5.70	-1.43	11.46	0.32	6.06	0.51
Asn	-1.19	114.90	1.66	-0.42	11.88	0.10	4.70	96.00	-0.31	-0.32	1.50	0.95	0.25	-1.01	4.76	0.43	0.66	0.43
Asp	-1.26	112.39	1.57	-0.33	11.04	0.10	4.57	96.00	-0.36	-0.38	1.42	0.89	0.00	-0.82	4.22	0.42	0.60	0.42
Cys	-0.90	101.85	0.94	-0.33	11.48	0.11	4.56	46.00	0.01	-0.04	0.43	0.19	0.00	-0.52	3.69	0.55	0.10	0.56
Gln	-	132.91	1.66	-0.42	13.71	0.10	5.41	136.00	-0.21	-0.23	3.30	2.73	1.42	-1.03	5.74	0.39	2.28	0.47
Glu	-1.18	129.38	1.57	-0.33	12.87	0.10	5.28	136.00	-0.16	-0.18	3.38	2.81	1.92	-1.20	6.39	0.39	2.37	0.46
Gly	-1.07	68.43	0.95	-0.33	6.64	0.10	2.64	18.00	0.34	0.23	0.01	0.004	0.00	-0.34	1.45	0.77	0.001	0.24
His	-0.59	137.90	1.53	-0.33	15.43	0.11	5.82	165.00	-0.01	-0.01	2.74	2.11	3.22	-1.06	7.31	0.42	1.65	0.68
Ile	-	135.50	0.94	-0.33	13.86	0.10	5.80	92.00	0.14	0.11	1.50	0.98	2.46	-0.77	6.61	0.41	0.72	0.55
Leu	-0.47	135.82	0.94	-0.33	13.86	0.10	5.79	96.00	0.19	0.15	0.90	0.47	1.61	-1.09	6.46	0.45	0.24	0.65
Lys	-0.93	148.91	1.27	-0.33	15.21	0.10	5.92	143.00	0.08	0.06	5.10	4.69	3.21	-1.15	8.26	0.37	4.29	0.48
Met	-0.55	137.48	0.94	-0.33	15.02	0.11	6.15	102.00	0.24	0.19	3.79	3.27	3.52	-0.52	7.25	0.51	2.83	0.56
Phe	-0.02	157.90	0.94	-0.33	18.14	0.11	6.60	212.00	0.33	0.30	3.96	3.40	4.33	-1.04	10.37	0.36	2.94	0.86
Pro	-0.90	108.70	0.93	-0.33	11.24	0.10	4.55	62.00	0.21	0.15	0.28	0.11	0.00	-0.97	4.06	0.55	0.05	0.53
Ser	-1.21	93.57	1.33	-0.39	9.12	0.10	3.66	46.00	-0.40	-0.46	0.23	0.09	0.00	-0.68	2.98	0.54	0.04	0.39
Thr	-	110.39	1.33	-0.39	10.83	0.10	4.54	65.00	-0.15	-0.19	0.27	0.11	0.00	-0.56	4.14	0.45	0.06	0.48
Trp	-	186.60	1.22	-0.33	22.32	0.12	8.10	396.00	0.19	0.18	5.87	5.48	6.88	-1.01	16.43	0.33	5.26	0.89
Tyr	-0.44	165.64	1.34	-0.39	18.78	0.11	6.97	268.00	0.11	0.08	5.39	4.99	4.14	-1.20	10.69	0.33	4.63	0.73
Val	-0.68	118.81	0.94	-0.33	12.02	0.10	5.09	65.00	0.01	-0.01	0.30	0.12	0.00	-0.74	5.15	0.46	0.07	0.51

*data values for lipophilicity parameters (R_{M0}) obtained on RP-18W chromatographic plates, according to the reference [16]

Table 2. The linear multiple regression models for lipophilicity prediction obtained by applying genetic algorithms on *Alchemy* and D*ragon* descriptors

ID	Size	Model	R^2 %	F	s	RSS	SDEC	Q^2 %	PRESS	SDEP
Alchemy										
A	5	*R_{MD}=14.01–0.14***Volume**+1.68***MaxQ**-+1.54***Polar** – 155.52***Sp.Pol** –0.008***WienI** ** R_{MD} =–11.08***Volume**+0.15***MaxQ**-+15.01***Polar**–2.61***Sp.Pol** –1.691***WienI**	89.19	16.51	0.143	0.206	0.113	76.37	0.450	0.168
B	4	* R_{MD} =13.38–0.14***Volume**+1.56***Polar**–156.11***Sp.Pol**–0.008***WieIn** ** R_{MD} = – 11.06***Volume** + 15.14***Polar** – 2.62***Sp.Pol** – 1.86***WieIn**	87.33	18.95	0.148	0.242	0.123	73.03	0.514	0.179
C	3	* R_{MD} = -0.97 – 0.68***$ABSQ_{ON}$** + 0.18***Polar** – 0.28*$^{\chi^{V}_{0}}$ ** R_{MD} = - 0.70***$ABSQ_{ON}$** + 1.79***Polar** – 0.94*$^{\chi^{V}_{0}}$	83.45	20.16	0.162	0.315	0.140	71.50	0.543	0.184
D	2	* R_{MD} =-1.17 – 0.66***$ABSQ_{ON}$** + 0.09***Polar** ** R_{MD} = - 0.68***$ABSQ_{ON}$** + 0.86***Polar**	80.95	27.62	0.167	0.363	0.151	68.96	0.591	0.192
Dragon										
E	5	*R_{MD}=-1.36+0.36***MATS3p**–0.22***DP11**+0.09***RDF070e**+0.37***Mor12u** + 0.20***Ap** ** R_{MD}=0.24***MATS3p**–1.37***DP11**+0.50***RDF070e**+0.32***Mor12u** +1.69***Ap**	99.83	1172.90	0.018	0.003	0.014	99.54	0.009	0.023
F	4	* R_{MD} = -3.05 – 0.22***DP12**+0.31***Mor12u**+0.32***Ap**+2.07***HATS2u** ** R_{MD} = -1.33***DP12** + 0.27***Mor12u** + 2.73***Ap** + 0.69***HATS2u**	**99.06**	290.00	0.040	0.018	0.034	**98.17**	0.035	0.047
G	3	* R_{MD} =-3.32 – 0.24***SP13** + 0.32***Ap** + 2.85***HATS2u** ** R_{MD} = -1.30***SP13** + 2.71***Ap** + 0.95***HATS2u**	**97.51**	156.50	0.063	0.047	0.055	**95.56**	0.085	0.073
H	2	* R_{MD} = -1.64 + 0.61***MATS3v** + 1.61***H1p** ** R_{MD} = 0.40***MATS3v** + 0.68***H1p**	88.45	49.80	0.130	0.220	0.117	84.97	0.286	0.134

**– non standardized coefficients*

*** –standardized coefficients*

Usually, the prediction ability of a model can be better characterized by an internal validation assessing the correlation coefficient between the experimental and predicted values. To evaluate the result of a large number of samples over the whole measurement range, usually, the regression analysis is preferred. The statistical parameters to evaluate the linear relationship between the experimental and predicted lipophilicity parameters for the training set of studied amino acids revealed that the models obtained with Dragon's descriptors have a good predictive capacity for R_{M0}, $Q^2 > 99\%$ and, in case of Alchemy's descriptors, $Q^2 > 76\%$.

Although satisfactory model robustness is a necessary condition to have a high prediction power, the real prediction ability of the model is assessed with the help of the external test set never used to build the models. So, the validation strategies should check the reliability of the developed models for their possible real application on a new set of data, and confidence of prediction can be judged.

In order to observe the ability of the obtained models to predict the lipophilicity the list of R_{M0} values both calculated with the model (Table 3) and predicted in the validation process (Table 4) has been compared with the experimental ones. Good correlation values were found for the training (sixteen amino acids) and training and test set (twenty amino acids) in the case of models using Dragon descriptors (Figure 1 c, d) and Alchemy descriptors (Figure 1 a, b), respectively. Based on the prediction criteria, the best model for lipophilicity could predict 99.83% of the variance in the case of Dragon descriptors and 76.37% in case of Alchemy descriptors. The test set used to validate models revealed that model C and D, although with better statistics, show a limited applicability. It may be also a good argument for robustness of model E that performs better predictability for both sets: training, and test, respectively (see Table 2). The model F has a better prediction for test sets. This is supported by the statistical parameters of regression ($R^2 = 99.06\%$, $Q^2 = 98.17\%$, $F = 290$, $s = 0.04$).

The predictive power of the models obtained with Alchemy descriptors is lower comparing with Dragon models because as we mentioned above, the set of amino acids do not form a homologous series. This is explaining by the fact that the retained descriptors do not contain sufficient information to describe the repartition behavior of all amino acids in thin layer chromatography (TLC) analysis. Lower prediction capacity is observed for amino acids with aliphatic side chain (Ala, Leu, Met, and Val) and for basic side chain (Arg and Lys) in comparison with experimental data. In Table 5 (the red marked) one can be observed that model E have a better prediction almost for all amino acids: basic side chain (Arg, His, Lys), hydrophobic side chain (aromatic) (Phe, Trp, Tyr), polar neutral side chain (Asn, Cys), unique amino acids (Gly, Pro). The most important selected descriptors indicate that the following descriptors are highly significant in the predictive lipophilicity models developed in this study: (a)

molecular descriptors obtained by radial basis functions centred on different interatomic distances (RDF descriptors – RDF070e); (b) molecular descriptors calculated by summing atoms weights viewed by a different angular scattering function (3D-MoRSE descriptors – Mor12u); (c) molecular descriptors obtained as statistical indices of the atoms projected onto the 3 principal components obtained from weighted covariance matrices of the atomic coordinates (WHIM descriptors – Ap); (d) molecular descriptors calculated from the molecular graph by summing the products of atom weights of the terminal atoms of all the paths (2D correlation – MATS3p, MATS3v); (e) molecular descriptors derived from the distance distribution moments of the geometry matrix (RMP descriptors – DP11, DP12).

Table 3. The R_{M0} values calculated with all MLR-GA models based on Alchemy and Dragon descriptors

Abv.	*$R_{M0\ exp}$	Model ID							
		Alchemy				Dragon			
		A	B	C	D	E	F	G	H
Ala	-1.138	-0.958	-0.981	-0.913	-0.891	-1.137	-1.093	-1.115	-1.201
Arg	-0.598	-0.741	-0.732	-0.838	-0.859	-0.589	-0.566	-0.553	-0.861
Asn	-1.187	-1.216	-1.085	-1.212	-1.218	-1.203	-1.147	-1.116	-1.144
Asp	-1.255	-1.191	-1.231	-1.272	-1.235	-1.263	-1.267	-1.304	-1.195
Cys	-0.896	-0.909	-0.919	-0.754	-0.777	-0.904	-0.909	-0.971	-0.770
Gln	-	-	-	-	-	-	-	-	-
Glu	-1.185	-1.237	-1.279	-1.130	-1.074	-1.156	-1.176	-1.109	-1.003
Gly	-1.071	-1.070	-1.122	-1.118	-1.208	-1.079	-1.085	-1.048	-1.005
His	-0.586	-0.624	-0.661	-0.778	-0.819	-0.607	-0.624	-0.567	-0.556
Ile	-	-	-	-	-	-	-	-	-
Leu	-0.472	-0.695	-0.697	-0.658	-0.567	-0.457	-0.466	-0.407	-0.507
Lys	-0.930	-0.817	-0.825	-0.668	-0.666	-0.945	-1.012	-1.009	-0.841
Met	-0.554	-0.309	-0.303	-0.541	-0.463	-0.532	-0.547	-0.607	-0.630
Phe	-0.017	-0.056	-0.089	-0.093	-0.187	-0.033	-0.037	-0.055	-0.072
Pro	-0.897	-0.911	-0.930	-0.786	-0.788	-0.895	-0.923	-0.855	-0.691
Ser	-1.214	-1.134	-1.058	-1.210	-1.246	-1.211	-1.188	-1.214	-1.301
Thr	-	-	-	-	-	-	-	-	-
Trp	-	-	-	-	-	-	-	-	-
Tyr	-0.439	-0.461	-0.409	-0.347	-0.393	-0.443	-0.389	-0.418	-0.414
Val	-0.681	-0.793	-0.800	-0.801	-0.729	-0.666	-0.691	-0.772	-0.829

*data values for lipophilicity parameters (R_{M0}) obtained on RP-18W chromatographic plates, according to the reference [16]

Table 4. The predicted (in cross-validation process) R_{M0} values with all MLR-GA models based on Alchemy and Dragon descriptors

Abv.	*$R_{M0\ exp}$	Model ID							
		Alchemy				Dragon			
		A	B	C	D	E	F	G	H
Ala	-1.138	-0.858	-0.899	-0.822	-0.796	-1.136	-1.083	-1.110	-1.215
Arg	-0.598	-0.784	-0.773	-0.941	-0.965	-0.583	-0.540	-0.522	-0.879
Asn	-1.187	-1.262	-1.070	-1.217	-1.225	-1.207	-1.137	-1.100	-1.136
Asp	-1.255	-1.172	-1.225	-1.276	-1.231	-1.267	-1.275	-1.326	-1.179
Cys	-0.896	-0.947	-0.988	-0.731	-0.759	-0.906	-0.912	-0.980	-0.761
Gln	-	-1.170	-1.040	-1.069	-1.056	-1.271	-1.310	-1.287	-1.030
Glu	-1.185	-1.259	-1.311	-1.117	-1.058	-1.145	-1.173	-1.090	-0.986
Gly	-1.071	-1.066	-1.214	-1.166	-1.278	-1.094	-1.112	-1.008	-1.178
His	-0.586	-0.635	-0.678	-0.807	-0.844	-0.619	-0.629	-0.565	-0.550
Ile	-	-0.666	-0.665	-0.658	-0.567	-0.382	-0.510	-0.578	-0.690
Leu	-0.472	-0.785	-0.788	-0.742	-0.582	-0.446	-0.462	-0.378	-0.512
Lys	-0.930	-0.776	-0.787	-0.646	-0.643	-0.954	-1.045	-1.042	-0.831
Met	-0.554	-0.170	-0.162	-0.536	-0.446	-0.511	-0.540	-0.619	-0.642
Phe	-0.017	-0.090	-0.144	-0.172	-0.268	-0.044	-0.051	-0.080	-0.110
Pro	-0.897	-0.914	-0.935	-0.768	-0.771	-0.894	-0.936	-0.849	-0.664
Ser	-1.214	-1.078	-1.006	-1.209	-1.254	-1.209	-1.183	-1.214	-1.334
Thr	-	-1.092	-1.008	-1.134	-1.092	-0.854	-0.978	-1.120	-0.985
Trp	-	0.262	0.152	0.071	-0.004	0.955	1.425	1.287	-0.095
Tyr	-0.439	-0.479	-0.390	-0.314	-0.380	-0.445	-0.373	-0.412	-0.408
Val	-0.681	-0.821	-0.829	-0.837	-0.736	-0.655	-0.694	-0.791	-0.839

*data values for lipophilicity parameters (R_{M0}) obtained on RP-18W chromatographic plates, according to the reference [16]

The predictive power of the models obtained with Alchemy descriptors is lower comparing with Dragon models because as we mentioned above, the set of amino acids do not form a homologous series. This is explaining by the fact that the retained descriptors do not contain sufficient information to describe the repartition behavior of all amino acids in thin layer chromatography (TLC) analysis. Lower prediction capacity is observed for amino acids with aliphatic side chain (Ala, Leu, Met, and Val) and for basic side chain (Arg and Lys) in comparison with experimental data. In Table 5 (the red marked) one can be observed that model E have a better prediction almost for all amino acids: basic side chain (Arg, His, Lys), hydrophobic side chain (aromatic) (Phe, Trp, Tyr), polar neutral side chain (Asn, Cys), unique amino acids (Gly, Pro). The most important selected descriptors indicate that the

following descriptors are highly significant in the predictive lipophilicity models developed in this study: (a) molecular descriptors obtained by radial basis functions centred on different interatomic distances (RDF descriptors – RDF070e); (b) molecular descriptors calculated by summing atoms weights viewed by a different angular scattering function (3D-MoRSE descriptors – Mor12u); (c) molecular descriptors obtained as statistical indices of the atoms projected onto the 3 principal components obtained from weighted covariance matrices of the atomic coordinates (WHIM descriptors – Ap); (d) molecular descriptors calculated from the molecular graph by summing the products of atom weights of the terminal atoms of all the paths (2D correlation – MATS3p, MATS3v); (e) molecular descriptors derived from the distance distribution moments of the geometry matrix (RMP descriptors – DP11, DP12).

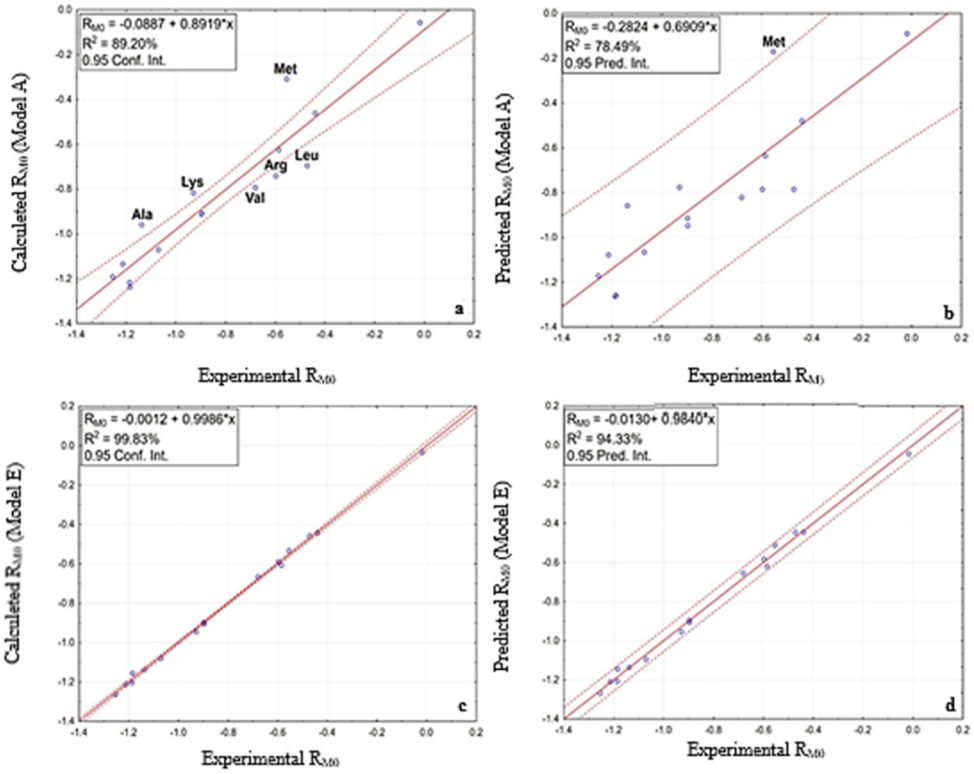

Figure 1. Calculated and predicted versus experimental R_{M0} values of amino acids for the training set (a, c); training and test set (b, d) for the best models developed using Dragon and Alchemy descriptors, respectively.

The most important descriptors in these models, accounting for 2D and 3D aspects of the molecular structure, can be classified as RDF (Radial Distribution Function), Randic molecular profiles, WHIM and GETAWAY signals. The selected RDF descriptors are related to the atomic van der Waals volumes (v) and atomic Sanderson electronegativities (e). The GETAWAY descriptors are related to the atomic Sanderson electronegativities (e). Also, the use of WHIM descriptors and GETAWAY descriptors show that atomic polarizabilities (p) and atomic van der Waals volumes (v) are the most important properties responsible for repartition coefficient of amino acids in TLC.

CONCLUSION

The chromatographic retention data for a set of proteinogenic amino acids have been modeled by a wide set of computational molecular descriptors using multiple linear regression and genetic algorithms methodologies. The best models, internally validated by leave-one-out procedure, revealed that only a small number of descriptors seem to be necessary in order to obtain statistically significant prediction models. The models derived from Dragon descriptors are more efficient comparing to the Alchemy descriptors. The descriptors selected as the best combinations correlated to the different lipophilicity response are not easily interpretable concerning the complex underlying lipophilicity mechanism. However, the most important descriptors, highly significant in the predictive lipophilicity models of amino acids, were related to the atomic polarizabilities, atomic Sanderson electronegativities and atomic van der Waals volumes of the molecules.

EXPERIMENTAL SECTION

Computation of the molecular descriptors

There are three common methods for structure representation: whole molecule 1D descriptors, 2D descriptors, and 3D descriptors. 1D descriptors attempt to express chemical information in a simple 1D molecular code and are designed for compact storage of information. 2D descriptors are calculated from a chemical structure which is represented as a connection table or a molecular graph. In the graphical representation of molecular structures, atoms in the molecular structure are represented as vertices while bonds are represented as edges. 3D molecular descriptors provide molecular information about the 3D arrangement of structural features and general molecular surfaces and volumes. There are many thousands of descriptors defined in a comprehensive handbook [18].

Dragon Plus version 5.4 (*www.talete.mi.it/dragon.htm*) [19] is widely used to calculate molecular descriptors for QSAR/QSPR/QSRR modeling. Generally, the Dragon calculated descriptors encoding the molecular structure of an analyte are categorized in 22 different types: constitutional (1D), molecular properties (1D), atom-centred fragments (1D), functional group counts (1D), charge (1D), information indices (2D), walk and path counts (2D), topological (2D), topological charge indices (2D), connectivity indices (2D), eigenvalue-based indices (2D), Burden eigenvalues (2D), 2D edge adjacency indices (2D), autocorrelation (2D), 2D binary fingerprints (2D), 2D frequency fingerprints (2D), geometrical descriptors (3D), Radial Distribution Function (RDF) descriptors (3D), Randic molecular profiles (3D), GETAWAY (Geometry, Topology and Atoms-Weighted Assembly) descriptors (3D), 3D-MoRSE (3D Molecular Representation of Structure based on Electron diffraction) descriptors (3D), and WHIM (Weighted Holistic Invariant Molecular) descriptors (3D). For this study were used 1056 descriptors.

The second set of descriptors related to charge dependent, 3D-structure-dependent parameters, topological and descriptors related to atom properties, formal and delocalized charge and molecular surface based on molecular mechanics for optimizing models, were computed using Alchemy^{2000} [20] (*http://www.tripos.com*). The descriptors used (19) are: the partition coefficient (ScilogP), the first-order ($^{1}\chi$) and third-order ($^{3}\chi$) connectivity indexes, the zero-order ($^{0}\chi^{V}$) and first-order ($^{V}\chi^{1}$) valence order connectivity indexes, the third-order shape index for molecule ($^{3}K_{a}$), the Wiener (WienI) index based on the graph of the molecule, the volume (Volume), the dipole moment (Dipole), the molecular polarizability (Polar), the specific molar polarizability (Sp.Pol), the largest positive/negative charges over the atoms in molecule, in electrons ($MaxQ^{+}$/$MaxQ^{-}$), the sum of absolute values of the charges on each atom of the molecule, in electrons (ABSQ), the sum of absolute values of the charges on the nitrogen and oxygen atoms in molecule, in electrons ($ABSQ_{ON}$), the surface area, the ovality (Ovality) of the molecule.

Chemometric methods

Multiple linear regression-genetic algorithm analysis [21, 22] was performed using the MobyDigs v.1.0 package [23]. Genetic algorithm procedure [24-26] was used to select the most significant variables. Models predictive performance [27, 28] was described by means of statistical parameters related to model goodness of fit (the determination coefficient R^2, Fisher function F, residual sum of squares RSS, standard error of estimate *s*, and predictive capability (cross-validation coefficient Q^2, predictive error sum of squares *PRESS*, and standard deviation error of prediction SDEP).

REFERENCES

1. C. Hansch, A. Leo (eds), Exploring QSAR: fundamentals and applications in chemistry and biology, American Chemical Society, Washington, D.C., **1995**.
2. M. Karelson, Molecular Descriptors in QSAR/QSPR, John Wiley & Sons, New York, **2000**.
3. M. Karthikeyan, V. Renu, Practical Bioinformatics, Springer, India, **2014**.
4. R. Kaliszan, Quantitative structure–chromatographic retention relationships, Wiley–Interscience, New York, **1987**.
5. R. Kaliszan, Structure and Retention in Chromatography. A Chemometric Approach, Harwood Academic Publishers, Amsterdam, **1997**.
6. Test No. 107, Partition coefficient (n-octanol/water), Shake-flask method, OECD, Paris, **1995**.
7. Test No. 123, Partition coefficient (n-octanol/water), Slow-stirring method, OECD, Paris, **2005**.
8. Test No. 117, Partition coefficient (n-octanol/water), HPLC method, OECD, Paris, **2004**.
9. A. Leo, C. Hansch, D. Elkins, *Chem. Rev.*, **1971**, *71*, 525–616.
10. J. Sangster, Octanol-water partition coefficients: fundamentals and physical chemistry, John Wiley & Sons, Inc., New York, **1997**.
11. H. Van de Waterbeemd, M. Kansy, B. Wagner, H. Fischer, Lipophilicity measurement by high-performance liquid chromatography (RP-HPLC). In: V. Pilska, B. Testa, H. Van de Waterbeemd (eds), Lipophilicity in drug action and toxicology, VCH, Weinheim, **1996**.
12. C. Sârbu, B. Malawska, *J. Liq. Chromatogr. Relat. Technol.*, **2000**, 23, 2143-2154.
13. C. Sârbu, R. D. Naşcu-Briciu, *Studia UBB CHEMIA*, **2015**, LX, *1*, 265-280.
14. R. D. Briciu, C. Sârbu, *Studia UBB CHEMIA*, **2010**, LV, *3*, 105-118.
15. D. Casoni, C. Sârbu, *J. Sep. Sci.*, **2012**, *35*, 915-921.
16. D. Casoni, C. Sârbu, *Studia UBB CHEMIA*, **2011***,* LVI, *1*, 45-61.
17. L. Xing, R.C. Glen, *J. Chem. Inf. Comput. Sci.*, **2002**, *47*, 796-805.
18. R. Todeschini, V. Consonni, Handbook of Molecules Descriptors, Wiley, Weinheim, **2000**.
19. Talete SRL, DRAGON for windows (software for molecular descriptor calculations). Version 5.4-2006. http://www.talete.mi.it
20. SciQSAR Application, Version 3.0, 1998 SciVision, Method: *Alchemy 2000* (software for molecular descriptor calculations). http://www.tripos.com
21. R. Kaliszan, *J. Chromatogr. A,* **1993**, *656*, 417-435.
22. R. Put, Y. Vander Heyden, *Anal. Chim. Acta*, **2007,** *602*, 164-172.
23. R. Todeschini, Moby Digs Academic version software for variable subset selection by genetic algorithms, Rel. 1.0 for Windows, Talete, Milan, **2004**.
24. R. Leardi, R. Boggia, M. Terrile, *J. Chemom.*, **1992**, *6*, 267–281.
25. S. Riahi, M.R. Ganjali, E. Pourbasheer, P. Norouzi, *Chromatographia*, **2008**, *67*, 917-922.
26. J. Devillers, Genetic algorithms in molecular modeling, Academic Press, Inc., San Diego, **1996**.
27. H. Kubinyi, *Quant. Struct.-Act. Relat.,* **1994**, *13*, 285–294.
28. P. Gramatica, A. Sangion, *J. Chem. Inf. Model.,* **2016**, *56*, 1127−1131.

STUDIA UBB CHEMIA, LXIV, 2,Tom I, 2019 (p. 255-264)
(RECOMMENDED CITATION)
DOI:10.24193/subbchem.2019.2.21

Dedicated to Professor Florin Dan Irimie on the Occasion of His 65th Anniversary

VALIDATED LC-MS/MS METHOD FOR THE DETERMINATION OF THE NONSTEROIDAL ANTI-INFLAMMATORY DRUG (NSAID) DICLOFENAC FROM HUMAN PLASMA

RÓBERT TŐTŐS[a*], JÓZSEF BALÁZSI[b]

ABSTRACT. The purpose of this study was the development and validation of an LC-MS/MS method, for the determination of diclofenac from human plasma. The sample workup involved a simple protein precipitation procedure. A core/shell type analytical column (50×2,1 mm, 2.6 Å) was used with C18 stationary phase. The mobile phase consisting of 52.5% acetonitrile and 47.5% water provided good peak shape, accuracy and precision (stable ionization). The mass spectrometer was operated in negative electrospray ionization mode for analyte and internal standard. The following parameters were evaluated for validation purpose: Selectivity, sensitivity, matrix effect, anticoagulant effect, linearity, precision and accuracy, recovery, short and long term analyte/IS stability in solvent/matrix and carryover. The validated calibration range was 3.9-1194 ng/ml. The correlation coefficient R^2 was at least 0.999 in all validation batches. The validated method has been successfully used for the evaluation of bioequivalence of a generic diclofenac potassium formulation of 12.5 mg strength.

Keywords: *diclofenac, NSAID, method validation, bioequivalence trial, LC-MS/MS*

[a] *Babeş-Bolyai University, Faculty of Chemstry and Chemical Engineering, Biocatalysis and Biotransformation Research Centre,11 Arany János str., RO-400028, Cluj-Napoca, Romania*
[b] *PharmacoKinetics SRL, 373 E/4 Corunca, RO-547367, Mures county, ROMANIA*
** Corresponding author totosr@chem.ubbcluj.ro*

INTRODUCTION

Diclofenac 2-[(2,6-dichlorophenyl)amino] benzeneacetic acid monopotassium salt with the empirical formula $C_{14}H_{10}Cl_2NKO_2$, is a nonsteroidal potent anti-inflammatory agent, an effective PGE (prostaglandin E) synthase inhibitor, platelet aggregation inhibitor, present analgesic and anti-pyretic effects. [1,7]. Inhibition of prostaglandin synthesis is considered fundamental to its mechanism of action, as prostaglandins play a major role of inflammation, pain and fever triggering. Diclofenac is generally used in form of sodium or potassium salt (Figure 1).

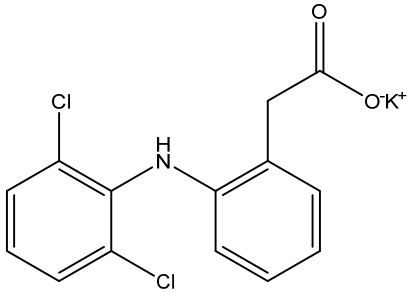

Figure 1. Structure of diclofenac potassium salt

RESULTS AND DISCUSSION

Determination of acquisition parameters

There are some methods known in the literature for the determination of diclofenac in human plasma or pharmaceutical formulations including topical products, using LC/UV [2,4,6] or LC-MS/MS methods [3,5,8].

The m/z transitions used for multiple reaction monitoring (MRM) were chosen based on the spectra from Figures 2 and 3. The monitored transitions should not interfere in their m/z value, specific for a given analyte. Their intensity should be convenient for the qualifiers, and the qualifier/quantifier ratio should remain stable over the time. Taking into account the considerations above the following transitions were chosen for the quantitative assay method:

Diclofenac: m/z 294.0→250.0, (296.1→252.0 qualifier ion) CE 5V,

Diclofenac acetophenyl ring-$^{13}C_6$ (IS): m/z 300.1→256.1

(302.1→258.1 qualifier ion) CE 5V. (CE – Collision Energy)

For analyte and IS (Internal Standard) the single charged molecular ions were used as precursors.

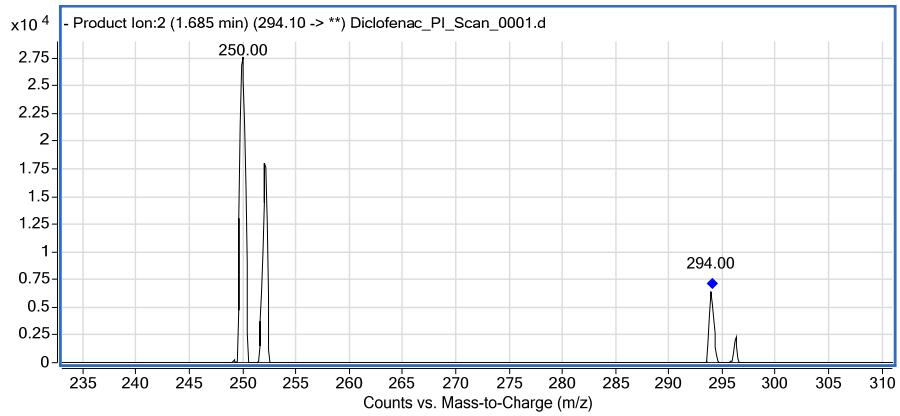

Figure 2. ESI(-) Spectrum of Diclofenac

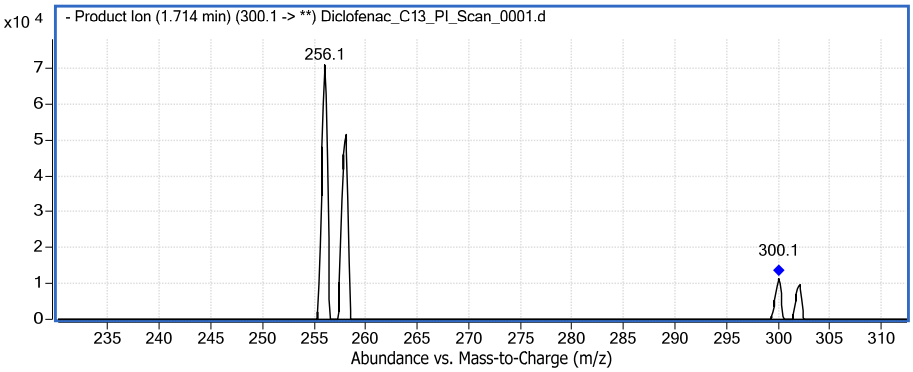

Figure 3. ESI(-) Spectrum of Diclofenac acetophenyl ring-$^{13}C_6$ (IS)

Figure 4 shows a typical MRM total ion chromatogram for an ULOQ (upper limit of calibration) sample. The analyte and IS are practically co-eluting at ca. 1.75 min. Values are back calculated concentrations for each analyte.

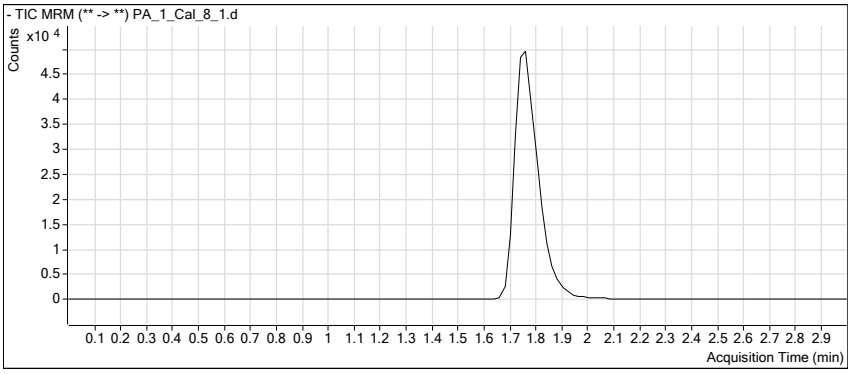

Figure 4. MRM chromatogram of Cal_8_1 (Diclofenac 1194 ng/ml, IS 58.9 ng/ml)

The use of the stable ^{13}C isotope labelled internal standard automatically leads to co-elution with the analyte. This is not an inconvenient in tandem mass spectrometry, also minimization of the matrix effect is achieved. It's noticeable, that no significant spectral response has been observed at the retention time of the analyte/IS in matrix blank samples (Figure 5.).

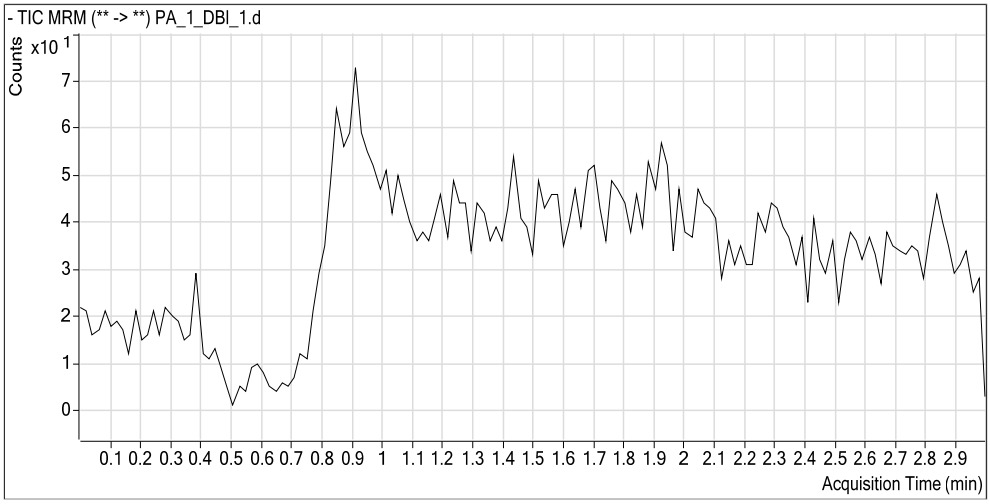

Figure 5. MRM chromatogram of DBI1 (matrix blank 0 ng/ml analyte/IS)

Bioanalytical method validation

The analytical method was validated according to the EMEA/CHMP/EWP/192217/2009 Guideline on validation of bioanalytical methods [11].

The tested parameters were: selectivity, sensitivity, matrix effect, intra/interbatch precision and accuracy, recovery, short/long term stability of stock solutions of analyte, short term stability of working solutions of analyte, bench top stability in biological matrix, freeze thaw stability in biological matrix, injector/autosampler stability of the processed samples, stability during delayed processing, dilution integrity, carryover. All tests were performed using 6 replicates at the mentioned QC (Quality Control) levels.

The calibration curve range is established according to literature data about plasma concentrations of the analyte. $C_{max\ average\ from\ literature}$ for diclofenac was found of ca. 450-600 ng/ml, after administration of a 25 mg dose. [2,9,10]

A summary of main results of validation batches is presented in Table 1.

The validated calibration range was 3.9-1194 ng/ml. The calibration curves were obtained using a linear weighted (1/x) regression analysis of the peak area ratio (analyte/internal standard) versus the nominal concentration of the calibration standards. The lower limit of quantitation was set smaller than 5% of expected average C_{max} values. A typical calibration curve is presented in Figure 6.

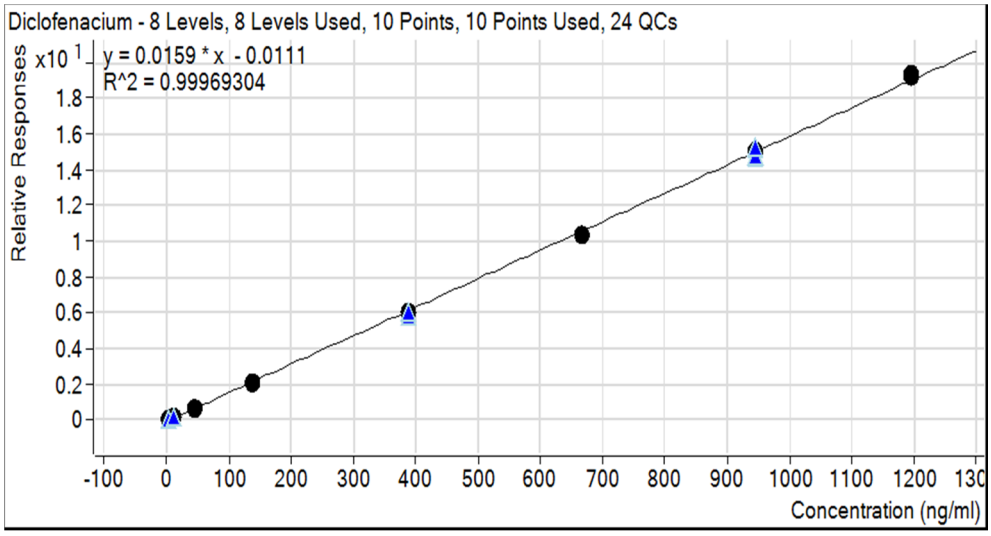

Figure 6. Calibration curve for diclofenac

Linearity summary results for diclofenac are presented in Table 2. The limit of quantitation was 3.9 ng/ml and the linear dynamic range of the curve was from 3.9-1194 ng/ml.

Summary of method validation

Table 1. Bioanalytical method validation summary for diclofenac

Calibration concentrations (ng/ml)	3.89, 11.11, 44.44, 138.88, 388.86, 666.62, 944.38, 1194.37
Lower limit of quantitation (ng/ml)	LLOQ, 3.89 Accuracy 103.28 %, RSD 4.52
QC Concentrations (ng/ml)	LLOQ-QC, LQC, MQC, HQC 3.89, 11.11, 388.86, 944.38
Between-run accuracy (%)	LLOQ-QC, LQC, MQC, HQC 104.67, 100.25, 101.47, 102.90
Between-run precision (RSD)	LLOQ-QC, LQC, MQC, HQC 1.49, 1.35, 2.28, 2.02
IS normalized Matrix factor (MF) RSD	LQC, HQC 1.06, 1.01 5.35, 0.95
Recovery (%)	LQC, MQC, HQC 94.04, 99.68, 98.60
Long term stability of stock solution and working solutions (Observed change %)	Confirmed up to 39 days at +4 °C LQC Stab. 98.99, change –1.01 % HQC Stab. 106.53, change +6.53 % IS Stab. 95.01, change – 4.99%
Short term stability in biological matrix at room temperature or at sample processing temperature. (Observed change %)	Confirmed up to 20.81(6) h LQC Stab. 104.91, change +4.91 % HQC Stab. 102.05, change +2.05 %
Long term stability in biological matrix (Observed change %)	Confirmed up to 125 days at –50 °C LQC Stab. 101.44, change +1.44 % HQC Stab. 96.21, change –3.79 %
Autosampler storage stability (Observed change %)	Confirmed up to 80.5(6) h LQC Stab. 104.87, change +4.87 % HQC Stab. 101.36, change +1.36 %
Freeze and thaw stability (Observed change %)	-50 °C, 3 cycles LQC Stab. 101.58, change +1.58 % HQC Stab. 101.14, change +1.14 %
Dilution integrity	Concentration diluted (2-fold) 101.26 %; RSD 1.04 % Concentration diluted (4-fold) 104.02 %; RSD 0.98 %

PA – Precision and Accuracy batch
LLOQ-QC/LQC/MQC/HQC – Lower Limit of Quantitation/Low/Medium/High Quality Control sample

Table 2. Linearity summary results for diclofenac

Calibration level	Nominal conc. (ng/ml)	Mean conc.±S.D. (ng/ml) n=3	RSD %	Accuracy %
Cal_1_1	3.89	4.08±0.20	4.97	104.96
Cal_1_2	3.89	4.23±0.32	7.60	108.74
Cal_2	11.11	10.45±0.32	3.03	94.02
Cal_3	44.44	41.93±1.83	4.37	94.35
Cal_4	138.88	136.85±3.12	2.28	98.54
Cal_5	388.86	386.87±3.48	0.90	99.49
Cal_6	666.62	655.00±11.88	1.81	98.26
Cal_7	944.38	949.32±8.34	0.88	100.52
Cal_8_1	1194.37	1198.59±21.73	1.81	100.35
Cal_8_2	1194.37	1203.49±23.86	1.98	100.76

CONCLUSIONS

A rapid, sensitive, and robust method has been developed and validated for the determination of diclofenac in human plasma. The quantitation was performed on an Agilent 1200 series HPLC system, coupled to an Agilent 6410 triple quadrupole mass spectrometer, using electrospray ionization technique. The components were detected in negative ionization mode. The method was successfully used for the evaluation of bioequivalence of a generic formulation of diclofenac potassium 12.5 mg film-coated tablets in human subjects. The administered dose was 25 mg (two tablets).

EXPERIMENTAL SECTION

Solvents and reference materials used

All used solvents are of HPLC grade. Acetonitrile was purchased from VWR, methanol from LGC Standards, formic acid and hydrochloric acid from Merck KGaA, ammonium acetate was purchased from Sigma-Aldrich, HPLC water was obtained using a Millipore Simplicity UV water purification system. Certified reference materials of Diclofenac sodium and Diclofenac acetophenyl ring-$^{13}C_6$ sodium salt heminonahydrate (internal standard-IS) were obtained from Sigma-Aldrich and are of analytical standard grade. Blank human plasma was obtained from Innovative Research/Dunn Labortechnik GmbH.

Instrumentation and working parameters

An Agilent 1200 series HPLC system with a Phenomenex Kynetex C18 column (50 × 2.10 mm) equipped with Phenomenex Security Guard (4 ×2.0 mm) was used for separation. The used mobile phase was an isocratic mixture of 52.5:47.5 acetonitrile:water (containing 1 ml 5% ammonium acetate and 1 ml formic acid per 1L of water). The used flow rate was 0.3 ml/min., the column temperature was set to 35 ºC. An Agilent 6410 triple Quadrupole Mass Spectrometer (Agilent Technologies, USA), equipped with electrospray ion source was used for the LC-MS/MS analyses. The runtime was 3 min/sample. The data acquisition and processing were carried out using MassHunter software. The whole system (software and hardware) was validated. The mass spectrometer was operated in negative ionization mode for analyte and IS. Nitrogen was used as nebulizing gas and collision cell gas. The temperature of the ESI source was set to 350 ºC, and the needle voltage to 4000V.

The quantitation was performed using MRM (multiple reaction monitoring) of the transitions: m/z 294.0→250.0, (296.1→252.0 qualifier ion) CE 5V, for diclofenac and 300.1→256.1 (302.1→258.1 qualifier ion) collision energy 5V for Diclofenac acetophenyl ring-$^{13}C_6$ (IS).

The mass spectrometer was operated at unit resolution with a dwell time of 300 ms per transition.

Stock and working solutions preparation

Stock solutions of diclofenac (1.0 mg/ml) were prepared in acetonitrile/water 50/50 (w/w) dissolving accurately weighed amounts of reference material. Stock solutions of IS (1.0 mg/ml) were prepared in acetonitrile/water 50/50 (w/w) dissolving accurately weighed amounts of diclofenac acetophenyl ring-$^{13}C_6$. They were stored between 2-8 °C. Correction factors were applied to the weighed amounts of reference materials to calculate the content of the pure substance (Table 3). Correction factors are derived from the purity and the chemical form (salt). Water content will be substracted from the purity.

Table 3. Correction factors for reference materials

Reference material	Diclofenac	Diclofenac $^{13}C_6$
Purity (%)	99.9	99.9
Water (%)	n/a	19.9
Chemical form correction factor	0.9309	0.9291
Correction factor	**0.9300**	**0.7432**

Working solutions of analyte and internal standard were prepared freshly before use by successive dilutions from stock solutions to appropriate levels, using acetonitrile/water 50/50 (w/w) as solvent. They were used for spiking human plasma used for calibrators and QC samples preparation.

Calibrators and QC samples preparation

To 400 µl of blank human plasma, 50 µl of spiking solution of analyte and 50 µl of spiking solution of internal standard were added in polypropylene tubes, to yield final concentrations of 3.89, 11.11, 44.44, 138.88, 388.86, 666.62, 944.38, 1194.37 ng/ml for diclofenac.

Sample preparation (workup)

To precipitate plasma proteins, 2 ml of methanol (containing 5 ml of 25% HCl/2.5 L) was added to the spiked samples, then vortexed for 10 minutes at 1500 rpm. Further the samples were centrifuged at 4 °C for 10 minutes at 4000 rpm. 500 µl of supernatant was transferred to HPLC autosampler vials diluted with 200 µl of water and injected into the analytical system (25 µl/sample).

Calibration curve parameters

The linearity of the method was evaluated using spiked plasma samples in the concentration range mentioned above using the method of least squares. Three linearity curves were analyzed.

Each calibration batch (curve) consisted of: blank samples in duplicate, zero samples (blank with IS) in duplicate and eight non-zero concentration levels, of which the lower and upper limit of quantitation samples were in duplicate. The calibration curves were obtained by using a linear weighted (1/x) regression analysis of the peak area ratio (analyte/internal standard) versus the nominal concentration of the calibration standards. Study samples concentrations were obtained by interpolation from the calibration curve.

The linearity results are summarized in Table 2 in the ‘Results and Discussion’ section.

ACKNOWLEDGMENTS

This work was performed using private funding of S.C KYNETYX HT SRL.

REFERENCES

1. *https://www.rxlist.com/voltaren-drug.htm#description:* ***Voltaren*** *(diclofenac sodium) Enteric-coated tablets; Viewed: 02.04.2019).*
2. B. Hinz, J. Chevts, B. Renner, H. Wuttke, T. Rau, A. Schmidt, I. Szelenyi, K. Brune, U. Werner, *Br. J. Clin. Pharmacol.*, **2005**, *59*, 80.
3. C. Chen, S. Bujanover, S. Kareht, A.M. Rapoport, *Headache*, **2015**, *55*, 265.
4. C.M. Adeyeye, Pui-Kai Li, Diclofenac Sodium in Analytical Profiles of Drug Substances, **1990**, *19*, 123-144.
5. J.F. Standing, R.F. Howard, Atholl Johnson, I. Savage, I.C.K. Wong, *Br.J. Clin. Pharmacol.*, **2008**, *66*, 846.
6. N.M. Idkaidek, G.L. Amidon, D.E. Smith, N.M. Najib, M.M. Hassan, *Biopharm. Drug Dispos.*, **1998**, *19*, 169.
7. B. Testa, S.D. Krämer, *Chemistry & Biodiversity*, **2009**, *6*, 651.
8. X.-J. Zhai, Y. Yu, F. Chen, Y.-N. Lu, *Curr. Ther. Res.*, **2013**, *75*, 53.
9. J.S. Lill, T. O'Sullivan, L.A. Bauer, J.R.H. Horn, R. Carithers Jr., E. Strandness, H. Lau, K. Chan, K. Thakker, *J. Clin. Pharmacol.*, **2000**, *40*, 250.
10. J.-L. Kienzler, M. Gold, F. Nollevaux, *J. Clin. Pharmacol.*, **2010**, *50*, 50.
11. EMEA/CHMP/EWP/192217/2009 Rev. 1 Corr. 2** Guideline on validation of bioanalytical method, 21 July 2011 (Updated 03/06/2015).

STUDIA UBB CHEMIA, LXIV, 2,Tom I, 2019 (p. 265-277)
(RECOMMENDED CITATION)
DOI:10.24193/subbchem.2019.2.22

Dedicated to Professor Florin Dan Irimie on the Occasion of His 65th Anniversary

SPECTROPHOTOMETRIC DETERMINATION AND ASSESSMENT OF POTENTIAL HEALTH RISK OF NITRITE FROM MEAT AND PROCESSED MEAT PRODUCTS

DORINA CASONI[a,b*], REBECCA ROXANA BADIU[a], TIBERIU FRENŢIU[b]

ABSTRACT. Nitrite content was determined in fresh meat of chicken and pork and in different processed meat products such as sausages, salami, ham and pate with declared and not declared nitrite addition. The spectrophotometric method based on diazo-coupling reaction was used. Under the optimum working conditions, the method showed a limit of detection of 0.4 mg kg^{-1} and a limit of quantification of 1.2 mg kg^{-1}. The method proved to be accurate with nitrite recovery of 98±14% from spiked samples. In the analyzed samples the nitrite content was in the range 1.1±0.1 to 26.4±2.5 mg Kg^{-1}, values that are below the maximum admitted level of nitrite in meat products (150 mg Kg^{-1}). The lowest nitrite concentration was found in chicken meat products (between 1.1±0.2 and 1.8±0.1 mg kg^{-1}) while in salami, ham and sausages products the content was high (26.4±2.5; 19.0±0.7 and 13.4±1.1 respectively). The health risk exposure parameters were between 4% and 94 % and between 2% and 50% from established Acceptable Daily Intake (ADI of 0.07 mg/kg body weight/day) in case of adults and children respectively. Higher values correspond to pork meat products as salami, sausages and ham. The risk exposure to nitrite estimated for occasional consumption of meat products proved to be much more informative than the nitrite concentration. For these products consumption should be limited to 150-300 g per week. Non-carcinogenic health effects, evaluated based on Target Hazard Quotient (THQ) were revealed for the investigated meat products by occasional consuming of 3 serving/week.

Keywords: *nitrite, meat products, UV/Vis spectrophotometry, risk exposure assessment*

[a] *Babeş-Bolyai University, Faculty of Chemistry and Chemical Engineering, Chemistry department, 11 Arany Janos str., RO-400028, Cluj-Napoca, Romania*

[b] *Research Center for Advanced Chemical Analysis, Instrumentation and Chemometrics – ANALYTICA, Babeş-Bolyai University 11 Arany Janos str., RO-400028, Cluj-Napoca, Romania*

** Corresponding author: dcasoni@chem.ubbcluj.ro*

INTRODUCTION

The salts of nitrite and nitrate are commonly added to perishable food products especially for their preservation and also to help hinder the growth of harmful microorganisms as in particular Clostridium botulinum (the bacterium responsible for botulism) [1-3]. The safety of their use has been contested especially because of toxicological aspects related to oxidation of hemoglobin to methemoglobin a compound incapable of transporting oxygen in the blood [4]. Moreover, dietary nitrites can form carcinogenic nitrosamines under acidic conditions or during food processing procedures [5-9]. As concern in this field, the Joint Expert Committee of the Food and Agriculture Organization (JECFA) / World Health Organization (WHO) established an Acceptable Daily Intake (ADI) of 0.07 mg nitrite kg^{-1} of body weight that appears to be safe for healthy neonates, children and adults [10].

It is well known that water and leafy vegetables are natural sources of dietary nitrate whereas cured meats are the major sources of dietary nitrite [11-13]. The use of nitrite in certain foodstuffs and meat products has been periodically regulated by European Comission (EC) and European Food Safety Authority (EFSA) [14-18]. In meat industry potassium nitrite (E249) and sodium nitrite (E250) are permitted additives with anti-microbial action, preservation effect, red color fixation and beneficial effect on flavour [19,20]. According to the European Comission Directive 95/2/EC their maximum amount in manufactured meat products is 150 mg Kg^{-1} [21]. Methods based on different analytical techniques, such as spectrophotometric, electrochemical, chromatographic, chemiluminescent, capillary electrophoresis and electrochemiluminescent methods have been reported for detection and determination of nitrite [22]. Though new methods have been published in the last years [23-25], the spectrophotometric ones are by far the most widely used for nitrite determination due to its simplicity and inexpensive analytical feasibility. These methods are mainly based on the reaction (diazotization or nitrosation) of nitrite with some detecting reagents and determination of nitrite concentration based on the absorbance measurement of the reaction product.

Based on sufficient evidence in humans that the consumption of processed meat causes colorectal cancer, the WHO's International Agency for Research on Cancer (IARC) classified in 2015 the consumption of processed meat as carcinogenic to humans (Group 1) [26]. However, the packaging information table of meat products does not contain relevant data on nitrate/nitrite content. In the best case the consumers are informed if the nitrite was added or not in certain meat products. As concern in the field, there is an emergent need to investigate the nitrite level in commercially available fresh meat as well as in processed meat products. The health risk exposure associated with their consumption should be evaluated especially for those products that are frequent consumed in the usually diet.

Based on these considerations, it was proposed to evaluate the nitrite risk exposure parameters in order to find which is more suggestive for the consumers. Thus, the aim of this paper was determination of nitrite content in meat based products and evaluation of the health risk exposure arising from usual consumption. For this study, spectrophotometric method based on Griess assay procedure was used. Fresh meat of chicken and pork and related sausages, salami, ham and pate processed meat products were taken into consideration. The health risk exposure arising from their usual consumption was evaluated both for adults and children for individual categories of meat products based on Acceptable Daily Intake (% ADI) and target hazard quotient (THQ) determination.

RESULTS AND DISCUSSION

Method performance and validation characteristics

Under the optimal working conditions, the calibration curve generated over the range 0-0.80 mg L^{-1} nitrite in the spectrophotometric assay had the correlation coefficient of 0.9999. The limit of detection and limit of quantification for nitrite were 0.4 mg kg^{-1} and 1.2 mg kg^{-1} respectively. Thus the proposed method is suitable for nitrite determination in fresh meat and processed meat products since the detection limit is 405 times lower than the current maximum concentration of 150 mg kg^{-1} admitted in meat products [16, 17], while the quantification capabilities are 135 fold lower.

The results for spiked samples of processed meat products, analyzed to check method accuracy, are presented in Table 1.

The developed methodology for nitrite determination provided good accuracy with an average recovery in the range 98±14%, consistent with the AOAC recommendations [27], namely 75-120% for 95% confidence level.

Table 1. Nitrite recovery in spiked samples

Sample name	*Nitrite (mg Kg^{-1})				Recovery (R±CI) (%)	Average recovery (R±CI) (%)
	Determined in original sample (C±CI)	Added (C_a)	Determined in spiked sample (C_s±CI)	Found C_a (C_{af}±CI)		
Salami	3.45±0.40	5.30	8.60±0.60	5.16±0.72	97±14	98±14
Sausage	12.54±0.56	5.30	17.60±0.50	5.06±0.75	95±15	
Pork ham	22.10±0.47	5.30	27.47±0.44	5.37±0.64	101±12	

* Mean values of five parallel samples; CI - is confidence interval for 95% confidence level (n=5)

Sample analysis and health risk exposure assessment

The results of nitrite determination in commonly consumed fresh meat and processed meat products are presented in Table 2.

Table 2. Nitrite concentration in meat and processed meat products

Sample no.	Sample Name / code	Declared content		Nitrite content (mg kg^{-1})	
		Kind of meat	Added nitrite	RSD (%)	Mean value (±CI)
1	Sausage (C)	pork	No	11.2	13.4±1.1
2	Sausage (D)	pork/beef	No	8.1	3.8±0.2
3	Sausage (D)	pork	No	5.7	2.8±0.1
4	Sausage (D)	pork/beef/horse	No	0.8	2.5±0.1
5	Salami (A)	pork	Yes	13.4	26.4±2.5
6	Salami (E)	pork	Yes	0.9	6.6±0.1
7	Salami (E)	pork	Yes	3.6	3.6±0.1
8	Salami (E)	pork	Yes	13.6	3.1±0.3
9	Pork ham (B)	pork	No	5.0	19.0±0.7
10	Pork meat (F)	pork	No	4.9	1.2±0.1
11	Chicken breast (G)	chicken	No	1.2	1.6±0.1
12	Chicken pulp (G)	chicken	No	3.6	1.1±0.1
13	Chicken pulp (G)	chicken	No	2.6	1.2±0.1
14	Chicken liver (G)	chicken	No	1.1	1.8±0.1
15	Chicken pate (G)	chicken	Yes	0.5	5.5±0.1
16	Chicken pate (G)	chicken	No	5.7	1.4±0.1
17	Goose pate (G)	goose/chicken	No	2.7	1.1±0.2
18	Pork pate (F)	pork	Yes	0.9	3.4±0.2
19	Pork pate (F)	pork	No	4.0	1.5±0.4
20	Pork pate (F)	pork /chicken	No	0.5	3.7±0.1

A, B, C – samples with high content of nitrite; D – samples of sausages with similar nitrite content; E – samples of salami with similar nitrite content; F – samples of pork meat and pork pate with similar nitrite content; G – samples of chicken meat (breast, pulp and liver) and chicken pate with similar nitrite content; RSD - Relative standard deviation (%); CI - Confidence Interval for 95% confidence level (n=5)

In all the analyzed samples the nitrite content was below the maximum admitted concentrations established by European Commission Regulations in meat products [17, 21]. The obtained results were evaluated considering as individual group each of the meat products category. For some of the meat products categories, the samples were divided into sub-groups based on

t-test results for 95% confidence level used to compare the mean nitrite content of the group with the individual values in the same group. Samples with significantly high content of nitrite ($p < 0.05$) such as kind of salami, pork ham and kind of sausages were considered separately and noted in the Table 2 with (A), (B) and (C) respectively. The pork meat products as sausages and salami in which the nitrite content was not significantly different from mean value were considered as groups and noted with (D) and (E) respectively. Using the same principle, pork meat and pork meat pate was considered as one group and noted with (F) while chicken meat (breast, pulp and liver) and chicken pate the group noted with (G).

The highest nitrite concentration was observed in salami (A), pork ham (B) and sausage (C) with values of 26.4±2.5 mg Kg^{-1}, 19.0±0.7 mg Kg^{-1} and 13.4±1.1 mg Kg^{-1} nitrite respectively (Figure 1). In other processed pork meat products such as salami (E), sausage (D) and pate (F) the nitrite content was lower with values in the range 3.1±0.3 and 6.6±0.1, 2.5±0.1 and 3.8±0.2, and 1.5±0.4 and 3.7±0.1 respectively.

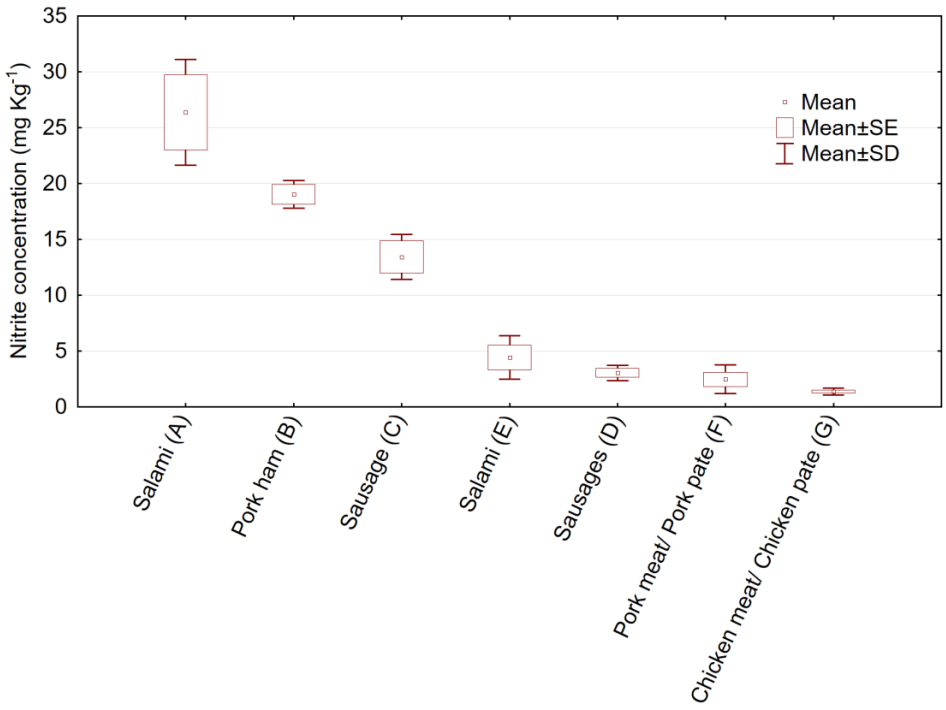

Figure 1. Nitrite concentration in categories of meat products (mg kg^{-1}, mean values / category of products)

The lowest nitrite concentrations were observed in chicken meat samples where the nitrite ranged from 1.1±0.1 to 1.8±0.1 mg Kg^{-1} with exception of one type of pate sample (5.5±0.1 mg Kg^{-1} nitrite) with declared added nitrite.

Thus, it can be concluded that the highest amount of nitrite was found in processed pork meat products, mainly salami, sausages and ham, while the lowest amount was found in fresh meat and pate of pork and chicken. Similar results were reported also in literature [25, 28].

As concern in food safety investigations, the danger of food nitrite still gives rise to debate in the scientific community. Recently new analysis methods were developed and new parameters were proposed for the evaluation of risk exposure to nitrite [29-31]. Rather than the nitrite concentration, %ADI would be more informative, since ADI was established based meat products consumption and nitrite concentration. According to data in Figure 2, the daily consumption of a portion of 150 g/20 g of meat products by a 60 kg adult/15 kg child body weight respectively, pose no health risk of exposure since the %ADI value are not exceeded in any of the cases.

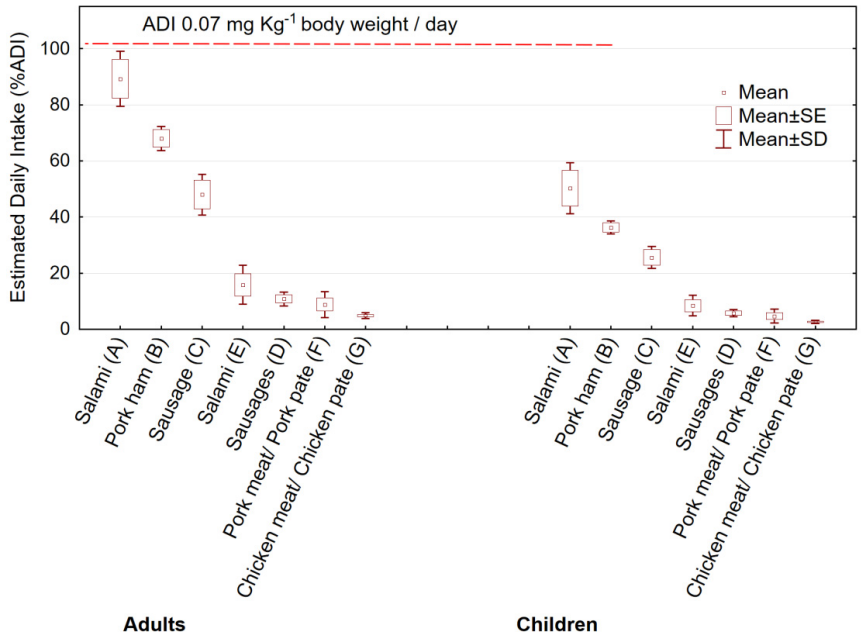

Figure 2. Daily risk exposure to nitrite via occasional consumption of a portion of 150 g meat product/day for a 60 kg body weight (bw) adult and 20 g meat product for a 15 kg body weight (bw) child, considering the current Acceptable Daily Intake (ADI) of 0.07 mg kg^{-1} body weight (bw)/day

It is important to note that processed pork meat products such as kind of salami (A), sausage (C) and pork ham (B) bring the highest values for %ADI being in the range 47-94% and 25-50% of nitrite ADI for adults and children respectively. These meat products with high nitrite content would be consumed with prudence. In these cases the weekly consumption should be limited to 150-300 g for adult which means 1-3 serving per week. The situation is also risk-free for children when consuming 40-150 g meat products, corresponding to 1-4 servings per week.

Other processed pork meat products such as salami (E) and susage (D) had lower %ADI values within the range 9-24% and 4-13% of nitrite ADI for adults and children respectively. For these products the weekly resk-free consumption is 600-900 g for adult and they could be daily consumed.

It is interesting to note that lowest %ADI were found for pork meat / pork pate (F) and chicken meat/chicken pate (G) products that have similar values within the range 4-13% and 2-7% for adults and children respectively. Thus for commercially available unprocessed meat and pate products from pork and chicken there is no health risk from exposure to nitrite and practically can be unlimited consumed.

From the carcinogenic point of view, the THQ parameter is more suggestive for nitrite risk exposure evaluation. According to data from Figure 3, for all of the investigated meat products non-carcinogenic effects are expected considering an exposure duration of 70 years with an average serving of 150 g for a 70 kg (bw) and an exposure frequency of 156 days (about 3 serving/week). It can be also observed that chicken meat and chicken products exhibits the lowest risk of exposure to nitrite.

CONCLUSIONS

The results of nitrite determination in commercially available fresh meat and processed meat products from pork and chicken revealed a nitrite concentration below the current maximum admitted limit established by European Comission Reglations at 150 mg kg^{-1}.

The highest nitrite concentration was found in pork processed meat products such as salami, sausages and ham, and some of these products should be consumed with prudence of 1-3 serving/week.

For unprocessed meat of chicken and pork there is no risk of exposure to nitrite and they could be practically unlimited consumed.

Non-carcinogenic health effects are expected by considering a consumption average of 3 serving/week.

The study highlighted that the risk assessment based on %ADI parameter is more suggestive. In order to better inform the consumer, %ADI values for a meal of 150/20 g for an adult/child would be provided in the table information on the packaging of the meat products.

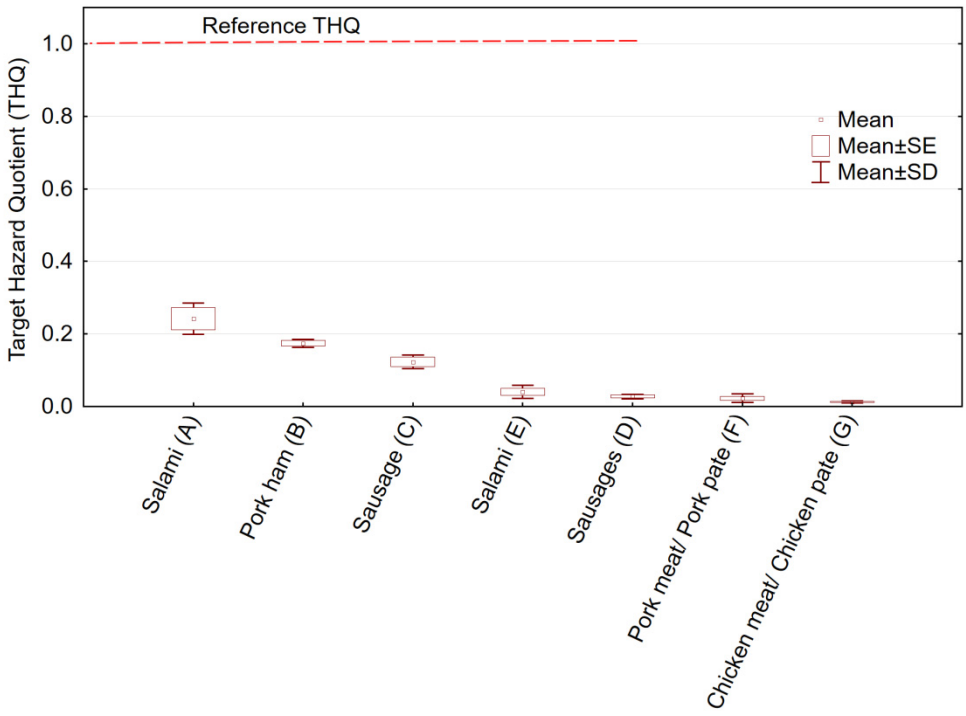

Figure 3. The health risk exposure to nitrite by occasional consumption of meat products (THQ - Target Hazard Quotient - calculated considering the exposure frequency to nitrite of 156 days, exposure duration of 70 years and an average serving of 150 g for a 70 kg (bw))

EXPERIMENTAL SECTION

Chemicals and solutions

All the chemicals were of analytical grade. Sodium nitrite ($NaNO_2$), sodium tetraborate (borax, $Na_2[B_4O_5(OH)_4]\cdot 10H_2O$), potassium hexacyanoferrate (II) ($K_4[Fe(CN)_6]$, zinc acetate ($Zn(CH_3COO)_2\cdot 2H_2O$), sulfanilic acid ($C_6H_7NO_3S$) , α-naphthylamine ($C_{10}H_9N$), glacial acetic acid (CH_3COOH) and sodium chloride (NaCl) were from Sigma-Aldrich (Steinheim, Germany).

For proteins precipitation solutions of potassium hexacyanoferrate II 10.6 % (m/V) in distilled water, zinc acetate 22% (m/V) in 3% acetic acid solution and borax 5% (m/V) in distilled water at 40-50°C were freshly prepared.

Griess reagent was freshly prepared as a mixture of equal volumes of sulfanilic acid solution with α-naphthylamine solution. For the preparation of sulfanilic acid solution 6.00 g of sulfanilic acid were dissolved in 200 mL

glacial acetic acid and 100 mL distilled water by heating on a water bath. After cooling, 200 mL of 10% (m/V) sodium chloride was added and the solution was diluted to 1000 mL with distilled water. The α-naphthylamine solution was prepared by dissolving 0.30 g of α-naphthylamine hydrochloride in 100 mL hot water. After cooling, 200 mL glacial acetic acid were added and the resulted solution was diluted to 1000 mL with distilled water.

Stock nitrite solution (4 mg/L) was obtained by dissolving appropriate quantity of sodium nitrite standard in distilled water.

Analytical procedure and equipment

For the spectrophotometric determination of nitrite in meat samples a modified version of Shinn method which is based on the Griess-Ilosvay diazo-coupling reaction was used [32]. The principle of the applied method is based on the ability of nitrite to react with sulfanilic acid in acidic medium to form a diazonium salt then coupling the diazotized sulfanilamide with 1-naphthylamine forming an intensely pink azo-dye [33] that can be determined by spectrophotometric measurements.

The absorbance measurement was carried out at λ=520 nm using T80 UV-Vis double beam Spectrophotometer (PG Instruments Ltd., Lutterworth UK).

Sample preparation and method development

Working standard solutions with a concentration from 0.08 to 0.80 mg/L nitrite were freshly prepared by adding 10 mL of Griess reagent to appropriate volume of stock solution and diluted to 50 mL with distilled water. The reagent blank was prepared by dilution of 10 mL of Griess reactive to 50 mL with distilled water but in absence of nitrite.

The fresh and processed meat products samples were treated according to the AOAC method (AOAC, 1980, technique number 24.041) and ISO 2918:1975 procedure (reference procedure) recommended by the International Standard Organization reviewed and confirmed as current reference version in 2018. This method is based on extraction of sample in a hot water bath followed by reaction of nitrite with sulfanilamide and N-(1-naphthyl) ethylenediamine dihydrochloride to form a pink dye whose absorbance is measured. According to recommended procedure, portion of 10.00 g of each grounded sample have been subjected to extraction with 100 mL hot water at 80°C and 5 mL borax in a 200 mL volumetric flask for 15 minutes using a water bath. After the sample cooling, the precipitation of proteins was made by addition of 2 mL of potassium hexacyanoferrate (II) and 2 mL of zinc acetate stirring after each addition for 15 minutes. The sample was diluted to 200 mL volumetric flask and filtered. In each case 10 mL of Griess reagent was

added over a 30 mL portion of the filtrate and diluted to 50 mL volumetric flask with distilled water. Resulted solutions were well homogenized and let for 15 minutes in a dark place at room temperature for complete reaction and formation of red-pink dye complex. The absorbance was measured at 520 nm. Five parallel samples were subjected to extraction procedure and replicate portions of 30 mL were prepared for Griess reagent reaction.

Assessment of method performance

For the method accuracy evaluation, meat products samples with low, medium and high level of nitrite content were spiked by adding 5.30 mg kg^{-1} nitrite in each sample and run through the whole extraction process as described above.

The spectrophotometric method was characterized in terms of limit of detection (LOD), limit of quantification (LOQ), precision and accuracy under the optimal working conditions. The LOD was calculated according to the $3S_{y/x}/m$ criterion (eq. (1)):

$$LOD = \frac{3S_{y/x}}{m} \quad (1)$$

where ($S_{y/x}$) is the residual standard deviation and (m) the slope of the calibration curve [34].

The LOD value was related to mass based on the sample preparation protocol while LOQ was calculated as 3xLOD.

The precision of the method as relative standard deviation (RSD) was estimated from confidence interval values for n=5 parallel samples.

Health risk assessment

The risk exposure to nitrite via occasional consumption of meat based products was evaluated accordingly with the Daily Intake (DI) estimation (eq. (2)):

$$DI = \frac{C \times m_s}{bw} \quad (2)$$

were *C* is the concentration of nitrite in meat product (mg Kg^{-1}), m_s is the amount of consumed meat product/one serving considered 150 g for adult and 20 g for child and *bw* is body weight considered as 60 kg for adult and 15 kg for child respectively.

The corresponding daily risk exposure to nitrite (%ADI) [35] was calculated as percent of Acceptable Daily Intake of 0.07 mg kg^{-1} bw (recommended ADI) [10] (eq. 3):

$$\%ADI = \frac{100 \times DI}{0.07} \quad (3)$$

The non-carcinogenic health risk posed by exposure to nitrite was evaluated based on the Target Hazard Quotient (THQ) parameter defined as the ratio of exposure to a toxic compound and the reference dose which is the highest level at which no adverse health effects are expected (eq. (4)).

$$THQ = \frac{E_{FR} \times E_d \times F_{IR} \times C}{RfD \times BW_a \times AT_n} \times 10^{-3} \quad (4)$$

where E_{FR} is the exposure frequency to nitrite (considered 156 days equivalent with about 3 serving/week)), E_d is the exposure duration (70 years), F_{IR} is the meat product ingestion rate (an average serving of 150 g/day), C is the concentration of nitrite in meat product, RfD is the oral reference dose of nitrite (0.07 mg Kg^{-1} bw/day), BW_a is the reference body weight (70 kg bw), AT_n is the averaged exposure time (365 days x 70years) and 10^{-3} is the unit conversion factor [36].

ACKNOWLEDGMENTS

This work was supported by a grant of Ministry of Research and Innovation, Romania, project number 33PFE/2018, within PNCDI III.

REFERENCES

1. D.L. Archer, *Journal of Food Protection*, **2002**, *65*, 872.
2. M. Armenteros, M.C., Aristoy, F. Toldrá, *Meat Science,* **2012**, *91*, 378.
3. M.P. Richards, *Antioxidants & Redox Signaling, **2013**, 18*, 2342.
4. P. Santamaria, *Journal of the Science of Food and Agriculture*, **2006**, *86*, 10.
5. A. Milkowski, H.K. Garg, J.R. Coughlin, N.S. Bryan, *Nitric Oxide- Biology and Chemistry,* **2010**, *22*, 110.
6. N.S. Bryan, D.D. Alexander, J.R. Coughlin, A.L. Milkowski, P. Boffetta, *Food and Chemical Toxicology*, **2012**, *50*, 3646.
7. M. Reinik, T. Tamme, M. Roasto, K. Juhkam, S. Jurtšenko, T. Tenńo, A. Kiis, *Food Additives and Contaminants,* **2005**, *22*, 1098.

8. S. Andrée, W. Jira, K.H. Schwind, H. Wagner, F. Schwägele, *Meat Science,* **2010**,*86*, 38.
9. 16. A. Cockburn, C.W. Heppner, J.L.C.M. Dorne, *Encyclopedia of Food Safety*, **2014**, *2*, 332.
10. FAO/WHO. Joint FAO/WHO Expert Committee on Food Additives, Summary and Conclusions of the Fifty-ninth Meeting; 2002 Jun 4–13; Geneva, World Health Organization, Geneva, 2002
11. A.A. Chetty, S. Prasad, *Food Chemistry,* **2009**, *116*, 561.
12. J. Hsu, J. Arcot, N.A. Lee, *Food Chemistry,* **2009**,*115*, 334.
13. A.H. Adam, N.E. Mustafa, I.M. Rietjens, *Food Additives and Contaminants, Part B Surveillance*, **2017**, *10,* 79.
14. European Commission. (2006). Commission Regulation (EC) No. 1882/2006 of 19 December 2006, laying down methods of sampling and analysis for the official control of the levels of nitrates in certain foodstuffs. *Official Journal of the European Union, L363*, 25.
15. European Commission. (2008). Regulation (EC) no 1333/2008 of the European Parliament and of the council of 16 December 2008 on food additives. *Official Journal of the European Union*, L354, 16.
16. European Commission. (2011). Regulation (EC) no 1129/2011 of the European Parliament and of the council of 12 November 2011 amending annex II to regulation (EC) no 1333/2008 of the European Parliament and of the council by establishing a union list of food additives. *Official Journal of the European Union*, L295, 1.
17. European Commission. (2014). Regulation (EC) no 601/2014 of the European Parliament and of the council of 4 June 2014 amending annex II to regulation (EC) no 1333/2008 of the European Parliament and of the council as regards the food categories of meat and the use of certain food additives in meat preparations. *Official Journal of the European Union*, L166, 11.
18. EFSA. (2010). EFSA panel on food additives and nutrient sources added to food (ANS); Statement on nitrites in meat products. *EFSA Journal*, *8*, 1538.
19. W. Bedale, J.J, A.L. Milkowski, *Meat Science*, **2016**, *120*, 85.
20. H.S. Lee, *Food Additives & Contaminants: Part A,* **2018**, *35,* 29.
21. European Commission. (1995). European Parlament and council directive No 95/2/EC of 20 February 1995 on food additives other than colours and sweeteners, *Official Journal of the European Union, L61*, 18.3.
22. Q.-H. Wang, L.-J. Yu, Y. Liu, L. Lin, R.-gang Lu, J.-ping Zhu, L. He, Z.-L. Lu, *Talanta*, **2017**, *165*, 709.
23. C. Lopez-Moreno, I.V. Perez, A.M. Urbano, *Food Chemistry,* **2016**, *194*, 687.
24. Z. Kalaycıoğlu, F.B. Erim, *Food Analytical Methods*, **2016**, 9, 706.
25. F. Della Betta, L. Morilla Pereira, M. Araújo Siqueira, A. Camargo Valese, H. Daguer, R. Fett, L. Vitali, A. C. Oliveira Costa, *Meat Science*, **2016**, 119, 62.
26. International Agency for Research on Cancer (2015). IARC Press release no 240.
27. AOAC. (2002). Standard Format and Guidance for AOAC Standard Method Performance Requirement (SMPR) Documents (Version 12.1; 31-Jan-11).

28. I. Tomasevic, M. Dodevska, M. Simić, S. Raicevic, V. Matovic, I. Djekic, *Meat Science*, **2017**, *134*, 76.
29. A.A. Chetty, S. Prasad, O. Castro Pinho, C. Medeiros de Morais, *Food Chemistry*, **2019**, *278*, 630.
30. H. Mejborn, M. Hansen, A. Biltoft-Jensen, T. Christensen, K.H. Ygil, P.T. Olesen, *Meat Science*, **2019**, *147*, 91.
31. S.M. Abdel Azeem, M.D. Madbouly, M.F. El-Shahat, *Journal of Food Composition and Analysis*, **2019**, In Press: https://doi.org/10.1016/j.jfca.2019.05.003
32. F. Van Staden, T. Vande Merwe, *South African Journal of Chemistry*, **1998**, *51*, 109.
33. T. Frentiu, A.C. Mot, E. Covaci, "Instrumental methods for analysis. Applications" (in Romanian), Cluj University Press, Cluj-Napoca, **2019**, chapter 5.
34. J.N. Miller, J.C. Miller, "Statistics and Chemometrics for Analytical Chemistry (4th ed.)", Pearson Education Ltd., Edinburgh Gate, England, 2000.
35. E. Covaci, M. Senilă, M. Ponta, E. Darvasi, M. Frentiu, T. Frentiu, *Food Control*, **2017**, *82*, 266.
36. J.M.R. Antoine, L.A. Hoo Fung, C.N. Grant, *Toxicology Reports*, **2017**, *4*, 181.

STUDIA UBB CHEMIA, LXIV, 2,Tom I, 2019 (p. 279-288)
(RECOMMENDED CITATION)
DOI:10.24193/subbchem.2019.2.23

Dedicated to Professor Florin Dan Irimie on the Occasion of His 65th Anniversary

DIELECTRIC SPECTROSCOPIC EVALUATION IN THE EXTREMELY LOW FREQUENCY RANGE OF AN ASPERGILLUS NIGER CULTURE

MÓNIKA LINGVAY[a,b], ALINA-RUXANA CARAMITU[c], ADRIANA-MARIANA BORȘ[d*], IOSIF LINGVAY[c]

ABSTRACT. By using the dielectric spectroscopy technique in the extremely low frequency (1–200Hz) range, dielectric loss *tg*δ was determined on both *Aspergillus niger* cultures in different growth stages and autoclaved biomass compared to the Czapex-Dox culture medium with sterile sucrose.

Experimental results have shown that living and sterile matter samples have different dielectric characteristics. In sterile probes, the evolutionary functions of tg*δ* depending on frequency are continuous, specific to α-relaxation governed by DC electrical conductivity. In living matter samples, the function of dielectric losses *tg*δ, depending on frequency, show several discontinuities that indicate the existence of some processes in which, at those frequencies, the number of charge carriers from investigated living matter is changing. It has also been found that the package of active processes differs depending on the growth stage of *Aspergillus niger*.

Keywords: *ELF electromagnetic fields, dielectric loss, relaxation dynamics, α-relaxation, fungi*

[a] *Babeş-Bolyai University, Faculty of Chemistry and Chemical Engineering, 11 Arany János str., RO-400028, Cluj-Napoca, Romania*
[b] Present affiliation: *University of Szeged, Faculty of Science and Informatics, Doctoral School of Physics, 9 Dóm tér, H-6720, Szeged, Hungary*
[c] *National Institute for Research and Development in Electrical Engineering INCDIE ICPE-CA, 313 Splaiul Unirii, RO-030138, Bucharest, Romania*
[d] *ICPE SA, 313 Splaiul Unirii, RO-030138, Bucharest, Romania*
** Corresponding author: adrianambors@gmail.com*

INTRODUCTION

In the perspective of sustainable development, ensuring healthy working and living conditions is a priority issue [1]. At present day, an essential condition for the quality of human life is to provide the necessary electricity.

The production, transmission / distribution and use of electricity involves generation of electromagnetic fields (EMF) which, by AC (alternating current) polarization, on the one hand, influence the mechanism and kinetics of the natural bioelectrochemical processes [2] specific to the living matter and, on the other hand, accelerate corrosion and / or material degradation processes (both oxide [3] and polymeric [4]) from the buildup media [5-8].

Research studies have shown that, depending on their intensity and frequency, EMF can modify certain biochemical processes and thus have an influence on the behavior of living matter [9-19] exposed to EMF of anthropogenic origin. Findings have shown that the EMF influences on the living matter are largely influenced by the experimental conditions, namely the frequency and intensity of the applied EMF, the dielectric characteristics of the sample materials, the geometry of the experimental cells / bioreactors [20], etc. EMF of anthropogenic origin can influence the organisms, both in a positive (growth stimulation [15, 21, 22]) and negative way (inhibition of growth [21, 23]). Growth stimulating of microorganisms (bacteria, microalgae, fungi etc.) and plants in EMF can be a way of streamlining various biotechnological processes such as biofuel production from algae, biodegradation of waste, water purification [21, 22]—including those containing xenobiotic substances—, etc. On the other hand, one can notice that excessive increase of the applied electric field leads to membrane permeabilization and subsequent leakage of intracellular compounds [15, 24].

The effects of exposure to EMF on living matter are differentiated according to the frequency of the perturbative field. Thus, several studies have emphasized that 50 Hz EMF diminishes melatonin production, thus causing disturbances of circadian rhythm with consequences on the immune system and increasing the incidence of different cancers [25-27]. Furthermore, researchers have also highlighted their influences on human leukemia cell line HL-60 [28] and on the intramicrovascular leukocyte behavior in mice [29]. Further various effects of exposure to 50 Hz EMF on human cells have been reported in [30-35]. In [36, 37], various biological effects of high- and very high frequency EMF have been presented. Associations between EMF and immune and oxidative response have been found in people professionally exposed to EMF in the 140–160 MHz band [38]. Various biological effects, namely modifications in enzymatic activity [39], cellular proliferation of nucleated erythropoietic cells [40-42], oxidative stress [43, 44], etc., have been reported for EMF exposures in the radio frequency band. Also, a lot of studies have shown the harmful effects of mobile telephony on the human brain [45-48].

Relaxation dynamics of protein solutions involves changes of the dielectric permittivity and conductivity of the living matter. Studies on the dielectric characteristics of protein solutions have been reported since 1938 [49]. The dielectric spectroscopy method allows analysis of the dielectric characteristics' evolution of the materials, as a function of the frequency of the applied electric signal [50]. Thus, many authors have applied this technique for studying the dielectric relaxation in biological systems or protein solutions [11, 51-56]. From these studies, can be concluded that the relaxation phenomena are differentiated according to the frequency band, respectively in the 1–1000 MHz band dominating is the β-relaxation (relaxation of the proteins in aqueous environment), in 0.1–10 GHz band the δ-dispersion (relaxation of the protein-bound water molecules), and over 10 GHz the γ-dispersion (rotational diffusion of water dipoles).

Mass and electrical charge transport have fundamental significance for the function and activity of biological systems. Cellular electrical polar structures with energy supply (such as microtubules) can become excited and generate an endogenous electric field. Endogenous electric field can have dominant effect on directed transport of molecules and electrons such that the probability to reach the target is enhanced in comparison with random thermal motion [57]. It is noted that by overlapping an external EMF on the endogenous electric field of biological systems, the field resulting from the vectorial composition of these can influence (favourably or unfavourably) the cellular transport processes of molecules and electrons and, implicitly, the behaviour of the organism. In this context, the effect of a transmembrane AC field in the 1 Hz – 10 kHz range on the biochemical activity of a native yeast vacuolar proton-ATPase (V-ATPase) had been reported recently [58], where the externally applied field generally inhibited the enzyme's rotational activity, except for a region peaking around 86 Hz, at which frequency, the field was able to synchronize the steps of ion-pumping in individual enzymes via a hold-and-release mechanism. It has been experimentally found that the 50 Hz electric field stimulates the growth and reproduction (production of spores) of *Aspergillus niger* [15].

Thus, the aim of present study is to probe a biomass of *Aspergillus niger* filamentous fungi in different stages of growth on sucrose medium by dielectric spectroscopy technique.

Results and Discussion

Dielectric losses tgδ in the 1–200Hz range have been determined applying the method of dielectric spectroscopy.

The ε dielectric permittivity of the materials is a frequency-dependent complex parameter and is given by the relation (1):

$$\varepsilon(\omega) = \varepsilon' + j\varepsilon'' \tag{1}$$

where j represents the imaginary unit ($\sqrt{-1}$), and the value of the imaginary component ε'', is determined by the electrical conductivity of the material, given by the number and the charge carriers mobility (at given temperature). The dielectric loss tgδ is the ratio between the imaginary ε'' and the real ε' component of the dielectric permittivity of the materials and is directly proportional with the electrical conductivity of the material, respectively (2):

$$\mathrm{tg}\delta = \frac{\varepsilon''}{\varepsilon'} \tag{2}$$

Experimental determinations were performed on samples of sterile Czapex–Dox culture medium with sucrose (reference), from an *Aspergillus niger* culture after 36 hours and 84 hours of incubation, as well as from the sterilized resulting biomass.

The comparative determination's results are presented in Figure 1.

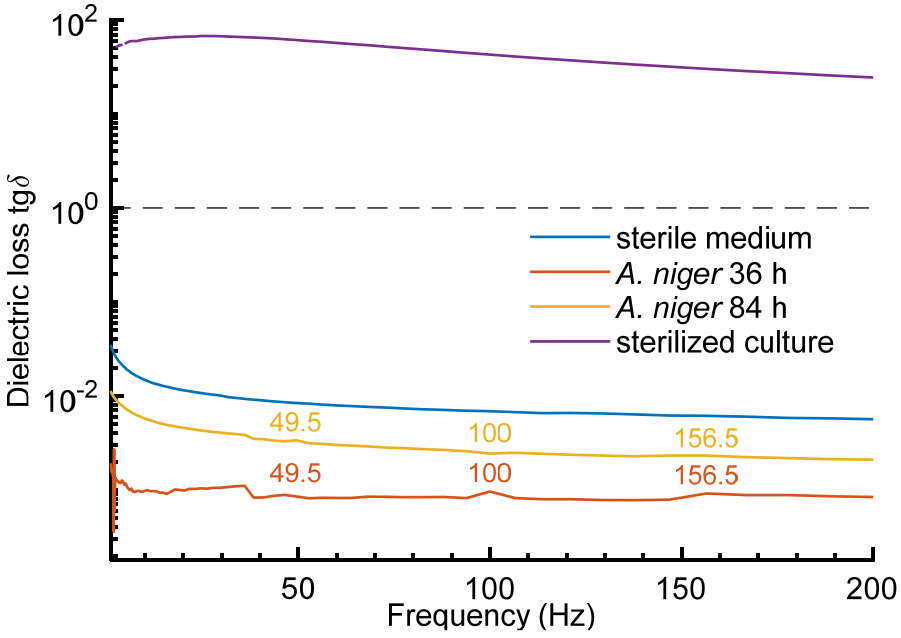

Figure 1. Dielectric losses of investigated samples

From the analyses of Figure 1 one can notice that the dielectric losses tgδ, both in the reference sample (blue curve) and in the incubated and sterilized sample (*Aspergillus niger* biomass in culture medium sterilized—violet curve) show a continuous evolution in function of frequency. Values smaller with about three order of magnitude obtained on the initial (reference) culture medium compared to those obtained on autoclaved biomass indicate that the number of charge carriers in the sample (and, implicitly, electrical conductivity) increases during the incubation (growth of *Aspergillus niger*). The number of charge carriers in the reference sample being given by the mineral salt content of the culture medium, this behaviour indicates that during the growth of *Aspergillus niger*, following the metabolism of sucrose, new electroconductive species were formed—such as proteins, which have a net-negative charge at neutral pH of cells, as well as the protons and anions of citric and oxalic acids formed by the metabolism of sucrose [14, 59].

By the comparative analysis of the dielectric behaviour of sterile samples (reference sample and autoclaved biomass) with those containing living matter (samples taken after 36 h—red curve—and 84 h of incubation—yellow curve), can be noticed that in the first 36 hours of growth tgδ decreases about tenfold relative to the reference sample, the decrease being less pronounced at 84 hours of incubation (about threefold). This behaviour can be explained by the fact that developing cells draw the necessary mineral ions from the culture medium to the cytoplasm across the plasma membrane—to maintain a relatively constant specific ionic composition of the cytosol—, reducing in this way the number of free charge carriers from the surrounding fluid and implicitly the electrical conductivity of the sample. The threefold increase of tgδ of the 84 h-sample compared to the 36 h-one is explained by the higher amount of charge carriers / metabolites formed during the growth of biomass and eliminated in the extracellular space. Under these conditions, the spectacular increase of tgδ following autoclaving (when disruption of bonds within cell walls and protein denaturation occurs) can be explained by “emptying” the intracellular space composition, together with dissociated inorganic salts and organic charged metabolites, into the extracellular space. The electrical conductivity of the sample is given by the total content of mineral salts and metabolic products originated from the cytoplasmic space.

Figure 1 shows a net-different dielectric behaviour of sterile samples (autoclaved medium and culture) from the living samples (36 h and 84 h of incubation). Unlike sterile samples, where tgδ evolution functions are continuous and specific to α-relaxation governed by DC electrical conductivity [50] in living matter samples these functions show discontinuities at certain frequencies (noticeable in Figure 1 and 2). These discontinuities indicate the presence of dynamic processes that are influenced at the respective frequencies by the electric field action generated by the measuring signal, so that the number of

charge carriers in the investigated matter changes. This kind of behaviour could be attributed to different transmembrane ion-transporting proteins—e.g. V-ATPase proton pumps, whose rotational rate can be determined by synchronizing the ion-pumping steps of individual enzymes with a transmembrane AC field [58]. Figure 2 shows the evolution of tgδ as function of frequency in the 1–60 Hz range (extension from Figure 1).

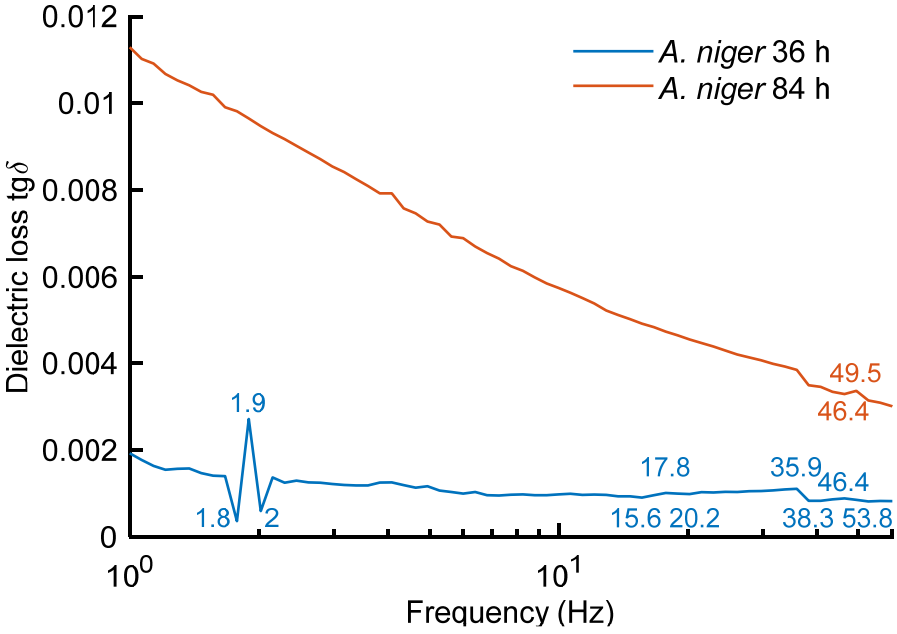

Figure 2. Dielectric losses of investigated samples with living matter

Analysing Figure 2 one can notice that in case of the 36 h-sample, beside the discontinuities from ~38.3, ~49.5, 100, and 156.5 Hz (with higher amplitude), those from 1.9 and 17.8 Hz can be also identified. This finding suggests that the package of proteins and enzymes operating at the early growth phase (formation of hyphae) and the phase of maturation growing stages of *Aspergillus niger* differ from each other at some extent, or several processes have different intensity at different times.

Under these conditions, it is very likely that by applying an external AC electric field it is possible to selectively control (stimulate/inhibit) the activity of proteins (especially ionic pumps) and implicitly the biochemical processes controlled by these. This aspect can explain both the stimulation of *Aspergillus niger* growth in the 50 Hz electric field [15], and the extremely low EMF effects reported [25-29].

CONCLUSIONS

By dielectric spectroscopy measurements in the 1–200Hz range, the dielectric loss tgδ was determined on both *Aspergillus niger* cultures in different growth stages and autoclaved biomass culture, compared to sterile medium (reference).

The experimental results have shown that samples with *Aspergillus niger* cultures had a different dielectric behaviour than sterile samples (culture medium and autoclaved biomass): for latter ones the evolution functions of tgδ are continuous, unlike samples of living matter, for which these functions have several discontinuities.

It has also been found that the processes performed in the first growing stage of the *Aspergillus niger* culture are different from those in the more advanced development stage (maturation).

These results suggest that an AC field with given frequency is able to selectively control the activity of several enzymes and other ion-transporting assemblies, which opens up the possibility of biotechnological exploitation.

EXPERIMENTAL SECTION

Sterile Czapex–Dox growth medium was prepared by autoclavation of 1000mL aqueous solution in which 30g sucrose, 2g $NaNO_3$, 0.7g KH_2PO_4, 0.3g K_2HPO_4, 0.5g KCl, 0.5g $MgSO_4 \times 7H_2O$, 0.01g $FeSO_4$, and 30g of Agar (for gelification) was dissolved. All reagents were of analytical grade and were purchased from Merck.

As inoculum, a suspension in basic mineral solution (about 10^6 spores/mL) of *Aspergillus niger* spores was used. Inoculated cultures were incubated in the dark for 84 h at 30 ± 2 °C, relative humidity 90 ± 5%.

Sterilization of the biomass grown on the culture medium was done by autoclavation for 30 min at 105 ± 3°C.

Growth medium samples were taken before inoculation (reference), after 36 h and 84 h of incubation, and after sterilization of the biomass, respectively.

Dielectric spectroscopic measurements in the 1–200Hz range were carried out using a 1296A Dielectric Interface System (Solartron Analytical / AMETEK Scientific Instruments, USA). Collected spectral data were analysed using the Spectr-O-Matic MATLAB® toolbox.

ACKNOWLEDGMENTS

The work was performed under contracts PN II no.100/2014 and 30PFE/2018 between National R&D Institute for Electrical Engineering ICPE-CA and Romanian Ministry of Research and Innovation (MCI).

REFERENCES

1. E.A. Stere, I. Popa; *Electrotehnica, Electronica, Automatica (EEA)*, **2018**, *66* (3), 125-136
2. I. Lingvay, C. Lingvay, A. Voina; *Rev. Roum. Sci. Tech. El.*, **2008**, *53* (2bis), 85-94
3. C. Lingvay, A. Cojocaru, T. Vişan, I. Lingvay; *U.P.B. Sci. Bull. Series B*, **2011**, *73* (4), 143-152
4. A. Caramitu, N. Butoi, T. Rus, A.M. Luchian, S. Mitrea; *Mat. Plast.,* **2017**, *54* (2), 331-337
5. I. Szatmari, M. Lingvay, L. Tudosie, A. Cojocaru, I. Lingvay; *Rev. Chim. (Bucharest),* **2015**, *66* (3), 304-311
6. I. Lingvay, M. Gabor, C. Lingvay, *Rev. Chim. (Bucharest),* **2006**, *57* (2), 180-183
7. I. Lingvay, C. Lingvay, C. Homan, O. Ciogescu; *Rev. Chim. (Bucharest),* **2006**, *57* (12), 1279-1282
8. I. Lingvay, A.M. Bors, D. Lingvay, L. Radermacher, V. Neagu; *Rev. Chim. (Bucharest)*, **2018**, *69* (12), 3593-3599
9. B. Yokus, M.Z. Akdag, S. Dasdag, D.U. Cakir, M. Kizil; *Int. J. Radiat. Biol.*, **2008**, *84* (10), 789-795
10. D. Sandu, I. Lingvay, S. Lányi, D.D. Micu, C.L. Popescu, J. Brem, L.C. Bencze, C. Paizs; *Stud. Univ. Babes-Bolyai, Chem.*, **2009**, *54* (4), 195-201
11. C. Stancu, M. Lingvay, I. Szatmári, I. Lingvay; *The 8th Int. Symp. on ATEE, Bucharest, Romania*, May 23-25, **2013**, 1-4
12. A.H. Hashish, M.A. El-Missiry, H.I. Abdelkader, R.H. Abou-Saleh; *Ecotoxicol. Environ. Saf.*, **2008**, *71*, 895-902
13. A. Amarolia, M.G. Chessaa, G. Bavestrello, B. Bianco; *Eur. J. Protistol.*, **2013**, *49*, 400-405
14. M. Gao, J. Zhang, H. Feng; *Bioelectromagnetics*, **2011**, *32*, 73-78
15. E. Radu, D. Lipcinski, N. Tănase, I. Lingvay; *Electrotehnica, Electronica, Automatica* (*EEA*), **2015**, *63* (3), 68-74
16. D.I. de Pomerai, B. Smith, A. Dawe, K. North, T. Smith, D.B. Archer, I.R. Duce, D. Jones, P. Candido; *IEEE Trans. Microw. Theory,* 2000, 48, 2076-2081
17. Y.J. Huang, J. Samorajski, R. Kreimer, P.C. Searson; *PLoS One*, 2013, 8 (3), e59447. DOI: 10.1371/journal.pone.0059447
18. S. Kwee, P. Raskmark, S. Velizarov; *Electro- Magnetobiol.*, **2001**, *20*, 141-152
19. T. Shigemitsu, K. Yamazaki, S. Nakasono, M. Kakikawa; *IEEJ Trans. Electr. Electron. Eng.*, **2007**, *2* (4), 405-412

20. M. Lingvay, L. Czumbil; *Electrotehnica, Electronica, Automatica* (*EEA*), **2014,** *62* (3), 84-89
21. R.W. Hunt, A. Zavalin, A. Bhatnagar, S. Chinnasamy, K.C. Das; *Int. J. Mol. Sci.*, **2009**, *10*, 4515-4558
22. J. Filipič, B. Kraigher, B. Tepuš, V. Kokol, I. Mandic-Mulec; *Bioresour Technol*. **2012**, *120,* 225-232
23. M. Racuciu, C. Iftode, S. Miclaus; *Rom. J. Phys.*, **2015**, *60* (3-4), 603-612
24. K. Aronsson, U. Rfnner, E. Borch, *Int. J. Food Microbiol.,* **2005**, *99*, 19-32
25. O. Hiwaki; *Engineering in Medicine and Biology Society*, *Proceedings of the 20th Annual International Conference of the IEEE*, 1998. DOI: 10.1109/IEMBS.1998.746203
26. Y. Touitou, B. Selmaoui; *Dialogues Clin Neurosci*. **2012**, *14* (4), 381-399
27. B. Lewczuk, G. Redlarski, A. Żak, N. Ziółkowska, B. Przybylska-Gornowicz, M. Krawczuk; *BioMed Res. Int.*, **2014**, ID 169459
28. D. Sztafrowski, Z. Wroblewski, M. Lukaszewicz, A. Sikorski, M. Majkowski; *10th EEEIC,* **2011**. DOI: 10.1109/EEEIC.2011.5874726
29. A. Ushiyama, Y. Suzuki, H. Masuda, S. Hirota, M. Taki, C. Ohkubo; Proceedings of *Radio Science Conference,* **2004** DOI: 10.1109/APRASC.2004.1422506
30. A.C. Mannerling, M. Simkó, K.H. Mild, M.O. Mattsson; *Radiat. Environ. Biophys.,* **2010**, *49*, 731-741
31. M.O. Mattsson, M. Simko; *Toxicology,* **2012**, *301*, 1-12
32. M. Lupke, J. Rollwitz, M. Simkó; *Free Radic. Res.,* **2004**, *38*, 985-993
33. M. Lupke, J. Frahm, M. Lantow, C. Maercker, D. Remondini, F. Bersani, M. Simkó; *Biochim. Biophys. Acta, **2006**, 1763*, 402-412
34. M.O. Mattsson, M. Simko; *Front. Public Health, **2014**, 2*, 132. DOI: 10.3389/fpubh.2014.00132
35. M. Simkó, M.O. Mattsson; *J. Cell. Biochem*., **2004**, *93* (1), 83-92
36. D. Popescu, R. Anton; *Arch. Biol. Sci*., **2015**, *67*, 895-897
37. E.S. Bechir, F. Bechir, B. Vladila; *Rev. Chim* (Bucharest), **2018**, *69* (12), 3705-3709
38. D. Dabala, D. Surcel, C. Szanto, S. Miclăus, M. Botoc, S. Toader, O. Rotaru; *Rev. Roum. Sci. Tech. El.,* **2008**, *53* (2bis), 21-30
39. R. Paulraj, J. Behari; *Electro- Magnetobiol*., **2002**, *21*, 221-231
40. S. Velizarov, P. Raskmark, S. Kwee; *Bioelectrochem. Bioenerg*., **1999**, *48*, 177-180
41. I. Trosic, I. Busljeta, V. Kasuba, R. Rozgaj; *Mutat. Res*., **2002**, *521*, 73-79
42. I. Busljeta, I. Trosic, S. Milkovic-Kraus; *Int. J. Hyg. Environ. Health*, **2004**, *207*, 549-554
43. M. Zmyslony, P. Politanski, E. Rajkowska, W. Szymczak, J. Jajte; *Bioelectromagnetics*, **2004**, *25*, 324-328
44. I. Meral, H. Mert, N. Mert, Y. Deger, I. Yoruk, A. Yetkin, S. Keskin; *Brain Res.,* **2007**, 1169, 120-124
45. N.D. Volkow, D. Tomasi, G.J. Wang, P. Vaska, J.S. Fowler, F. Telang, D. Alexoff, J. Logan, C. Wong; *JAMA*, **2011**, *305* (8), 808-813. DOI: 10.1001/jama.2011.186

46. R.B. Dubey, M. Hanmandlu, S.K. Gupta; *J Comput Assist Tomogr*, **2010**, *34* (6), 799-807
47. N.D. Volkow, D. Tomasi, G.J. Wang, J.S. Fowler, F. Telang, R. Wang, D. Alexoff, J. Logan, C. Wong, K. Pradhan, E.C. Caparelli, Y. Ma, M. Jayne; *Neuroimage*., **2010**, *51* (2), 623-628
48. M. Barteri, A. Pala, S. Rotella; *Biophys. Chem*., **2004**, *113*, 245-253
49. J.L. Oncley; *J. Am. Chem. Soc*.,**1938**, *60*, 1115-1123
50. Valerică Raicu, Yuri Feldman; *Dielectric Relaxation in Biological Systems – Physical Principles, Methods, and Applications*, OXFORD University Press, New York, **2015**, Chapter 2.
51. I. Wolf, R. Gulich, P. Lunkenheimer, A. Loidl; *Biochim. Biophys. Acta*, *Proteins Proteomics*, **2012**,*1824* (5), 723-730
52. K. Asami; *Bioelectrochemistry*, **2013**, *92*, 14-21
53. J.L. Sebastian Franco, A. Sanchis Otero, J. R. Madronero, S. M. San Martin; *Prog. Electromagn. Res*., **2013**, *134*, 211-222
54. M. Lingvay, C. Stancu, I. Szatmári, I. Lingvay; *Electrotehnica, Electronica*, *Automatica* (*EEA*), **2013**, *61* (1), 43-47
55. M. Stoneman, A. Chaturvedi, D. Jansma, M. Kosempa, C. Zeng, V. Raicu; *Bioelectrochemistry*; **2007**, *70* (2), 542-550
56. I. Rodríguez-Arteche, S. Cerveny, Á. Alegría, J. Colmenero; *Phys. Chem. Chem.* Phys., **2012**, *14* (32), 11352-11362
57. J. Pokorný, J. Hašek, F. Jelínek; *J. Biol. Phys.,* **2005**, *31* (3-4), 501-514
58. C.M. Ferencz, P. Petrovszki, A. Dér, K. Sebők-Nagy, Z. Kóta, T. Páli, *Sci. Rep.,* **2017**, *7*, 45309. DOI: 10.1038/srep45309
59. Y.L. Ramachandra, G. Narayanamurthy, S. Jois; *Adv. Biol. Res*., **2013**, *7*, 234-240

STUDIA UBB CHEMIA, LXIV, 2,Tom I, 2019 (p. 289-296)
(RECOMMENDED CITATION)
DOI:10.24193/subbchem.2019.2.24

Dedicated to Professor Florin Dan Irimie on the Occasion of His 65th Anniversary

VALIDATED LC-MS/MS METHOD FOR THE DETERMINATION OF THE MUSCARINIC RECEPTOR ANTAGONIST (MRA) SOLIFENACIN FROM HUMAN PLASMA

RÓBERT TŐTŐS[a*], JÓZSEF BALÁZSI[b]

ABSTRACT. The purpose of this study was the development and validation of an LC-MS/MS method, for the determination of solifenacin from human plasma. The sample workup involved a simple protein precipitation procedure. A core/shell type analytical column (50×2,1 mm, 2.6 Å) was used with C18 stationary phase. The mobile phase consisting of 65% acetonitril and 35% water provided good peak shape, accuracy and precision. The mass spectrometer was operated in positive electrospray ionization mode for analyte and internal standard. The following parameters were evaluated for validation purpose: Selectivity, sensitivity, matrix effect, anticoagulant effect, linearity, precision and accuracy, recovery, short and long term analyte/IS stability in solvent/matrix and carryover. The validated calibration range was 0.71-71.28 ng/ml. The correlation coefficient R^2 was at least 0.99 in all validation batches. The validated method has been successfully used for the evaluation of bioequivalence of generic solifenacin 10 mg formulations.

Keywords: *solifenacin, muscarinic antagonist, method validation, bioequivalence trial, LC-MS/MS*

INTRODUCTION

Solifenacin (1*S*,3′*R*)-1-Azabicyclo[2.2.2]oct-8-yl-1-phenyl-3,4-dihydro-1*H*-isochinolin-2-carboxylate with the empirical formula $C_{23}H_{26}N_2O_2$ is a competitive muscarinic receptor antagonist indicated for the treatment of the overactive bladder with associated symptoms such as urge urinary incontinence

[a] *Babeş-Bolyai University, Faculty of Chemistry and Chemical Engineering, Biocatalysis and Biotransformation Research Centre,11 Arany János str., RO-400028, Cluj-Napoca, Romania*
[b] *PharmacoKinetics SRL, 373 E/4 Corunca, RO-547367, Mures county, Romania*
** Corresponding author: totosr@chem.ubbcluj.ro*

and increased urination frequency. Although acetylcholine and muscarinic receptors mediate different actions in various organs, the major therapeutic target organ for solifenacin is the urological tract [1,2]. Solifenacin is generally used in form of succinate salt (Figure 1).

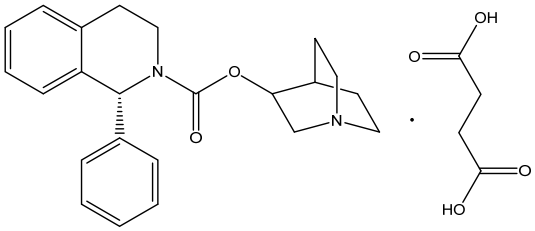

Figure 1. Structure of solifenacin succinate

RESULTS AND DISCUSSION

Determination of acquisition parameters

There are only a few methods known in the literature for the determination of solifenacin in human plasma or pharmaceutical formulations, using LC, UV [3,7] or LC-MS/MS methods [4-6].

The LC/UV methods presented in papers [3,7] uses UV only detection, with LLOQ values of 2ng/ml and 10 µg/ml, unsuitable for bioanalytical assays. Besides there are MS incompatible buffers used for setting the pH of the mobile phase (phosphate). Retention times of up to 25 min are unsuitable for a high throughput analysis.

The LC-MS/MS methods reviewed [4-6] are of a suitable sensitivity (LLOQ between 0.47-0.60 ng/ml), they used a more laborious and time consuming liquid-liquid extraction method. However, analysis time of 3 min. assure a rapid analysis more than 350 samples/day.

The m/z transitions used for multiple reaction monitoring (MRM) were chosen based on the spectra from Figures 2 and 3. The monitored transitions should not interfere in their m/z value, specific for a given analyte. Their intensity should be convenient for the qualifiers, and the qualifier/quantifier ratio should remain stable over the time. Taking into account the considerations above the following transitions were chosen for the quantitative assay method:

Solifenacin: m/z 363.3→110.2, (363.3→193.2 qualifier ion) CE 30V,

Losartan (IS): m/z 423.2→207.2 (423.2→377.3 qualifier ion) CE 15V.

(CE – Collision Energy)

For analyte and IS (Internal Standard) the single charged molecular ions were used as precursors.

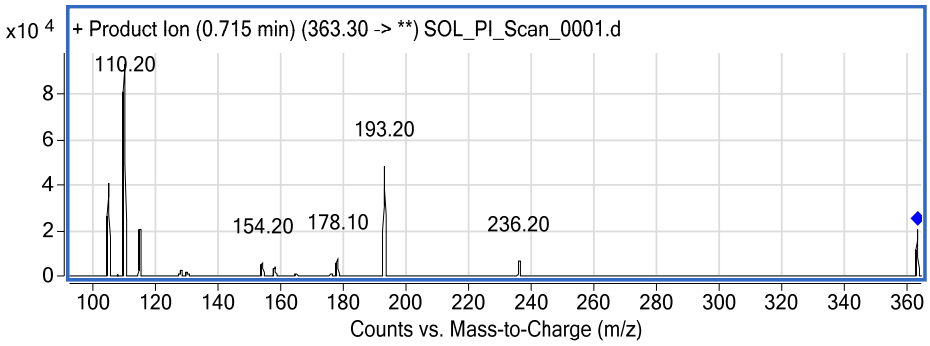

Figure 2. ESI (+) Spectrum of Solifenacin

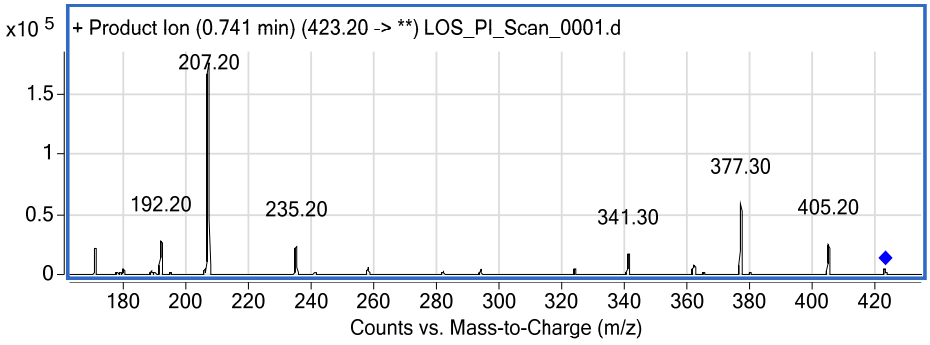

Figure 3. ESI (+) Spectrum Losartan (IS)

Figure 4 shows a typical MRM total ion chromatogram for an ULOQ (upper limit of calibration) sample. The analyte and IS are practically co-eluting at 0.73 min. Values are back calculated concentrations for each analyte.

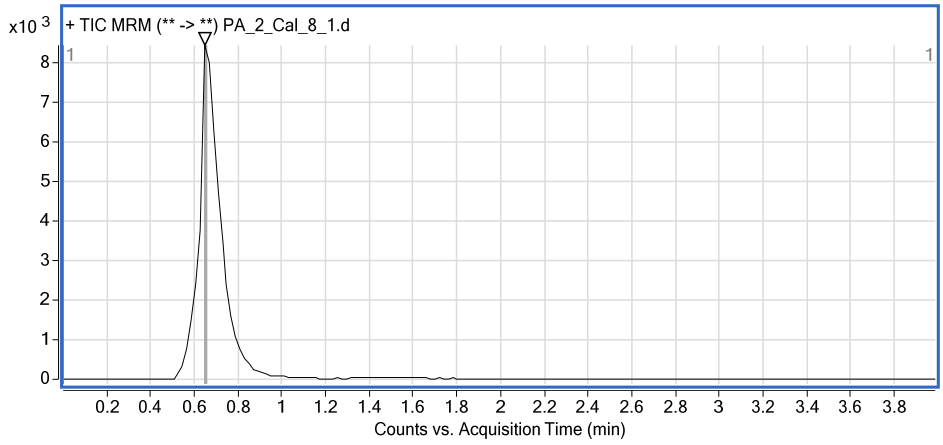

Figure 4. MRM chromatogram of Cal8 (solifenacin 71.28 ng/ml, Losartan 100.75 ng/ml)

The use of the co-eluting internal standard will compensate the matrix effect, and it's a convenient alternative to the stable isotope labeled solifenacin. Moreover, it is easily soluble in the sample solvent resulting after plasma protein precipitation (methanol:water 3:1).

It's noticeable, that no significant spectral response has been observed at the retention time of the analyte/IS in matrix blank samples (Figure 5.).

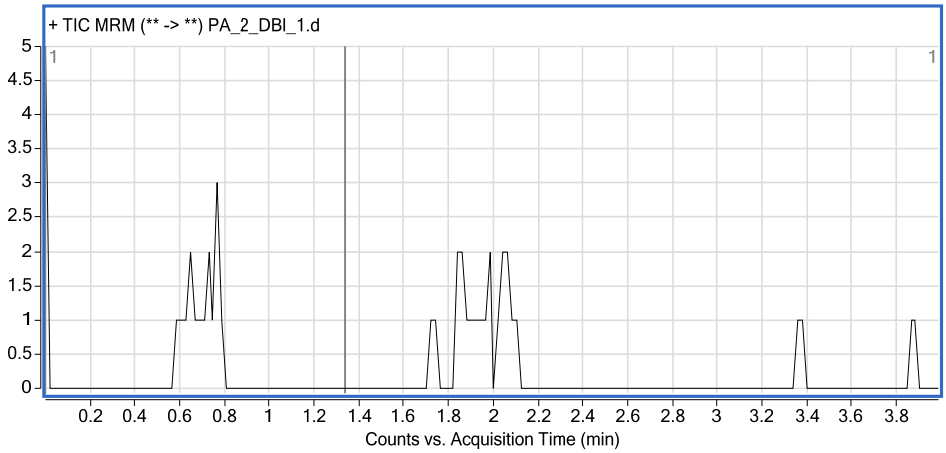

Figure 5. MRM chromatogram of DBI1 (matrix blank 0 ng/ml analyte/IS)

Bioanalytical method validation

The analytical method was validated according to the EMEA/ CHMP/EWP/192217/2009 Guideline on validation of bioanalytical methods [8].

The tested parameters were: selectivity, sensitivity, matrix effect, anticoagulant effect, intra/interbatch precision and accuracy, recovery, short/long term stability of stock solutions of analyte, short term stability of working solutions of analyte, bench top stability in biological matrix, freeze thaw stability in biological matrix, injector/autosampler stability of the processed samples, stability during delayed processing, dilution integrity, carryover. All tests were performed using 6 replicates at the mentioned QC (Quality Control) levels.

The calibration curve range is established according to literature data about plasma concentrations of the analyte. $C_{max\ average\ from\ literature}$ for Solifenacin was found of ca. 15 ng/ml, after administration of a 10 mg dose. [2,6]

A summary of main results of validation batches is presented in Table 1.

The validated calibration range was 0.71-71.28 ng/ml. The calibration curves were obtained using a linear weighted (1/x) regression analysis of the

peak area ratio (analyte/internal standard) versus the nominal concentration of the calibration standards. The lower limit of quantitation was set smaller than 5% of expected average C_{max} values.

Linearity summary results for solifenacin are presented in Table 2. The limit of quantitation was 0.71 ng/ml and the linear dynamic range of the curve was from 0.71 to 71.28 ng/ml.

Summary of method validation

Table 1. Bioanalytical method validation summary for solifenacin

Calibration concentrations (ng/ml)	0.71, 2.14, 5.35, 10.69, 21.39, 32.08, 42.77, 71.28
Lower limit of quantitation (ng/ml)	LLOQ, 0.71 Accuracy 98.84 %, RSD 2.91
QC Concentrations (ng/ml)	LLOQ-QC, LQC, MQC, HQC 0.71, 2.14, 21.39, 42.77
Between-run accuracy (%)	LLOQ-QC, LQC, MQC, HQC 104.99, 103.65, 102.23, 100.81
Between-run precision (RSD)	LLOQ-QC, LQC, MQC, HQC 9.08, 3.67, 2.39, 4.07
IS normalized Matrix factor (MF) RSD	LQC 1.21 4.44
Recovery (%)	LQC MQC HQC 100.32 97.97 101.17
Long term stability of stock solution and working solutions (Observed change %)	Confirmed up to 53 days at +4 °C LQC Stab. 101.09, change +1.09 % HQC Stab. 94.35 change –5.65 % IS Stab. 101.38 change + 1.62%
Short term stability in biological matrix at room temperature or at sample processing temperature. (Observed change %)	Confirmed up to 23.80 h LQC Stab. 102.68, change +2.68 % HQC Stab. 101.70 change +1.70 %
Long term stability in biological matrix (Observed change %)	Confirmed up to 189 days at –50 °C LQC Stab. 94.97, change –5.03 % HQC Stab. 93.79 change –6.21 %
Autosampler storage stability (Observed change %)	Confirmed up to 76.1(6) h LQC Stab. 95.34, change –4.66 % HQC Stab. 92.21 change –7.79 %
Freeze and thaw stability (Observed change %)	-50 °C , 3 cycles LQC Stab. 101.58, change +1.58% HQC Stab. 102.09, change +2.09%
Dilution integrity	Concentration diluted (2-fold) 103.97 %; RSD 3.78 % Concentration diluted (4-fold) 105.87%; RSD 3.04 %

PA – Precision and Accuracy batch
LLOQ-QC/LQC/MQC/HQC – Lower Limit of Quantitation/Low/Medium/High Quality Control sample

Table 2. Linearity summary results for solifenacin

Calibration level	Nominal conc. (ng/ml)	Mean conc.±S.D. (ng/ml)	RSD %	Accuracy %
Cal_1_1	0.71	0.71±0.05	7.21	100.29
Cal_1_2	0.71	0.70±0.06	8.19	98.62
Cal_2	2.14	2.11±0.03	1.49	98.60
Cal_3	5.35	5.39±0.08	1.49	100.78
Cal_4	10.69	10.86±0.05	0.45	101.55
Cal_5	21.39	21.59±0.41	1.92	100.93
Cal_6	32.08	32.28±0.72	2.22	100.64
Cal_7	42.77	42.12±1.18	2.80	98.49
Cal_8_1	71.28	71.62±1.46	2.03	100.47
Cal_8_2	71.28	71.02±1.05	1.48	99.63

CONCLUSIONS

A rapid and robust method has been developed and validated for the determination of solifenacin in human plasma. The quantitation was performed on an Agilent 1200 series HPLC system, coupled to an Agilent 6410 triple quadrupole mass spectrometer, using electrospray ionization technique. The components were detected in positive ionization mode.

The developed method involves a rapid sample workup using protein precipitation versus liquid-liquid extraction. Even so, the sample matrix presents no interferences or significant matrix effects at the retention time on analyte/IS. An analysis time of 4 min. is adequate for the elution of all analytes/matrix components from the column, and ensures a capacity of more than 350 samples/day on the used LC-MS/MS system. The usage of a non-labeled internal standard beside the protein precipitation, makes the method more cost-effective.

The method was successfully used for the evaluation of bioequivalence of a generic formulation of solifenacin 10 mg film-coated tablets in human subjects.

EXPERIMENTAL SECTION

Solvents and reference materials used

All used solvents are of HPLC grade. Acetonitril was purchased from VWR, formic acid from Merck KGaA, HPLC water was obtained using a Millipore Simplicity UV water purification system. Certified reference materials of Solifenacin succinate and Losartan potassium (internal standard-IS) were obtained from Ak Scientific Inc., respectively Sigma-Aldrich and are of analytical standard grade. Blank human plasma was obtained from the regional blood transfusion center (CRTS) Cluj.

Instrumentation and working parameters

An Agilent 1200 series HPLC system with a Phenomenex Kynetex C18 column (50 × 2.10 mm) equipped with Phenomenex Security Guard (4 ×2.0 mm) was used for separation. The used mobile phase was an isocratic mixture of 65:35 acetonitrile:water (containing 0.5% formic acid). The used flow rate was 0.3 ml/min, the column temperature was set to 35 ºC. An Agilent 6410 triple Quadrupole Mass Spectrometer (Agilent Technologies, USA), equipped with electrospray ion source was used for the LC-MS/MS analyses. The runtime was 4 min/sample. The data acquisition and processing were carried out using MassHunter software. The whole system (software and hardware) was validated. The mass spectrometer was operated in positive ionization mode for analyte and IS. Nitrogen was used as nebulizing gas and collision cell gas. The temperature of the ESI source was set to 350 ºC, and the needle voltage to 4000V.

The quantitation was performed using MRM (multiple reaction monitoring) of the transitions: m/z 363.3→110.2, (363.3→193.2 qualifier ion) collision energy 30V, for solifenacin and 423.2→207.2 (423.2→377.3 qualifier ion) collision energy 15V for losartan (IS).

The mass spectrometer was operated at unit resolution with a dwell time of 300 ms per transition.

Stock and working solutions preparation

Stock solutions of solifenacin (1.0 mg/ml) were prepared in ultrapure water dissolving accurately weighed amounts of reference material. Stock solutions of losartan (1.0 mg/ml) were prepared in methanol/water 50/50 (w/w) dissolving accurately weighed amounts of losartan. They were stored between 2-8 °C. Correction factors were applied to the weighed amounts of reference materials to calculate the content of the pure substance (Table 3). Correction factors are derived from the purity and the chemical form (salt, etc.). Water content will be substracted from the purity.

Table 3. Correction factors for reference materials

Reference material	**Solifenacin succinate**	**Losartan potassium**
Purity (%)	98.3	99.6
Water (%)	0.23	0.27
Chemical form correction factor	0.7543	0.9174
Correction factor	**0.7397**	**0.9113**

Working solutions of analyte and internal standard were prepared freshly before use by successive dilutions from stock solutions to appropriate levels, using water as solvent. They were used for spiking human plasma used for calibrators and QC samples preparation.

Calibrators and QC samples preparation

To 400 µl of blank human plasma, 50 µl of spiking solution of analyte and 50 µl of spiking solution of internal standard were added in polypropylene tubes, to yield final concentrations of 0.71, 2.14, 5.35, 10.69, 21.39, 32.08, 42.77, 71.28 ng/ml for solifenacin.

Sample preparation (workup)

To precipitate plasma proteins, 1500 µl of acetonitrile was added to the spiked samples, then vortexed for 20 minutes at 1500 rpm. Further the samples were centrifuged at 4 °C for 10 minutes at 4000 rpm. 800 µl of supernatant was transferred to HPLC autosampler vials and injected into the analytical system (20 µl/sample).

Calibration curve parameters

The linearity of the method was evaluated using spiked plasma samples in the concentration range mentioned above using the method of least squares. Three linearity curves were analyzed.
Each calibration batch (curve) consisted of: blank samples in duplicate, zero samples (blank with IS) in duplicate and eight non-zero concentration levels, of which the lower and upper limit of quantitation samples were in duplicate. The calibration curves were obtained by using a linear weighted (1/x) regression analysis of the peak area ratio (analyte/internal standard) versus the nominal concentration of the calibration standards. Study samples concentrations were obtained by interpolation from the calibration curve.

The linearity results are summarized in Table 2 in the 'Results and Discussion' section.

ACKNOWLEDGMENTS

This work was performed using private funding of S.C KYNETYX HT SRL.

REFERENCES

1. *https://www.rxlist.com/vesicare-drug.htm:* ***VESIcare*** *(solifenacin succinate) Tablets; Viewed: 02.11.2018).*
2. O. Doroshyenko, U. Fuhr, *Clin. Phramacokinet*., **2009**, *48*, 281.
3. L. Singh, S. Nanda, Pharmaceutical Methods, **2011**, *2*, 21.
4. H.N. Mistri, A.G. Jangid, A. Pudage, D.M. Rathod, P.S. Shrivastav, *Journal of Chromatography B*, **2008**, *876*, 236.
5. J. Macek, P. Ptáček, J. Klíma, *Jorunal of Chromatography B*, **2010**, *878*, 3327.
6. T. Uchida, W.J. Krauwinkel, H. Mulder, R.A. Smulders, *Br. J. Clin. Pharmacol.,* **2004**, *58*, 4.
7. Yanagihara T, Aoki T, Soeishi Y, Iwatsubo T, Kamimura H., *Journal of Chromatography B.,* **2007**, *859*, 241.
8. EMEA/CHMP/EWP/192217/2009 Rev. 1 Corr. 2** Guideline on validation of bioanalytical method, 21 July 2011 (Updated 03/06/2015).

STUDIA UBB CHEMIA, LXIV, 2,Tom I, 2019 (p. 297-308)
(RECOMMENDED CITATION)
DOI:10.24193/subbchem.2019.2.25

Dedicated to Professor Florin Dan Irimie on the Occasion of His 65th Anniversary

KINETICS OF DAPAGLIFLOZIN AFTER SINGLE DOSE ORAL ADMINISTRATION OF A 10 MG IMMEDIATE RELEASE TABLET

MONICA OROIAN[a,b], ADRIANA MARCOVICI[b], DIANA IOANA POP[a,b], SANDEEP BHARDWAJ[b], ARSHAD KHUROO[c], ANA-MARIA GHELDIU[d,*], LAURIAN VLASE[a]

ABSTRACT. The present study aimed to elucidate and describe the basic pharmacokinetics of dapagliflozin after a single dose oral administration of a 10 mg immediate release tablet developed by Sun Pharmaceutical Industries Limited, India. Ten competing models were created in order to analyze the experimental data obtained from the 71 subjects who were enrolled and finalized two bioequivalence clinical trials, under fasting and fed state. The studies took place at the Clinical Pharmacology and Pharmacokinetics Department of Terapia S.A. Considering the Akaike index value for a rational model discrimination, model number 8 (M8) was found to be the best that fits the experimental data. The representative pharmacokinetic model involves zero order absorption kinetics with a lag time of approximately 0.3 hours, first order systemic metabolism and elimination and two-compartmental distribution. Furthermore, by using M8, the most important pharmacokinetic parameters of dapagliflozin were determined. All calculations were performed by Phoenix WinNonlin® version 6.3 (Certara, USA).

Keywords: *dapagliflozin, compartmental pharmacokinetic analysis, subjects, bioequivalence clinical trials*

[a] *University of Medicine and Pharmacy 'Iuliu Hatieganu', Faculty of Pharmacy, Department of Pharmaceutical Technology and Biopharmaceutics, 8 Victor Babes str., RO-400012, Cluj-Napoca, Romania*

[b] *Terapia SA – a Sun Pharma Company, Department of Clinical Pharmacology and Pharmacokinetics, 124 Fabricii str., RO-400632, Cluj-Napoca, Romania*

[c] *Clinical Pharmacology and Pharmacokinetics Department, Sun Pharma Gurugram, India*

[d] *University of Medicine and Pharmacy 'Iuliu Hatieganu', Faculty of Pharmacy, Department of Pharmaceutical Botany, 23 Marinescu str., RO-400337, Cluj-Napoca, Romania*

** Corresponding author: anamaria.gheldiu@yahoo.com*

INTRODUCTION

Dapagliflozin (see Figure 1) is an inhibitor of the human sodium-glucose co-transporter 2 (SGLT2), which is present in the proximal tubule and is responsible for the glucose reabsorption [1]. By inhibiting the SGLT2, the glucose reabsorption can be reduced while urinary excretion of the glucose is increased [2].

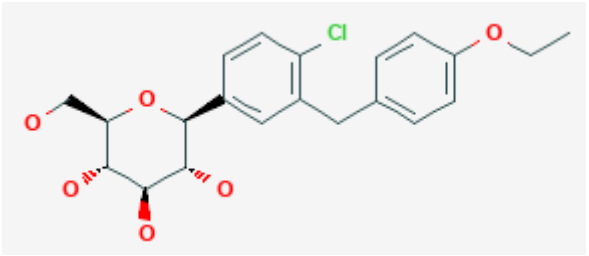

Figure 1. Chemical structure of dapagliflozin (IUPAC name: (2S,3R,4R,5S,6R)-2-{4-chloro-3-[(4-ethoxyphenyl)methyl]phenyl}-6-(hydroxymethyl)oxane-3,4,5-triol) [14]

Dapagliflozin was demonstrated to improve glycemic control and to prevent administration of increased doses of insulin in patients with type 2 diabetes mellitus (T2DM) while also helping them lose weight, when diet and exercise alone do not provide adequate response and when metformin administration is considered inappropriate due to intolerance [3,4]. Dapagliflozin is prescribed as monotherapy or associated with other oral anti-diabetes substances in order to assure an improved glycemic control in patients with T2DM [5].

Dapagliflozin is metabolized via the enzyme UGT1A9 (uridine diphosphate glucuronosyltransferase 1A9), present in the liver and kidneys, to dapagliflozin 3-O-glucuronide. Its metabolite is devoid of pharmacological activity [6].

Compartmental pharmacokinetic analysis offers a better understanding of the relationship between the pharmacological effect and the administered dose. This mathematical approach deals with the quantitative analysis of the pharmacokinetic (PK) processes that occur in the human body after drug administration until its irreversible removal from the body, namely it describes the following processes: absorption, distribution, metabolism, and elimination (ADME) [7,8]. After the active drug substance/active pharmaceutical ingredient (API) is released from the pharmaceutical formulation, it is molecularly dispersed in the internal aqueous medium (or dissolved) and then is absorbed by crossing through various biological membranes, eventually reaching the blood stream [9]. From this site, which is named the central compartment and consists of highly

hydrophilic tissues and organs in addition to the blood stream, the API can be distributed to peripheral compartments, which is formed by the organs and tissues with lipophilic character. Thus, the API is exchanged both-ways in between these compartments (central and peripheral) in accordance with its chemical affinities [9]. The API can also suffer metabolism prior to elimination, process that usually inactivates the API and leads to formation of more polar metabolites, which are easier to eliminate. The process of elimination always takes place from the central compartmental and can occur by metabolism and/or excretion. Therefore, if the API undergoes distribution, it then has to return to the central compartment to be further irreversible removed from the body by the process of elimination [10]. All the aforementioned kinetic processes can be characterized by transfer rate constants. Moreover, each compartment is described by a system of differential equations for which the constant coefficients are the PK parameters. By using specific PK software, the differential equations are solved for each compartment and the values for the PK parameters are determined [10].

The knowledge of drug kinetics in the body (namely the kinetic model) is important for predicting the drug plasma levels after different doses or after multiple-dose administration. The chosen kinetic model can further be used for PK population modelling, therapeutic drug monitoring, mathematical correlations between drug kinetics and the intensity of the pharmacological effect. It also gives a deeper insight of drug interactions with other drugs administered concomitantly or with food intake. Likewise, it permits a better calculation and choice of dosage regimen for a drug in particular situations, when the PK processes of absorption, distribution, metabolism and elimination are modified consequently to disease state or altered physiology [7,8].

The aim of this study was to create and use a PK model that can accurately describe the kinetic processes involved in dapagliflozin's disposition in the body (ADME), after oral administration of a single dose (10 mg) dapagliflozin in healthy Caucasian subjects. This was assayed by comparing the predicted values with actual experimental data, obtained from two bioequivalence clinical trials performed at the Clinical Pharmacology and Pharmacokinetics Department of Terapia S.A., under fasting and fed state of the subjects.

RESULTS AND DISCUSSION

A number of 10 distinct mathematical models were created in order to evaluate the PK of dapagliflozin. The characteristics for each kinetic model are given in Table 1.

Table 1. Pharmacokinetic models for dapagliflozin used in compartmental analysis

Pharmacokinetic model	Absorption kinetics	Lag time	Number of compartment
M1	1st order	No	1
M2	1st order	Yes	1
M3	Zero order	No	1
M4	Zero order	Yes	1
M5	1st order	No	2
M6	1st order	Yes	2
M7	Zero order	No	2
M8	Zero order	Yes	2
M9	1st order and zero order	Yes	1
M10	1st order and zero order	Yes	2

The differences between the evaluated mathematical models consisted in suppositions about the kinetic order for the process of absorption (zero order or 1st order), the existence of the lag time prior to absorption, and the number of compartments for dapagliflozin. For instance, the first PK model (M1) assumes absorption follows a 1st order kinetics without lag time and monocompartmental distribution for dapagliflozin. The M10 model employs the existence of a mixed order absorption process (zero order and 1st order), with lag time, and a bicompartmental distribution. For each tested model, the processes of metabolism and elimination were regarded as 1st order kinetic processes.

The schematic representation of the kinetic processes from model M8 are depicted in Figure 2.

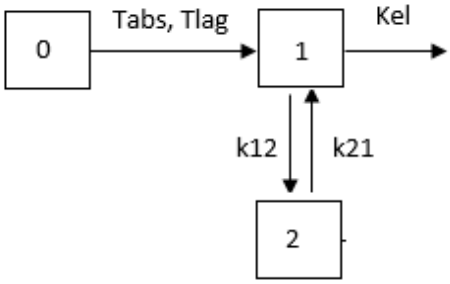

Figure 2. Schematic representation of kinetic processes for model M8, where "0" is absorption compartment of dapagliflozin; "1" is the central compartment of dapagliflozin, while "2" is the peripheral compartment; T_{lag} is the latency time for absorption; T_{abs} is the time needed for zero order absorption of dapagliflozin; k_{12} and k_{21} are the distribution rate constants; K_{el} is the the elimination rate constant for dapagliflozin. The kinetic processes are depicted as straight arrows.

For each kinetic model, the corresponding mathematical differential system of equations were written and run by the software Phoenix WinNonlin®, version 6.3 (Certara, SUA). The equations for model M8 are shown in Figure 3.

M8

$$\begin{cases} \frac{\partial Qabs}{\partial t} = -\frac{Qabs}{Tabs} \\ \frac{\partial Qc}{\partial t} = \frac{Qabs}{Tabs} - kel * Qc - k12 * Qc + k21 * Qp \\ \frac{\partial Qc}{\partial t} = \frac{Qabs}{Tabs} - kel * Qc - k12 * Qc + k21 * Qp \\ ConcDc = \frac{Qc}{V\_F} \end{cases}$$

Figure 3. The mathematical equations of kinetic model M8, where Q_{abs} is the amount of dapagliflozin at the site of absorption; Q_c and Q_p are the amount of dapagliflozin in the central and peripheral compartment, respectively; ConcDc is the plasma concentration of dapagliflozin; Q_{abs}/T_{abs} is the rate constant of the zero order kinetic absorption; V_F is the apparent volume of distribution of the central compartment. The other parameters were previously described.

The ten kinetic models previously presented were implemented in Phoenix WinNonlin® software and were further used to evaluate the mean plasma concentrations versus time of dapagliflozin. For each model analysis, the settings of the software minimization engine were the following: the chosen weighting scheme was 1/y (1/observed concentration), minimization method used was Gauss-Newton (Levenberg and Hartley variant), and the convergence criterion was set at 0.0001.

For rational discrimination between the assessed kinetic models, the Akaike index value (AIC) was elected. This index considers the number of observations and number of parameters of the specific model and evaluates the goodness of fit between experimental and predicted values. The analysis software automatically calculated it and the model that best fit the experimental data was characterised by a smaller AIC value [11].

The first set of data for which was assessed the PK profile of dapagliflozin was obtained in a bioequivalence study conducted under the fasting state. Likewise, the second set of data corresponded to the clinical data of the bioequivalence test performed under the fed state of the subjects.

Therefore, the AIC values for the ten evaluated models are presented in Figure 4 (fasting state), respectively Figure 5 (fed state).

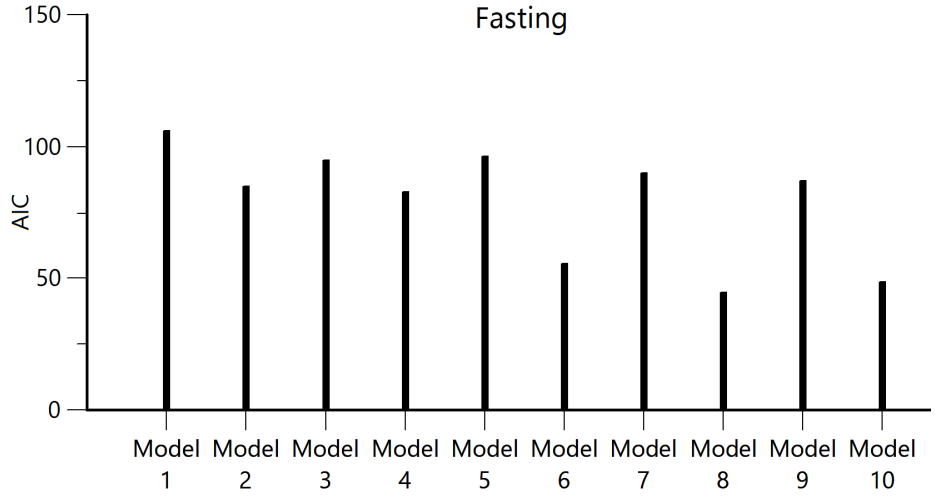

Figure 4. Akaike index values (AIC) for kinetic models used for characterization of dapagliflozin pharmacokinetics from data obtained in bioequivalence study under fasting state of subjects

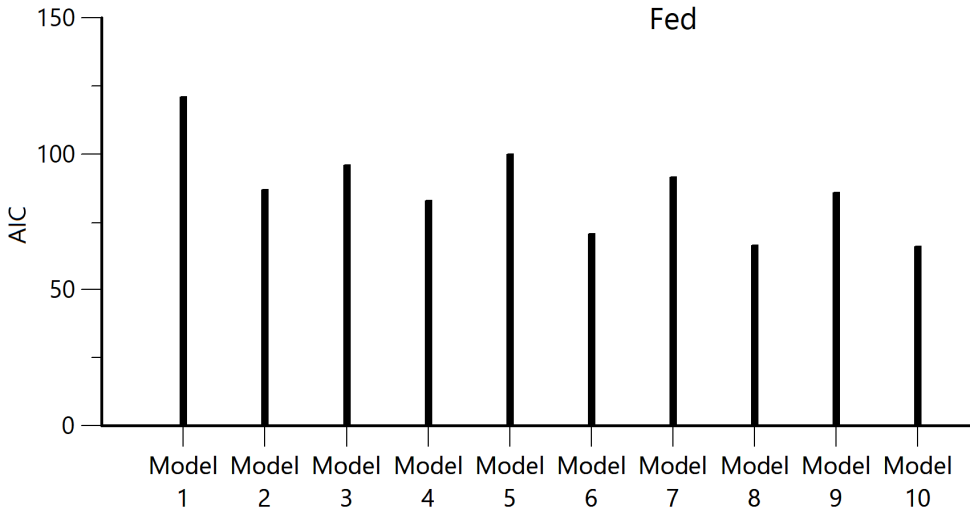

Figure 5. Akaike index values (AIC) for kinetic models used for characterization of dapagliflozin pharmacokinetics from data obtained in bioequivalence study under fed state of subjects

By visual inspection of the AIC values presented in figures 4 and 5, it can be concluded that model M8 fits the experimental data from both clinical trials better than its concurrent models. For this model were obtained the smallest AIC values and it was further selected as representative for the description of dapagliflozin disposition in the body after oral administration of a single dose of 10 mg immediate release tablet.

In figure 6 is presented the typical fitting for subject 1 dataset to representative model M8, for both clinical trials, under fasting and fed state. Similar good fitting were obtained for the other 70 datasets (data not shown).

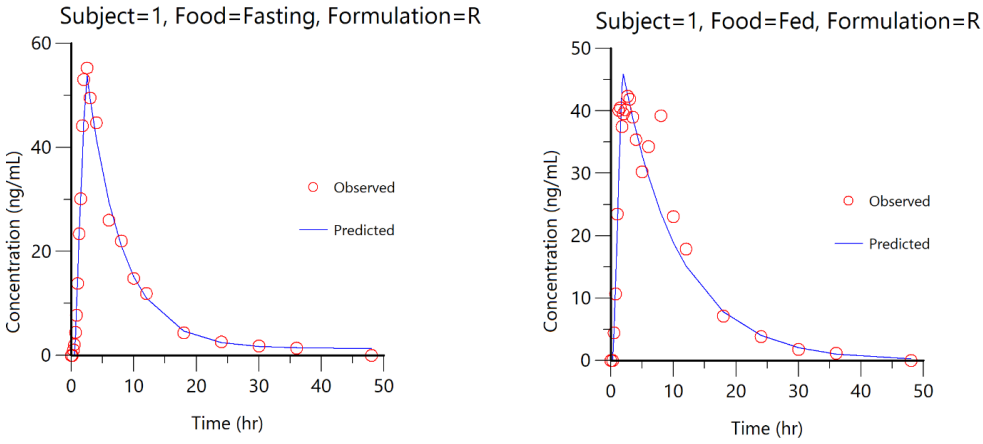

Figure 6. Typical fitting of kinetic model M8 to subject 1 dataset, for fasting and fed state of the subject in the bioequivalence clinical trial (○ represents the experimental/observed plasma drug concentrations of dapagliflozin, the blue line represents the computed concentrations predicted by model M8)

According to kinetic model M8, the PK of dapagliflozin is characterized by a zero order absorption kinetics with lag time, bicompartmental distribution, and first order kinetics of elimination. By using this representative PK model for dapagliflozin, its characteristic PK parameters were further determined and are shown in Table 2. In the below table are summarized the main PK parameters calculated for datasets obtained in both clinical trials, under fasting and fed state of subjects, and the statistical evaluation of the differences performed with ANOVA test.

Table 2. The kinetic parameters of dapagliflozin calculated with model M8 and the statistical evaluation of the differences between clinical trials

Variable (units)	Food						
	Fasting			Fed			*p* value[3] (ANOVA)
	Mean	SD[1]	CV%[2]	Mean	SD	CV %	
T_{lag} (hr)	0.290	0.102	35.2	0.342	0.268	78.3	0.949
T_{abs} (hr)	1.181	0.645	54.6	3.229	2.537	78.6	0.001
K_{12} (hr^{-1})	0.088	0.054	60.9	0.144	0.237	164.1	0.142
K_{21} (hr^{-1})	0.063	0.042	66.4	0.118	0.226	191.8	0.952
K_{el} (hr^{-1})	0.189	0.072	38.2	0.162	0.100	61.8	0.010
Vd_F (L)	110.685	28.415	25.7	147.542	71.802	48.7	0.005

[1]SD – standard deviation; [2]CV% - coefficient of variation; [3]*p* value <0.05 was considered statistically significant.

Dapagliflozin's basic PK profile was assessed from data obtained in two bioequivalence clinical trials, under fasting and fed state of subjects. For both cases, kinetic model M8 best fit the experimental data, even though the modified values of the calculated PK parameters in between trials showed that food intake influenced the rate constants of the kinetic processes that describe its disposition. More precisely, three PK parameters displayed statistically significant different values between studies. Firstly, the time needed for zero-order absorption process (T_{abs}) varied from 1.181 ± 0.645 hr during the fasting study to 3.229 ± 2.537 hr for the fed study. Secondly, the rate constant of first-order elimination process (K_{el}) was 0.189 ± 0.072 hr^{-1} for the fasting state, while for the fed state was 0.162 ± 0.1 hr^{-1}. Thirdly, the apparent volume of distribution (Vd_F) was 110.685 ± 28.415 L for fasting state, 147.542 ± 71.802 L for fed state, respectively.

The Vd_F for central compartment of dapagliflozin was high due to high protein binding of the drug (approximately 91%) [12]. This PK parameter was influenced by the bioavailability of dapagliflozin after oral administration. The increase of Vd_F during the fed state study with approximately 33% was apparent, since the oral bioavailability of dapagliflozin was modified because of food intake.

It is acknowledged that food intake can influence the absorption process and the bioavailability of certain drugs [13]. In the case of dapagliflozin, the absorption onset was delayed since the lag time increased from 0.290 ± 0.102 hr (fasting state) to 0.342 ± 0.268 hr (fed state). This was

due to an increased time necessary for gastric emptying and reach into duodenum, where the absorption begun. The time needed for the zero-order absorption process to take place registered a 2.7-fold increase for fed state of the subjects.

According to M8, dapagliflozin displayed bi-compartmental distribution. As expected, the distribution processes from the central compartment to the peripheral compartment and reverse were not influenced by the food intake. The values for the rate constants of distribution processes (K_{12} and K_{21}, with $K_{12}>K_{21}$) did not register a statistically significant difference between clinical trials.

Dapagliflozin was eliminated following a first-order kinetic process, characterised by a rate constant of 0.189 ± 0.072 hr^{-1}, under the fasting state. The intake of food modified the K_{el} to 0.162 ± 0.1 hr^{-1}; this decrease was caused by the modification of the bioavailability of dapagliflozin following oral administration. K_{el} depends upon two physiological parameters: clearance – in a directly proportional manner - and Vd_F – inversely proportional [9,10], thus it was expected that an increase in the apparent volume of distribution (due to modified oral bioavailability) would lead to a decreased value for K_{el}. However, this alteration of the K_{el} value lacks actual clinical importance.

The increase of the variability for the calculated PK parameters between clinical trials was due to food-effect in addition to natural biological and physiological differences between subjects (inter-subject variability).

CONCLUSIONS

Ten different mathematical models were evaluated in order to find the model that best fit the experimental data (plasma concentration versus time) of dapagliflozin obtained from two clinical trials. After data analysis, according to AIC values, the model M8 was found to best fit the data from both studies, conducted under fasting and fed state of subjects. Even though the food intake led to a modification of the values for certain calculated PK parameters, the basic PK profile of dapagliflozin was not influenced. The kinetics of dapagliflozin is characterised by zero-order absorption process after a lag time of approximately 0.3 hr. Following absorption, the drug is distributed between the central and peripheral compartment ($K_{12}>K_{21}$) and is further eliminated from the body following first-order kinetic process.

EXPERIMENTAL SECTION

Subjects: Both fasting and fed research studies were carried out in accordance with the Basic Principles defined in US 21 CFR Part 320, the ICH E6 (R1) (CPMP/ICH/135/95) 'Guideline for Good Clinical Practice' and the principles of the Declaration of Helsinki. The protocols of the studies were approved by National Agency for Medicines and Medical Devices, Romania and the Bioethics National Committee of the Medicines and Medical Devices, Romania. After the subjects gave their written informed consent for participation in the study, the investigators performed the screening procedures and subjects further included in studies were declared healthy and filling all inclusion criteria of the studies.

The study was conducted in the Clinical Unit of the Clinical Pharmacology and Pharmacokinetics Department of Terapia SA, Romania.

The studies were design as open label, balanced, randomized, two-period, two-sequence, single-dose, crossover study in fasting condition and under fed condition, respectively.

Up-to-date, no differences regarding the PK profile between genders were reported in the scientific literature, furthermore no gender effect was observed in the bioequivalence studies conducted by Clinical Unit of the Clinical Pharmacology and Pharmacokinetics Department of Terapia SA, Romania. Consequently, the subjects were of mixed gender, women and men, respectively.

Sample size estimation for both studies was based on available in-house study data on Dapagliflozin tablets. 48 Caucasian subjects were enrolled in the fasting study planned based on the assumptions that Test/Reference ratio is in the range of 90-110%, an expected intra-subject CV of approximately 20%, power of 80% and possible dropouts and/or withdrawals. A number of 38 subjects finalized the fasting study, of which 12 were women and 26 were men. Considering a Test/Reference ratio of 95-105% and intra-subject CV of approximately 24% and a power of 90% to show bioequivalence under bioequivalence assumptions and to allow for possible dropouts and/or withdrawals, 44 subjects were considered to be included in the fed study out of which 33 subjects finalized (9 women and 24 men). Thus, from the 92 subjects initially enrolled in both bioequivalence study, 71 subjects finalized the studies (21 women and 50 men). Their datasets were further used for PK modeling assay (n=71).

Study protocol

Fasting study: After an overnight fasting state of at least 10 hours, the subjects were administered the drug product containing dapagliflozin 10 mg with 240 mL of a 20 % glucose solution in water at ambient temperature. Approximately 60 mL of 20% glucose solution was administered every 15

minutes for up to 4 hours post dosing to prevent hypoglycemia. During housing subjects received standard meals, identical for both periods. For complete elimination of dapagliflozin from the body, the wash-out between study periods was 7-days.

The blood samples were collected predose and at 0.16, 0.33, 0.5, 0.67, 0.83, 1, 1.25, 1.5, 1.75, 2, 2.5, 3, 4, 6, 8, 10, 12, 18, 24, 30, 36 and 48 hours post-dose in each period of the study

Fed study: Following fasting period of at least 10 hours, the subjects started the recommended high-fat high-calorie standard meal, 30 minutes prior to administration of the drug product. The drug product was administered with 240 mL of 20 % glucose solution. Approximately 60 mL of 20% glucose solution was administered in approximately every 15 minutes for up to 4 hours post dose. During housing subjects received standard meals, identical for both periods. The wash-out between study periods was 7-days.

Blood samples were collected predose and at 0.25, 0.5, 0.75, 1, 1.25, 1.5, 1.75, 2, 2.33, 2.67, 3, 3.5, 4, 5, 6, 8, 10, 12, 18, 24, 30, 36 and 48 hours post-dose in each period of the study.

For both studies drinking water was not allowed for 1 hour before and after dosing. Thereafter, it was allowed at all times. Also, no food was allowed for 4 hours post dose.

Drug analysis from plasma: All samples were collected and processed under low light condition. The samples were collected in K3EDTA vacutainers. After collection, the blood samples were maintained in ice cold water bath. The blood samples were centrifuged under cooling condition (4-10°C), within 90 minutes post blood sample collection, for 15 minutes at a speed of 4000 rpm and a set temperature of 4ºC, to separate plasma that was maintained in ice cold water bath until storage.

Mass spectrometry was performed in the negative-ion multiple reaction–monitoring mode with m/z transitions of 407.10→329.20 for dapagliflozin and 412.10→334.10 for internal standard, which was dapagliflozin-D5.

Analyst software version 1.6.3 was used to determine peak areas of dapagliflozin and the internal standard. Subject sample concentrations were calculated from peak area ratios.

Calibration curves were linear over plasma dapagliflozin concentration ranges of 1.01 to 352.50 ng/mL.

During validation the between-run accuracy was 88.79% to 95.10%, between-run precision was 0.65% to 2.49%, within-run accuracy was 89.44% to 94.39% and within-run precision was 1.12% to 5.64%.

Pharmacokinetic analysis: The compartmental PK analysis was performed in order to analyse the plasma concentrations versus time of dapagliflozin for each individual dataset obtained from subjects who took part in two bioequivalence studies (71 dataset).

Ten distinct kinetic models were created and implemented in Phoenix WinNonlin® software, version 6.3 (Certara, SUA) in order to assess the basic PK profile of dapagliflozin (see Table 1).

ACKNOWLEDGMENTS

Financial disclosures: Ana-Maria Gheldiu and Laurian Vlase are full-time employees of the University of Medicine and Pharmacy "Iuliu Hatieganu", Cluj-Napoca, Romania.

Conflicts of interest: Monica Oroian, Adriana Marcovici, Diana Ioana Pop, Sandeep Bhardwaj were employees of the Sun Pharmaceutical Industries Limited, India, during the conduct of this study.

REFERENCES

1. M. Hankins, K. Tsai, J. Kim, N. Hammar, *Diabetes Research and Clinical Practice*, **2017**, *125*, 29.
2. J.F. List, J.M. Whaley, *Kidney International*, **2011**, *79(Suppl 120)*, S20.
3. J. Bolinder, Ö. Ljunggren, J. Kullberg, et al., *The Journal of Clinical Endocrinology and Metabolism*, **2012**, *97(3)*, 1020.
4. J.P.-H. Wilding, V. Woo, N.G. Soler, et al., *Annals of Internal Medicine*, **2012**, *156*, 405.
5. B. Vakkalagadda, M.L. Vetter, J. Rana, et al., *Pharmacology Research and Perspectives*, **2015**, *3(6)*, e00201, doi: 10.1002/prp2.201.
6. S. Kasichayanula, X. Liu, M. Pe Benito, et al., *British Journal of Clinical Pharmacology*, **2012**, *76(3)*, 432.
7. A.-M. Gheldiu, A. Csavdari, M. Achim, L. Vlase, I. Tomuta, D.M. Muntean, *Studia UBB Chemia*, **2017**, *LXII (2)*, 179.
8. A.-M. Gheldiu. D.M. Muntean, I. Cristea, I. Antonescu, R. Chira, C. Ureche, L. Vlase, *Revista de chimie (Bucharest)*, **2016**, *67(4)*, 702.
9. L. Shargel, A.B.C. Yu, "Applied Biopharmaceutics and Pharmacokinetics", 7th edition, McGraw Hill Education, New York, **2016**, chapter 1.
10. S.S. Jambhekar, P.J. Breen, "Basic Pharmacokinetics", 2nd edition, Pharmaceutical Press, London, **2012**, chapter 19.
11. W. Pan, *Biometrics*, **2001**, *57*, 120.
12. M.A. Saeed, P. Narendran, *Drug Design, Development and Therapy*, **2014**, *8*, 2493.
13. D. Pop, A.-M. Gheldiu, M. Oroian, A. Marcovici, S. Bhardwaj, A. Khuroo, R. Kochhar, L. Vlase, *Acta Medica Marisiensis*, **2018**, *64(4)*, 161.
14. Chemical structure of dapagliflozin, available at: https://pubchem.ncbi.nlm.nih.gov/substance/135257266#section=2D-Structure. Accessed on the 22nd of May 2019.